DOCTOR OF PHILOSOPHY

Circulation, mixing and renewal in the Clyde Sea

Midgley, Rik

Award date:
1998

Awarding institution:
Bangor University

CIRCULATION, MIXING AND RENEWAL IN THE CLYDE SEA.

A thesis submitted in accordance with the requirements of the University of Wales, Bangor, for the degree Doctor of Philosophy.

by RIK MIDGLEY.

University of Wales, Bangor,
School of Ocean Sciences,
Menai Bridge,
Gwynedd LL59 5EY.
U.K.

July 1998.

CIRCULATION, MIXING AND RENEWAL IN THE CLYDE SEA.

ABSTRACT.

The first continous set of observations made over the seasonal cycle of the vertical structure and currents in the Clyde Sea, Scotland's largest fjord, are used to show that the vertical structure is controlled by a balance between mixing and stratifying processes within the basin, and exchange with the North Channel of the Irish Sea. Stratification was observed to change from being entirely saline in the winter to being thermally dominated in the summer. Deep water renewal occurred throughout the winter. The inflow rate peaked in the early spring and also in the summer, resulting in an annual mean flushing time of ~3.5 months, in satisfactory agreement with previous estimates. Within the basin, a two layered flow structure was observed throughout the year, and a residual anti-cyclonic surface circulation was seen to be persistent. A 3-dimensional modelling study supports the hypothesis that this flow is driven by currents associated with the density gradients at the basin's mouth.

A positive density difference across the sill is a necessary but not sufficient condition for deep water renewal; when the difference was maximum in the winter, the rate of exchange was below average. Renewal was generally episodic, which is suggestive of wind induced exchange. The 3-dimensional model confirmed that changes in the wind direction could substantially increase or diminish exchange by enhancing or blocking the estuarine circulation. Rapid renewals in the spring time of 1993 and 1994 were initiated by storm events. In the summer of 1993, persistently high rates of exchange were observed. 3-dimensional modelling supported the hypothesis that this was due to the presence of saline water over the sill, which results from the summer time retreat of the front at the mouth of the Clyde Sea due to low freshwater inflow. An existing 1-dimensional filling-box model was developed in the light of the new observations. It showed that significant entrainment of Clyde Sea bottom water into this summer inflow was a possible mechanism to explain the deep water properties in the summer.

Mixing was found to be predominantly wind driven. A positive correlation was found between the wind and the amplitude of internal oscillations at sub-tidal frequencies, which dominated the velocity field in winter. A mode 1 internal tide at the M_2 frequency was observed, and had a horizontal velocity at the mooring sites of ~2 cms^{-1} throughout the year. The mixing associated with the internal tide was ~0.01 mWm^{-2}, which is 2 orders of magnitude lower than the wind mixing. The residual surface anti-cyclonic circulation prevents surface fresh water from entering the Kilbrannan Sound, which reduces the potential energy anomaly by ~60 Jm^{-3} relative to than that of the Arran Deep. Consequently, the wind induces relatively deeper mixing in the Kilbrannan Sound, which in the winter resulted in the reduction of the bottom water temperature without a significant decrease in salinity, and explains how the Clyde Sea bottom water may cool more rapidly than the deeper North Channel.

To imagine that 'good' can be done by means of an 'evil' is an illusion - a nightmare.

- Sayagyi U Ba Khin.

ACKNOWLEDGEMENTS.

Firstly, I would like to thank my supervisor, John Simpson, for his advise and criticism throughout my work. He planned and initiated this project, assisted by Tom Rippeth, whilst I was in sunny Bermuda anchoring current meters to the coral reefs. Thanks to Pat Hyder, who in my absence, between March and September 1993, organised the deployment and servicing of the moorings discussed in this thesis.

I would like to thank the members of the Dynamical Oceanography group at UWB for providing a stimulating environment in which to work, and all my fellow students and staff who have made my work here so enjoyable. Thanks goes to Toby Sherwin for his discussions on internal waves, and to Alex Souza for the discussions of ROFI systems. Thanks to Tom Rippeth for his help in the preparation and calibration of the Anderra RCM data, and to Joseph Cheok for his patients whilst teaching me the intricacies of UNIRAS graphics.

I express my thanks to the officers and crew of the R. V. Prince Madog, the R. V. Calanus, and the R. R. V. Challenger, whose friendly co-operation enabled the experimental work to go smoothly and enjoyably. Thanks to Ivan Ezzi and Ken Jones (Dunstaffnage Marine Laboratory) with whom I shared data from CTD surveys. Technical support was expertly provided by Dave Boon, Ann Hammerstein, Alan Nield, Ray Wilton, and Nigel Mathers with his mastery of the SEAROVER. Thanks to Ed Hill for the use of the drogues. Thanks to James Curran (Clyde River Purification Board) for the river flow data, Jannet Allen (Porterin Marine Laboratory) for the Porterin salinity data, and John Fullwood and Colin Henton (Meterological Office) for the meterological data.

A special thanks goes to Ian James (POL) who did much of the work involved in developing the 3-D Clyde Sea model, and with whom I had useful discussion of the results.

This research was undertaken as a component of the Processes in Regions of Freshwater Influence (PROFILE) MAST II E.U. project grant MAS2-CT93-0054.

CIRCULATION, MIXING AND RENEWAL THE CLYDE SEA.

CONTENTS.

LIST OF FIGURES.

LIST OF TABLES.

CHAPTER 1. INTRODUCTION.

1.1 OCEANOGRAPHY, AN ENVIRONMENTAL SCIENCE?

In modern times, people have developed a great trust in science, to the extent that it is commonly termed 'the new religion of the Western world'. Without doubt, science, and the technology which follows it, has radically transformed our lives. Many of the mundane and menial tasks of daily life are no longer necessary, while advances in health care and medicine dramatically extend our life expectancy. However, many environmental problems have risen in the wake of this new technology. Indeed, it seems that, the more rapidly science and technology are developed to solve the daily problems faced by man, the more rapidly new, maybe unforeseen, problems are created. The environmental consequence of these developments, is that the deterioration of the quality of the air we breath, the water we drink, and the soil from which we grow our food, has been so rapid and widespread that we must question whether mankind is undermining our own life support system.

In the shelf seas and coastal waters, the recent rapid expansion in the exploitation of natural resources, such as fossil fuels, aggregates and fisheries, and their increased use as dumping grounds for industrial, agricultural, and sewage effluent, has proceeded with little knowledge and consideration of the impact upon the ecosystem. Examples, all in the North Sea, are overfishing, which has resulted in the near extinction of cod, the reduction in the biodiversity occurring within 500 m - 6 km of waste piles of metals and toxic diesel from the 1500 oil rigs, (New Scientist, 6/11/96), and the increasing frequency of 'nuisance' blooms of phytoplankton, caused by anthropogenic nutrient inputs, which can cause hypoxia and have toxic effects on the local benthic ecology, which may be transferred into the food chain.

As these threats increase, it becomes even more important to monitor the coastal environment, and to control anthropogenic impacts. Water quality models are required, which should be used in an informed manner as predictive tools to determine the effects of future inputs. To implement and test these models, it is first necessary to improve our understanding of the basic processes, many of which are poorly understood, partly as a result of the lack of investment into relevant research over recent decades.

It is the scientists job to describe and understand nature in an objective fashion. However, the world unknown to science is immense, and only a tiny fraction may be selected for study. It is part of the scientists job to ensure that the areas selected for research are chosen objectively. With the large sums of money being channelled into research on, for example weaponry and genetics, it is evident that this is not the case.

The application of discoveries and developments are in the hands of the policy makers and politicians. However, the profitability of protecting our coastal waters has not been proven in a language that is understandable to people in government. Environmental management tends to be seen as a technical issue which is not fully understood by those in control, and attention is focused only upon visible phenomena. On the contrary, their discussions are full of production-orientated concepts like profits and development. The current political trend for privatisation ensures that science is increasingly done in collaboration with multinational corporations, which guarantees that many of the strategic and ethical decisions remain in the hands of an unaccountable élite.

In this scenario, the future of coastal oceanography appears murky and turbulent! However, in recent years we have witnessed projects such as the North Sea Programme, LOIS (Land Ocean Interaction Study), and more recently PROFILE (Processes in Regions of Freshwater Influence), and SES (Shelf Edge Study), which begin to address some of the major uncertainties concerning the dynamics of our coastal seas. Urgent areas for further study are the semi-enclosed seas, because of their inability to dilute anthropogenic inputs, an example of which are fjords. The work presented in this thesis is a part of the PROFILE project and focuses upon the dynamics of the Clyde Sea, Scotland's largest fjord.

1.2 INTRODUCTION TO FJORDIC OCEANOGRAPHY.

Fjords are deep estuaries, usually semi-enclosed by one or more relatively shallow sills which separate them from the ocean. Being of glacial origin they occur at the high latitudes of Scandinavia, North and South America, New Zealand, and along much of the Arctic coastline. People living on the shores of fjords use them as sources of food, for the disposal of waste and for recreation, and the military enjoy playing in them.

A typical fjord has a three layer structure (Figure 1.1). Freshwater flowing into a fjord mixes to form a brackish surface layer, which drives a baroclinic circulation known as estuarine circulation. This buoyant layer flows seaward, entraining saline water from below, to the extent that its volume increases by 1 or 2 orders of magnitude (Stigenbrandt, 1990). Beneath this layer, seawater has to flow landward to replace the entrained water. The presence of a sill complicates this scenario by preventing landward flow from reaching the deep water, defined as water below sill depth, and may lead to the formation of a stagnant deep layer (Gade & Edwards, 1980). Many fjords are sufficiently deep that for much of the time the estuarine flow tends not extend to the full depth, but is confined to a relatively shallow surface layer (Farmer & Freeland, 1983).

Water that is advected across the sill, into the basin, will, if it is denser than the ambient water, sink to a level at which it is neutrally buoyant, displacing the resident water upwards (Gade & Edwards, 1980). Such events are termed deep water inflows and lead to a renewal of the deep water. Partial renewal may occur if the renewal event is too short or if the intrusions are not sufficiently dense to replace the bottom water.

At times when there are no deep water inflows, the deep water is isolated from the open ocean, and changes due to vertical mixing tend to dominate (Gade & Edwards, 1980). These have the effect of changing the value of the deep water properties towards those found near the surface. Density is reduced, thus enhancing the fjord's liability to renew. Figure 1.2 shows the variation in deep water properties in Indian Arm over an 11 year period (de Young & Pond, 1988). Bottom water renewals, which occur here over periods of years, are indicated by an increase in deep water density and salinity. Following these events, these properties show a steady decrease, resulting in a saw-toothed shape of the time series, which is common in many fjords. Partial renewal events are highlighted by temperature fluctuations at 100 m, with none at 200 m.

A further consequence of the isolation of the deep water is the steady accumulation of dissolved nutrients and the decrease in dissolved oxygen concentration due to biological activity. In extreme cases, this may lead to anoxic conditions and the presence of hydrogen sulphide, which may destroy marine life. Figure 1.2 shows such an anoxic event occurring in the spring of 1982 in the deep water of Indian Arm. When deep water inflows occur, highly oxygenated inflowing waters cause dramatic increases in the deep water oxygen concentrations. The uplifted water, rich in hydrogen sulphide, has been reported to kill fish in Lake Nitinat, Vancouver Island (Ozretich, 1975).

The classification of fjords is not straightforward. Since in many, possibly most, fjords more than one process governs the characteristics of the circulation and stratification. Hansen & Rattray (1966) began by classifying estuaries by comparing relative stratification with the ratio of mean surface velocity to net river run-off flow velocity. This scheme distinguished deep fjords with relatively thin, relatively highly sheared near surface circulation from other types of estuaries, but gives little information on the dominant scales or intensity of turbulent processes. Stigenbrandt (1981) proposed a simple classification based on the assumption of steady internal hydraulic control of a two layer flow at the estuary mouth. However, this scheme breaks down if conditions are strongly time dependent, or two layer flow does not occur, for example in fjords subject to rapidly changing meteorological forcing or tides. Any practical classification scheme must look closely at the kinds of processes and scales of variability which actually occur in nature. In this review, a detailed discussion of the physical character of fjords is divided into processes which directly control the rate of cross-sill exchange, processes which result in mixing

within the basin, and a discussion of circulation within wide fjords. The section on renewal is subdivided into 2 sub-sections dealing with (i) the mechanisms by which the dimensions of the sill can affect renewal, and (ii) the processes which act to control the gradients, both barotropic and baroclinic, across the sill.

1.3 DEEP WATER RENEWAL.

1.3.1 THE SILL TOPOGRAPHY.

Generally, the sill is a region of increased currents and shears and consequently increased vertical mixing. The dimensions of the entrance sill define much of the hydrological character of a fjord, by governing the nature of the cross-sill flows. The sill may be shallow or deep, relative to the pycnocline, and this will determine whether barotropic or baroclinic forcing is important. A sill may also be long or short, in comparison to a tidal excursion, and this determines whether cross-sill exchange occurs at times of low or high barotropic forcing, such as during spring tides or strong winds. Finally the sill may be narrow or wide in comparison to the internal Rossby radius of deformation, which determines whether or not inflow will be affected by the Earth's rotation.

If a sill is sufficiently shallow the barotropic flow may reverse the baroclinic flow. Even though the baroclinic flow may even be turned off during the ebb tide, it is augmented on the flood to the degree that the carrying capacity of the sill is increased (Stigenbrandt, 1977). Renewal over the shallow sill (~10 m) of Loch Eil, a Scottish loch, is governed by the amplitude of the barotropic tide; it stagnates during neap tides, and is renewed regularly during springs (Edwards *et al.*, 1980). Other fjords are controlled similarly by the spring/neap cycle, if the sill is sufficiently shallow, but the timing of renewal events is controlled by the availability of dense water at the sill (e.g. Oslofjord; Gade & Edwards, 1980; and Indian Arm; de Young & Pond, 1988). Elliott *et al.* (1990) note that turbulence is evident during spring tides over the ~10 m deep sill of Loch Sunart as a 'boiling' of the surface waters.

If the tidal excursion is less than the sill length, mixing becomes critically important. Here renewal tends to occur on the neap tide, with dense inflow over the surface of the sill continuing even during the ebb tide, e.g. Rupert and Holberg Inlets (Drinkwater & Osborn, 1975), Indian Arm (de Young & Pond, 1988), and Puget Sound (Geyer & Cannon, 1982; Cannon *et al.*, 1990). Cannon *et al.* (1990) also describe the significance of the density gradient across the sill in Puget Sound where intrusions on the neap tide occasionally begin during springs, a phenomena illustrated in Figure 1.3. The final inflow has undergone a degree of dilution.

Fjords often have constrictions at their mouths, which enhances the importance of barotropic forcing by ensuing complete mixing, and possibly result in the existence of a tidal jet. Loch Linnhe in Scotland is such a fjord, and exchange is augmented in the spring tide (Allen, 1995). An extreme example is the sill known as the Quatsino Narrows, near Vancouver Island, the dimensions of which are length 6 km, width 500 m, and depth 18 m, and include a sharp bend (Drinkwater & Osborn, 1975). Water in the Narrows is a well mixed combination of basin and outside water, which on the flood tide is injected into the basin, below the low salinity surface layer. On the other hand, fjords which have large mouths in comparison to their volume will have low tidal energy and associated mixing.

Deeper silled fjords are less constrained by topographic effects, and estuarine flow may continue unimpeded. The timing of renewals is governed by variations in the density of the water over the sill. If no other complicating factors exist, this condition often occurs in the late summer, at a time when the salinity reaches its annual maximum, e.g. the Gulf of Alaska (Gade & Edwards, 1980), Hardanger Fjord, Norway (Dyer, 1977). Studies of deep water mixing in thirty Norwegian fjords by Stigenbrandt & Aure (1989) show that fjords with either deeper sills or more shallow basins have better aerated (i.e. better mixed) deep water.

Rotational effects are important in fjords with wide sills, (where the channel width, W, is much greater than the internal Rossby radius, λ). Many studies of flows over wide sills have assumed that conditions vary slowly downstream, so that flows crossing the sill are much larger than those along sill, a condition not satisfied in the Clyde Sea where there is a front over the sill (e.g. Edwards *et al.*, 1986). Recent research into rotating hydraulics over wide sills has concentrated upon either homogeneous systems (Borenas & Pratt, 1990) or a simple 1.5 layer approach (Pratt & Lundberg, 1991). Whitehead *et al.* (1974) made a preliminary study of rotation on a 2 layer flow and found rotation to be important when $\lambda \sim W$. The equations of flow of a homogeneous inviscid fluid down a rotating channel of slowly varying cross-section were later formalised (Gill, 1977) and extended to include two active layers and a simple sill (Daziel, 1990). However, the description of the flow field is complicated and obscured by formidable algebra. For $\lambda \sim W$, Daziel found rotation caused a stronger coupling between layers and a decrease in the exchange transport. For wider sills, the exchange was found to be independent of channel width. The effects of longitudinal winds in broad fjords was investigated by Cushman-Roisin & Svendsen (1994). They find that the wider and deeper a sill, the greater the horizontal separation of in- and out-flow, and the less exchange is frictionally inhibited and they illustrate this phenomena with observations from Porsanerfjord.

If there is variation in the axial topography along wide sills, inflow will be enhanced along the channel. This is exemplified by research in semi-enclosed estuaries such as Chesapeake Bay

(Valle-Levinson & O'Donnell, 1994; Valle-Levinson *et al.*, 1995), and Delaware Bay (Münchow & Garvine, 1993; Wong, 1994). Outflow may either be enhanced over the channels or the shoals, depending upon the interaction between topography and Coriolis (Valle-Levinson & O'Donnell, 1994), and whether the circulation is driven by gravitational, wind or remote atmospheric forcing (Wong, 1994).

1.3.2 GRADIENTS ACROSS THE SILL.

In addition to the sill topography, the renewal of the deep water is governed by the relative density of the water within the basin, and that near the sill, and by barotropic forcing between the two. Variations in density of the basin water may result from variations in the mixing or run-off rates, while the density of water at the sill fluctuates seasonally, with the tidal cycles, and with meteorological events. Consequently deep water renewal tends to be intermittent. However, the majority of fjords repond, to some extent, to seasonal forcing of the coastal oceanographic climate. Whenever the annual variation is large in comparison with shorter term variations the annual cycle is likely to appear in the deep water, such as in the Bonnefjord basin of the Oslofjord (Gade & Edwards, 1980) and Indian Arm (de Young & Pond, 1988). Mixing will be discussed in detail in Section 1.5.

Stanton (1986) suggested that the availability of dense water offshore precipitates the deep water inflow in four New Zealand Fjords. Salinity changes outside the sill of Puget Sound appear as the result of northerly winds on the Pacific coast and force the upwelling of dense water into the mouth of the fjord (Geyer & Cannon, 1982; Cannon *et al.*, 1990). Figure 1.4 illustrates that these salinity fluctuations result in the periodic renewal of Puget Sound over a winter period. If the fjord is open to a sea which is also semi-enclosed, renewal may be restricted to periods of low freshwater run-off in the outside waters, such as in Lake Nitinate, Vancouver Island (Ozretich, 1975), and fjord Skjoman (Skreslet & Loeng, 1977).

Renewal of Loch Etive, a Scottish fjord, occurs, on average less than once a year, in response to very dry conditions. Here, renewal is prevented at times when the density of the water near the sill, which is controlled by run-off, is less than that of the deep water (Edwards & Edelsten, 1977). In extreme cases of fresh water discharge the surface layer extends to the sill depth and blocks the incoming flow. In other fjords, freshwater run-off can accelerate baroclinic currents which supply the replacement water. In McBride Inlet, a small glacial fjord on the Alaskan coast, bottom water flushing occurs only in summer, when the freshwater input is increased by glacial melt, enhancing the density gradients and the estuarine flow (Cowan, 1992).

In highly stratified fjords, meteorological effects may also become important. Wind and atmospheric pressure gradient can enhance the barotropic flow, and also drive baroclinic flows in the sill region. The frictional drag of a down-fjord wind may enhance the estuarine flow, while in some fjords the wind effects upon the density field becomes important (Gade & Edwards, 1980). At times of low freshwater run-off, Scottish fjords Loch Sunart (Gillibrand *et al.*, 1995), and Loch Ailort (Gillibrand *et al.*, 1996), episodic renewal occurs on timescales of weeks, which is indicative of a wind driven exchange. Periods of easterly winds enhance the estuarine circulation and renewal in Ofotfjord, North Norway. This in turn brings saline water to the entrance of Skjomen fjord, resulting in renewal (Skreslet & Loeng, 1977). A similar situation occurs in Upper Loch Linnhe, which is separated from Loch Linnhe by a shallow sill. With a seaward wind blowing down the fjords, the pycnocline in Loch Linnhe is upwelled, bringing denser water to an area immediately seaward of the sill, from where it is advected across the sill by the barotropic tidal currents (Allen, 1995).

1.4 MIXING IN FJORDS.

All vertical mixing processes within a fjord serve to reduce the density of the bottom water by mixing down brackish surface water, thereby predisposing the fjord to further deep water inflows. Without mixing, renewal could only occur when water seaward of the sill attained a density greater than at any time in the past. Much of the energy available for mixing derives from the barotropic tide and meteorological forcing. Molecular diffusion can generally be assumed negligible in comparison with large scale eddy transports, although in highly stratified areas, a higher eddy diffusivity has been observed for heat than salt (Edwards & Edelsen, 1979).

There is a flux of energy into the fjord with the barotropic tidal wave. There are three main sinks for this energy: boundary mixing, internal waves at tidal and higher frequencies and tidal jets and plumes. The dominant mechanism will vary between fjords. Boundary mixing is a strong function of velocity and varies greatly within the basin. Barotropic currents in most fjords will be small away from the sill. Frictional energy losses in Knight Inlet from the barotropic tide are estimated to be less than 3% of the total loss (Farmer & Freeland, 1980). In fjords with constricted sills, much of the energy in the barotropic tide is channelled into a jet and an internal tide may not be generated (Stigebrandt, 1976). Stigebrandt & Aure (1989) estimated that 1% of the energy of such jets is used in mixing the deep water.

The barotropic tide passing over the sill induces a vertical velocity which displaces the isopycnals in an oscillatory manner. This generates a vertical buoyancy force which drives internal gravity waves at tidal frequencies, known as the internal tide (Phillips, 1977; Baines, 1982). These

waves are particularly well developed if the sill reaches up to the pycnocline (e.g. Stigebrandt, 1976; Elliott *et al.*, 1990). They may be manifest on the surface as bands of roughened and smooth water, which have been observed from satellites (Hughes, 1978), while the flow itself can be visualised using high frequency echo-sounders operating in the 50-200 kHz range (Figure 1.5). These use passive acoustic scatterers such as plankton and temperature inhomogeneities to outline the motions of the water column (e.g. Farmer & Freeland, 1982, Stacy & Zedel, 1986, who use this technique to observe an hydraulic jump in the flow in the lee of a sill).

The internal tides in Oslofjord diminish rapidly away from the sill indicating energy is dissipated into turbulent motion, maybe at the boundary (Stigebrandt, 1979; Gade & Edwards, 1980). Stigebrandt (1976) suggested that mixing results as internal waves break on the sloping basin walls, thus dissipating energy. He supported his arguments with laboratory experiments, where the induced turbulence was found to extend appreciably below the pycnocline, thus creating a similar effect to that of localised boundary mixing. A corollary of the concept of breaking internal waves driving deep water mixing is that the internal tide is not reflected and, hence, is purely progressive. However, evidence of reflection of internal tides has been presented in Alice Arm, British Columbia (Keeley, 1984); Indian Arm (de Young & Pond, 1987), and Knight Inlet (Marsden & Greenwood, 1994). The mixing associated with internal tides has been prescribed as the unaccounted for process, which must be acting to explain observed high flushing rates in a number of fjords (Stigebrandt, 1976,1979; Seibert *et al.*, 1979; Farmer & Freeland, 1980; Simpson & Rippeth, 1993).

Modelling results suggest that, in Loch Sunart, increases in the near-surface stratification following a run-off event may cause the internal tide to strengthen. This will generate an increased shear across the halocline (which is deeper than the 10 m sill depth), which maintains the vertical mixing and may actually reduce renewal (Elliott *et al.*, 1990). Internal tides may also be modified by a pulsed dense water inflow, which will carry the energy downward, so that dissipation occurs at a lower level (Perkins & Lewis, 1978).

The role of the wind has received little attention, but may contribute to mixing through internal seiching and increased shear (Gade & Edwards, 1980). Surface wind stress is important in producing a surface mixed layer. Wind drift of the surface layer can lead to changes in the depth of the pycnocline which may occur either in the form of standing waves (i.e. seiches) or as frictionally damped progressive waves. For example rapid changes in the pycnocline depth near the head of Alberni Inlet propagate back along the channel for several tens of kilometres (Farmer & Freeland, 1982). The pycnocline depth doubles in less than six hours and the theory of long internal waves appears to provide a good description of its subsequent behaviour.

In the winter, if fresh water run-off is low, surface cooling results in thermal instabilities which drives convective mixing. Typical cooling rates in Knight Inlet are 150 Wm^{-2} (Farmer & Freeland, 1982), while in the Clyde Sea values an order of magnitude higher have been observed (Rippeth & Simpson, 1995). In both Alice Arm and Knight Inlet, British Columbia, mixing reaches depths of 225 m (Farmer & Freeland, 1982). Although wind mixing may have been responsible for the formation of such a deeply mixed layer, it seems more likely that thermal convection would serve to maintain it. A similar situation exits in Arctic fjords where convection is driven by salt exclusion from growing ice sheets (e.g. Cambridge Bay, Perkins & Lewis, 1978).

Once over the sill, inflowing water enters the fjord as a gravity current (e.g. Turner, 1973; Pedersen, 1980). A gravity current is essentially an internal bore in which a fluid of higher density moves under one of lower density. The buoyancy contrast drives the flow against frictional losses at the bed and upper interface. Generally, the relatively static ambient water is entrained into the inflow at a rate proportional to the velocity of the plume. However, on more gentle slopes the flow is more stable and mixing is suppressed. In Saguenay Fjord, entrainment is sufficiently strong that, at times, the density contrast may vanish before reaching the bottom and the inflow is at mid-depth (Seibert *et al.*, 1979). Cannon *et al.* (1990) followed an intrusion which propagated along Puget Sound at around 10 cms^{-1} as a density perturbation, and noted a compensatory flow above. The flow was deflected by topography and by Coriolis acceleration, which highlights the difficulties in quantifying these flows using a single vertical section (Geyer & Cannon, 1982; Bretschneider *et al.*, 1985).

1.5 CIRCULATION IN WIDE FJORDS.

It is usual to ignore the effect of rotation in studies of fjords, and approximate the dynamics along an axial section. In wide fjords however, (those in which the width is greater than the internal Rossby radius), rotational dynamics may be important. Examples are some northern Norwegian fjords, where the Coriolis parameter becomes large (Svendsen, 1995), and in the large fjords of the North Baltic, such as Bothnian Bay, Gulf of Finland, and Gulf of Riga (Rodh, 1995).

A wind blowing along the axis of Porsangerfjord in northern Norway induced upwelling on one side and downwelling on the other, in a similar fashion to classical coastal upwelling, except that here, the upwelling and downwelling interfere with one another (Cushman-Roisin *et al.*, 1994). An up-fjord wind is believed to induce a surface cyclonic rotation in Altafjord and Malangen, in northern Norway, while a down-fjord wind is ambiguously described as creating a 'similar circulation' (Svendsen, 1995). Asplin (1995) showed numerically that for a generalised wide fjord, an up-fjord wind (blowing towards the head) induced a cyclonic circulation which induced

exchanges with the coastal waters of the order of 100 m^3s^{-1}.

Evidence for the existence of a residual anti-cyclonic circulation within the basin has been observed in Ise Bay, Tokyo Bay, and Osaka Bay, all in Japan (Fujiwara *et al.*, 1997). The seasonally averaged distribution of residual surface currents are part of the evidence for the anti-cyclonic circulation in Ise Bay, which is both smaller and shallower than the Clyde Sea (Figure 1.6). From spring until autumn a front lies in an forward position near the mouth of the gulf, while in the winter, when freshwater inflow is minimum, the front retreats towards the head of the bay. In the autumn an anti-cyclonic gyre occupies much of the bay. Fresh surface water is carried across the mouth by the frontal jet to the coast, where upon the flow diverges, partially outflowing, and partially returning into the bay as a part of the anti-cyclonic gyre. In winter, the divergence point moves with the front, which retreats to the head of the bay, and the anti-cyclonic gyre is restricted to a small area near the head.

Fujiwara *et al.* (1997) presented an explanation which entailed the combined effects of classical estuarine circulation and the Earth's rotation. Their arguments required that potential vorticity be conserved as the bottom layer is entrained into the upper. However, in order that potential vorticity be conserved, the isobars must be parallel to the isopycnals and frictional effects must be negligible. The former is not the case in an estuarine environment, and the frictional effects of topographic steering, bottom and surface mixing, (not to mention entrainment!), are important in a shallow gulf.

1.6 THE CLYDE SEA, AND THESIS OBJECTIVES.

The new observations, analysis and modelling of the Clyde Sea presented in this thesis, were undertaken as a component of the MAST II EU PROFILE project (grant no. MAS2-CT93-0054). The project aimed to study processes in Regions Of Freshwater Influence (ROFIs) on a regional scale. It undertook to make new observations of several European ROFIs; the Thermaikos Gulf, the German Bight, the Rhine, and the Po, in addition to the Clyde Sea. The Clyde Sea was chosen as being the low tidal energy regime.

The Clyde Sea, situated on the west coast of Scotland, is a basin of 200 m depth covering some 2500 km^2. Land locked on three sides, to the south it is partially cut off from the North Channel of the Irish Sea by a sill of depth 40 m.

The Clyde Sea annually receives large inputs of freshwater (~300 m^3s^{-1}), which generally results in the existence of a strong halocline in the basin. In addition, thermal stratification becomes

important in the summer, which leads to the relative isolation of the bottom waters in the basin. This 'stagnant' deep water becomes depleted in oxygen, and nutrients are trapped below the pycnocline. Understanding the mechanisms by which this deep water is diluted by mixing with the surface waters or renewed by inflow from the shelf sea, is essential in understanding the effects and fate of anthropogenic inputs intofjords.

The Clyde Sea is unusual among fjords in that it has a wide mouth, which results in there being relatively little local intensification of tidal mixing, while rotational effects become important. Consequently, many of its characteristics are more typical of many gulf type ROFIs, where lateral flows are important. Rotation influences both the mechanism by which water is exchanged over the sill and the circulation within the basin. There have been few studies of this type of fjordic circulation, and these features have not been previously studied in the Clyde Sea.

Edwards *et al.* (1986) and Simpson & Rippeth (1993) have studied the dynamics of the Clyde Sea. Rippeth (1993) identified the mechanism of cross-sill exchange and mixing associated with internal waves as two areas of uncertainty. These are both important processes which control the character of the deep water, and are relevant to many fjords.

The aim of this study was to further our understanding of the processes which control the circulation, mixing and renewal of the Clyde Sea. Of particular interest was the degree of isolation of the bottom waters in the summer, and the processes which affect it. This included a re-evaluation of the relevant significance and timing of the various mixing mechanisms, and an identification of the mechanisms which control the rate and timing of cross-sill exchange.

The specific objectives of this study are:

(i) To make a definitive, continuous and duplicated set of observations of the vertical structure over a period greater than one year.

(ii) Compare the new observations with results from the 1-dimensional filling-box model of Simpson & Rippeth (1993).

(iii) Observe the internal tide, and estimate the magnitude of the associated mixing.

(iv) Observe the flows over the sill at periods of both high and low cross-sill exchange.

(v) Develop a 3-dimensional model of the sill region, and use it to determine the necessary and sufficient conditions for cross sill exchange.

1.7 LAYOUT OF THESIS.

Following this introductory chapter, there is a detailed description of the Clyde Sea and previous relevant work. There follows chapters on the observational techniques and data analysis methods used in this thesis. In Chapter 5 the observational results from the seasonal survey are presented, along with some interpretation. Processes involved in mixing are considered in Chapter 6. The 1-dimensional model is run over the observation period, and modified in Chapter 7. In Chapter 8, the new observations from the sill region are presented, along with inferences. A new 3-dimensional model of the Clyde Sea, which focuses upon the sill region, is used to synthesize the new results in Chapter 9. The thesis is concluded with a summary of the findings and a discussion of the results in Chapter 10.

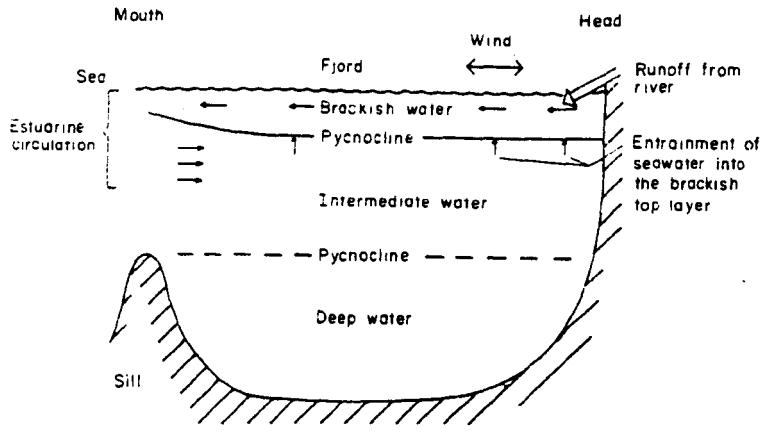

Figure 1.1. Vertical cross section along a typical fjord showing the different types of water and the estuarine circulation. (Reproduced from Stigebrandt, 1981).

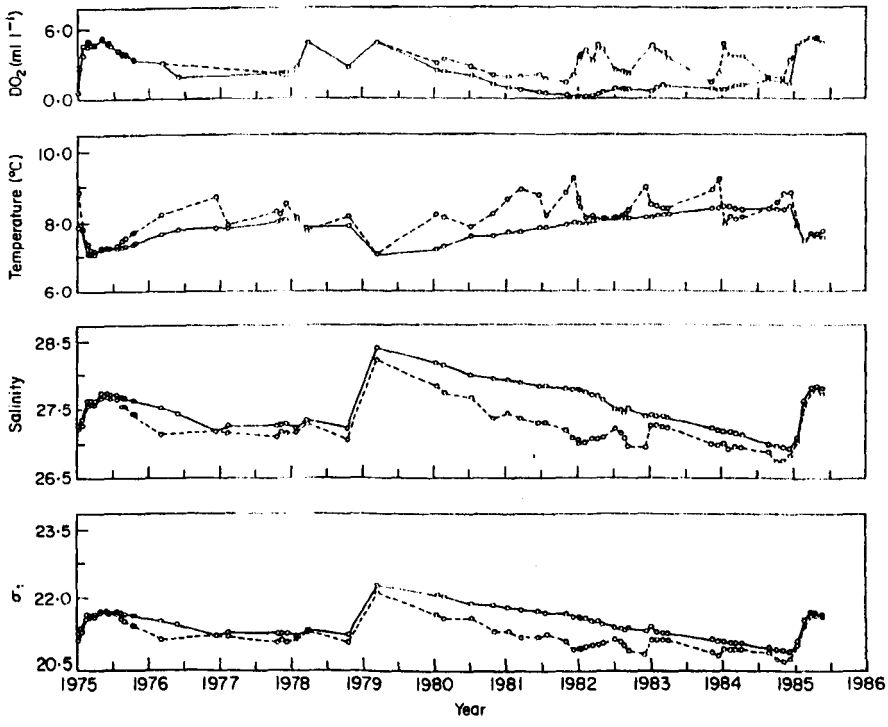

Figure 1.2. Timeseries of dissolved oxygen concentration DO_2, temperature, salinity, and σ_t in Indian Arm. (__) data at 200 m, (---) data at 100 m. (Reproduced from de Young & Pond, 1988).

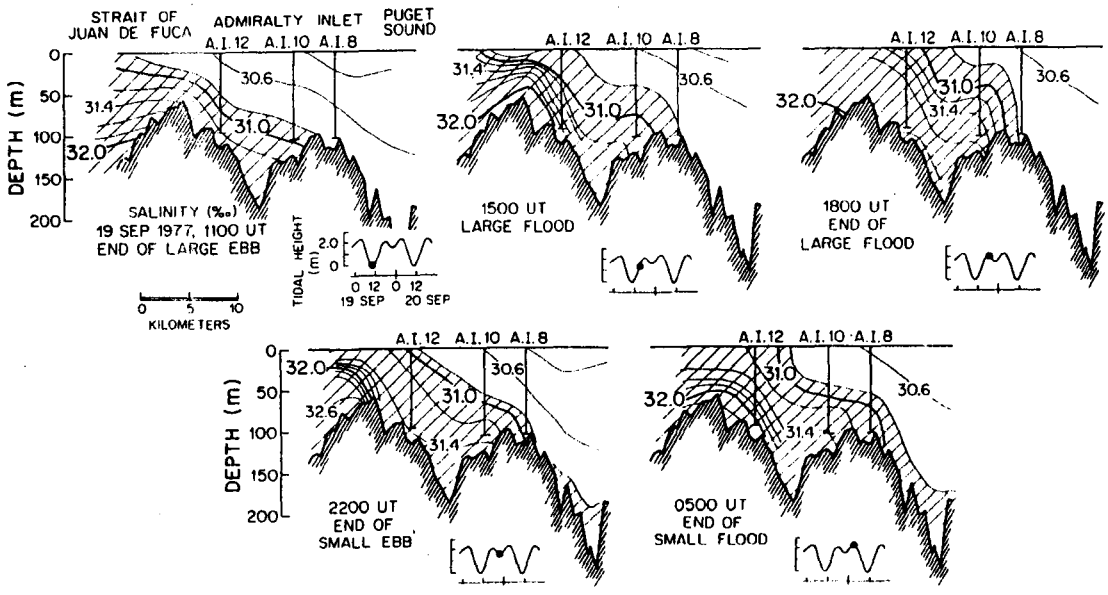

Figure 1.3. Salinity sections at Admirality Inlet at various phases of the tide during the neap part of the cycle. The tidal height at nearby Seattle is shown for each section in the inset. The shaded region indicates water more saline than the ambient in Puget Sound. (Reproduced from Geyer & Cannon, 1982).

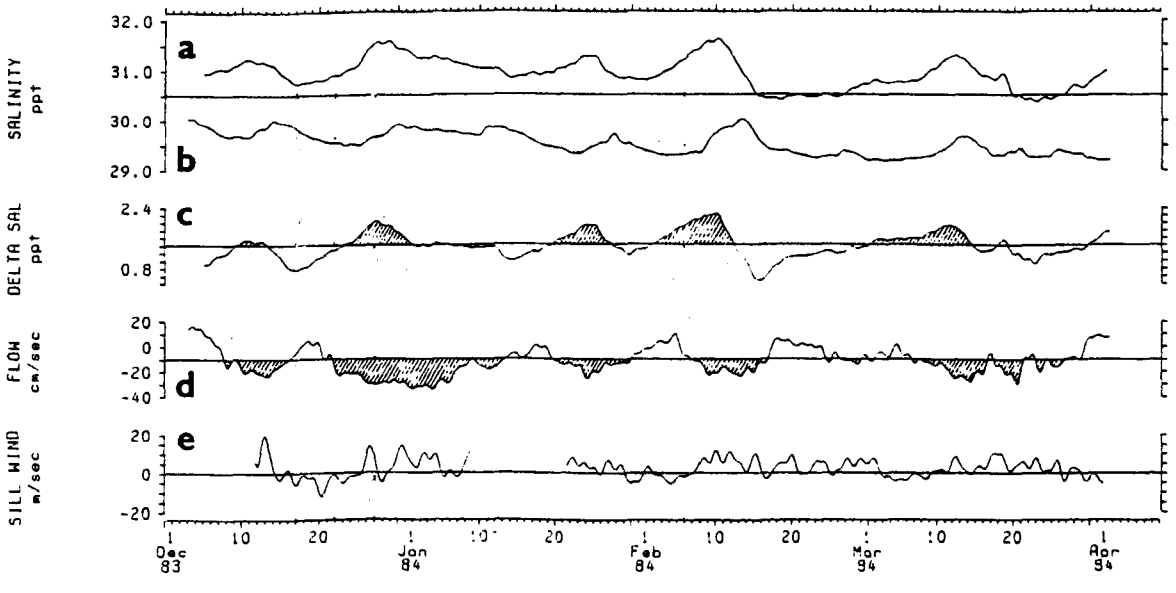

Figure 1.4. (a) Low pass filtered salinity at sill depth outside the sill; (b) salinity at the bottom in Puget Sound; (c) the difference between the two; (d) bottom flow in the sound, and; (e) along channel winds. Inflow greater than 10 cms^{-1} and salinity differences greater than 1.4‰ are shaded. (Reproduced from Geyer *et al.*, 1990).

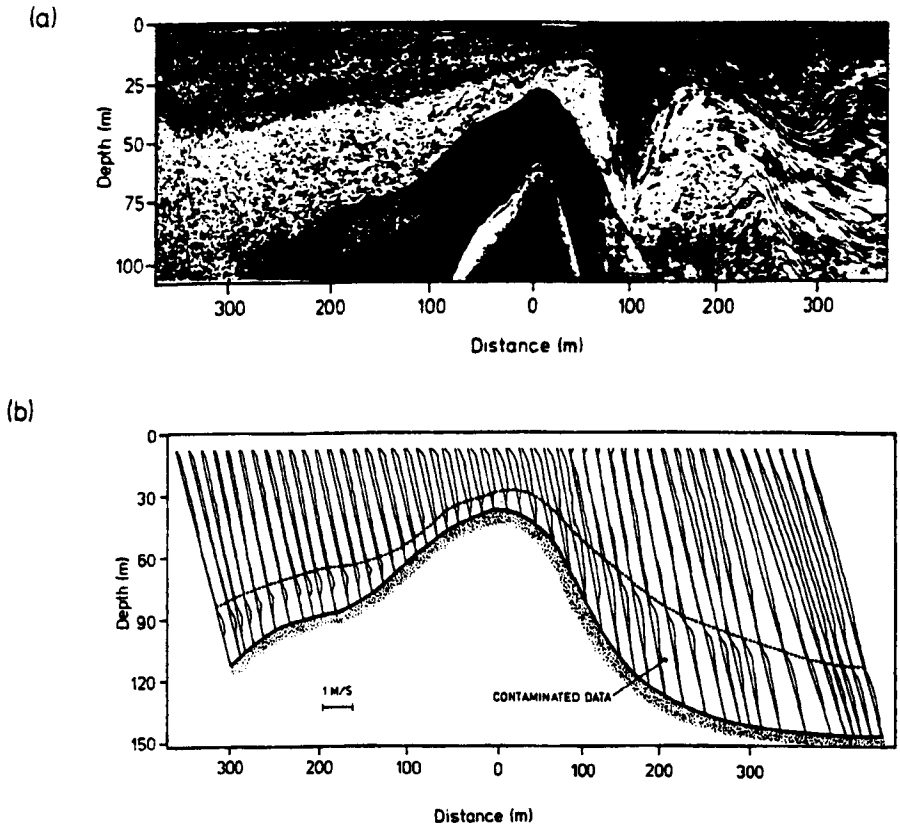

Figure 1.5. (a) Streamlines of the ebb tide in Observatory Inlet, British Columbia, from a 100 kHz echo-sounder. The flow is from left to right towards the mouth of the inlet. (b) Profiles of velocity measured along the acoustic beam. Flow to the right (left) is indicated by the profile curve being located on the right- (left-) hand side of the reference line. Below the dashed line the measurements are biased by bottom reflections. (Reproduced from Stacy & Zedel, 1986).

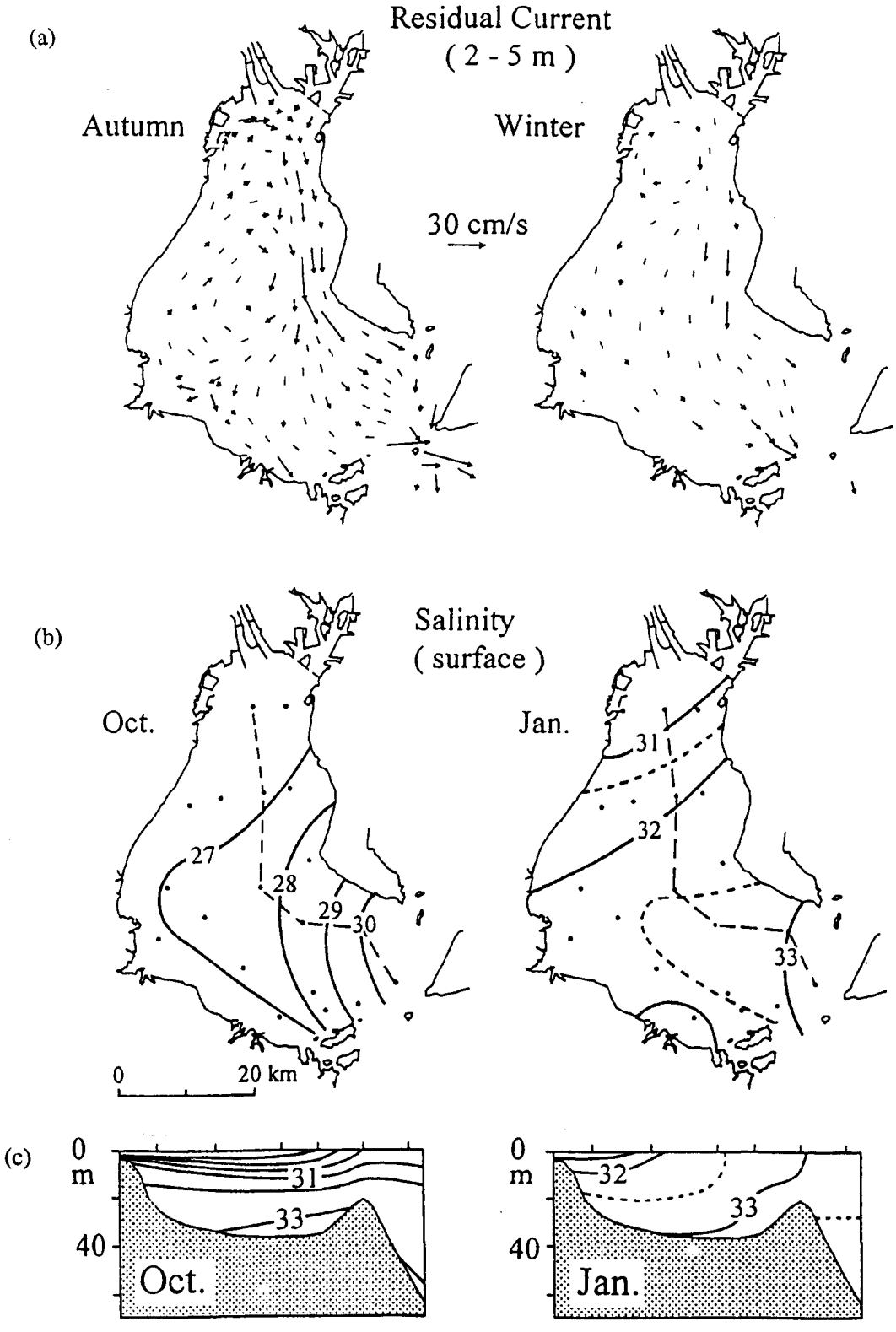

Figure 1.6. Salinity and currents in Ise Bay, Japan. a) Residual surface currents during autumn and winter; b) surface salinity distributions during October and January (1982-1991 means); and c) salinity along section AB during October and January (1982-1991 means). (Reproduced from Fijiwara, In Press).

CHAPTER 2. INTRODUCTION TO THE CLYDE SEA.

2.1 GEOGRAPHICAL BACKGROUND.

The Clyde Sea is Scotland's largest fjord, located at 55.5° N, 5° W (Figure 2.1). It is a deep semi-enclosed basin covering some 2500 km^2. It communicates with the North Channel of the Irish Sea via the Great Plateau, a relatively shallow sill at its entrance (of maximum depth 50 m). At its northern limit, the Clyde Sea is connected to a series of fjordic sea lochs and the shallow, drowned-valley estuary of the Clyde River.

The Clyde Sea is itself divided by the island of Arran. To the east of Arran is the Firth of Clyde, the largest part, which includes a basin of depth 180 m, known as the Arran Deep. To the west of Arran lies the Kilbrannan Sound, a basin some 160 m deep which is bounded to the north by a sill of 100 m depth, and to the south by the Davaar Sill, depth ~25 m. The deep waters of the Kilbrannan Sound and the Arran Deep meet in Inchmarnock water, north of Arran, where the maximum depth is 200 m. This deep water extends northwards into Lower Loch Fyne, to a sill of depth 30 m at Otter Point.

To the north of the Firth of Clyde lies the Highland Boundary Fault. This forms a major geological divide between the ancient, highly deformed igneous and metamorphic rocks to the north, and the younger, less deformed sedimentary structures to the south (Tivy, 1986). The area experienced several major glaciations during the Quaternary period. Glacial erosion and deposition during the Devensian (18000 BP), the most recent cold period, resulted in the Clyde's present distinctive form (Jardine, 1986). Marine invasion had commenced by 14000 BP, but occurred predominantly during the period of rapid sea level rise in the Holocene (8400 - 5500 BP).

A catchment area of over 10,500 km^2 collects an average of ~350 m^3s^{-1} of freshwater (Poodle, 1986). Of the total freshwater, ~46% enters from the Clyde Estuary, ~15% from the Ayrshire coast, ~9% from Loch Fyne, ~7% from Arran, ~4% from the Kyles of Bute, and ~13% goes directly into the sea. Freshwater flows are highly variable with the most frequently occurring rate being only 50% of the average, while winter flows have been observed which are twenty times this figure (Poodle, 1986).

Maritime air from the North Atlantic dominates the atmospheric circulation, which is often vigorous. The winds are variable in direction with south-westerlies being marginally more frequent. Smith (1986) quotes a mean wind velocity of 3 ms^{-1}, which seems somewhat low in comparison to Figure 5.1, and notes that wind speeds of 15 ms^{-1} are recorded for 1% of the time.

The Kintyre peninsula and Arran offer shelter from westerly winds, and the mountainous terrain tends to funnel winds within the Clyde into a north-south orientation.

2.2 HUMAN INFLUENCE.

The Clyde Sea attracted early settlement with its rich fishing grounds and sheltered harbours. The Clyde Estuary was one of the major foci of the Industrial Revolution in Britain, particularly in the fields of marine transport and engineering. Following the Second World War, the naturally sheltered deep water harbours in the Firth of Clyde attracted the larger cargo vessels of the time. Consequently the heavy industries in Glasgow and Lanarkshire were relocated to the Firth on the Ayrshire coast. More recently economic recession, combined with a shift in North American trade-routes from Britain direct to continental Europe, has led to a decline in the Clyde's port activity. Increasing emphasis is now directed to the Clyde Sea's amenity and recreational value. Improved road access has aided the rapid growth in the number and size of large marinas, water sports and other holiday facilities (Tivy, 1986).

Herring fisheries have been important for hundreds of years, providing the only source of income for some of the isolated Kintyre villages. The area also has important demersal and shell-fisheries (Hislop, 1986; Mason & Fraser, 1986). Due to recent over-fishing, catches are greatly reduced in size and nephrops fishing now dominates. More recently Lochs Fyne and Striven were among the first Scottish sites for salmon farming (Tett *et al.*, 1986).

Over a million people live in the watershed of the Clyde Sea, which includes the city of Glasgow. Significant levels of pollution occur, notably in the Clyde Estuary, along the Ayrshire coast and at the sewage dumping ground at Garroch Head (Boyd, 1986). A clear example of impact was during the last 2 weeks of September 1980; discoloured surface water was observed in the northern sealochs, enriched by nutrients from recent high freshwater runoff, and containing dense blooms of dinoflagellate *Gyrodinium Aureolum*. A fish farm in Loch Fyne suffered a mortality of 3000 salmon (Jones *et al.*, 1982). In recent years, the water quality of the Clyde Sea has improved, not as a result of any goodwill or intentional legislation, but as a consequence of economic recession.

2.3 THE SEASONAL CYCLE OF STRATIFICATION OF THE CLYDE SEA.

Unlike most fjords, the Clyde Sea is relatively wide at its mouth (Section 1.2), and consequently the intensification of mixing at the sill is limited. The waters within the basin are generally well

stratified, with relatively weak horizontal gradients, the stratification varying from being predominantly thermal during the summer, to entirely haline during the winter.

Observations dating back to Mills (1892) show the isolation of the bottom waters in the summer, beneath the thermocline. Craig (1959) describes how the bottom water 'loses its identity during October or early November'. At this time, the North Channel water cools, and thus becomes sufficiently dense to replace the bottom water in the basin. Deep water properties then follow those over the sill until late spring, suggesting continual North Channel inflow over this period (Edwards *et al.*, 1986).

The concentration of radiocaesium in the Clyde Sea waters, released from the nuclear fuel reprocessing plant in Cumbria, on the north east of the Irish Sea, shows a marked degree of spatial uniformity indicative of a well mixed system (Baxter *et al.*, 1979). Over a three year survey period, they estimated, using a simple box model, the residence time to be ~4.5 months. Edwards *et al.* (1986) estimated the seasonal mean volume of fresh water in the surface 50 m to be equivalent to only 2 months mean supply. This shorter period is presumably balanced by a longer residence time in the deep waters. Baxter *et al.* (1979) also estimated the long term average composition of the Clyde Sea water to have originated 92% from the Irish Sea, 7% from the Atlantic, with the remaining 1% being fresh water.

A seasonal time series of archive data, compiled at a station in the Arran Deep indicates a summer thermal stratification of ~6 °C, and a winter thermal inversion of ~1 °C (Figure 2.2). The springtime warming of the bottom waters lags the surface by 3 months, and continues to do so until the thermal inversion is created in the autumn. The available data do not show any obvious seasonality in the salinity.

2.4 CIRCULATION IN THE CLYDE SEA.

A total of 6 CTD surveys have been made of the Clyde Sea and Lower Loch Fyne (Edwards *et al.*, 1986; Mitchelson-Jacob *et al.*, 1989; Simpson & Rippeth 1993). These show that within the Clyde Sea horizontal gradients are weak (Figure 2.3). The most saline, densest water is observed in the Arran Deep, and generally appears to be associated with inflows from the North Channel. Horizontal uniformity within the basin becomes particularly apparent in the summer months, when the thermocline is strong and wind mixing is weak (Edwards *et al.*, 1986; Simpson & Rippeth 1993).

Figure 2.3 also shows the existence of a front over the Great Plateau, which divides the stratified

Clyde Sea from the tidally well mixed North Channel. This front is often visible on satellite sea surface temperature images. It is primarily a surface phenomena, with weaker horizontal gradients near the bed (Craig, 1959; Dooley, 1979; Edwards *et al.*, 1986; Mitchelson-Jacob *et al.*, 1989; Simpson & Rippeth 1993). Winter and summer distributions of surface temperature and salinity indicate that, at the surface, it is predominantly a haline phenomenon (Figure 2.4). Stratification in the Clyde leads to greater seasonal extremes of surface temperature than in the North Channel; the surface waters are significantly warmer in the summer months and cooler in the winter. Run-off is high in the winter due to high precipitation, and in the spring from melt water (Poodle, 1986). Edwards *et al.* (1986) suggest that the increase in freshwater input in the winter, results in the observed 10 km southward advancement of the front (Edwards *et al.*, 1986; Mitchelson-Jacob *et al.*, 1989; Elliott *et al.*, 1991).

Craig (1959) noted a general clock-wise surface circulation about Arran of some 7 cms^{-1}. Surface drift bottles experiments during a prevailing southerly wind, identified a northerly drift up the Kilbrannan Sound, with a southerly return flow along the Arran Deep (Barnes & Goodley, 1961). A deeper flow opposing this circulation, was inferred by assuming that water flows along isopycnal surfaces, which descend anti-clockwise about the Isle of Arran in February and May 1985 (Figure 2.5). Thus, the deep water in the Kilbrannan Sound arrives from the North. The Davaar Sill, with a depth of only 25 m, is an effective obstacle to inflow, at least in the spring when the density contrast between the bottom and the Plateau diminishes.

MacKay & Halcrow (1976), in a nutrient survey, found surface transport to be dominated by local wind stress and horizontal density gradients, resulting in extremely variable patches of water. Dooley (1979) found that the weak horizontal density gradients ($\sim 2 \times 10^{-5}$ $kgm^{-3}m^{-1}$) within the basin were in approximate geostrophic balance, and suggested that they were a result of wind forcing and fresh water input.

Simpson and Rippeth (1993) observed a complete break down in stratification in November 1990. They argued that this was a due to the combined effects of wind mixing and convective cooling. As the strong wind stirring diminished the horizontal gradients began to relax under gravity, re-stratifying the Kilbrannan Sound waters within two days. The observed 1°C drop in water column temperature over a three day period represented a cooling rate of greater than 1 kWm^{-2}. This intense cooling perpetuates the convective process, thus prolonging the mixed state (Rippeth & Simpson, 1996). Following this event, the bottom water intrusions, together with high freshwater inflow in the winter months, serve to re-establish the density gradient, and thus restrict the depth to which wind may mix the water column (Edwards *et al.*, 1986).

The rotation of the Earth will effect the exchange flows over the sill, since the width of the sill

is several times larger than the internal Rossby radius. In addition, the sill has its maximum depth towards the eastern extreme of the sill. A compilation of many years of archive observations of wintertime data shows that the bottom salinity is enhanced towards the Ayrshire coast, indicating that inflow occurs predominantly towards the east (Figure 2.6). Barnes & Goodley (1961) also observed a considerable amount of rotatory flow over the Great Plateau, indicating the complexity of the dynamics.

It is possible to infer the speed and spatial extent of the inflows from moorings observations, deployed between 4 - 18 November 1973 at stations 111 (near CS6, Figure 3.1), station 112 (near AD2) and 110 (near AD6) (Dooley, 1979). Central in the Firth at 111 (at 77 m) the deep water flows showed little directional coherence, while towards the Ayrshire coast, the flows at 112 and 110 were persistently to the north and had amplitudes 10 - 20 cms^{-1} at 63 m and 40 m respectively, and ~10 cms^{-1} at 27 m and 17 m respectively. This indicates that rotation restricts the inflow to at least the eastern half of the Firth, and can have an amplitude of >10 cms^{-1}, which would take less than a week to reach CS8 (Figure 3.1).

2.5 THE NORTH CHANNEL OF THE IRISH SEA.

The Clyde Sea is connected to the North Channel, which is the Irish Sea's northern connection with the Atlantic. Tidal currents in the North Channel are large, reaching a maximum of over 2 ms^{-1} southwest of Kintyre (Ellet & Edwards 1983), and the consequent mixing ensures that stratification is low. Edwards *et al.* (1986) argue that the transverse horizontal gradients will also be weak, since the tidal excursion is similar to the width of the North Channel, implying the existence of eddies of this length scale.

Radiocaesium concentrations, released at the Windscale nuclear fuel reprocessing plant in Cumbria, U.K., act as an excellent tracer of residual flows in the northern Irish Sea. Observations during 1970 to 1978 indicate a northward residual flow of ~0.06 Sv (1 Sv = 1 x 10^6 m^3s^{-1}), equivalent to a mean flow of 0.02 ms^{-1}, with considerable variability over the observation period (Jefferies *et al.*, 1982). Current velocity observations by Brown & Gmitrowicz (1995) show that the along channel flow is controlled largely by the large scale wind field, both as a consequence of the generation of an along-channel pressure gradient and direct wind forcing. At times of low wind, a northward residual was observed, which possibly indicates a tidal residual. However, a 2-dimensional depth integrated model indicates that there is little tidal residual (Prandle, 1984). Brown & Gmitrowicz (1995) estimate a mean northwards transport of about 0.12 Sv, which includes a persistent southward flow in the east of 0.04 Sv. A November section off Kintyre, shows bottom salinity to be enhanced near the Irish coast, an indicator of

Atlantic Inflow (Harker, 1994). This across channel variability is approximately consistent with the density differential between the Irish Sea and the Malin Shelf.

ADCP profile observations off The Rhins of Galloway, at a depth of 140 m, between July 1993 and October 1994, show a surface southward residual of ~0.03 ms^{-1}, with a weaker northward bottom flow of ~0.02 ms^{-1} (Howarth *et al.*, 1995). Coincident OSCR measurements show that the mean surface flows are highly spatially variable, with the ADCP located where a residual surface eddy is moving water southward. Temporal variation in the bottom flows indicate fluctuations on the timescale of months. In particular, during November to January 1994, the northwards bottom flow is enhanced to about 0.04 ms^{-1} (Howarth, personnel communication).

2.6 MODELLING STUDIES.

2-dimensional modelling studies have been undertaken by Townsend & Collar (1986) to investigate storm surges and by Elliott *et al.* (1992) to determine the tidal currents. The latter study was verified against ADCP and RCM data in the region. Figure 2.7 shows co-range, co-tidal, and tidal ellipses of the M_2 tide in the model domain. The tidal current amplitude decreases dramatically at the sill, tidal velocities within the Clyde Sea are generally less than 0.1 ms^{-1}, while to the southwestern tip of Kintyre peninsula, they exceed 2.5 ms^{-1}.

Simpson and Rippeth (1993) have tested the balance between the basic stratifying and stirring processes in the Clyde Sea in a one dimensional filling box model. The model parameterises the mixing energy associated with winds, the tide, and gravitational inflow, and incorporates the stratifying influences of surface heating, freshwater input and saline inflow. The model assumes that the Clyde Sea is horizontally uniform, and that the exchange flow with the North Channel is proportional to the density difference across the sill. The model did not reproduce the observed summer time warming of the bottom waters, which led the authors to infer the existence of an additional bottom mixing mechanism. The mechanism, first proposed by Stigebrandt (1976), involved internal waves generated by tidal flows at the sill, which bring about mixing when they break at the side walls. The contributions of different sources of mechanical stirring in the model are shown in Figure 2.8. Rippeth & Simpson (1996) ran the model for the period 1985-1991, during which limited archive data was available. In order to reproduce the observed bottom warming, an internal wave mixing efficiency, $\epsilon = 0.18$ was required, 3 times greater than the value estimated from the study of a large number of Norwegian fjords (Stigebrandt & Aure, 1989), and approaching the theoretical maximum of 20 % (Ivey & Nokes, 1989).

The new mooring and CTD data presented in this thesis constitutes the first comprehensive

oceanographic survey of the seasonal cycle in the Clyde Sea. A selection of the new mooring data has been presented in Rippeth, Midgley & Simpson (1995), along with a model run over the same period, using the parameters from Rippeth & Simpson (1996). For the first time, it was possible to compare the model output with an observed time series. The results indicate that the physical processes governing the seasonal cycle in the Clyde Sea were incompletely represented in the model. This will be discussed in detail later in this thesis.

2.7 SUMMARY.

The generally stratified waters of the Clyde Sea are separated from the tidally well mixed water of the North Channel by a front over the sill. In the summer, thermal stratification becomes sufficiently strong to isolate the deep water in the basin beneath the thermocline. Deep water renewal commences in the autumn, and continues through to the springtime, when the inflowing waters become too warm, and hence buoyant, to penetrate to the bottom. Mixing within the Clyde Sea is dominated by the wind, which peaks in the winter months, but mixing associated with internal tides may play an important role in the summer months.

To further our understanding of the dynamics in the Clyde Sea, the next stage is to make continuous observations of the vertical structure over an entire seasonal cycle. These observations could then be compared with the results from the 1-dimensional filling-box model of Simpson & Rippeth (1993). As discussed in Chapter 1, Rippeth (1993) identified two main areas of uncertainty, related to the importance of internal tide mixing in the region, and the dynamics of cross sill exchange. The new observations should be made in such a way that the amplitude of the internal tide and its seasonal variation may be identified. A full 3-dimensional model is required to investigate the nature of the cross-sill exchange, since flows are expected to be influenced by the Earth's rotation. It would then be necessary to verify these results with new observations in the sill region.

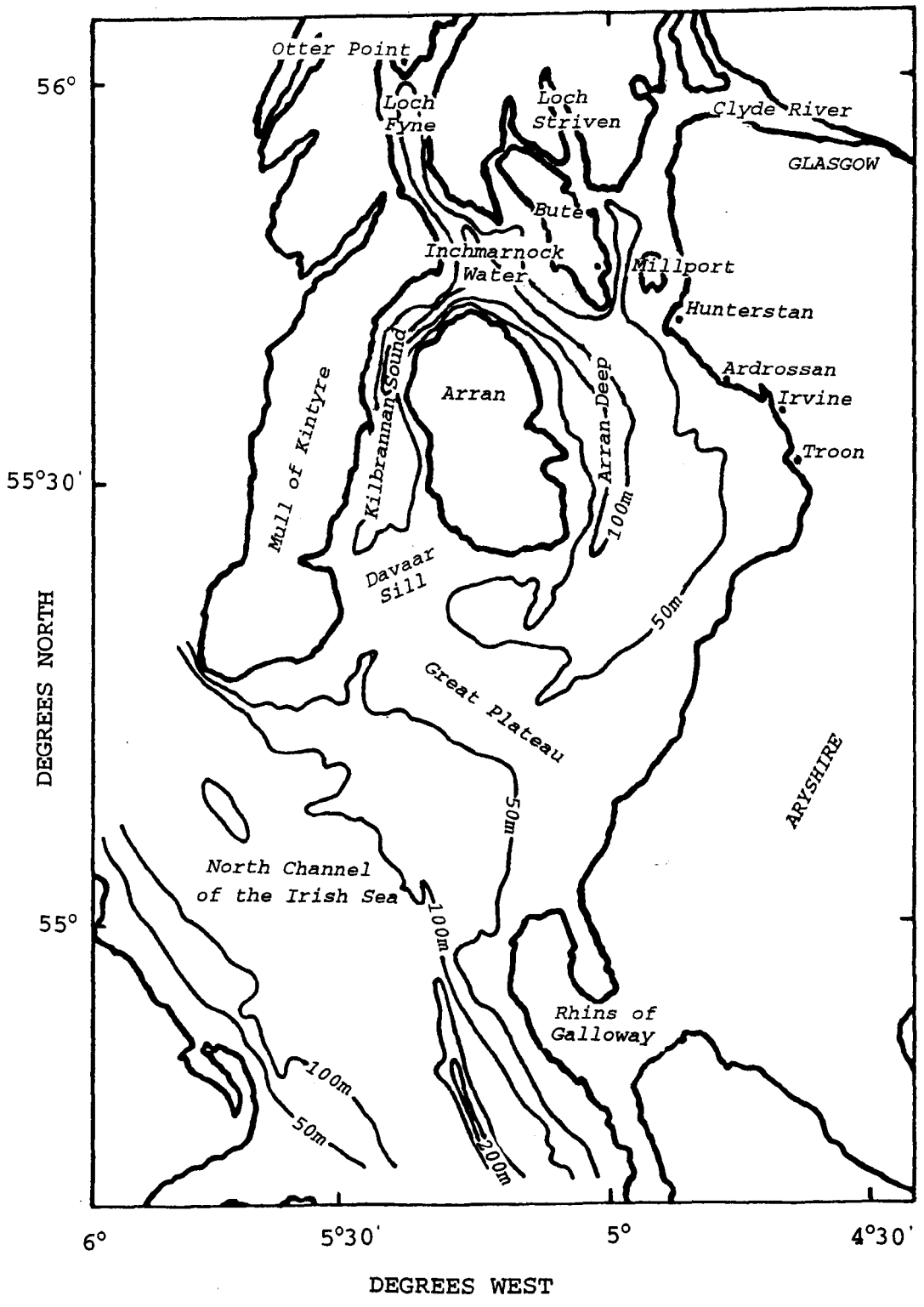

Figure 2.1. A map of the Clyde Sea region, showing the bathymetry.

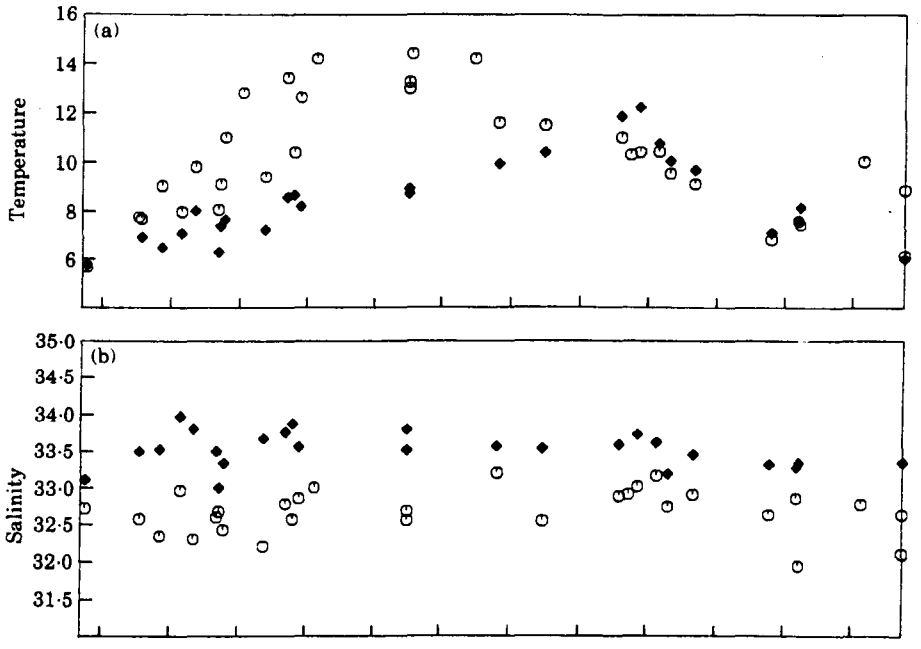

Figure 2.2. Seasonal timeseries for a station in the Arran Deep based on composites of all available data from different years. (a) temperature; (b) salinity. ◆, near bed; ○, near surface values. (Reproduced from Simpson & Rippeth, 1993).

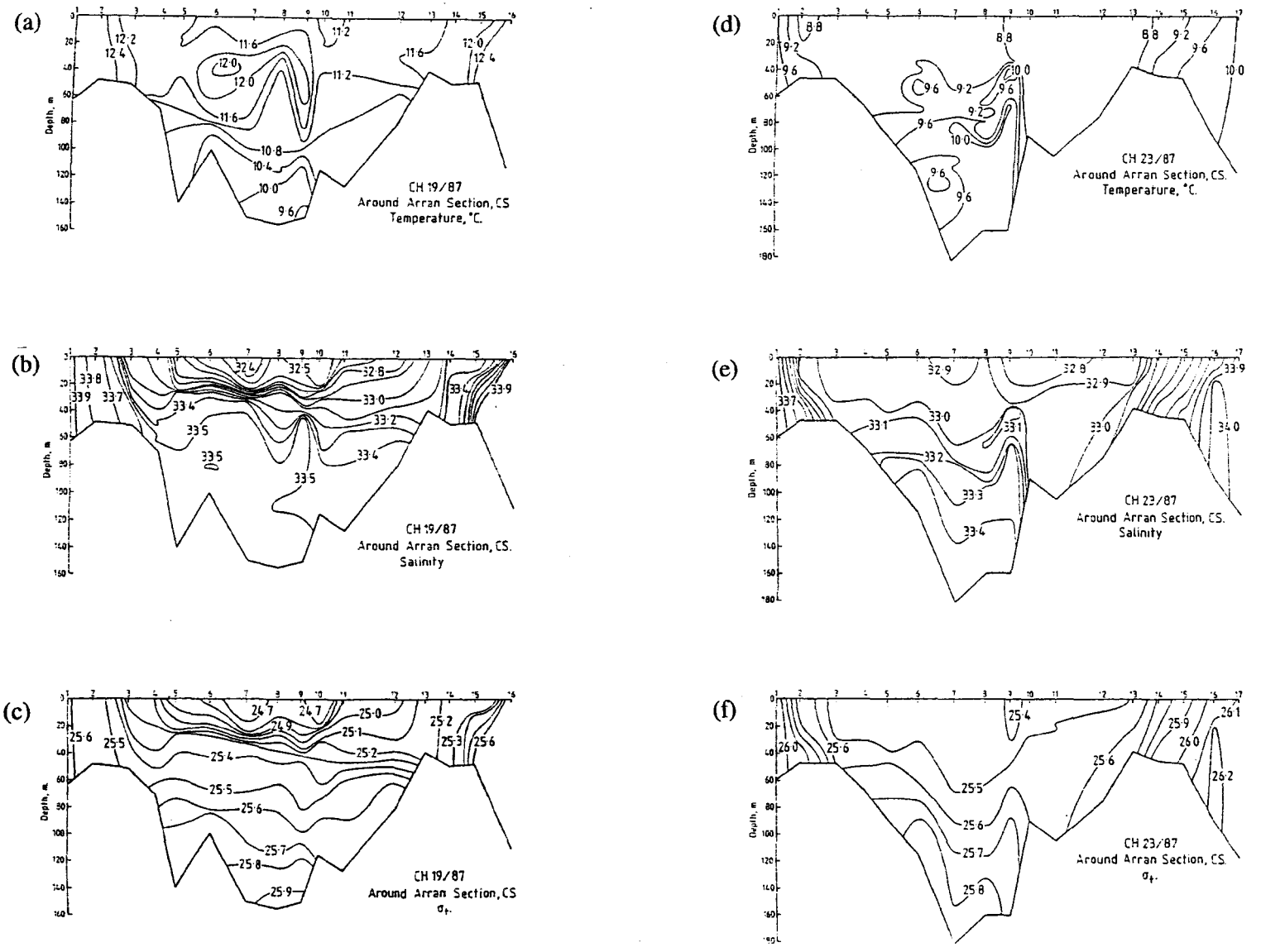

Figure 2.3. Temperature, salinity and σ_t on a section from the North Channel, anti-clockwise around Arran. Numbers indicate positions of CTD stations. (a)-(c) 12/13 October *1987*, (d)-(f) *18 December 1987*. (Reproduced from Michelson-Jacob *et al.*, 1989).

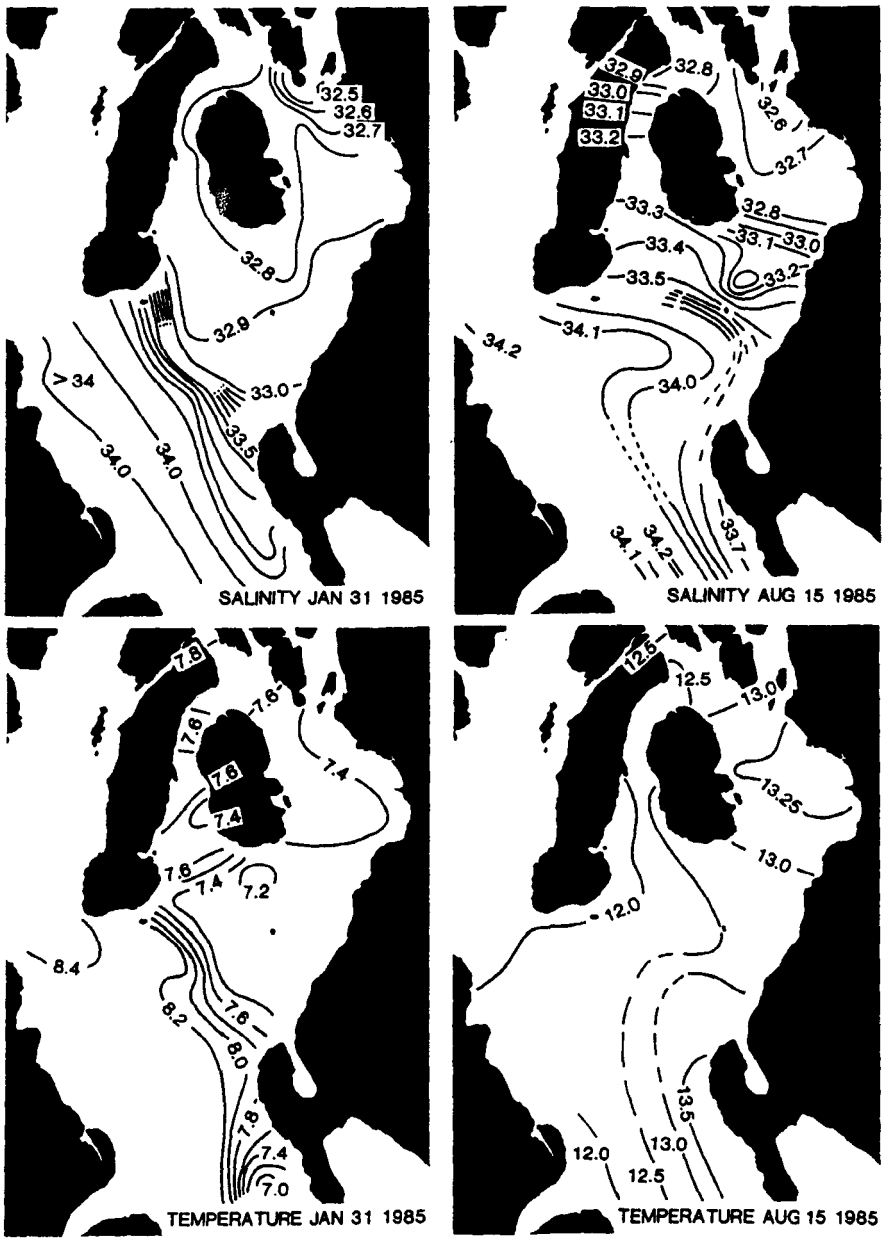

Figure 2.4. Winter and summer distributions of surface temperature and salinity. Note the depression of salinity in the Firth of Clyde and off the Rhins of Galloway during February, May and August, 1995. (Reproduced from Edwards *et al.*, 1986).

Figure 2.5. The depth and temperature of isopycnal surfaces over the Great Plateau. (Reproduced from Edwards *et al.*, 1986).

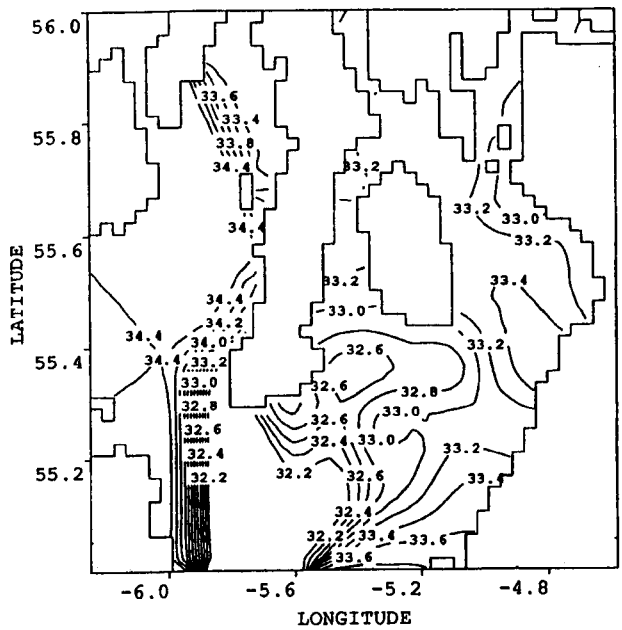

Figure 2.6. Bottom salinity during winter (December-February), based on 225 salinity and 535 temperature archive measurements. (Reproduced from Elliot *et al.*, 1991).

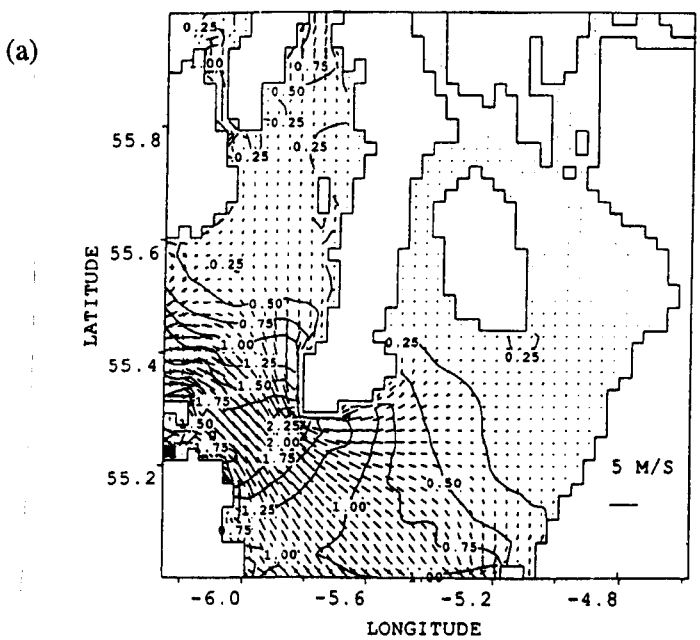

Figure 2.7. Results from a depth averaged model of the Clyde Sea for the M_2 tidal harmonic; a) tidal ellipses; b) co-range; and c) co-tidal plots. (Reproduced from Elliot *et al.*, 1992).

(b)

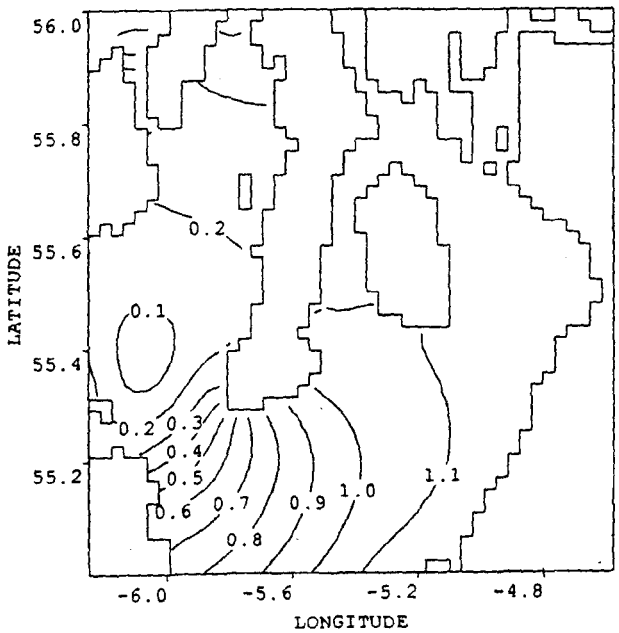

(c)

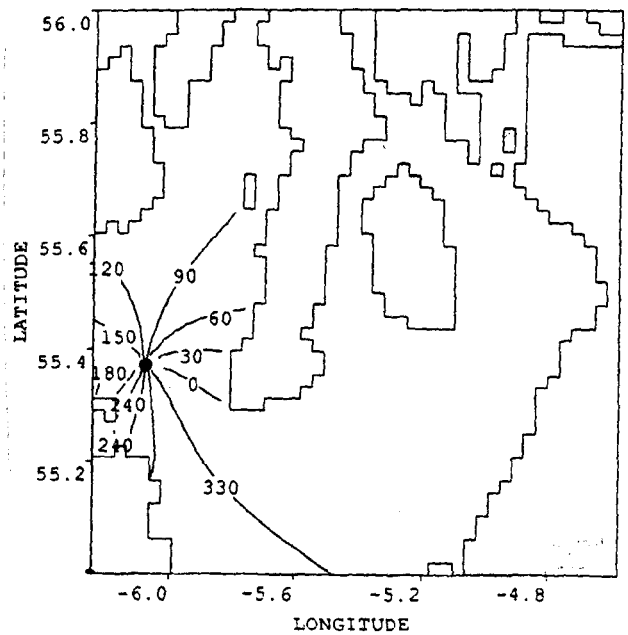

Figure 2.7. Continued.

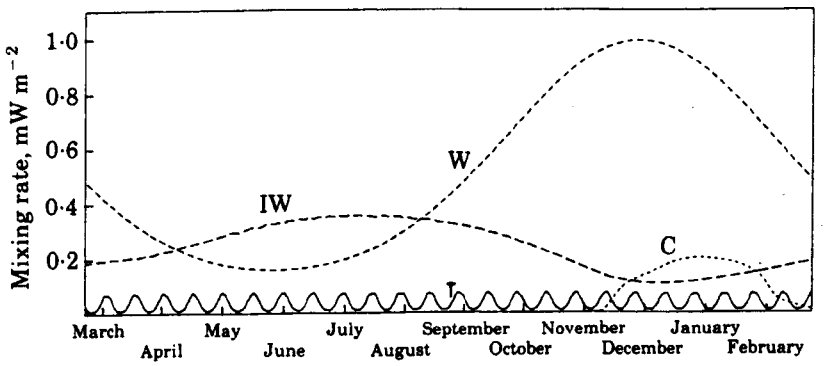

Figure 2.8. Estimates of the contribution to mechanical stirring from different energy sources, over the seasonal cycle: T, tidal mixing; W, wind mixing; C, convection inflow mixing; IW, internal tide mixing. (Reproduced from Simpson & Rippeth, 1993).

CHAPTER 3. OBSERVATIONS AND INSTRUMENTATION.

3.1 INTRODUCTION.

The initial aim of the observational programme was to make a continuous set of observations of the vertical structure in the Clyde Sea over the seasonal cycle. To this end, two moorings fitted with arrays of recording current meters (RCMs) were deployed in deep water in the Firth of Clyde. Spatial CTD (conductivity, temperature, depth) surveys of the Clyde Sea and North Channel were taken at intervals of approximately one month, to put the mooring data into a spatial context. In total there were nineteen cruises between 17 March 1993 and 13 May 1994, utilising the vessels *R.R.S. Challenger*, *R.V. Prince Madog* and *R.V. Calanus*, the choice of vessel being essentially one of availability and convenience. The cruise dates and vessel used are shown in Table 3.1.

Two further cruises were taken to make observations of the density and flow structure in the sill region, using profiling and undulating CTDs, shipborne ADCP, and 2 Argos drifters. These cruises were each of two week duration and took place in March and September 1995.

3.2 OBSERVATIONAL STRATEGY AND DEPLOYMENT DETAILS.

3.2.1 OBSERVATIONS OVER THE SEASONAL CYCLE.

Two moorings were deployed in the Firth of Clyde, in the deep water, with the aim of obtaining a continual and duplicated set of observations over the seasonal cycle. The planned deployment period was 27/3/1993 - 11/5/1994, longer than a full seasonal cycle. The moorings were deployed at stations named MCS6 (80 m deep, 55° 33.4'N, 04° 55.7'W) and MCS8 (170 m deep, 55° 44.3'N, 05° 11.6'W) (Figure 3.1).

The moorings were of a standard U-shaped design (Figure 3.2). An array of 4 Aanderra RCMs measuring temperature, salinity and current velocity, were mounted on an instrument chain, with a fifth mounted on the surface marker buoy in order to record near surface measurements of temperature and salinity. The depths at which the RCMs were deployed is shown in Table 3.2, along with the name assigned to each RCM position. These names will be used consistently throughout this thesis. The RCMs were initially set to sample at 10 minute intervals. This was increased to 20 minutes on the November cruise as a precaution against bad weather conditions delaying the winter cruises. The specific instruments used are shown in Table 3.3.

MCS6		MCS8	
RCM Name	Depth (m)	RCM Name	Depth (m)
60	surface	80	surface
61	17	81	15
62	23	82	37
63	63	83	119
64	79	84	165

Table 3.2. *Name and depth of RCMs deployed on each mooring.*

The monthly servicing of the moorings was necessary to download the data and service the instruments, but meant that the moorings were out of the water for about 24 hours. As a result, the 409 day deployment was separated into 10 deployments intervals. Other lacunae occurred as a result of instrument failure. Also, data was lost as a result of a delay in the deployment of MCS6 due to problems over its position. Towards the end of the period, MCS6 was damaged by a ship colliding with the mooring, which resulted in the loss of several instruments. Consequently MCS6 was only fully deployed between 9/6/1993 - 26/3/1994. Overall, the RCM data return was good, being ~80% of the maximum possible (Figure 3.3).

A total of twelve, approximately monthly, CTD surveys were made during the fourteen month observation period. Each survey consisted of a core set of stations (CS1-17, Figure 3.1) which provided 2 transect lines across the Great Plateau, through the Kilbrannan Sound and the Firth of Clyde, as far north as Lower Loch Fyne. Additional stations were occupied when ship time and weather conditions permitted. Good coverage was achieved throughout the seasonal cycle, with the exception of early winter (November and December) when the planned cruise had to be cancelled due to bad weather conditions. The stations sampled are shown in Table 3.4 and correspond to those used in previous studies.

3.2.2 OBSERVATIONS IN THE SILL REGION.

Two cruises were undertaken to observe the density and current structure in the region of the Great Plateau between 13/3/1995 - 23/3/1995 and 11/9/1995 - 21/9/1995, on the *R.V. Prince Madog*. These periods were selected on the basis of available data, as being times of high and low cross-sill exchange respectively.

The shipborne ADCP on the R.V. Prince Madog was used in these experiments. Manufactured

by R.D. Instruments, it operates at 300 kHz. It was set to record ensemble averages in 2 m depth bins, the first of which was centred at a depth of 6.6 m. No data is returned from the bottom 15% of the water column due to side lobe interference of the return signal. In bottom tracking mode, the ADCP measures the apparent velocity of the sea floor and vectorially subtracts it from the measured velocity. Thus the water velocity is measured relative to the sea floor. For the above settings, the short term error, inherent to the individual velocity profiles deduced from the return signal is ~0.9 cms^{-1}. There is also a bias error of 0.5-1.0 cms^{-1}. (R.D.I., 1989).

The observational strategy was to make measurements on a transect along the sill (stations A-F) with a profiling CTD and shipborne ADCP. These transects were made between 10:40 18/3/1995 - 07:20 20/3/1995 and 04:15 12/9/1995 - 06:50 14/9/1995, in both cases coinciding with the spring tide. The transect was repeated 6 times over a 48 hour period. Deliberate delays in the start of some transects were included to avoid aliasing of the data with the semi-diurnal tide, so as to allow the calculation of a non-tidal residual. At each station, the ship remained stationary for a period of 15 minutes, while recording an ADCP measurement. This method of sampling minimised the correction for the ship's movement, a procedure considered necessary since the residual velocities were expected to be of the order of a few cms^{-1}, which is not much greater than the resolution of the ADCP. On the transect taken during the September cruise, station A1 was added to the end of the transect. This additional station did not affect the timing of the experiment.

During both cruises, CTD profiles were also taken in the North Channel, and in the deep water within the basin. This provided observations of the boundary conditions for the exchange flows, and enabled comparison of the new observations with the earlier observations.

Additional observations were made during each cruise. On the March cruise, the transect experiment showed that the bottom salinity at stations D and F were close to the North Channel value, indicating inflow, and were thus chosen for a higher temporal resolution survey. These stations were observed alternately (approximately every 45 minutes), using profiling CTD and shipborne ADCP in a similar manner to the transect. These observations were repeated between 18:45 21/3/1995 and 08:30 23/3/1995, to give a temporarily coherent data set over 3 semidiurnal tidal cycles.

On the September cruise, observations were made on a cross-sill transect between stations CS1 and CS5, a distance of 38 km, using the SEAROVER undulating CTD in conjunction with shipborne ADCP. Six passes of the transect were made during a 24 hour period, near the spring tide, allowing the removal of the tidal signal. ARGOS drifters 3945 and 3947 were deployed on 12/9/1995; at 55^0 20.0' N 5^0 12.0' W at 05:15 and at 55^0 18.0' N 5^0 12.0' W (station C) at 04:55

respectively. They were allowed to free drift over the entire September cruise, and were recovered on 20/9/1995. The Argos drifters consisted of a 7 m long drogue, suspended from a surface buoy, so that the centre of the drogue was at a depth of 23 m. The position of the drifter was tracked by the Argos Global Positioning Centre in Toulose, France. Typically, 10-14 positions are received daily, depending upon the transit times of the NOAA satellites. With the usual 3 satellite fix, the standard deviation in the position is 150 m.

3.3 CALIBRATION.

It is important that any systematic differences between instruments are minimised, particularly when deriving spatial variability from both moored and shipborne instruments. The CTD temperature and conductivity were calibrated against in-situ measurements taken throughout each of the cruises, using SIS RTM4002 reversing thermometers and water samples, the salinity of which was determined using a Guideline Autosal. Calibration normally involves a linear correction requiring both an additive value and a multiplicative factor. However, applying this method the final calibrations proved to be sensitive to the removal of individual measurements. A simpler method of calibration was devised in which the temperature was corrected by an additive factor, ΔT_{CTD}, derived from the mean difference between the CTD and the calibration values, and the conductivity was corrected using a multiplication factor, f_{CTD}, derived from the mean ratio of the conductivity of the CTD to the calibration values.

For cruises using the same CTD hardware, the student t-test indicated that there were no systematic differences between the calibrations. On some cruises, however, the sample number was too low to be statistically significant. Therefore, for each instrument and CTD combination, ensemble mean calibration factors were calculated using all available data, and applied to each of the data sets. The values of the coefficients and resultant standard error, $\sigma/(\sqrt{N-1})$, where σ is the standard deviation and N the number of samples, are show in Table 3.5. In all cases the standard errors in the calibration factor were equivalent to less than 0.005 °C and 0.01 psu, for temperature and salinity respectively.

The calibration of the RCMs was more problematic. Immediately before a mooring was deployed, and on occasions, immediately following recovery, the RCMs were mounted onto a specially made frame which was attached below the CTD frame. This was lowered into well mixed water, and left for sufficient time to record between 3-5 calibration readings. Additional calibration points were obtained from CTD dips taken shortly after the mooring was deployed, and prior to recovery. In order to reduce standard errors from the calibration, when possible, the individual instrument at each position on the mooring remained unchanged. Calibration of RCM

speed and direction was not possible as the relevant facilities were not available, though the compasses had previously been calibrated at Research Vessel Services, Barry.

In the same way as for the calibration of the CTD, discrepancies between temperature measured by the RCM and the CTD were best represented by a simple difference, ΔT. Changes in the conductivity cell arise from small changes in cell geometry, which are best corrected using a form factor, *ff*, a ratio of the conductivity, measured by the CTD to that measured by the RCM (Aanderraa, 1992).

The calibration factors were derived separately for each of the mooring deployments using the measurements taken in the calibration frame. However with the application of this calibration, there were some significant departures from the in-situ CTD calibration. This resulted from the combination of several factors:

i) In all cases, too few calibrations were available for the result to be statistically significant.

ii) The range of T and S calibrated did not cover the range over which the observations were made. In order to not risk instrument loss, the calibration was usually made near the surface, and consequently the calibration of temperature and salinity was restricted to near surface values. Thus the deeper the RCMs were deployed, the less accurate is the calibration.

iii) The calibrations were usually taken consecutively in the same water mass and consequently were similar.

iv) Time constraints or conditions did not always allow the calibration to be made in homogeneous water, and a compromise had to be made with calibration in weakly stratified water.

v) The CTD was often not lowered to the depth of the bottom RCM, which resulted in no in-situ calibration for the bottom RCM.

In many cases no systematic differences between successive calibrations were apparent, and variation was well within the level of uncertainty. At these times, the calibrations were grouped together. This reduced the uncertainty in the RCM calibration coefficients by increasing the sample size. At other times, when the changes were statistically apparent, new calibration coefficients were applied. The calibration coefficients are shown in Table 3.6. The absolute accuracy of the temperature and salinity observations are estimated to be ~0.1 °C and ~0.1 psu respectively. However, the relative accuracy, between consecutive deployments is about half this value.

3.4 PRELIMINARY PROCESSING.

Once the temperature and conductivity were calibrated, the salinity and sigma-t were calculated using the Practical Salinity Scales and the International Equation of State, respectively (UNESCO, 1981). The CTD and RCM data was de-spiked and converted to hourly values with a block average. It is this hourly data which is presented in later chapters. A magnetic correction of 8° to compass direction, appropriate for the Clyde region, was applied. The principal axes were defined as being N-S at MCS6 and 320° at MCS8, which is roughly along the channel.

In the later discussion, the data is usually referred its Julian Day, which is defined here to begin on 1/1/1993, and continue into 1994. Thus the deployment period of MCS8 is days 86 - 495. For readers unfamiliar with this system, on some diagrams the solar equanox and solstice are marked.

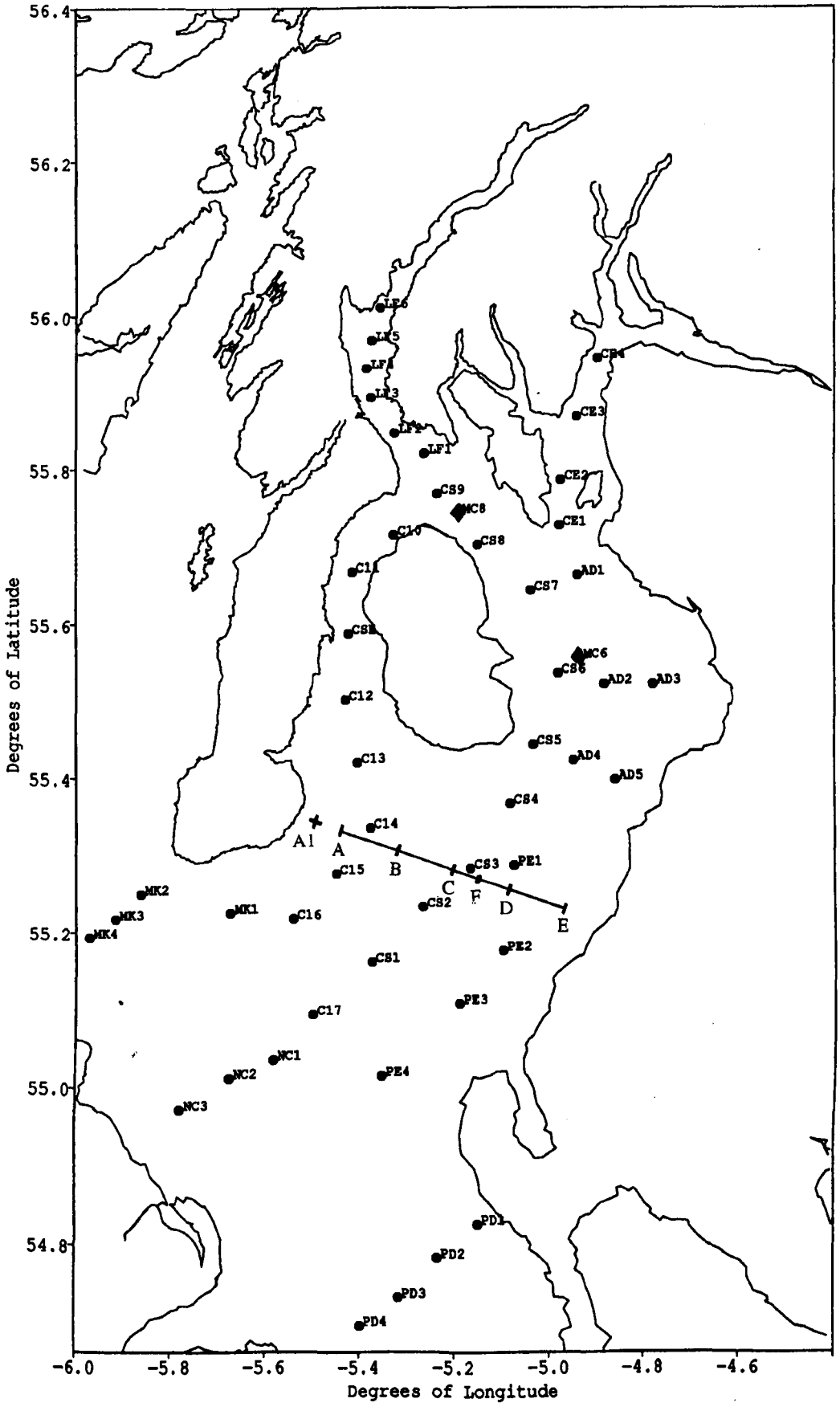

Figure 3.1. A map of the Clyde Sea region, showing the positions of CTD stations (•), the stations used in the sill survey (†), and the moorings (✦).

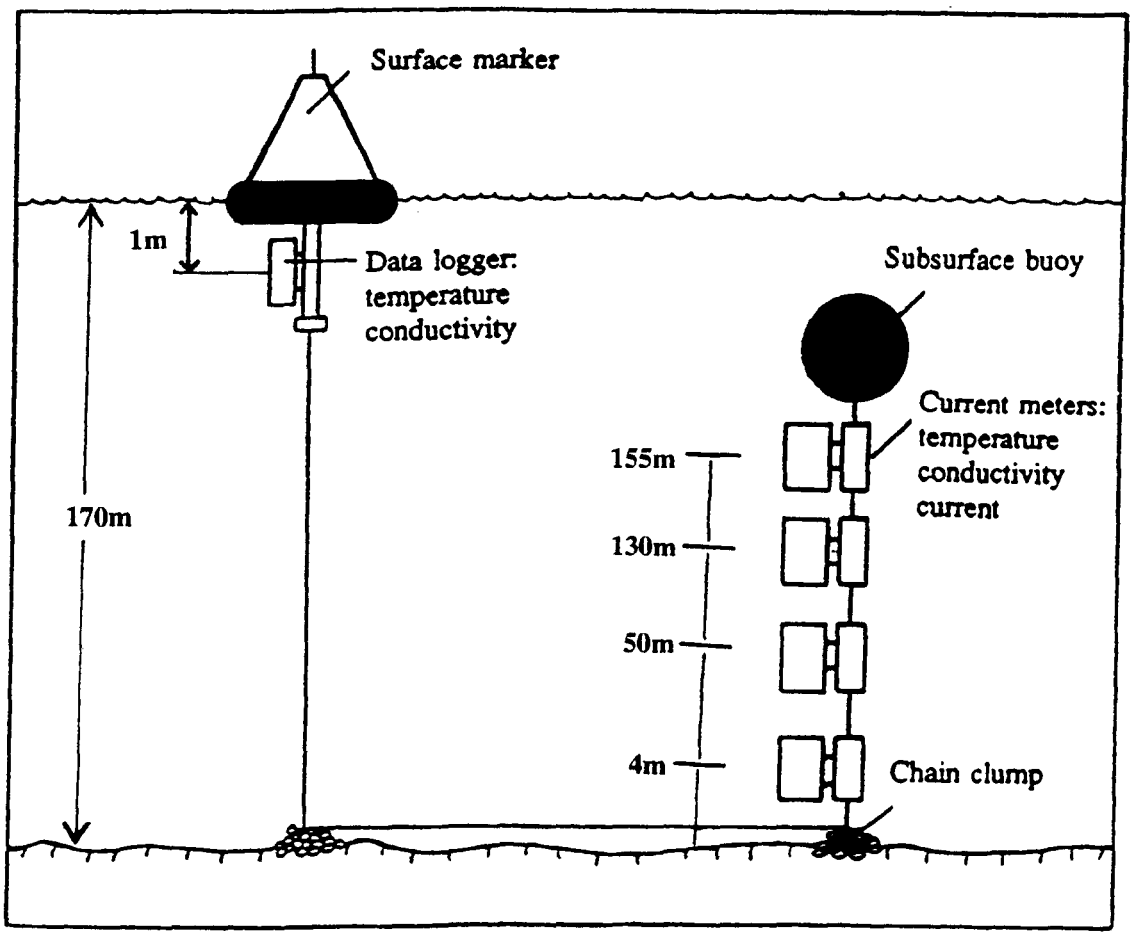

Figure 3.2. Design of u-shaped mooring at station MCS8.

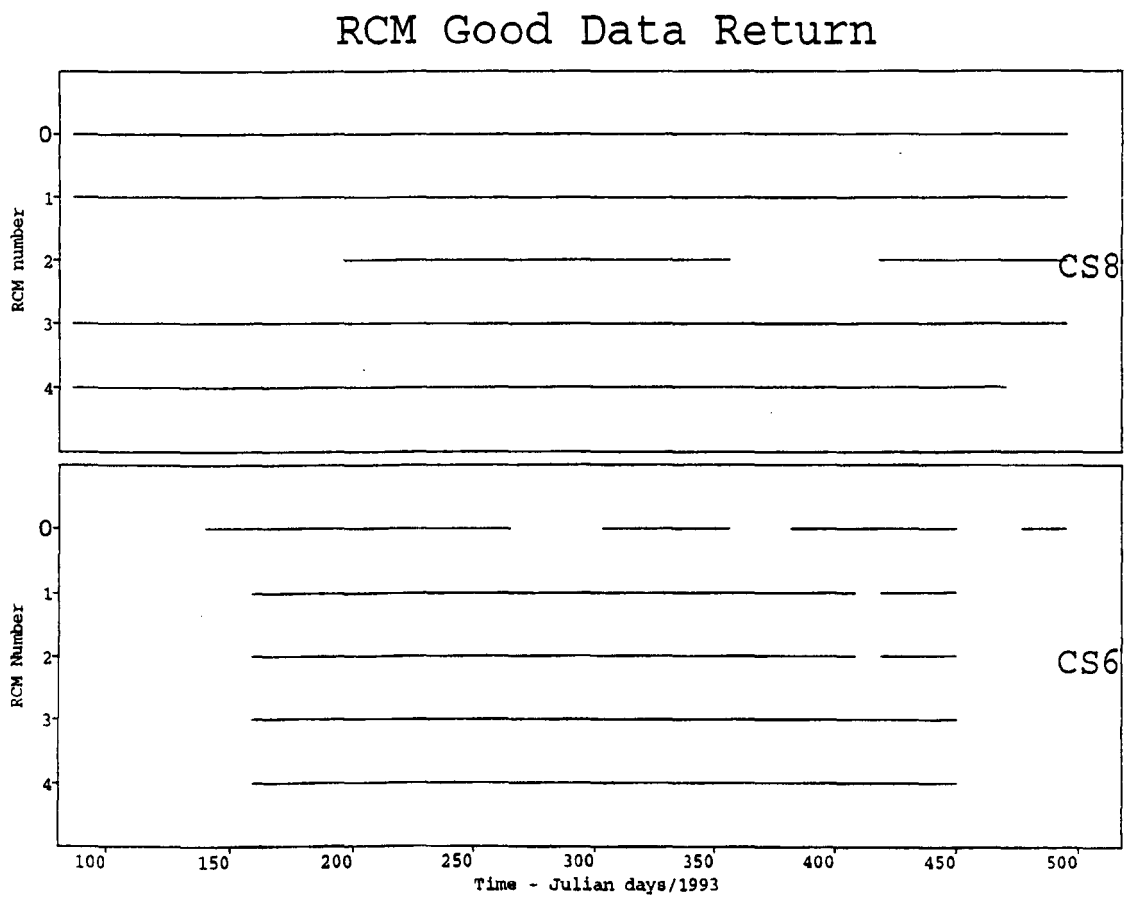

Figure 3.3. Good data return from the mooring sites; a) MCS6; b) MCS8. 0: surface RCM; 1-4: upper to lower RCMs deployed on the anchor chain.

Dates in Clyde Sea	Vessel and Cruise Number	Purpose of Cruise
17-18 March 1993	Challenger C10193	CTD Survey
23-24 March 1993	Challenger C10293	Mooring Service
4-7 May 1993	Prince Madog	CTD Survey Mooring Service
21-23 May 1993	Challenger C10393	CTD Survey
7-10 June 1993	Prince Madog	CTD Survey Mooring Service
12-16 July 1993	Prince Madog	CTD Survey Mooring Service
16-26 August 1993	Calanus	CTD Survey Mooring Service
14-15 September 1993	Challenger C10593	CTD Survey
20-22 September 1993	Calanus	Mooring Service
25-27 October 1993	Calanus CA0593	CTD Survey
29-31 October 1993	Challenger C10793	Mooring Service
16-20 January 1993	Calanus CA0194	CTD Survey Mooring Service
14-17 February 1994	Calanus CA0294	CTD Survey
21-24 February 1994	Prince Madog	Mooring Service
10-12 March 1994	Challenger C11094	CTD Survey
25-28 March 1994	Calanus CA0394	Mooring Service
11-13 April 1994	Calanus CA0494	CTD Survey
25-29 April 1994	Prince Madog	Side-Scan Survey Only
9-13 May 1994	Prince Madog	Mooring Service

Table 3.1. Cruise dates and vessel used.

(a)

JULIAN DATE OF DEPLOYMENT 1993/4	RCM POSITION NUMBER ON MCS6				
	60	61	62	63	64
NEW LOCATION	NONE	NONE	NONE	NONE	NONE
159.54-195.30	6750	6152	8240	8247	8249
195.58-228.43	6750	10666	11165	8240	9069
229.44-263.61	6750	10666	11165	8240	9069
264.46-302.65	6750	11184	11185	11188	9069
303.36-380.44	6750	11184	11185	11188	9069
382.46-418.31	6750	11184	11185	11188	9069
419.49-449.43	6750	11184	11188	11185	9069
450-LOST	LOST	LOST	LOST	LOST	LOST

(b)

JULIAN DATE OF DEPLOYMENT 1993/4	RCM POSITION NUMBER ON MCS8				
	80	81	82	83	84
86.49-125.24	3295	3321	9580	8248	9415
125.50-158.32	3295	3321	9580	8248	9415
158.48-195.68	3295	3321	9580	8248	9415
196.38-229.53	3295	3321	10525	8248	9415
230.45-264.54	3295	3321	10525	8248	9415
264.77-303.43	3295	11186	11183	8248	10525
303.71-380.44	3295	11186	11183	8248	10525
381.76-418.47	3295	11186	11183	8248	10525
420.67-450.54	3295	11186	11183	8248	10525
451.42-495.31	3295	11186	11183	8248	10525

Table 3.3. Mooring deployment times and instrument used for (a) MCS6 and (b) MCS8.

\ DATE \ STATION	23 3 93	4 5 93	21 5 93	7 6 93	12 7 93	16 8 93	14 9 93	25 10 93	29 10 93	16 1 94	14 2 94	10 3 94	11 4 94	11 5 94
MCS6				*	*	*	*		*	*	*	*		*
MCS8	*	*		*	*	*	*		*	*	*	*		*
CS1		*	*	*	*	*	*	*			*	*	*	
CS2		*	*	*	*	*	*	*			*	*	*	
CS3		*	*	*	*	*	*	*	*		*	*	*	
CS4		*	*	*	*	*	*	*	*	*	*	*	*	
CS5		*	*	*	*	*	*	*	*	*	*	*	*	
CS6		*	*	*	*	*	*	*		*	*	*	*	
CS7		*	*	*	*	*	*	*	*	*	*	*	*	
CS8		*	*	*		*	*	*	*	*	*	*	*	
CS9		*	*	*		*	*	*	*	*	*	*	*	
CS10		*	*	*	*	*	*	*	*	*	*	*	*	
CS11		*	*	*		*	*	*	*	*	*	*	*	
CSE			*	*	*	*	*	*	*	*		*	*	
CS12		*	*	*		*	*	*	*	*	*	*	*	
CS13			*	*		*		*	*	*		*	*	
CS14		*	*	*		*		*		*	*	*	*	
CS15		*	*	*	*	*	*	*	*	*	*	*	*	
CS16		*		*	*	*		*	*		*	*	*	
CS17				*	*	*								
MK1		*		*	*	*			*					
MK2		*		*	*				*					
MK3		*		*					*					
MK4		*		*			*		*					
CE1		*		*		*								
CE2		*	*	*		*	*	*			*		*	

continued on next page.

CE3		*		*										
CE4		*		*										
LF1		*		*		*								
LF2			*	*		*	*	*		*	*	*	*	
LF3		*	*	*		*		*		*	*	*	*	
LF4						*		*						
LF5		*		*				*						
AD1		*		*		*		*	*		*	*	*	
AD2		*	*	*	*	*		*	*		*	*	*	
AD3		*		*	*	*			*					
AD4		*	*	*	*	*	*	*	*		*	*	*	
AD5		*	*	*	*	*	*	*	*		*	*	*	
PE1		*												
PE2		*		*										
PE3		*		*										
PE4		*			*									
NC1		*		*										
NC2		*												
NC3		*												
GP1					*									
GP4				*					*					
GP5				*					*					

Table 3.4. Table of CTD stations visited. Date given is within 24 hours.

DATES IN THE CLYDE SEA	CTD CALIBRATION	
	Conductivity Ratio and resultant uncertainty (psu)	Temperature Difference (°C) and resultant uncertainty (°C)
23-24 March 1993	.99402 S +.1846 *	1.000912 T +.0084 *
4-7 May 1993	1.000506 ±.003	-.10018 ±.001
7-10 June 1993	1.000506 ±.003	-.10018 ±.001
12-16 July 1993	1.000506 ±.003	-.10018 ±.001
16-26 August 1993	.9999395 ±.009	.0222 ±.003
20-22 September 1993	.9999395 ±.009	.0222 ±.003
29-31 October 1993	1.001787 ±.004	-.005274 ±.001
16-20 January 1993	.9999395 ±.009	.0222 ±.003
21-24 February 1994	1.008945 ±.01	.0068 ±.005
25-28 March 1994	.9999395 ±.009	.0222 ±.003
9-13 May 1994	1.008945 ±.01	.0068 ±.005

Table 3.5. The CTD calibrations. The errors shown are the estimated uncertainty in salinity (psu) and in temperature (°C) resulting from the CTD calibration. The exception is the calibration made on the Challenger C10193 cruise (*) where the both the intersept and ratio are given for both temperature and salinity, with no estimate of the resultant uncertainty.

JULIAN DAY 1993/4 OF DEPLOYMENT	ΔT / ff	60	61	62	63	64
159-195	ΔT	-0.13	1.44	-0.043	2.78	
	ff	1.0028	1.0566	1.0050	1.031	
195-228	ΔT	-0.13	0.012	-0.60	-0.074	-0.08
	ff	1.0028	0.99298	0.99418	1.0050	1.003
229-263	ΔT	-0.13	0.012	-0.017	-0.013	-0.08
	ff	1.0028	0.99298	0.99418	1.0050	1.003
264-302	ΔT	-0.13	0.17	0.165	0.15	-0.08
	ff	1.0028	1.000	0.9997	0.998	1.003
303-380	ΔT	-0.13	0.17	0.165	0.14	-0.08
	ff	1.0008	1.001	0.9997	0.998	1.003
382-418	ΔT	-0.095	0.087	0.084	0.057	-0.016
	ff	1.0008	1.001	0.9997	0.998	1.0022
419-449	ΔT	-0.095	0.052	0.054	0.042	0.0
	ff	1.0008	1.001	0.99915	0.99975	1.0022

Table 3.6a. Calibrations for MCS6. Temperature difference ΔT in °C.

JULIAN DAY 1993/4 OF DEPLOYMENT	ΔT / ff	80	81	82	83	84
86-125	ΔT	0.063	-0.32	0.01	0.1	0.04
	ff	1.0016	1.0012	N/A	0.9945	1.00246
125-128	ΔT	0.063	-0.32	0.01	0.135	0.04
	ff	1.0016	1.0012	N/A	0.9956	1.00246
158-195	ΔT	0.063	0.01	0.01	-0.069	0.04
	ff	1.0016	1.0012	N/A	0.992	1.00246
196-229	ΔT	0.063	0.01	0.10	0.058	-0.041
	ff	1.0016	1.0012	0.998	0.992	1.00246
230-264	ΔT	0.063	-0.042	0.126	0.058	-0.041
	ff	1.0016	1.0012	0.998	0.992	1.00246
264-303	ΔT	0.063	0.155	0.153	0.058	0.046
	ff	1.0016	0.998	0.9975	0.993	0.998
303-380	ΔT	0.063	0.155	0.153	0.1	0.046
	ff	0.9942	0.998	0.9975	0.994	0.998
381-418	ΔT	0.152	0.050	0.057	0.150	0.046
	ff	0.991	N/A	0.9975	0.9941	0.998
420-450	ΔT	0.152	0.050	0.057	0.150	0.046
	ff	0.991	N/A	0.9985	0.997	0.9985
451-495	ΔT	0.201	0.071	0.057	0.006	0.046
	ff	0.9984	N/A	1.00308	1.0006	0.999

Table 3.6b. Calibrations for MSC8. Temperature difference ΔT in °C.

CHAPTER 4. DATA ANALYSIS AND THEORY.

4.1 INTRODUCTION.

In this chapter some of the methods of analysis used in later chapters are discussed, along with the relevant associated theory. Standard mathematical techniques, such as the use of filters, correlations and cubic splines are applied in many parts of this work, and detailed mathematical descriptions will not be given.

4.2 FILTERING.

Unless otherwise specified, ninth order *Butterworth filters* were used. Butterworth filters sacrifice rolloff steepness for evenness of gradient in the pass- and stop bands, which was generally considered of greater importance.

4.3 HARMONIC TIDAL ANALYSIS.

The harmonic method of tidal analysis is based on the idea that the time variation of a scalar parameter Z(t), observed at a single location, may be interpreted as the linear combination of a number of waves. The frequencies of these waves are determined from the astronomical arguments, which are well known (Godin, 1972). $Z_{tidal}(t)$ is an estimate of the parameter Z(t), fitted to N such waves:

$$Z_{tidal}(t_i) = Z_0 + \sum_{n=1}^{N} H_n f_n \cos[\sigma_n t_i - g_n + (V_n + u_n)] \qquad (4.1)$$

where the amplitude and phase of the n^{th} constituents, $\{H_n, g_n\}$, and the mean, Z_0, are to be determined. The parameters f_n and u_n are the nodal adjustments to the amplitude and phase respectively, which are known, and σ_n and V_n are the tidal frequency and equilibrium phase angle for each of the constituent waves (Pugh, 1987).

Estimates of Z_0 and the set of $\{H_n, g_n\}$ may be made by fitting Equation 4.1 to the observations, in a least squares sense. The unknown parameters are selected so that the sum of the square of the errors of residuals, χ^2, is minimised. Given a set of M observations, χ^2 is given by:

$$\chi^2 = \sum_{i=1}^{M} [Z(t_i) - Z_{tidal}(t_i)]^2 \qquad (4.2)$$

The character of the data set defines the number of tidal constituents, N, it is possible to identify. If two frequencies are to be distinguished it is generally accepted that the *Rayleigh Criterion* be satisfied. This requires, that the signal length be greater than $1/\Delta f$, where Δf is the frequency difference between the two oscillations.

In order to observe the seasonal variation in tidal amplitudes in the RCM data (Section 5.4), the period chosen for harmonic analysis should be a small fraction of a year. In coastal seas, oscillations at the M_2 and the S_2 frequencies are expected to dominate the tidal record, and a period of 15 days is necessary to differentiate the two. With the length of each deployment being $\geq$30 days, these periods were divided into two for analysis.

Observations using the shipborne ADCP, presented in Chapter 8, were taken over periods of 24 - 48 hours. This is not of sufficient length to differentiate between the M_2 and S_2 signals. As many of the observations were made near the spring tide, a mean *semi-diurnal* tide with a frequency weighted by the relative amplitudes of the M_2 and S_2 was used (Amin, 1982; Elliott *et al.*, 1991), and had a period of 12.3 hours. On occasions a *quarter-diurnal* tide was calculated, the period assumed to be half of that of the semi-diurnal tide.

4.4 HARMONIC ANALYSIS OF THE TIDAL ELLIPSE.

For a vector signal such as current, it is advantageous to identify the rotary components of the tidal signal. For example, Souza & Simpson (1995) used rotary component analysis to elucidate changes in the tidal regime of the Rhine ROFI system. From the amplitude and phase of the U- and V- components, at a specific frequency, the clockwise and anti-clockwise rotatory components can be calculated (Godin, 1974, p147):

$$
\begin{aligned}
Q_c &= \frac{1}{2}\left\{u^2+v^2-2uv\sin(g_v-g_u)\right\}^{\frac{1}{2}} \\
Q_{ac} &= \frac{1}{2}\left\{u^2+v^2+2uv\sin(g_v-g_u)\right\}^{\frac{1}{2}} \\
g_c &= \arctan\left\{\frac{v\cos g_v+u\sin g_u}{u\cos g_u-v\sin g_v}\right\} \\
g_{ac} &= \arctan\left\{\frac{v\cos g_v-u\sin g_u}{u\cos g_u+v\sin g_v}\right\}
\end{aligned}
\tag{4.3}
$$

where Q_c, Q_{ac}, g_c and g_{ac} are the amplitudes and phases of the clockwise and anticlockwise rotary components respectively. These rotary components are then used to determine the tidal ellipse properties:

$$
\begin{aligned}
m &= Q_{ac}-Q_c \\
M &= Q_{ac}+Q_c \\
\psi &= \frac{g_{ac}+g_c}{2} \\
\phi &= \frac{g_{ac}-g_c}{2} \\
\epsilon &= \frac{m}{M}
\end{aligned}
\tag{4.4}
$$

where M is the semi-major axis, m is the semi-minor axis, ψ is the orientation (positive anti-clockwise from the east), and ϕ the phase angle of the semi-major axis. The ellipticity, ϵ, is defined as the ratio of the semi-minor to the semi-major axis. ϵ is equal to zero when the ellipse becomes degenerate, $|\epsilon|=1$ when the ellipse is a circle, and the sign gives the sense of rotation (i.e. positive anti-clockwise and negative clockwise).

Bottom friction will tend to reduce both clockwise and anti-clockwise components of current. However, in the Northern Hemisphere, the characteristic boundary layer thickness is greater for clockwise than for anti-clockwise rotation. Thus, within the bottom boundary layer, there is a general tendency for the current ellipse to become more clockwise with increasing distance from the seabed. This gradient is enhanced if the water is stably stratified, since the vertical transfer of momentum is inhibited. Above the pycnocline, the ellipticity acquires its 'free-stream' value, which is a function of local conditions such as topography and density gradient. This phenomena is relevant to the analysis in Section 8.3.

4.5 SPECTRAL ANALYSIS.

Spectral analysis seeks to describe the frequency content of a regularly sampled record. Unlike tidal analysis, it assumes no prior knowledge of the frequencies. The record, x(t), consists of N discrete observations, sampled at intervals of Δt. The n^{th} constituent, $x_n(t)=x(n\Delta t)$. The transform of the record, X(f), is related to x(t) by the Discrete Fourier Transform (e.g. Lynn & Fuerst, 1990).

$$X_k(f) = \frac{1}{\sqrt{N}} \sum_{n=1}^{N} x_n(t)\, e^{\left\{\frac{-i2\pi kn}{N}\right\}} \tag{4.5}$$

where the k^{th} constituent of the transform, $X_k(f)=X(k\Delta f)$, $\Delta f=1/T$ is the discrete frequency band, and T is the length of the original record. The power spectral density is then estimated by:

$$P_k(f) = \frac{X_k(f)\, X_k^*(f)}{N} \tag{4.6}$$

where * indicates the complex conjugate. This is the basic method of estimating the power spectral density, and is known as the *periodogram*. The problem with the periodogram estimate is that the variance is large and does not decrease with record length. The *Welch method* (e.g. Kay, 1988) is one way of reducing the variance at the loss of resolution. The record is divided into number of overlapping sections, the periodograms of each of these sections then being averaged. However, due to the overlap, these sections are statistically dependent, which again results in an increase in the variance. This problem is overcome by applying a non-rectangular data window to the sections prior to computing the periodogram. The analysis is not sensitive to the choice of window, and in the work presented here, a Kaiser N-point window, with a β parameter of 5 was chosen. Overlap rates of half the section length are found to significantly decrease the variance estimate.

Parseval's Relation states that the integral of the power spectrum density is a measure of the total energy in the signal. The fraction of energy in each frequency band is simply the sum of the periodogram over that band, divided by the total energy in the periodogram. In Section 6.2, the sample period of the RCM data, L, was typically 37 days, giving a frequency resolution (1/L) of better than 0.03 day^{-1}, but for consistency, the energy spectra was integrated into frequency bands of 0.1 day^{-1}.

4.6 INTERNAL WAVE MODAL THEORY.

A linear internal wave may be interpreted as the sum of a series of vertical modes. This is a commonly used technique in the study of internal waves in the open ocean (e.g. Baines, 1982). For normal mode theory to be retained in the case of a sloping bed, the ray characteristics (the direction along which the energy propagates) must be steeper than the bottom slope (Le Blond & Mysak, 1978). This is generally not satisfied in the vicinity of sills, where topographic gradients are large. However, reasonable success in describing internal tides in fjords has been made using modal theory in fjord Skjomen (Cushman-Roisin & Svendsen, 1983), Knight Inlet (Webb & Pond, 1986; Marsden & Greenwood, 1994), and Upper Loch Linnhe (Allen, 1995).

The method consists of two parts. Firstly, the derivation of the theoretical profile of the internal tide currents from observed density profile. Secondly, the calculation of the amplitude and phase lag of the internal tide by fitting the theoretical profile to the observed complex profile of the harmonic amplitude and phase. Detailed accounts of normal mode theory and the derivation of the linear internal wave equation may be found in many standard physical oceanographic textbooks (e.g. Phillips, 1977; Le Blond & Mysak, 1978; Gill 1982).

By assuming separable solutions of the linear hydrostatic equations of motion under the Boussinesq approximation, it can be shown that internal waves can be interpreted as the sum of a series of horizontally propagating modes, which are eigensolutions of the equation:

$$\frac{\partial^2 \bar{w}(z)}{\partial z^2} + \left\{\frac{N^2-\omega^2}{\omega^2-f^2}\right\} k^2 \bar{w}(z) = 0 \qquad (4.7)$$

$$\textit{where vertical velocity} \quad w(x,z,t) = \bar{w}(z) e^{i(kx-\omega t)}, \quad i = \sqrt{-1}$$

k is the horizontal wavenumber, N is the Brunt-Väisälä frequency, $N^2=-(g/\rho)\partial\rho/\partial z$, f is the Coriolis parameter, and ω is the frequency of the wave. Equation 4.7 is constrained by the boundary conditions w(z)=0 at the upper and lower boundaries.

For a given latitude, the structure of the modes are dependent only upon N, which is calculated from the CTD profile at the mooring sites. Modes characterised by the lowest wavenumbers tend to occur preferentially. In a study of internal waves formed on the Malin Shelf, 77% of the energy was found to be concentrated in mode 1 (Sherwin, 1988). The shapes of the first two vertical modes, for observed profiles of N in the Clyde Sea, were computed iteratively using a space-centred numerical scheme. The horizontal current modes are then calculated from continuity from the relation:

$$\bar{u}(z) = \frac{1}{k}\frac{\partial \bar{w}(z)}{\partial z} \tag{4.8}$$

The eigenfunctions are often referred to as *normal modes*. The modes are normal in the sense that for a given frequency and stratification, any two modes are orthogonal to each other, i.e.:

$$\int_{-H}^{0} \tilde{u}_n(z)\tilde{u}_m(z)\,dz = 0 \quad \text{if } m \neq n \tag{4.9}$$

where H is the depth of the water column. The normal modes prescribe the theoretical vertical structure of the velocity components; they do not provide any information on the absolute magnitude of the internal tidal currents. To estimate the actual magnitude of the velocity components for each mode, the theoretical profile must be fitted to the observed profile of harmonic amplitudes and phases.

The total energy in an internal wave is divided between kinetic and potential forms. The ratio of potential energy (PE) to kinetic energy (KE) for low frequency waves ($N^2 >> \omega^2$), is given by (e.g. Gill, 1977, p255):

$$PE = \frac{\omega^2 - f^2}{\omega^2 + f^2} KE \tag{4.10}$$

In the analysis in Section 6.3, only the M_2 frequency will be considered. Thus $\omega = 1.405 \times 10^{-4}$ s^{-1}, and using $f = 1.200 \times 10^{-4}$ s^{-1}, gives a ratio PE = 0.156 KE.

4.7 ANALYSIS OF STRATIFICATION.

A convenient measure of vertical stratification is the potential energy anomaly, ϕ, which is the energy required to vertically mix the water column. It is defined as (e.g. Simpson 1981):

$$\phi = \frac{1}{H}\int_{-H}^{0} (\bar{\rho} - \rho) g z\,dz, \qquad \bar{\rho} = \frac{1}{H}\int_{-H}^{0} \rho\,dz \tag{4.11}$$

where H is the depth of the water column, and $g = 9.81$ ms^{-2}. This is appropriate for CTD data, but the mooring data has observations only at discrete depths. If the RCMs are given subscripts i=0-4 descending the water column (Table 3.2), with ρ_i being the density at each RCM and d_i its depth, then ϕ may be defined in discrete form:

$$\phi = \frac{g}{12}\sum_{i=1}^{4}\left\{\frac{3}{H}(2\bar{\rho}-\rho_i-\rho_{i-1})(d_i^2-d_{i-1}^2) + 2(d_i-d_{i-1})(\rho_i-\rho_{i-1})\right\}$$

$$\text{where} \quad \bar{\rho} = \frac{1}{2H}\sum_{i=1}^{4}(\rho_i+\rho_{i-1})(d_i-d_{i-1}) \tag{4.12}$$

The second term in Equation 4.12 represents the energy required to vertically mix each of the individual layers, while the first term is the energy required to mix these four homogeneous layers throughout the entire water column. If data was not available at RCMs 1 or 3, the summation was made over layers 0-2 or 2-4 respectively, which led to only a small increase in the uncertainty in ϕ, since the pycnocline was generally near the depth of RCM 2.

Both salinity and temperature play an important role in the seasonal stratification in the Clyde Sea, and it is useful to observe their effects independently. The sigma-t difference, $(\Delta\sigma_t)_T$, which results from the temperature, T, differing from a reference temperature T_o, may be estimated from the reduced equation of state:

$$(\Delta\sigma_t)_T \simeq \alpha(T-T_0) \tag{4.13}$$

where α is the coefficient of thermal expansion of sea water, which at 33.0 psu, and over a range of temperatures observed in the Clyde Sea, 6-13 °C, varies approximately linearly (Gill, 1982), such that:

$$\alpha \simeq (0.596+0.1022T)\,x\,10^{-4} \tag{4.14}$$

where T is the local temperature (°C). Fluctuations in salinity between 32-34.0 psu lead to a 2% uncertainty in α. The variation in density was calculated relative to the well mixed water column at MCS8 on day 323, where temperature T_0=10.30°C, salinity S_0=33.00 psu, and sigma-t σ_0=25.34 kgm^{-3}. The remainder of the density variation is assumed to result from variation in salinity.

5 THE SEASONAL CYCLE IN THE CLYDE SEA.

5.1 INTRODUCTION.

In this chapter, the new observations from both the mooring sites and the CTD surveys, taken over the period 27/3/1993 - 11/5/1994, are presented. The new data are used to describe the seasonal cycle of stratification and circulation, and to investigate the rate and timing of cross-sill exchange. Internal oscillations are discussed separately in Chapter 6.

5.2 WIND AND FRESHWATER RUN-OFF.

The estimated total river run-off into the Clyde Sea was derived from the combined gauged outflow of 12 rivers, and enhanced by a factor of 1.67 to account for ungauged sources (Poodle 1986). The mean run-off over the observation period was 310 m^3s^{-1}, with a strong seasonal variation of ±200 m^3s^{-1} (Figure 5.1a). The run-off was marginally greater than the 1975-94 average of 280 m^3s^{-1}.

The wind speed observed at Machrihanish over the observation period was 6.5 ms^{-1} with a root mean square of 4 ms^{-1}, and a strong seasonal signal (Figure 5.1b). It should be noted that winds over the Clyde Sea are often gusty in nature, a phenomena which enhances the mixing, which is related to the cube of the wind speed.

5.3 STRATIFICATION AT THE MOORING SITES.

The daily averaged RCM and the CTD data from the mooring sites was compiled to give a single comprehensive set of depth-time plots of the hydrological conditions at each mooring (Figure 5.2). The plotting routine had a similar effect to passing a filter of period several days through the data. The main features are observed to be similar at both sites.

In the summer time (days 150-250), thermal stratification was strong (Figure 5.2). At MCS8 the vertical temperature difference over the water column peaked at ~6 °C, equivalent to a stratification of ~0.8 kgm^{-3} (Figure 5.3). During this period the potential energy anomaly, ϕ, (as calculated from Equation 4.12) indicated consistently greater stratification at MCS8 than MCS6 with typical values of ~150 Jm^{-3} and 100 Jm^{-3} respectively (Figure 5.4).

Between days ~250-310, the surface waters cooled, while the temperature of the bottom waters

continued to rise. This period was characterised by a decrease in ϕ, with the exception of near day 280, when the combined effects of high freshwater inflows and low winds resulted in an increase in the surface stratification (Figures 5.1, 5.2). Over the following months (days ~310-420), the entire water column cooled at a fairly uniform rate, from ~11 °C in the early autumn, to the winter minimum of ~6 °C. During this period, the surface waters were persistently ~1 °C cooler than those at the bottom, which amounted to a thermal instability of ~0.15 kgm^{-3}.

During the period of thermal inversion (days ~310-420), freshwater run-off increased the surface stratification at MCS8, except following severe wind events, such as the storm on day 323 which mixed the water column to a depth >120 m (Figures 5.1, 5.2, 5.4). However, over this period, the water column at MCS6 was persistently mixed to a depth of about 60 m, and on a number of occasions became fully mixed. The only significant stratification resulted from the saline inflow at the bottom. Since the stratification was low, so too was the internal Rossby radius, which dropped from its average value of ~4 km at MCS6, to ~2 km. Consequently, much of the fresh water entering the Firth of Clyde may have been constrained sufficiently close to the Arran coast to not be detected at MCS6.

In the month following both days 90 and 410 (i.e. day 45, 1994), the deep water salinity rose by ~0.4 psu at MCS8, indicating saline inflow (Figure 5.2). At these times, the haline stratification reached its seasonal maxima of ~1.2 kgm^{-3} (Figure 5.3). A ~0.6 psu rise was also observed at MCS6 commencing at about day 430. In all cases the salinity continued to rise for about a month, indicating the time span for the inflow event. ϕ reached its seasonal maximum of ~170 Jm^{-3} at MCS8 near day 420, and ~120 Jm^{-3} at MCS6 near day 440. The time delay of the salinity and ϕ observations between the 2 mooring sites cannot be related to the propagation time of the inflow, since MCS6 is closer to the sill than MCS8, but may be due to the dense inflow first filling the deepest parts of the basin.

A third, weaker, episode of increasing deep water salinity was observed in the summer, around days 200-250 (Figure 5.2). At MCS6 only the bottom most RCM recorded an enhanced salinity. This saline, dense water, was presumably flowing into the deep waters to the north. At MCS8, this inflow was apparent as a salinity rise of ~0.2 psu at mid-depths, centred at ~90 m, and resulted in a distinct salinity inversion, which was compensated for by the inflow's higher temperature.

During this period of inflow, the water from the North Channel (temperature 11 - 13 °C, and salinity 33.7 - 33.8 psu) would have been neutrally buoyant in the Clyde Sea at ~40 m. To be neutrally buoyant at a greater depth, the inflow must have entrained relatively dense, cool, yet less saline water. The Clyde Sea bottom water was the only near-by water mass with these

properties. The observed inflow has a temperature and salinity equivalent to approximately a 50 : 50 mix of North Channel and Clyde Sea bottom water. Assuming that these two water masses mixed, much of this entrainment must have occurred south of station MCS6, presumably in the vicinity of the sill. However, at this stage it is not possible to identify the mechanism by which these water masses mixed.

At other times of the year vertical mixing dominates over inflow, resulting in the observed reduction in the deep water salinity. Even during these mixing dominated periods, inflow may occur, but not at a sufficient rate to increase the deep water salinity.

5.4 CURRENTS AT THE MOORING SITES.

The amplitude of the barotropic tidal current at the M_2 frequency, estimated from the seasonal average depth-mean amplitude of the along axis current, was 7.23 cms^{-1} and 3.74 cms^{-1} at MCS6 and MCS8 respectively. These figures are consistent with estimates from continuity arguments. Observations of the internal tide are discussed in Section 6.3.

The non-tidal residual currents generally exhibited a 2-layer flow at both moorings, where the along-channel velocity at the lower two RCMs were in the opposite direction to the upper two (Figure 5.5). The mean velocity difference between near-surface and near-bed flows was ~1.5 cms^{-1} and ~3.0 cms^{-1} at MCS6 and MSC8 respectively. At MCS6, periods of strong two layer flow roughly correlate with periods of strong stratification (Figure 5.2a). At times of low stratification, the surface flow may have been constrained too near the Ayrshire coast by the Earth's rotation to be visible at MCS6.

If the outflow from the Clyde Estuary flowed into a stationary and stratified Clyde Sea, it would turn to the right under the influence of the Earth's rotation, and flow into the Kilbrannan Sound, (the entrance of which is ~5 km wide, whilst the internal Rossby radius at MSC8 was typically <3 km). However, the residual surface flow at MCS8 was persistently in the opposite direction, and would carry the freshwater into the Firth. It will be discussed in Section 10.3 how these flows constituted part of a clockwise (anti-cyclonic) circulation about Arran and may be related to the front at the mouth of the Clyde.

5.5 THE CTD SPATIAL SURVEYS.

A transect, which tracks anti-clockwise about the Isle of Arran, beginning and ending in the

North Channel (Figures 3.1 & 5.6) is used in this section to display some of the CTD data. The surface temperature tended to be generally uniform over the Clyde Sea, as indicated by the parallel nature of the contours in Figure 5.7a, while the gentle turning of the contours at the extremes of the section show a phase lag of a few weeks between changes in temperature of the surface waters in the Clyde and the well mixed North Channel.

The surface salinity is rather more variable (Figure 5.7b). The high salinities observed at the ends of the section are those of the North Channel. Marked reductions in the mean surface salinity across the entire Clyde Sea occurred at the beginning and end of the time series (observed on days 126 & 467), which was not co-incident with an increase in run-off (Figure 5.1). As discussed in Section 5.3, these times follow periods of rapid saline inflow, and presumably the rising halocline inhibits wind mixing, trapping the freshwater in a thin surface layer (Figure 5.2).

The surface salinity observed in the Kilbrannan Sound was generally greater than in the Arran Deep by ~0.3 psu. The spatial variation of surface salinity on day 157 (Figure 5.8) shows the minimum to occur in the Firth, while the salinity at the mouth of the Firth is similar to that observed at the most northern part of the Kilbrannan Sound. These data are consistent with the surface water flowing clockwise about Arran, forcing the freshwater outflow from the Clyde Estuary into the Firth, and saline water from the sill region into the Kilbrannan Sound, as discussed in Sections 5.4 & 10.3.

Figure 5.7c shows the depth of the 33.2 psu isohaline, or the bottom, if the salinity was lower than this. The level of this isohaline was raised to a depth of ~50 m and ~70 m near days 130 and 440 respectively, which followed the spring periods of rapid saline inflow (Section 5.3). Between days 160-200 and around day 400 this halocline was below 100 m, indicative of periods of low inflow rate, again in agreement with the mooring data. During the period of summer inflow (days ~200-250), the level of this halocline became progressively deeper away from the sill, reaching a maximum depth of >70 m in the Kilbrannan Sound. Assuming that inflow occurs along contours of constant salinity, this suggests an anti-clockwise flow in the deep water about Arran, in agreement with the observations of Edwards *et al.* (1986). However, at other times this halocline rises in the Kilbrannan Sound, a phenomena which may be related to wind mixing, and will be discussed in Section 10.5.

A maximum in the potential energy anomaly, ϕ, occurred in the Arran Deep, in the deepest part near CS7 and CS8 (Figure 5.7d). From the start of the timeseries to day ~250, ϕ remained steady at ~140 Jm^{-3}, during which stratification changed from being thermal to haline dominated. It decreased, over the entire basin, following the onset of surface cooling near day 250, and was still <90 Jm^{-3} on day 380. By day 434 ϕ it was rising strongly, and reached ~160 Jm^{-3} on day

458, due to a combination of saline inflow and freshening of the surface waters, as discussed above.

At times of high ϕ, the value in the deep water of the Kilbrannan Sound was typically ~60 Jm^{-3} less than in the Arran Deep (Figure 5.7d). This is expected in the light of the salinity distributions of Figures 5.7b & c; the surface water in the Arran Deep was less saline and the deep water more saline than in the Kilbrannan Sound. Consequently the Kilbrannan Sound will be relatively vulnerable to mixing by the wind, the effects of which will be discussed in Section 10.5.

It was previously thought that in the winter inflow acted to cool the Clyde Sea's bottom waters (Edwards *et al.*, 1986, Simpson & Rippeth 1993). However, the basin bottom salinity dropped over the winter of 1993/4 (Figure 5.9) and was lower in December than in October 1987 (Figure 2.3). This indicates that bottom water properties are primarily governed by the effects of mixing, rather than inflow, at these times. In addition, the North Channel water is marginally warmer than the Clyde Sea bottom water during much of this period, due to its greater depth and thus heat capacity, and so cannot be responsible for cooling the basin bottom waters.

5.6 EXCHANGE.

Theoretically, inflows to the Clyde basin may occur at all times of the year, at a level at which the inflowing water is neutrally buoyant, but bottom water renewal can only occur when the water on the North Channel side of the sill is denser than the bottom water in the Clyde Sea. The properties of the sill water were estimated from CTD observations at 50 m at CS1, and interpolated using a heat budget applying wind speeds from Machrihanish and daily solar radiation from Auchincruive, near Prestwick. These were plotted alongside timeseries of the daily averaged properties of the deep water at both moorings (Figure 5.9).

The sill water became denser than the bottom water at MCS6 on day ~260, but not until day ~290 at MCS8 at 120 m, which is 40 m deeper. Following these times there were bottom salinity fluctuations of 0.2 - 0.5 psu on timescales of weeks, indicating that bottom water renewal occurred, but was episodic. The sharp rise in deep water salinity near day 410 was coincidental with the time at which the bottom waters reached their seasonal temperature minimum. Since seasonal density variations in the North Channel are dominated by temperature variations, this is also the time of seasonal maximum density, and this will be discussed later in Section 10.4. Near day 440, the North Channel water had warmed to the extent that it had become too buoyant to renew the bottom water (Figure 5.9).

A reasonable estimate of the volume of cross-sill exchange occurring between CTD surveys may be obtained by a study of the salt and mass budgets. The fresh water inflow is well known, and the salt mass of the Clyde Sea may be estimated from the CTD surveys. CTD stations CS4, CS7, CS10, MCS6, MCS8 and LF2, which were all sampled regularly, were chosen as being representative of the entire Clyde Sea. The mean salinity was taken as the average from the CTD profiles, each weighted with the general hypsographic function of the Clyde Sea (from Edwards & Sarples, 1988).

If, between any 2 CTD surveys, Q_R is the rate of freshwater inflow, Q_{in} is the rate inflow over the sill, then by conservation of volume, the rate of outflow, $Q_{out}=Q_{in}+Q_R$. The salinity balance is:

$$V\frac{\Delta S}{\Delta t} = Q_R S_R + Q_{in} S_{NC} - Q_{out} S_{out} \qquad (5.1)$$

where ΔS is the change in mean salinity over time Δt, S_{NC} and S_{out} are the mean salinities of the inflowing and outflow waters respectively, the river salinity, $S_R=0$, and the volume of the Clyde, $V \approx 1.0 \times 10^{11}$ m^3. Thus the rate of inflow is given by:

$$Q_{in} = \frac{V\frac{\Delta S}{\Delta t} + Q_R S_{out}}{S_{NC} - S_{out}} \qquad (5.2)$$

S_{out} was estimated as being equal to the average salinity of the surface 40 m observed at CS4, since the results of chapter 8 indicate that the water at this site is typical of the outflow, and it was sampled regularly. The errors in Q_{in} were estimated by varying S_{out} by ± 0.2 psu, where the uncertainty in S_{out} was estimated from data taken along the sill (Sections 8.4 & 8.5). The error should be larger/smaller than this in the winter/summer, since the spatial variability of salinity in the sill region is greater/smaller than average.

The results show maximum inflow in the spring of both 1993 and 1994, followed by periods of very low exchange, and persistently high inflow during the summer (Figure 5.10). It is important to note that the volume of inflow between surveys, during the high inflow period in spring 1994 (days 409-433), was sufficient to upwell the bottom water to above sill level. Thus a quantity of the inflow may also have flowed out between the observations. With this consideration, the spring peak inflow rate was estimated to be ~4 x 10^4 m^{3}s^{-1}. The mean rate of exchange is 1.3 x 10^4 m^{3}s^{-1}, over the observation period, or ~1.1 x 10^4 m^{3}s^{-1} over a season, equivalent to a flushing time in the Clyde Sea of 3-4 months, in agreement with estimates from surveys of radiocaesium concentration (Baxter *et al.*, 1981).

The high rates of exchange observed in the spring of 1993 and 1994 have repercussions upon the

North Channel. The volume of exchange over these periods was ~1 x 10^{11} m^3, which is roughly the volume of the Clyde Sea and about half the volume of the North Channel. Figure 5.11 shows the salinity at all stations in the North Channel which were sampled more than once over the observation period. Distinct salinity minima are observed near day 150 and after 460, which follow the episodes of strong exchange. The magnitude of the salinity drop was not inconsistent with the observed salinity in the Clyde Sea. The reduction in density associated with this salinity drop will have acted as a negative feedback upon exchange.

5.7 MIXING.

In this section the main mixing mechanisms in the Clyde Sea are evaluated, together with discussion of their seasonal variation. These are surface mixing from the wind, bottom mixing from the tidal currents, and inflow mixing. Mixing associated with the internal tide and low frequency wind driven internal seiching is considered in the next chapter.

The rate of wind mixing in the open ocean may be estimated as $\delta k_s \rho_a w^3$, where w is the wind speed at 10 m, ρ_a is the air density, the drag coefficient times the slippage factor $k_s = 6.4 \times 10^{-5}$, and the efficiency of mixing $\delta = 0.023$ (Simpson & Bowers, 1981). Over the winter months (days 320-460) wind mixing is of the order 1.0 mWm^{-2}, whilst during the summer it is typically closer to 0.1 mWm^{-2}.

Friction on the sea bed results in boundary mixing, estimated by $4/(3\pi)\epsilon k_b \rho u^3$, where the efficiency of mixing $\epsilon = 0.0037$, the bottom drag coefficient $k_b = 2.5 \times 10^{-3}$, ρ is the water density, and u is the depth averaged current (Simpson & Bowers, 1981). A tide gauge at Millport, Great Cumbrae Island shows that ~70% of the tidal energy is at semidiurnal frequencies, of which ~69% and ~18% are at the M_2 and S_2 frequencies respectively (Amin, 1982). Thus bottom mixing at springs at MCS6 is ~2.7 x 10^{-6} Wm^{-3}. This value is 2 orders of magnitude lower than the wind mixing, and can thus be considered as negligible.

North Channel water entering the Clyde Sea will descend into the basin to a level at which it is neutrally buoyant. The rate at which potential energy, P, is released, is:

$$P = \gamma \frac{Q \Delta h g (\rho_0 - \bar{\rho}(z))}{A_0} \qquad (5.3)$$

where Q is the inflow rate, Δh is the depth below the sill to which the inflow descends, ρ_0 the density of the inflowing water, $\rho(z)$ the mean density between the sill and the depth of neutral

buoyancy, g = 9.81 ms^{-1}, and the surface area $A_0 = 2.1 \times 10^9$ m^2. Gade & Edwards (1980) estimate from laboratory experiments, that the fraction of this energy available for mixing, γ, is less than 10%, while the best estimate of Stigebrandt (1985) is 5%. Using the maximum observed values in the springtime; $Q = 4 \times 10^4$ m^3, $\Delta h = 150$ m, and $\Delta\rho = 0.5$ kgm^{-3}, gives P = 0.7 mWm^{-2}, which is comparable to the wind mixing, but only occurs for a short duration. More typical values of Q and $\Delta\rho$ (Figures 5.9, 5.10) imply a value of P more than an order of magnitude smaller.

5.8 SUMMARY AND DISCUSSION.

The seasonal cycle of stratification and circulation has been observed. Strong thermal stratification occurred in the summer, resulting in a relative isolation of the bottom waters, while a thermal inversion of ~1°C was persistent throughout the winter. North Channel water inflowed intermittently throughout the season, but only between the early autumn and the early spring was it sufficiently dense to renew the bottom water. The mean rate of exchange was estimated from the salinity and mass budgets to be 1.3×10^4 m^3s^{-1}, equivalent to a flushing time of 3-4 months, which is consistent with previous estimates.

Three periods of rising deep water salinity were observed, indicating periods when the effects of inflow dominated over vertical mixing. Following day 90 in 1993, and day 50 in 1994, the inflow rate averaged ~4×10^4 m^3s^{-1} over about a month; a sufficient volume to flush the entire Clyde Sea. This exchange resulted in a reduction in the salinity of the North Channel, which would have acted as a negative feedback upon exchange. A relatively persistent inflow during the summer entered the basin at mid-depths, which cannot be explained by either cross-sill gradients, which are maximum in the late winter, or by wind forcing which was relatively weak in the summer. Fluctuations in the bottom salinity indicated that these inflows were episodic, and so were probably influenced by the wind.

The increase in exchange in the summer may be associated with the seasonal migration of the front at the mouth of the Clyde. The low freshwater run-off in the summer leads to a retreat of the front towards the basin head (Section 2.4). The front would then be closer to the sill, and saline North Channel water could inflow relatively unimpeded. This phenomena will be addressed during the 3-dimensional modelling study of Chapter 9. Since the summer inflow serves to warm the deep water (Figure 5.2), the 1-dimensional model of Simpson & Rippeth (1993) may not require the inclusion of bottom mixing associated with the breaking of the internal tide (Section 2.6). The internal tide and its potential to mix are discussed in Chapter 6, while in Chapter 7, the 1-dimensional model is developed to include the summer inflow.

The seasonal minimum in the deep water salinity occurred at the end of the winter indicating a period of strong vertical mixing. During this period, wind mixing was particularly strong. Cooling of the bottom waters in the winter cannot be attributed to inflow, as previously thought (Edwards *et al.*, 1986; Simpson & Rippeth, 1993), since this would entail a rise in bottom salinity. Consequently, a mechanism for cooling the bottom water must act within the Clyde Sea itself. It is suggested in Section 10.5 that this mechanism is associated with deep mixing by the wind in the Kilbrannan Sound.

A 2-layer flow has been observed at both mooring sites. At MCS8 the residual surface flow is southward, indicating the existence of a clockwise (anti-cyclonic) surface residual flow about the Isle of Arran. In addition, the surface salinity in the Kilbrannan Sound is persistently ~0.3 psu higher than that in the Arran Deep, which is consistent with the fresh outflow from the Clyde Estuary being blocked from entering the Kilbrannan Sound by this clockwise surface flow. This is further discussed in section 10.5.

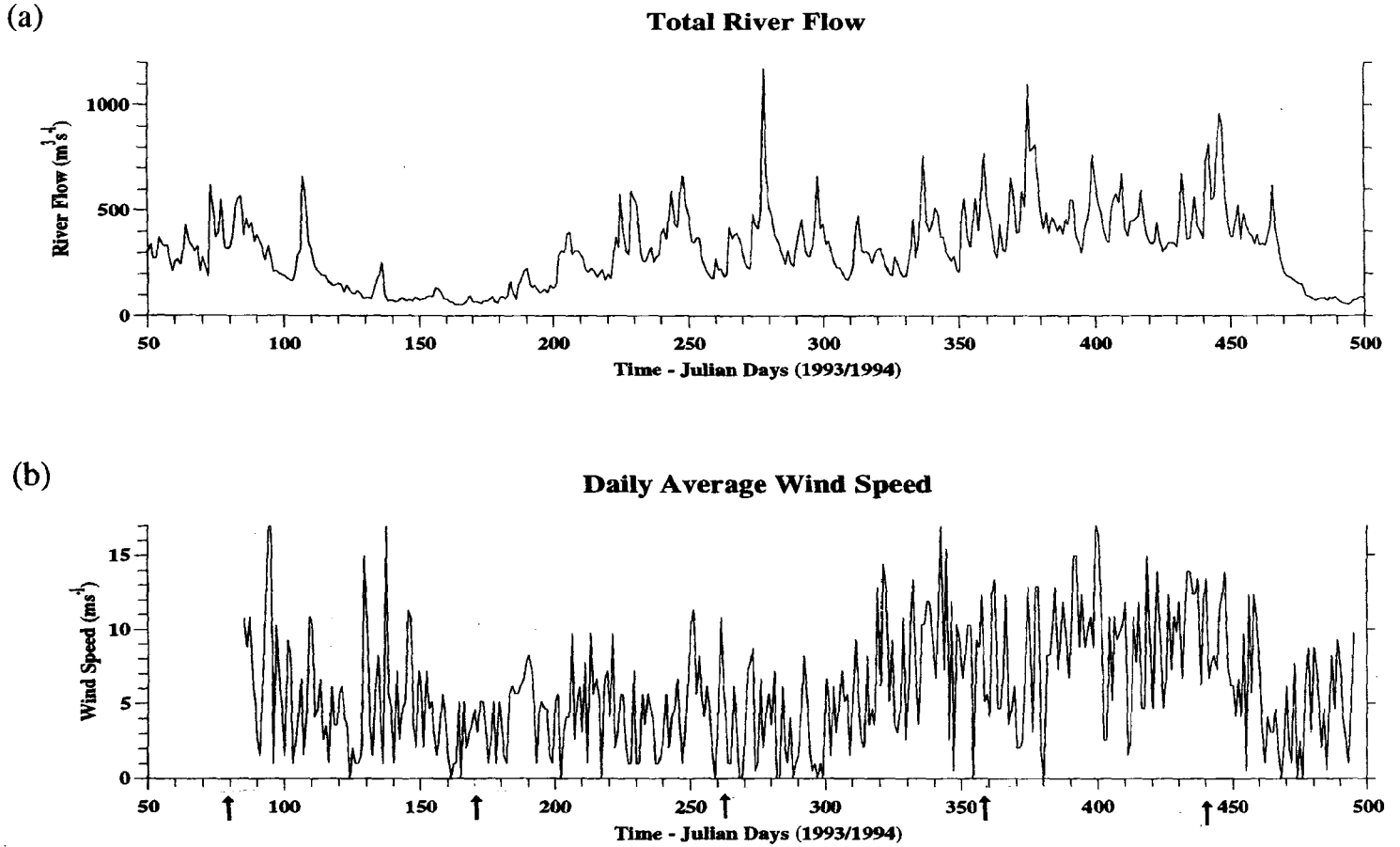

Figure 5.1. (a) Total river flow into the Clyde Sea from the outflow of 12 gauged rivers and corrected to account for other sources. (Data from the Clyde River Protection Board). (b) Daily averaged wind speeds observed at Machrihanish, Mull of Kintyre (Data from the Meterological Office).

(a)

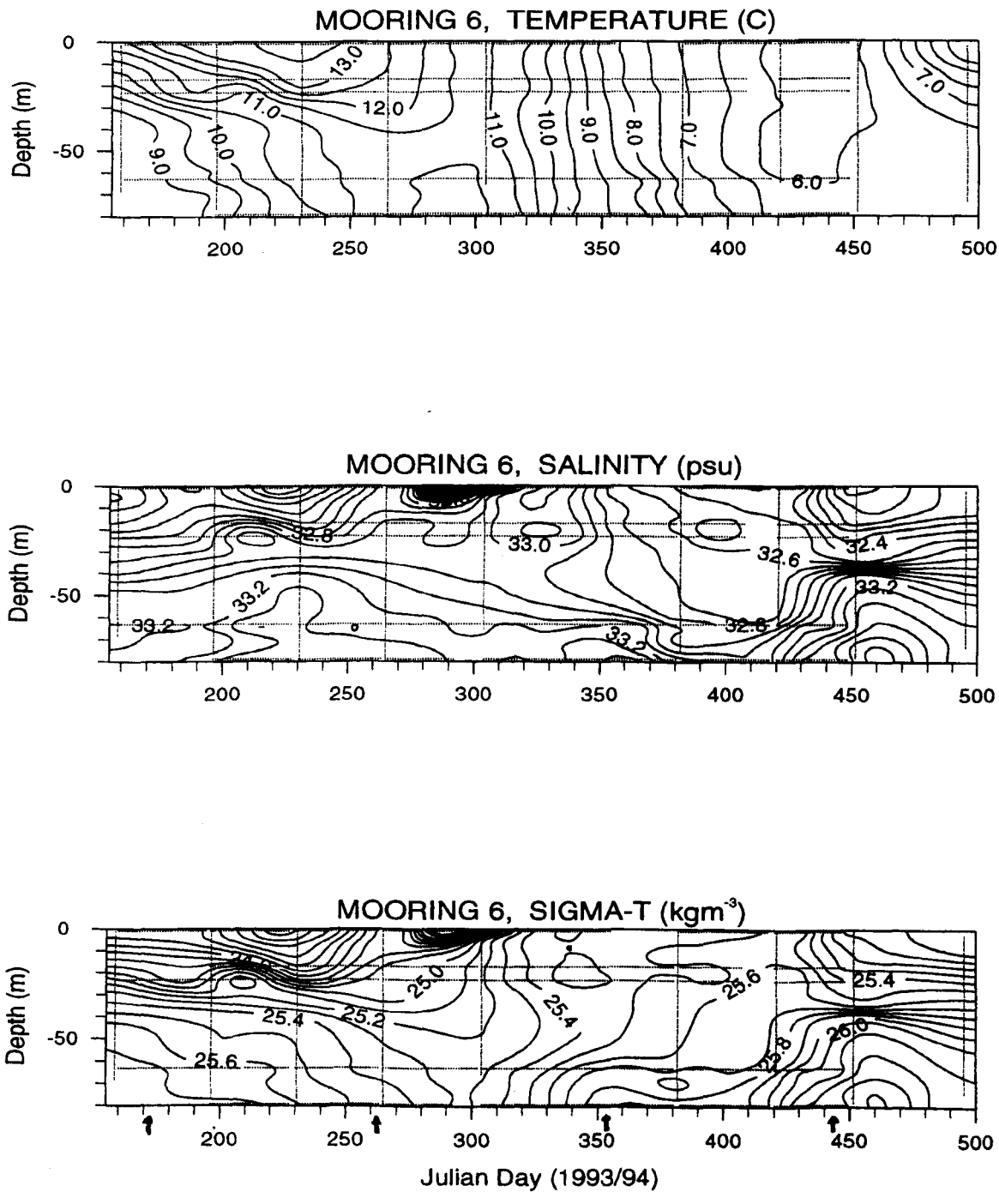

Figure 5.2. Timeseries of temperature, salinity, and σ_t at the mooring sites combining both the daily averaged RCM data and the CTD profiles. (a) MCS6, (b) MCS8.

(b)

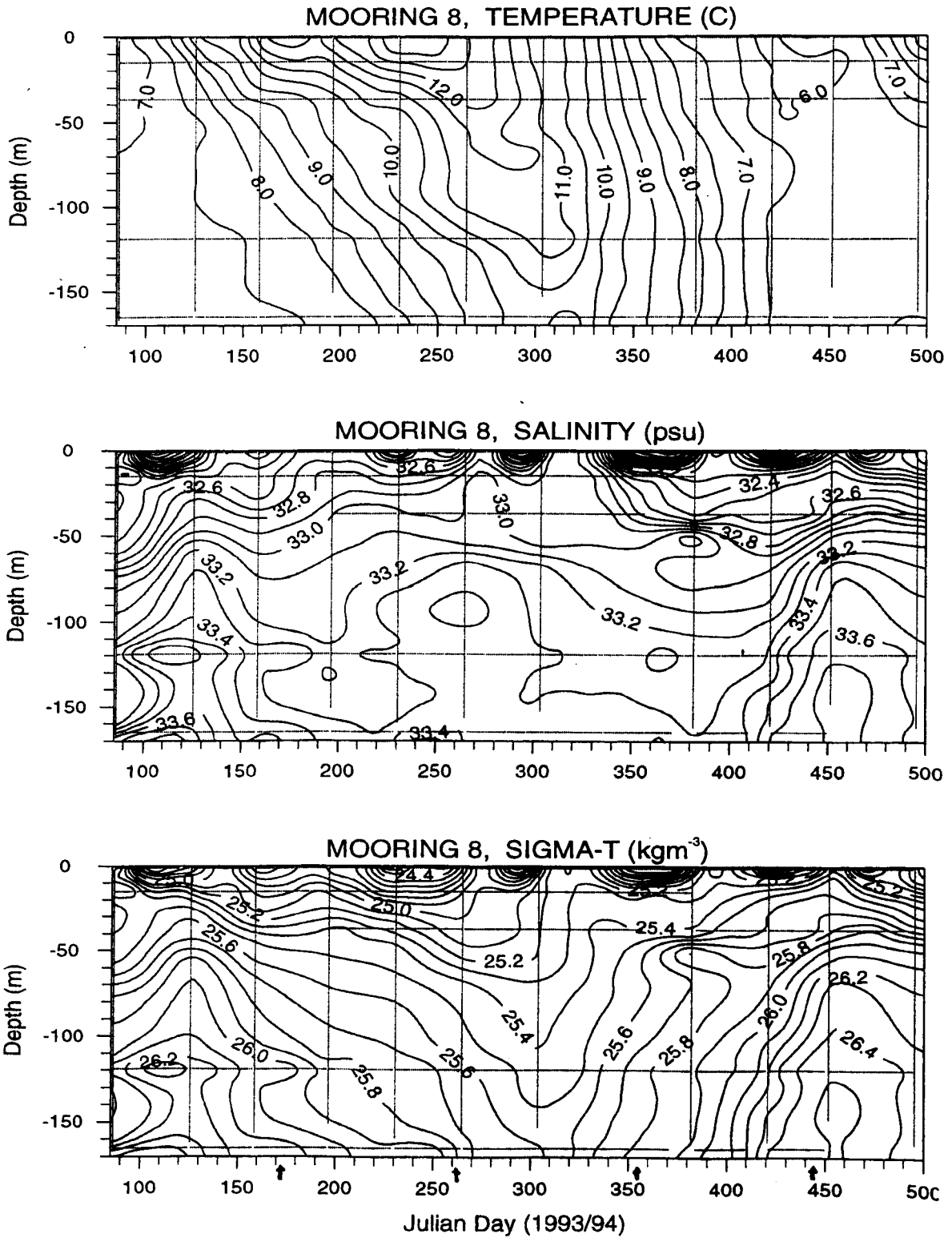

Figure 5.2. Continued.

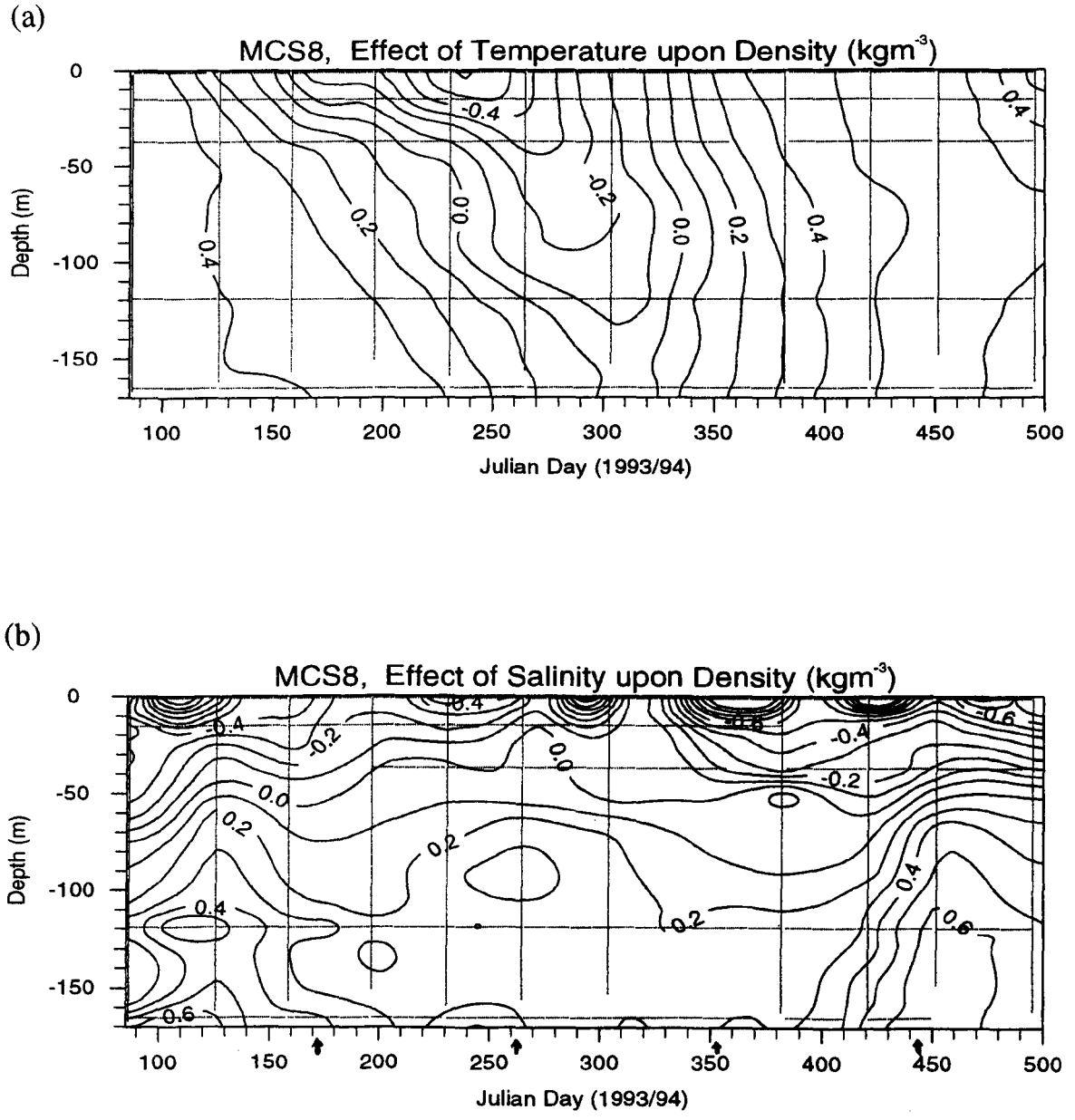

Figure 5.3. The independent effect of (a) temperature and (b) salinity upon sigma-t at MCS8. The variation in sigma-t was calculated relative to the well mixed water column at MCS8 on day 323, where temperature T_0=10.30°C, salinity S_0=33.00 psu, and sigma-t σ_0=25.34 kgm^{-3}.

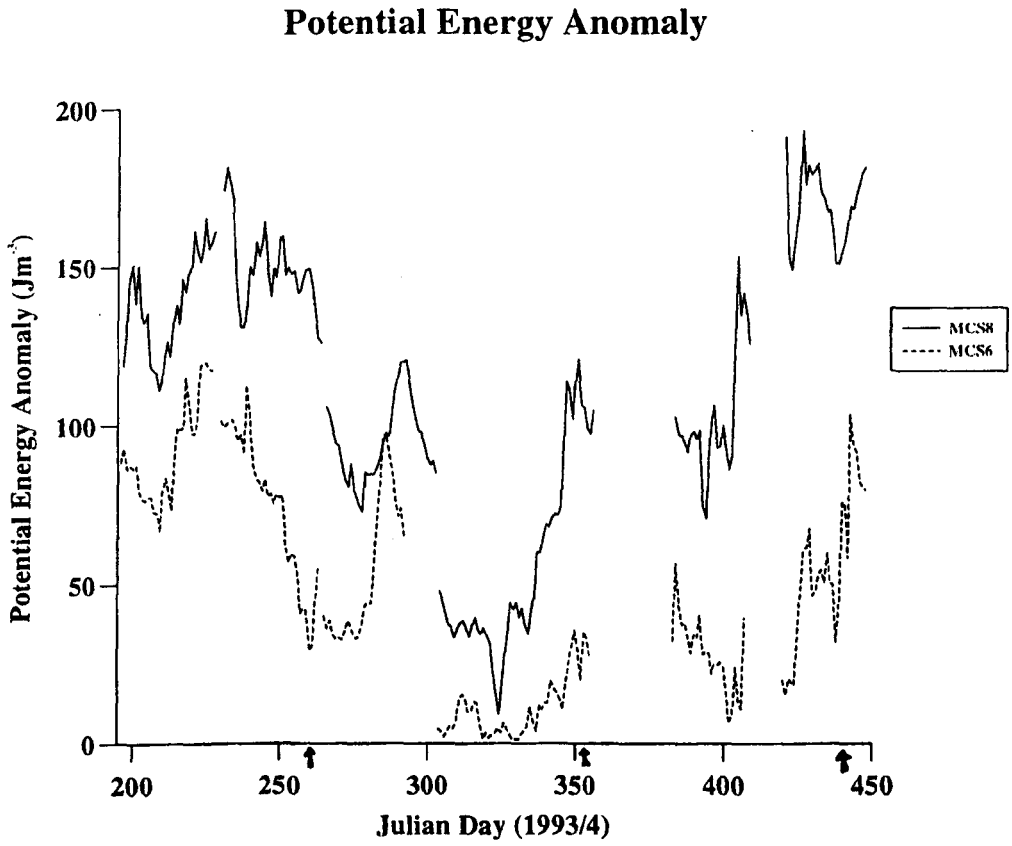

Figure 5.4. Potential energy anomoly, estimated from the RCM data (Jm^{-3}).

(a)

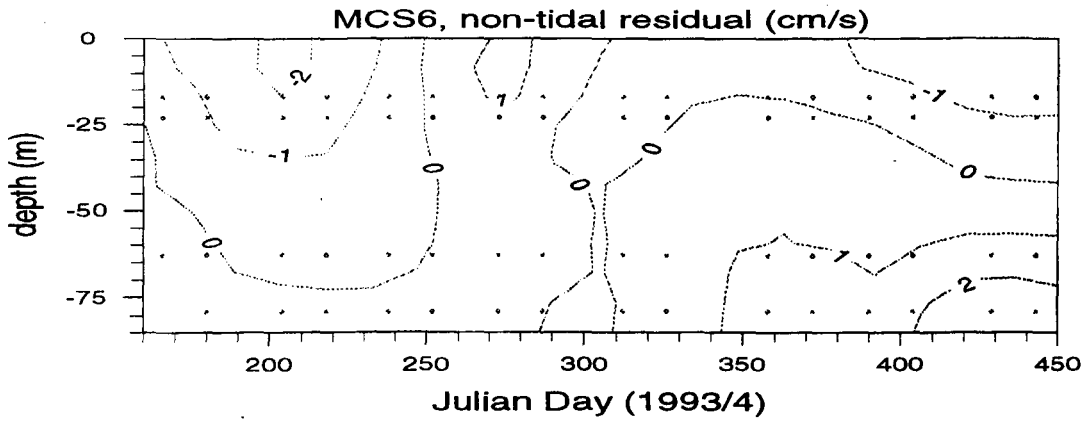

(b)

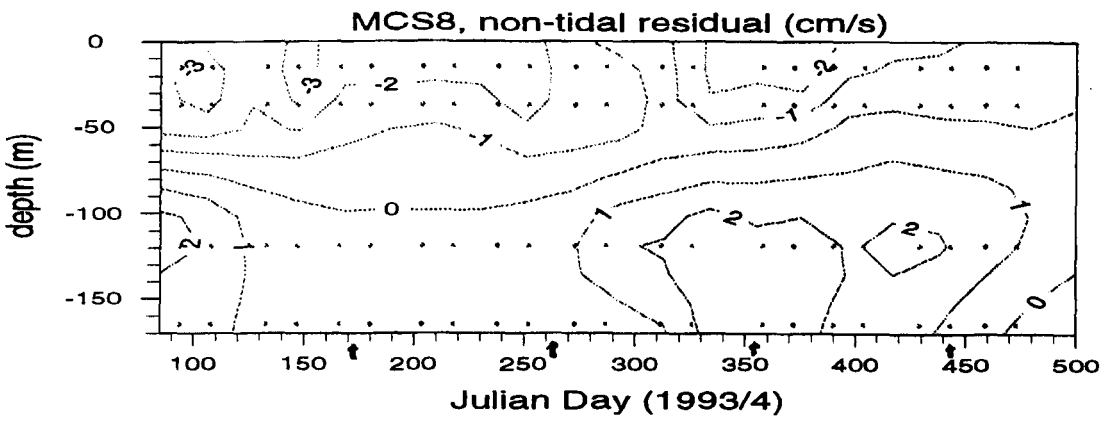

Figure 5.5. Along channel tidal residuals at (a) MCS6, northwards positive, and (b) MCS8, 320° positive.

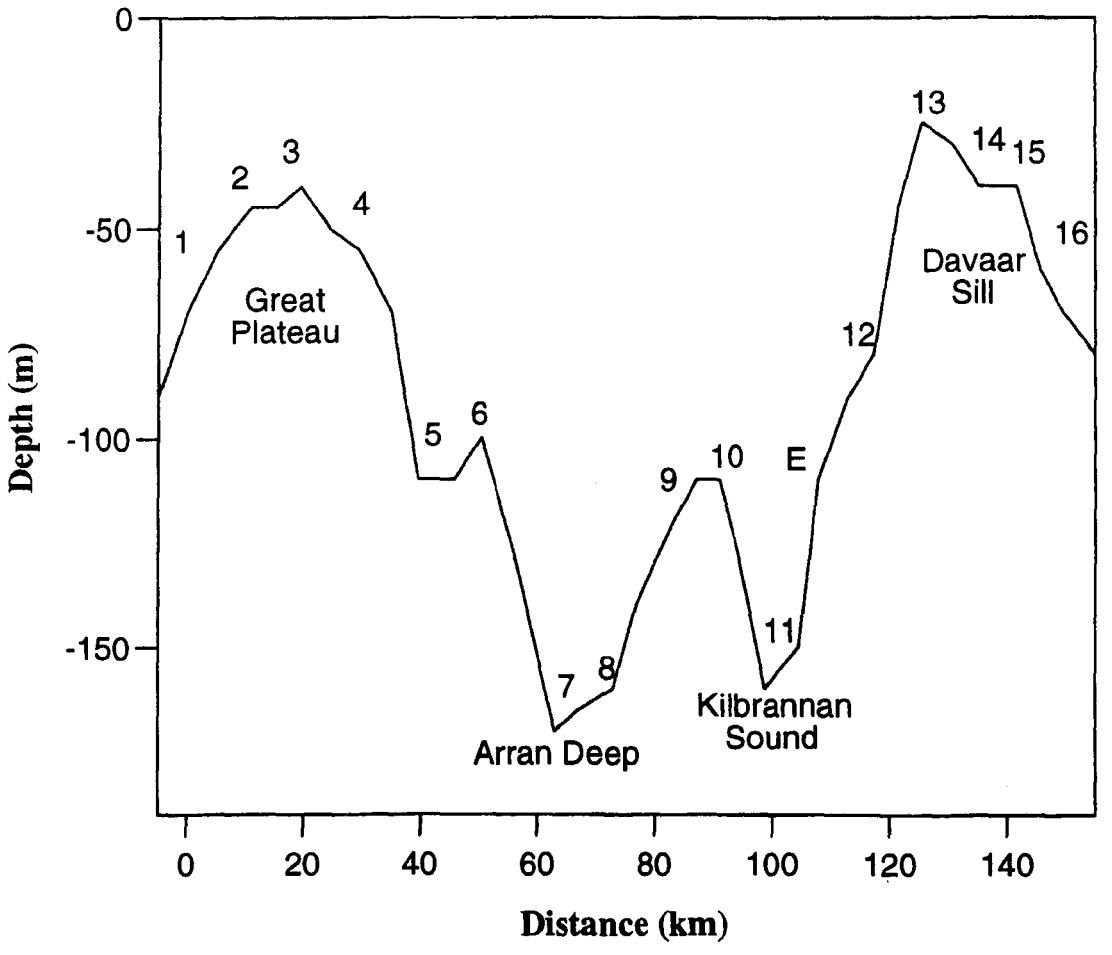

Figure 5.6. Depth profile of CTD stations CS1-16, a section anti-clockwise about the Isle of Arran, along which data is plotted in Figure 5.7.

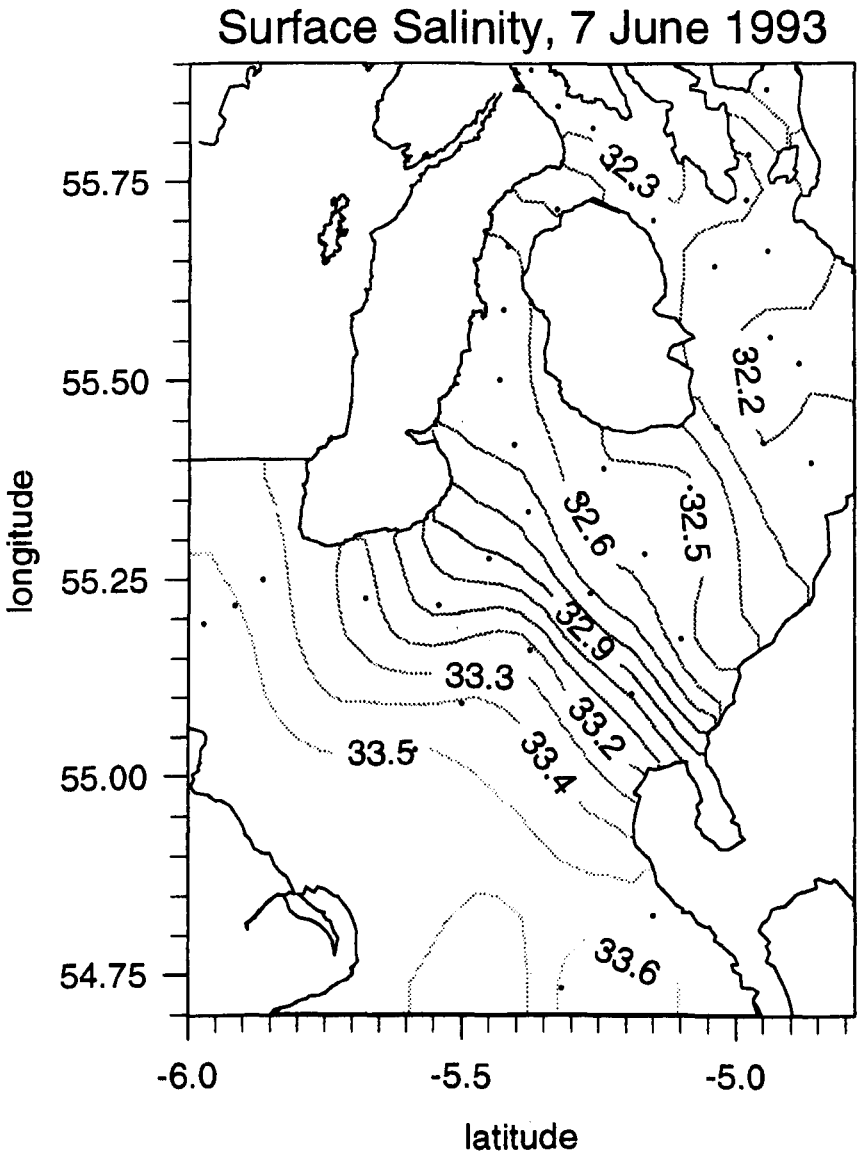

Figure 5.8. The surface salinity distribution on day 157, 1993. Dots are locations of CTD observations.

(a)

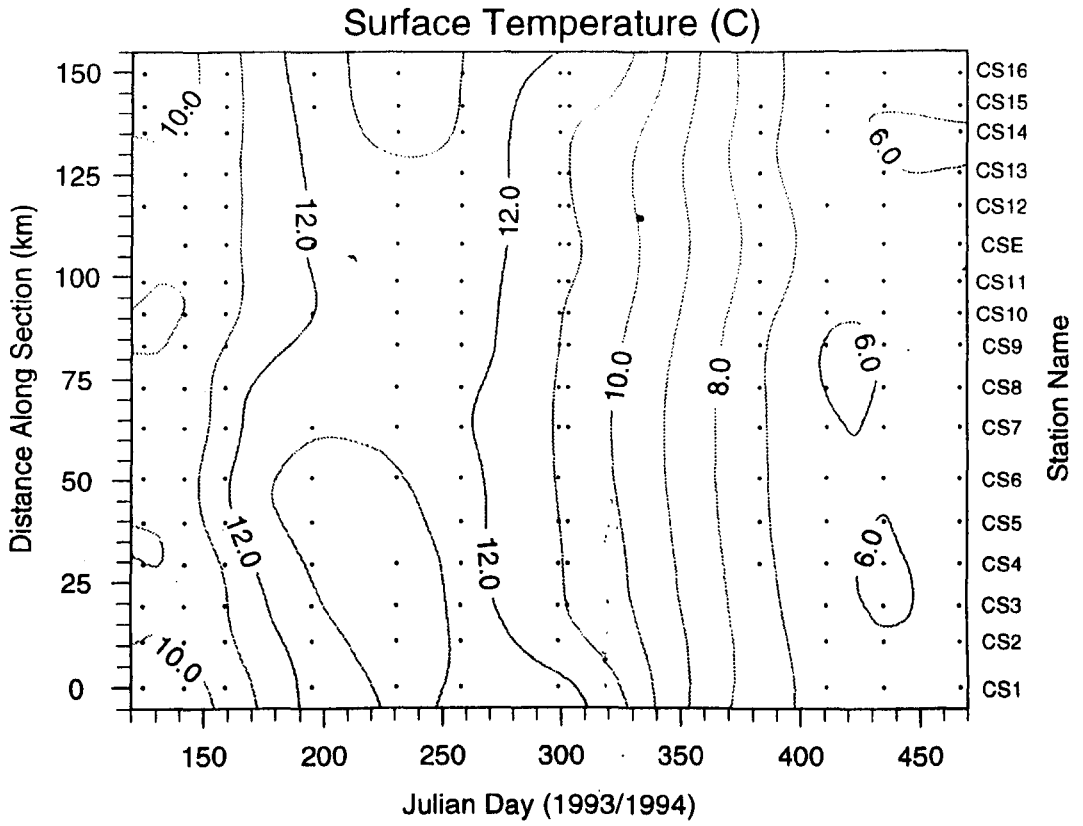

(b)

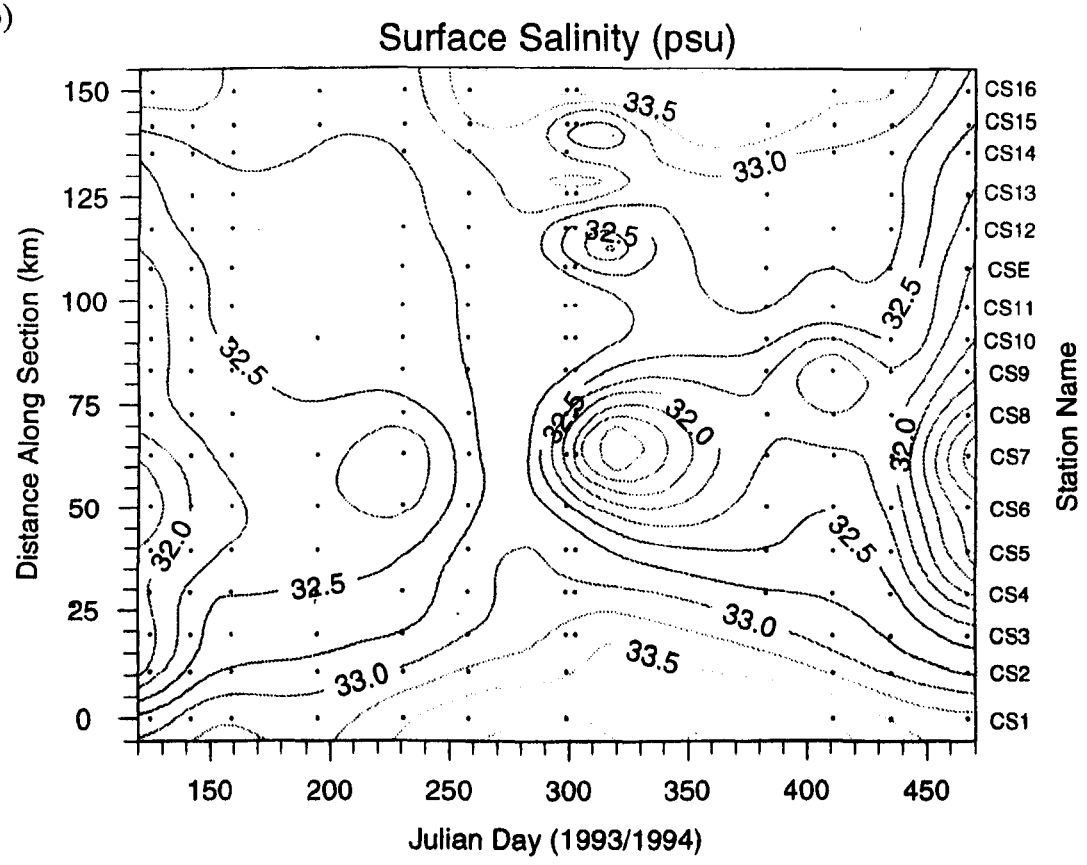

Figure 5.7. Position/time plots of conditions along the section detailed in Figure 5.6. (a) surface temperature; (b) surface salinity; (c) the depth above which salinity is lower than 33.2 psu, and; (d) potential energy anomaly (Jm^{-3}).

(c)

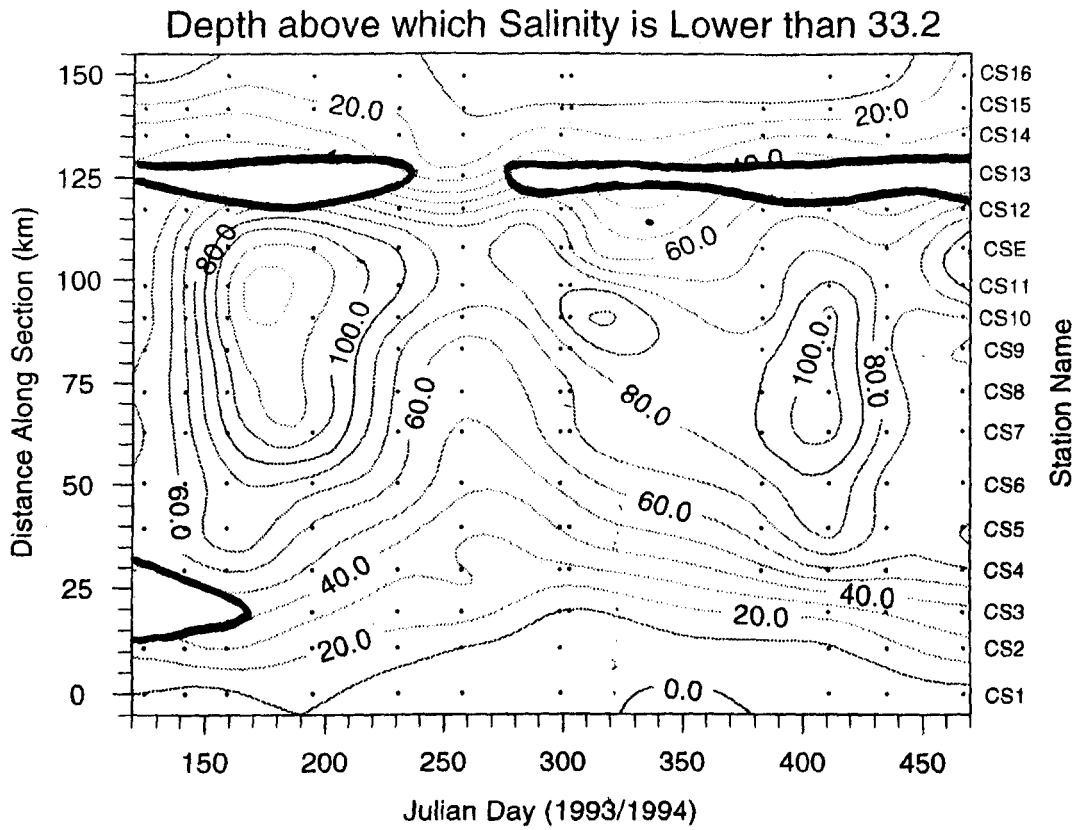

(d)

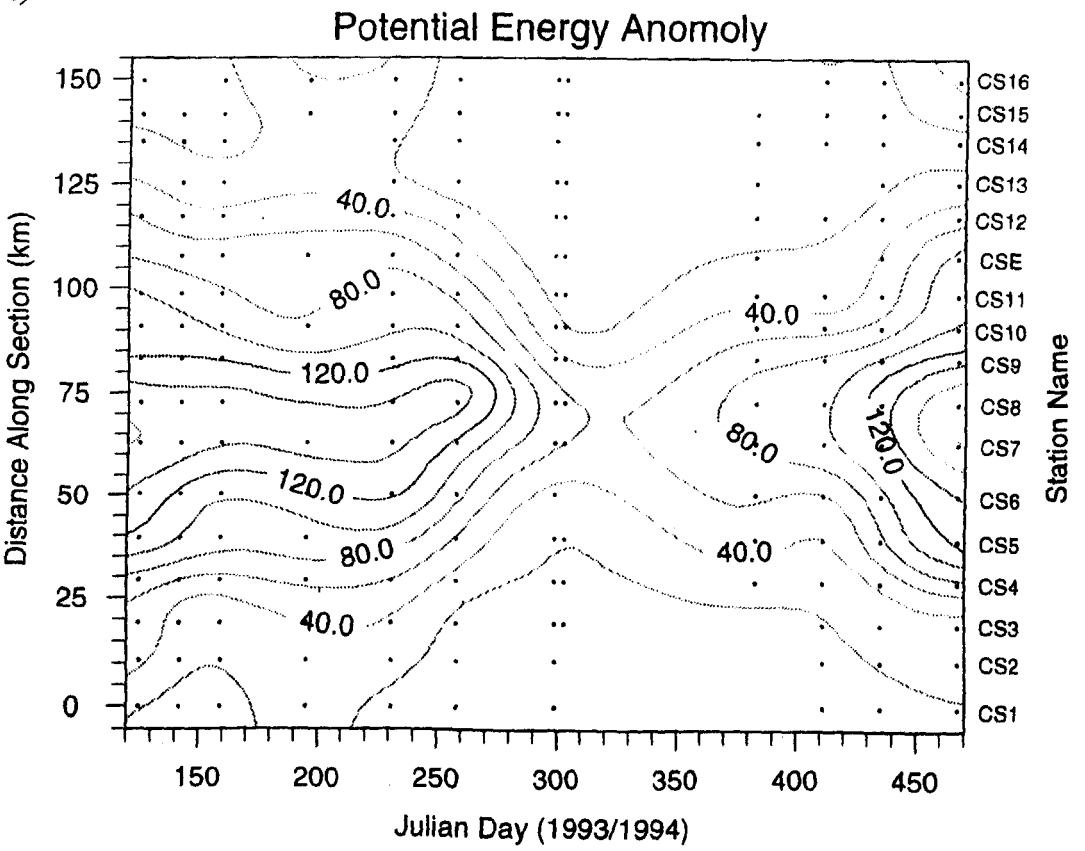

Figure 5.7. Continued.

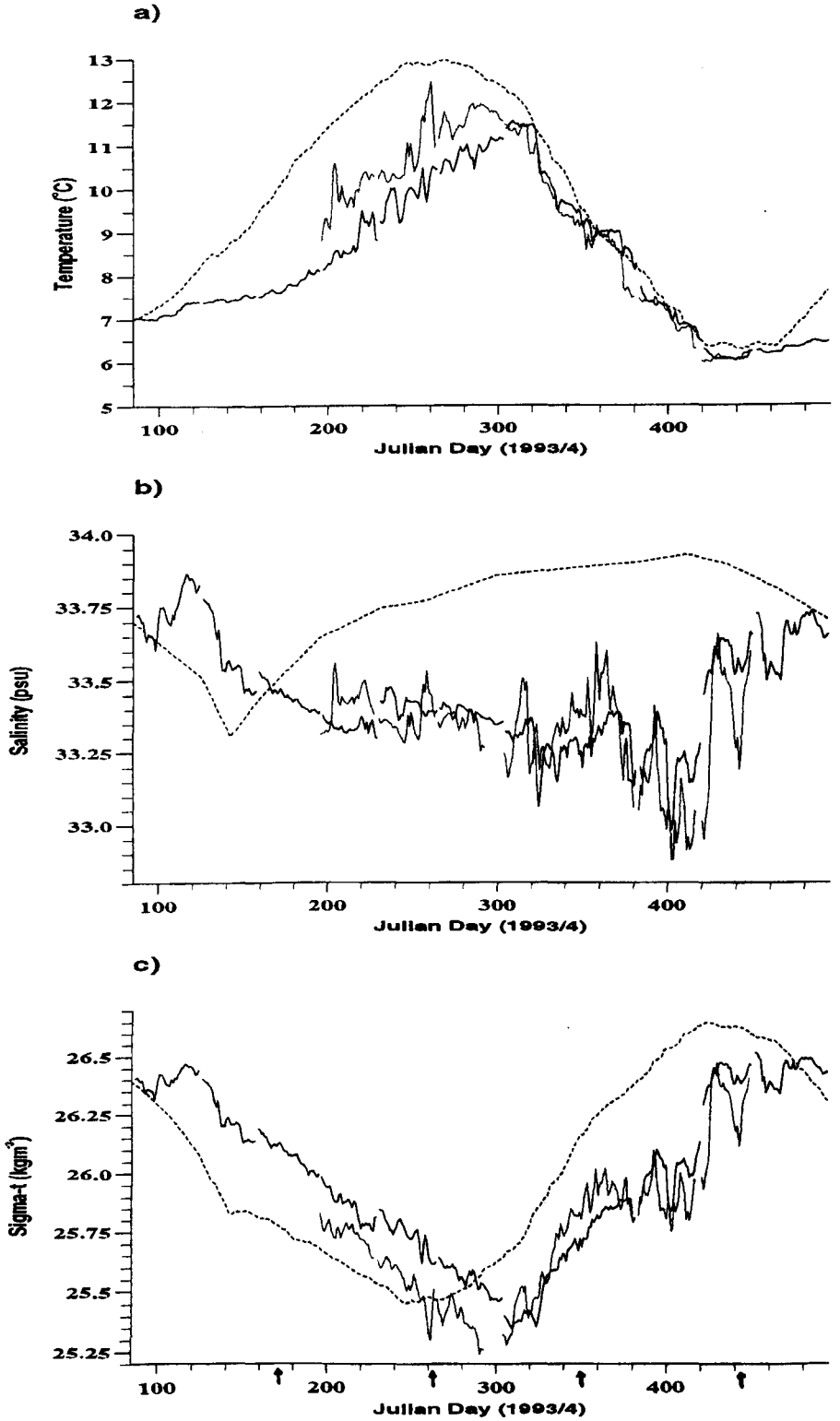

Figure 5.9. Timeseries of temperature, salinity and σ_t at MCS6 at 80 m (...); MCS8 at 120 m (__); and the North Channel (--). The North Channel values are from the CTD observations at CS1 at 50 m, and interploated using a heat budget for temperature, and linearly for salinity.

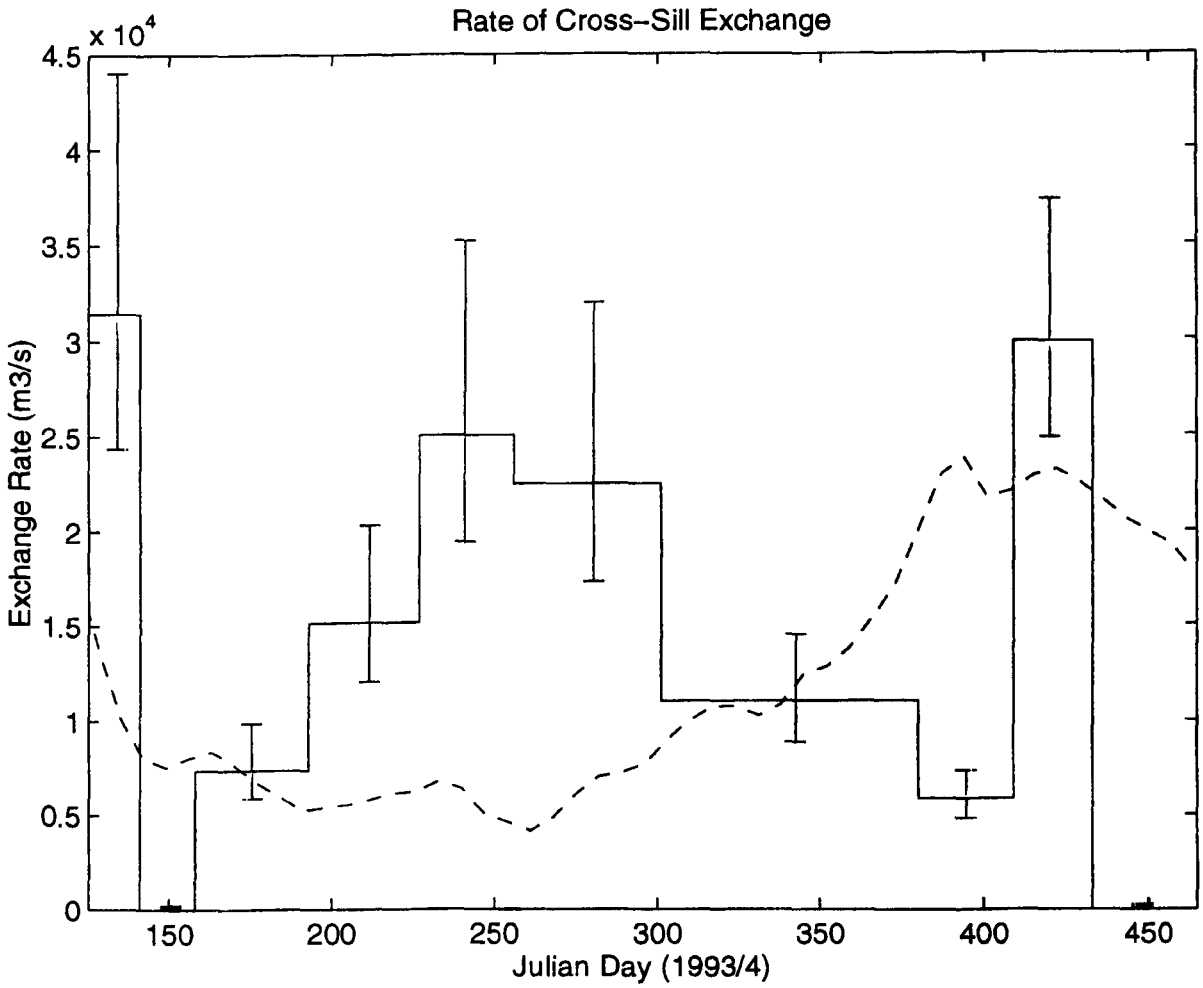

Figure 5.10. The rate of cross-sill exchange, as estimated from the salt/mass budget from the CTD surveys, with an error inferred from a 0.2 psu uncertainty in the salinity of the outflow. The dashed line is the rate of cross-sill exchange hindcast by the 1-D model described in Rippeth *et al.* (1995).

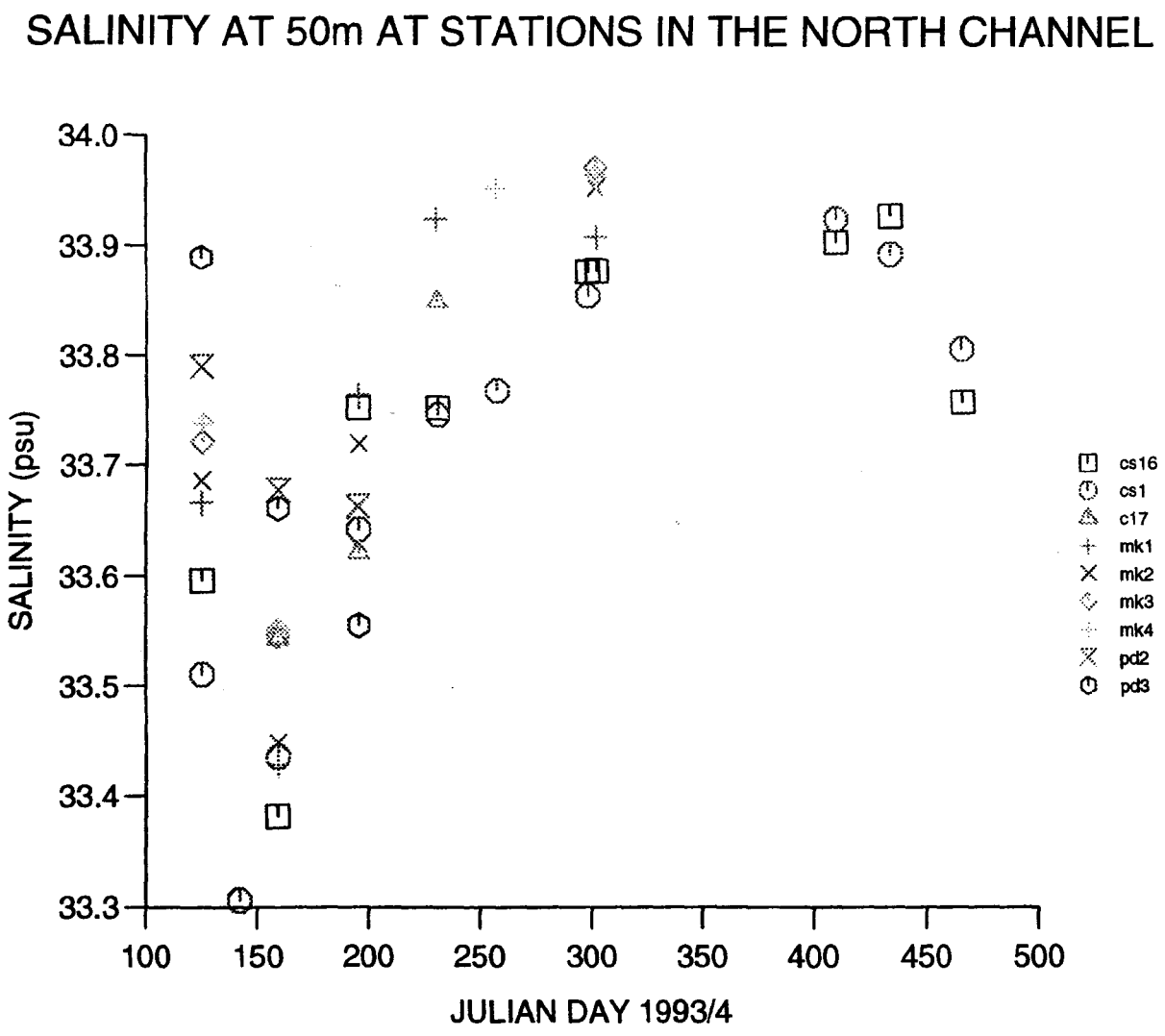

Figure 5.11. Salinity at 50 m, at stations in the North Channel of the Irish Sea.

CHAPTER 6. INTERNAL OSCILLATIONS.

6.1 INTRODUCTION.

In this chapter the new data are used to investigate the nature of internal oscillations in the Clyde Sea, with an emphasis on their potential to cause mixing. The internal tide has not previously been observed in the Clyde. However, Simpson & Rippeth (1993) suggested that bottom mixing produced when the internal tide broke on the basin walls (a mechanism first proposed by Stigebrandt, 1976) was sufficiently strong to mix the warm summer surface water downwards, and thus warm the bottom water (Sections 1.4, 2.6).

An analysis of motions at sub-tidal frequencies is considered first, and evidence that they are wind driven is presented. There follows a description of the observed internal tide in the Clyde Sea, and a comparison with the theoretical estimates of the bottom mixing caused when the internal tide breaks on the side walls.

6.2 WIND DRIVEN MOTIONS.

The Clyde Sea is largely land-locked, and generally stratified. Winds may excite low frequency baroclinic motions, which can lead to mixing. In this section, this mechanism is investigated by using spectral analysis to investigate the frequency distribution of the energy in the velocity recorded at the mooring sites.

The power spectrum density of the along channel velocity from each of the RCMs was calculated, as described in Section 4.5. The spectra from each mooring were then averaged to give an estimate of the mean spectral energy density down the water column (Figure 6.1). There was a concentration of energy at low frequencies (< 0.5 day^{-1}), and at the semi-diurnal frequency, with a weaker signal at quarter diurnal frequency.

The low frequency signal was defined here to include all oscillations with frequencies < 1.0 day^{-1}. The low frequency motions at MCS8 have about twice the energy of those at MCS6 (Table 6.1). This may be due to the topography near MCS8 being more favourable to supporting internal seiches, or that the motions are concentrated by rotation to the Ayrshire coast, and thus not visible at MCS6. The energy in the semi-diurnal tide was estimated by integrating the energy in the frequency band 1.8-2.1 day^{-1}, and the amplitude of the M_2 velocity was then calculated, assuming that the M_2 accounts 69% of the energy in the semi-diurnal tide (Amin, 1982). This amplitude is similar to that calculated in the tidal analysis.

MOORING	Low Frequency Spectral Energy (Jm^{-3})	1.8-2.1 day^{-1} Spectral Energy (Jm^{-3})	M_2 Amplitude (cms^{-1})	Tidal Analysis Amplitude at M_2 (cms^{-1})
MCS6	3.13	3.24	7.75	7.23
MCS8	6.94	0.96	4.21	3.74

Table 6.1. *The vertical mean energy at low frequencies (< 1.0 day^{-1}) and at semi-diurnal frequencies, with a comparison of the implied M_2 velocity amplitude with that calculated in the tidal analysis.*

The seasonal variation of this low frequency signal has a minimum in the summer (days 180-300), followed by a marked rise over the winter months (Figure 6.2). The 7 day filtered square of the wind speed, observed at Machrihanish, which is proportional to the wind drag, is also shown. A positive correlation is apparent.

One mechanism by which these low frequency motions may enhance mixing in the Clyde is by increasing the bottom velocity, and consequently bottom stirring. The power, P, available for bottom mixing as a result of non-tidal currents is estimated by:

$$P = |B\rho(\overline{u_{obs}^3} - \overline{u_{tidal}^3})| \qquad (6.1)$$

where $\bar{u}_{obs}$ is the observed bottom velocity (including the tidal component), $\bar{u}_{tidal}$ is the depth averaged tidal current amplitude, and $B=3.9 \times 10^{-6}$ (see Section 5.7). This bottom mixing contribution, for both MCS6 and MCS8, has a winter maximum of ~0.02 mWm^{-2}. This is an order of magnitude larger than the bottom mixing resulting from the tidal currents alone, but still does not represent a significant source of mixing in the Clyde. There may, however, be other mechanisms by which these low frequency seiches contribute to mixing, associated with the shear at the pycnocline or bottom friction. These mechanisms are hard to quantify.

6.3 OBSERVATION OF THE INTERNAL TIDE.

The internal tide will be dispersed by the complex topography of the Clyde, such that any reflected wave is likely to be small, i.e. it will tend to be progressive (c.f. fjord Skjomen, Cushman-Roisin & Svendsen, 1983). The internal tide will also be modified by the effects of rotation, since the internal Rossby radius is smaller than the channel width. The incoming wave will be concentrated along the Ayrshire coast, so the full amplitude will not be observed at

MCS6, which is approximately 2 Rossby radii from the coast. At MSC8 the channel is narrower, but it is also further from the source region, so that the amount of internal tide energy dissipated before arrival will be greater. Therefore, the amplitude of the internal tide observed at both moorings is expected to be lower than that entering the basin.

Since the barotropic tide is the driving force for the internal tide, it is reasonable to assume that the M_2 will be the most energetic constituent in the internal tide. In the new data, the variation of horizontal velocity best indicates the nature of the internal tide.

Using the analytical methods of Section 4.6, the theoretical modal structure at the mooring sites was calculated from the density profiles, and normalised to a potential energy of 1 Jm^{-3}. Although the density profile varied substantially over time at MCS8, at the depths of the RCMs the shape of the 1st mode is rather similar for each of the profiles (Figure 6.3). The velocity reversal always occurred at a depth between the second and third RCMs down. Thus, it was possible to simplify the analysis by considering the 1st mode as a tidal oscillation of constant amplitude down the water column, with the two surface RCMs 180° out of phase from the bottom two. The same assumption was made for the 1st mode at MCS6. However, in the winter, prior to the spring inflows, (days 320-420) the wind often mixed the pycnocline to beneath the depth of the 3rd RCM down the mooring chain. At these times, the velocity reversal may have occurred between the third and fourth RCM down, and consequently the simple shape assumed for the 1st mode was not applicable.

The depths at which velocity reversals occur for the 2nd mode was more variable, and were sensitive to changes in the stratification. Thus with a vertical resolution of only 4 RCMs it was not generally possible to extract this mode.

Assuming that the influence of friction is limited to a relatively thin boundary layer, and can therefore be neglected, the barotropic wave may be considered to have constant amplitude and phase down the water column. A residual baroclinic signal was calculated by vectorially subtracting the barotropic tide. This was then fitted, in a least squares fashion, to the simplified first mode baroclinic profile (Figure 6.4).

The mean amplitude of the 1st mode was ~1.9 cms^{-1} and ~2.4 cms^{-1} at MCS6 and MCS8 respectively (Figure 6.4a), which was of the same order as the root mean square residual variance (~2 cms^{-1}). Two characteristics confirm that the internal tide had actually been observed. Firstly, the observed phase varied in a coherent and gradual manner, indicating a real signal. Secondly, for a few days following day 323, the water column at MCS8 became homogeneous, and consequently could not support any baroclinic oscillations. At this time, the observed 1st mode

was reduced to ~0.4 cms^{-1}.

Seasonal and spatial variations in the stratification lead to variation in the theoretical mode 1 internal wavelength, λ_1. These variations tended to be significant and incoherent spatially, indicating the uncertainty resulting from estimating λ_1 from a single profile Very roughly, near MCS8, λ_1 is generally ~20 km, but gradually increased to ~30 km between days ~270-430, while near MCS6 and in the Firth of Clyde, λ_1 ~20 km throughout the year. Near days 270 and 430, gradual phase shifts of ~60° were observed at MCS8 (Figure 6.4b). Taking MCS6 and MCS8 to be 35 km and 65 km from the sill respectively, this phase shift indicates an increase in λ_1 of ~1 km (an average from the sill to MCS8) between days 270-430. This is small relative to the estimates from modal theory.

The total energy in the 1st mode, E_1, the kinetic energy ($\rho u^2/4$) plus the potential energy (Equation 4.10), was estimated to be E_1= 0.11 Jm^{-3} and 0.17 Jm^{-3}, at MSC6 and MSC8 respectively. Assuming that the energy observed at each mooring is typical of a section across the fjord, the rate at which energy is transported away from the sill is given by:

$$P_T = BE_1c_1 \qquad (6.2)$$

where c_1 is the group velocity of the 1st mode, (which is approximately equal to the phase velocity given in the modal theory), and the cross-sectional area of the fjord; B ≈ 1.4 x 10^6 m^2 and 7.0 x 10^5 m^2, at MCS6 and MCS8 respectively. The results (Table 6.2) have been split into three seasons, characterised by different stratifications and internal wave speeds; winter (days 320-420), spring (days 80-200, 420-500) and summer (days 200-320). MCS6 is closer to the sill than MCS8, and therefore the internal tide energy flux must be larger. The lower observed value indicates that rotation restricts much of the energy to the Ayrshire coast.

Season and Approximate Julian Date (1993/4)	Winter (320-420)		Spring (80-200,420-500)		Summer (200-320)	
Mooring Number	6	8	6	8	6	8
Velocity c_1 (ms^{-1})	0.5	0.9	0.4	0.5	0.4	0.7
Observed Internal Tide Power, P_T (10^6 W)	0.08	0.11	0.06	0.06	0.06	0.08

Table 6.2. *The calculated internal tide power, over three seasons characterised by changes in typical stratification.*

Stigebrandt and Aure (1989) estimated the efficiency of the mixing resulting from the breaking of internal waves in a large number of Norwegian fjords to be $\epsilon = 0.056 \pm 0.011$. Using this estimate, and accounting for higher internal modes and other tidal frequencies, the amount of mixing due to this mechanism in the Clyde is ~0.01 mWm^{-2}. This estimate is a low limit, since, the moorings were not suitably located to observe the maximum internal tide. However, this figure is more than two orders of magnitude smaller than the surface wind mixing. Unless much of the internal tide energy is dissipated in the vicinity of the sill, it is unlikely that the breaking of internal tides will result in significant mixing in the Clyde Sea. In their 1-dimensional model, Simpson & Rippeth (1993) required a peak internal tide mixing of ~0.4 mWm^{-2} to produce the observed bottom warming. Following the above analysis, this would imply an internal tide velocity amplitude of ~30 - 40 cms^{-1}, which is substantially larger than that observed.

6.4 THEORETICAL ESTIMATE OF THE INTERNAL TIDE ENERGY FLUX.

In the previous section, the observations were used to make an estimate of the mixing energy resulting from the breaking of the internal tide on the side walls of the basin. Simpson & Rippeth (1993) used a theoretical estimate of the internal tide energy flux to calculate the induced bottom mixing, following Stigebrandt (1976), and a similar calculation is made here using the new observations of the stratification.

Regions of internal wave formation are characterised by large values of $(\delta H/\delta x)/H$, where x is the cross-sill coordinate and H the depth (Baines, 1982). In the Clyde Sea there are two distinct regions of internal tide formation; over the Davaar sill at the entrance of the Kilbrannan Sound (KS), and over the Great Plateaux in the entrance to the Firth of Clyde (FC). According to Stigebrandt (1976), the rate of energy transfer to the internal wave field in a two layer system, with the pycnocline at sill depth, is given by:

$$I = 0.5\rho\omega^2 a_0^2 \left\{ g\frac{\Delta\rho}{\rho} \right\}^{0.5} \frac{A_0^2}{A_s} \left\{ \frac{h_1 h_2^3}{(h_1 + h_2)^3} \right\}^{0.5} \qquad (6.3)$$

where h_1 and h_2 are the depth of the surface and bottom layers respectively, A_s is the fjord entrance area, the tidal elevation a_0 ~ 1.5 m, the frequency of the M_2; $\omega = 1.405 \times 10^{-4}\ s^{-1}$, and the area of the Clyde Sea north of the Great Plateaux A_0 ~ $2.1 \times 10^9\ m^2$. Taking typical values; in the Kilbrannan Sound $h_1 = 30$ m, $h_2 = 70$ m, $A_s = 15$ km x 30 m, and in the Firth of Clyde $h_1 = 40$ m, $h_2 = 50$ m, $A_s = 20$ km x 45 m. Thus:

$$I = 1.3 \times 10^7 \sqrt{\Delta\rho_{FC}} + 7.8 \times 10^6 \sqrt{\Delta\rho_{KS}} \qquad (6.4)$$

where $\Delta\rho_{FC}$ and $\Delta\rho_{KS}$ are the stratification in the Firth of Clyde and the Kilbrannan Sound respectively. Typical stratification of each of the Kilbrannan Sound and Firth of Clyde are shown in Table 6.3, along with the implied value of I.

Season and Approximate Julian Date (1993/4)	Winter (320-420)	Spring (80-200,420-500)	Summer (200-320)
Typical $\Delta\rho_{FC}$ (kgm^{-3})	0.3	1.5	1.1
Typical $\Delta\rho_{KS}$ (kgm^{-3})	0.2	1.2	0.8
Calculated Internal Tide Power, I (10^6 W)	11	24	21

Table 6.3. *The theoretical internal tide power, over three seasons characterised by changes in typical stratification.*

The observed power, P_T, is roughly 2 orders of magnitude lower than the theoretical, I. Craig (1987) offers an explanation. In addition to the factors described in Equation 6.3, the magnitude of the internal tide is dependent upon the ratio of topographic to baroclinic length scales, α. If the bottom slope is assumed to be $\Delta H/L$, where ΔH is the increase in depth over a distance L, then the angle of the ray characteristic, θ, by geometry, is given by (Craig, 1987):

$$\theta = 2\frac{H}{\lambda_1} \tag{6.5}$$

Then α is given by:

$$\alpha = \frac{\Delta H \lambda_1}{2HL} \tag{6.6}$$

For supercritical slopes ($\alpha>1$), the energy flux varies approximately linearly with α, while for subcritical slopes ($\alpha<1$), it varies as α^5. To highlight the differences in the internal tide formation characteristics between the Clyde Sea, and Vestfjord, to the north of Oslofjord, as described in Stigebrandt (1976), α will be estimated for both fjords.

Within the sill at Vestfjord, the depth increases from 20 to 60 m over 5 km, implying an approximate topographic slope of 8×10^{-3}. From the Oslofjord parameters given, λ_1~35 km, H ~60 m, and therefore $\alpha = 2.3$, which is supercritical, indicating that Stigebrandt's energetics will be valid with little modification for Vestfjord. Repeating this calculation for the Clyde Sea;

within the sill the topographic gradient is about 2 x 10^{-3}, λ_1 ~25 km, H ~70 m; and so α ~0.36, which is subcritical. Hence the energy flux varies with α^5 ~0.006. This indicates that in the Clyde Sea, the topographic gradients are too gentle for the efficient production of an internal tide and the flux will be greatly reduced from the above estimate.

6.5 SUMMARY.

Low frequency internal motions have been observed to have an energy of comparable magnitude to the barotropic tide at MCS6 and an order of magnitude greater at MCS8. A visual correlation was found between this energy and the square of the wind speed, indicating that they are wind driven. The data available did not allow an estimate of the rate of production or dissipation of these waves, but it is possible that they make a significant contribution to the mixing budget.

A 1st mode internal tide has been observed in the Clyde Sea, to have a horizontal velocity amplitude of ~2 cms^{-1}. An estimate of the associated mixing is ~ 0.01 mWm^{-2}, which is two orders of magnitude lower than theoretical estimate following Stigebrandt (1976). This is not a significant contribution to the mixing budget in the Clyde Sea, and therefore the internal tide is unlikely to be responsible for the summer time warming of the deep water as suggested by Simpson & Rippeth (1993). It is argued that the sill topography is too gentle to efficiently produce an internal tide. However, there remains the possibility that mixing near the sill by a rapidly dissipated internal tide is significant.

In the summer, mixing associated with low frequency internal motions will be small since wind speeds are generally low, and mixing associated with the internal tide is negligible. There are no other apparent mechanisms to produce the summer time bottom mixing inferred by Simpson & Rippeth (1993). As discussed in Section 5.8, the summer time deep water warming may be related to inflow, and modelling studies associated with this are presented in Sections 7.33 & 9.3.3, followed by a discussion in Section 10.4.

(a)

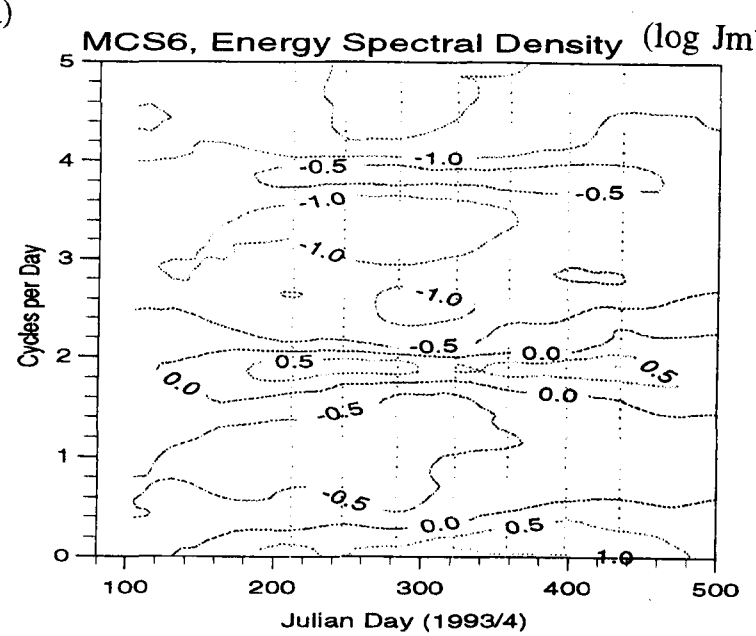

(b)

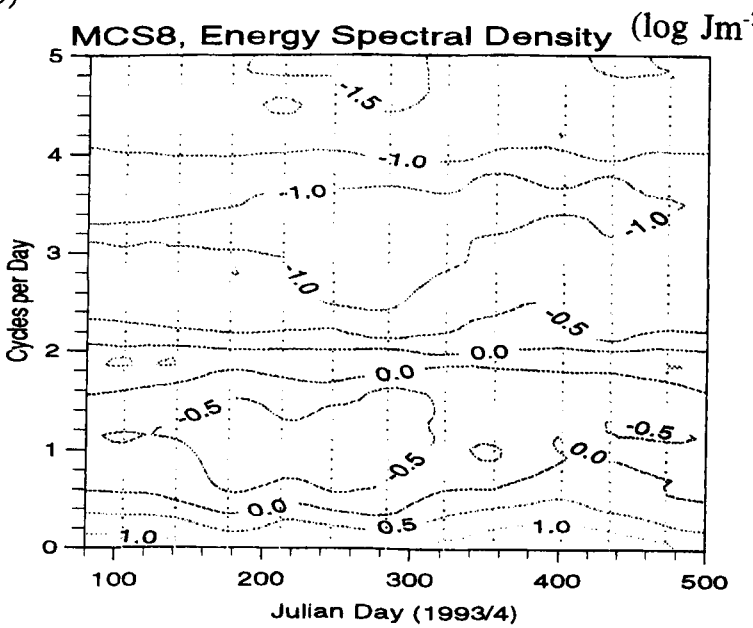

Figure 6.1. Frequency/time plot of the energy spectral density (log Jm^{-3} per unit frequency) estimated from a) MCS6; b) MCS8. The energy at frequencies higher than 5 day^{-1} was negligable.

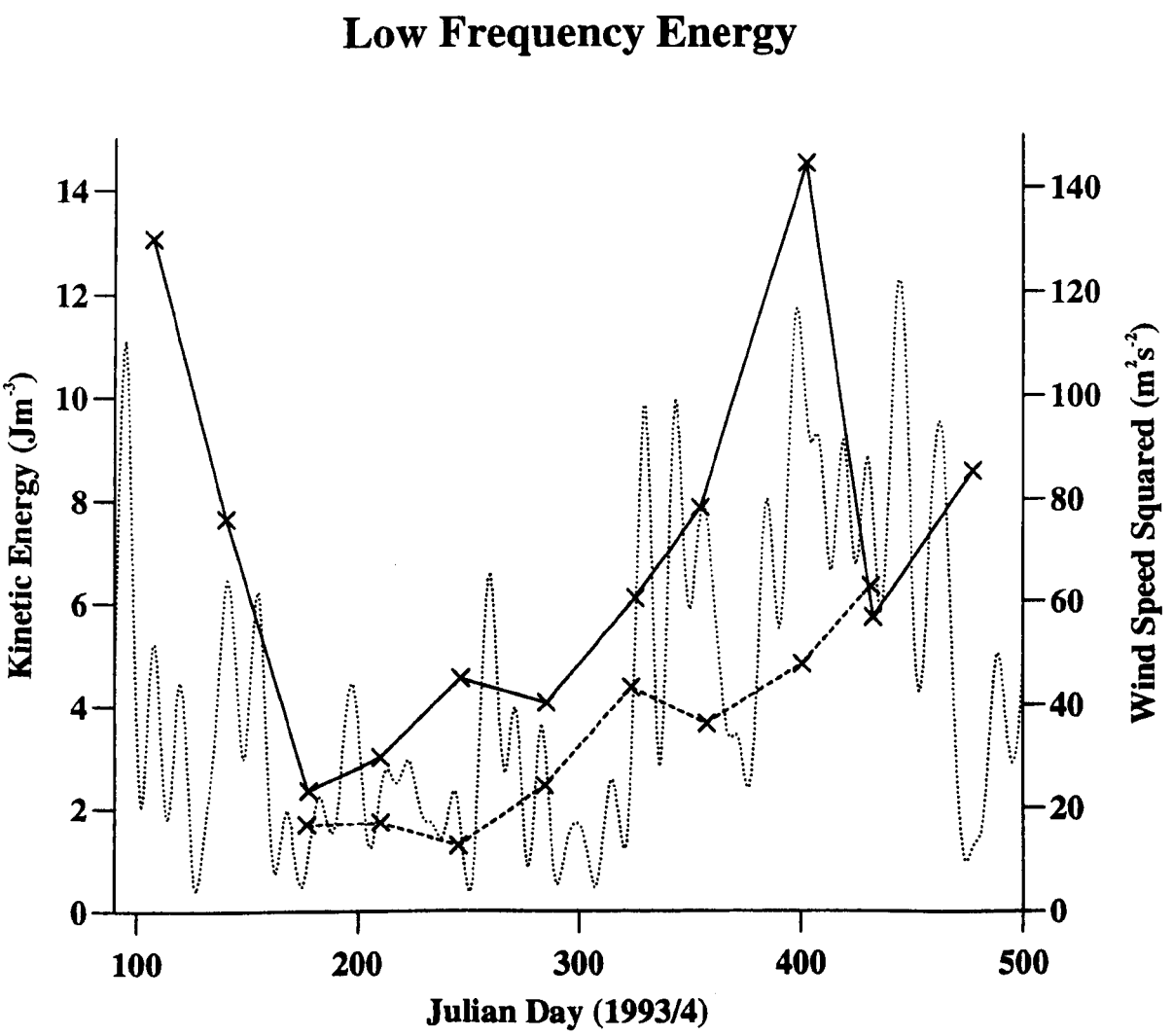

Figure 6.2. Integrated low frequency kinetic energy, defined as oscillations with periods of greater than a day, for MCS6 (---) and MCS8 (__). The 7 day averaged square of the wind speed is also shown (....).

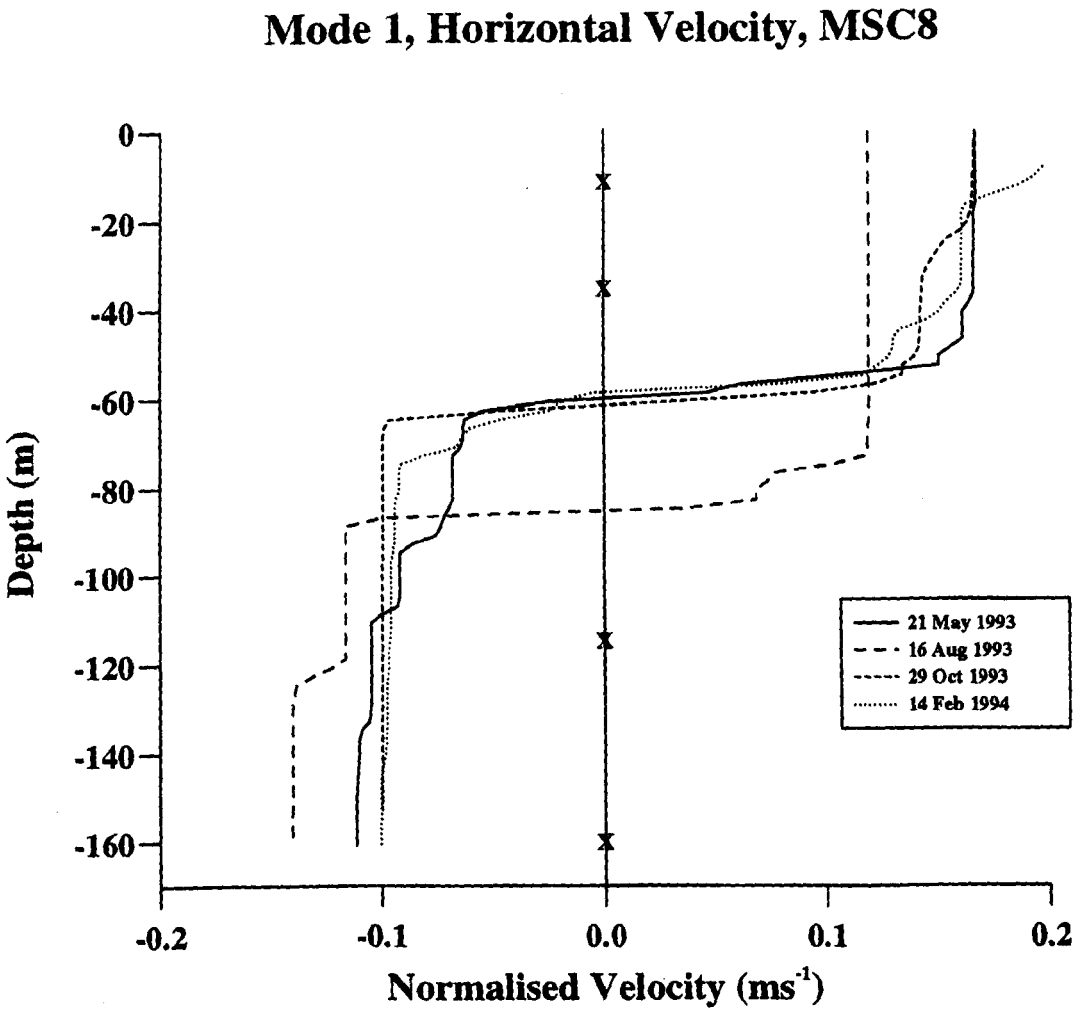

Figure 6.3. Depth profile of the theoretical mode 1 normalised horizontal velocity, at the M_2 frequency, at MSC8, calculated from selected CTD profiles over the observation period. The depths of the RCMs are marked with an x.

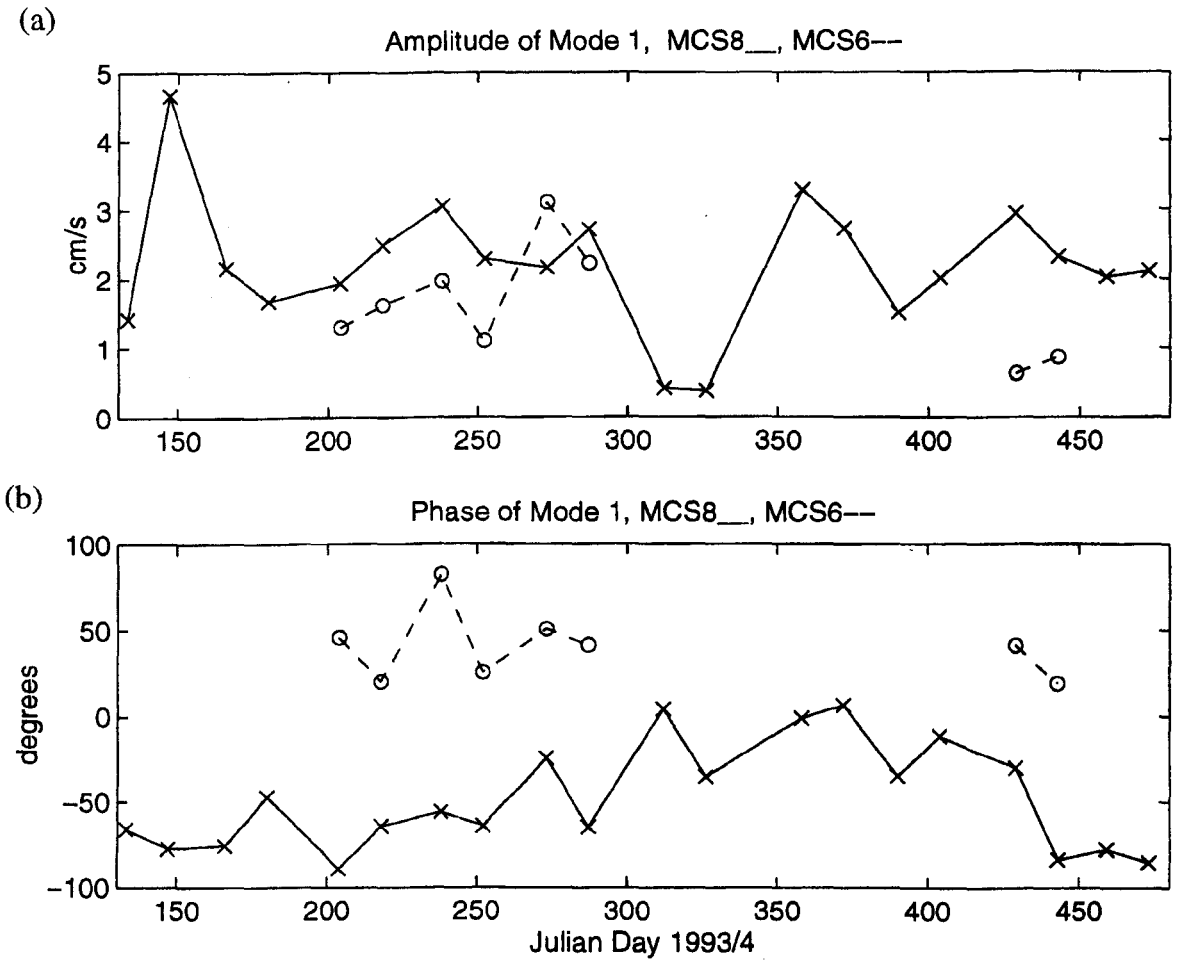

Figure 6.4. a) Amplitude and b) phase lag of the mode 1 internal tide, at M_2 frequency, at MCS6 (---) and MCS8 (__).

CHAPTER 7. THE 1-DIMENSIONAL MODEL OF THE CLYDE SEA.

7.1 INTRODUCTION.

A 1-dimensional filling-box model was developed for the Clyde Sea by Simpson & Rippeth (1993). It was used to examine the competition between the basic stratifying and stirring processes which control the vertical structure. The model was later adapted by Allen (1995) to study the seasonal cycle of stratification in Upper Loch Linnhe, and by Jones *et al.* (1995) to study the controls on phytoplankton and nutrient cycles in the Clyde Sea. Only a brief description of the model will be given here, and the reader is referred to the original paper for a more detailed description. In this chapter, the model is further developed, applying the insight from the new observations.

The objective of this modelling work was not to produce a predictive model, capable of simulating the detailed physics of the seasonal cycle in the Clyde Sea. Rather, the objective was to further our understanding of the Clyde Sea system by testing the extent to which a model based on a simple set of physical assumptions reproduces the main, low frequency, features of the observations. Using the new data, for the first time it has been possible to compare the model simulation with an observed annual timeseries.

The model domain consists of discrete horizontal layers representing the profile, each 1 m in depth. Within each layer, conditions were assumed to be homogeneous, which is in reasonable agreement with the observations from the Firth. The change of surface area with depth (the hypsographic function) was taken as that previously used, originally derived from Edwards & Sharples (1988).

The model assumes that the stratifying influence of freshwater and surface heating are opposed by mixing due to the surface wind stress, the barotropic and baroclinic tides, convection due to surface cooling, and inflow mixing. These processes bring about changes in the potential energy, which follow from the energy arguments used in the shelf sea heating/stirring problem (Simpson & Bowers, 1984). The rate of exchange was calculated, by analogy with the Hansen-Rattray estuarine circulation, to be proportional to the density difference between the North Channel and the basin bottom.

When the model was originally run over a typical seasonal cycle, it did not reproduce the observed summer time warming of the bottom waters (Simpson & Rippeth, 1993). This led the authors to seek an additional source of bottom water mixing (to mix down heat from the warm surface waters). They incorporated a mechanism, first proposed by Stigebrandt (1976), by which

internal waves generated by tidal flows at the sill bring about mixing when they break at the side walls.

The model effectively contained two tunable parameters; the internal wave mixing efficiency, ϵ, and H_R, an arbitrary constant, which when multiplied by the cross-sill density difference gives the inflow rate. Rippeth & Simpson (1996) tuned the model for the period 1985-1991, during which limited archival CTD data was available.

This version of the model was run, applying meterological and boundary forcing as observed over the mooring deployment period, in order that the model run be compared with an observed time-series. This comparison has already been made by Rippeth *et al.* (1995), and shows that the variation in both surface and bottom salinity was not well reproduced (Figure 7.1). In part, this is due to the timing of the inflows not being well represented in the model, as discussed in Section 5.6. Thus, the physical processes governing the rate of inflow were incompletely represented in the model.

7.2 MODEL DEVELOPMENT.

The model was run over the period of the new mooring data, with meteorological forcing derived from the hourly observations of wind velocity and dew point temperature, and the daily freshwater inflows. CTD data from CS1 at 50 m was assumed to be representative of the well mixed North Channel. The salinity was linearly interpolated between the observations, whilst the temperature was interpolated using a heat budget. Wind, and bottom mixing efficiencies were set to those given by Simpson & Bowers (1981), which represented a 56% increase on the value used by Rippeth *et al.* (1995). Inflow mixing efficiency was set to 5%, which is the best estimate for mechanically generated turbulence (Stigebrandt, 1985). The model was initiated with the profile at MCS8 on 28/3/1993, as this was the only CTD station visited in the Firth of Clyde at the time.

A series of 3 model runs are presented. In the first run (run A), parameterisations similar to that of Rippeth & Simpson (1996) were made, with the above alterations. The inflow was set to be proportional to the cross-sill density difference and internal wave mixing was applied to the bottom boundary, as before. In run B the parameterisation is modified, in the light of the new observations (Chapter 5). This involved reducing the internal wave mixing to a constant value, and forcing the rate of inflow to be that estimated from the salt/mass budgets (Figure 5.10). Thus both tunable parameters (ϵ and H_R) are eliminated, so that all the parameterisation has come from either the literature or directly from the observations. Run C is similar to run B, but includes a

parameterisation representing mixing associated with the entrainment of inflowing water. The differences between the runs are summarised in Table 7.1.

RUN	Internal Wave Mixing Mechanism	Entrainment Mixing Included	H-R or Observed Exchange Rate
A	Stigebrandt (1976)	NO	H-R
B	1 x 10^{-5} Wm^{-2}	NO	Observed
C	1 x 10^{-5} Wm^{-2}	YES	Observed

Table 7.1. Summary of differences between the model runs.

7.3 RESULTS.

7.3.1 RUN A - Original Parameterisation.

Run A applies the parameterisation given by Rippeth & Simpson (1996); the cross-sill exchange coefficient, $H_R = 2.0 \times 10^4$, and internal tide mixing efficiency, $\epsilon = 0.18$. This run is equivalent to that presented in Rippeth, Midgley & Simpson (1995). The results are shown in a depth-time plot in Figure 7.2. One striking feature is that the water column is vertically homogeneous below the pycnocline due to the strong internal wave mixing (typically > 1.0 x 10^{-3} Wm^{-2}) applied directly to the bottom. In the summer this mixed layer reaches 20 m from the surface, well above sill depth. The pycnocline is eroded from below, mixing warm, brackish water into the bottom mixed layer. Consequently, the bottom salinity drops over the summer, and the bottom temperature rises.

In contrast, the observed *deep water* has a stratification of ~0.5 kgm^{-3} throughout the summer, and there is no observed summer minimum in bottom salinity (Figure 5.2b). The simulated bottom water temperature peaks, with a minimum in density, near day 280, a month earlier than the observations. This indicates that the rate at which the model mixes heat down the water column is too fast. In the simulation, inflow forces the deep water salinity to rise sharply near day 370, a month earlier than observed.

7.3.2 RUN B - Best Parameterisation from the Observations.

The rate of inflow in run B was taken from the estimate from the salt/mass budgets (Figure 5.9) extrapolated over the observation period and smoothed with a 7 day filter. The mixing associated

with internal waves was assumed constant at 0.01 mWm^{-2}, which is a negligible contribution to the mixing budget (Section 6.3).

The results of run B (Figure 7.3) show that the bottom water is strongly isolated below sill depth throughout the summer (days 120-320), since during this time there is now no significant source of bottom mixing. The summer inflow is confined to the surface 50 m, and is apparent in Figure 7.3 as a weak salinity maximum. A salinity inversion also occurs in the observations at this time, albeit at a greater depth.

Bottom water renewal begins in the autumn (day ~360), resulting in a rise in the bottom salinity. This is associated with a distinct warming of the bottom water (days 360-400), which is not apparent in the observations. This may be due to an overestimate of the wind speed, and consequently an overestimate of the cooling in the Clyde Sea. In the original model, and thus all runs described here, the observed wind speed over land was enhanced by 30% to estimate its value over the sea (following Lavin-Peregrin, 1984). However, the Clyde Sea is relatively sheltered in comparison to the Irish Sea (where the original observations were made), and consequently this factor may be too large.

7.3.3 RUN C - The Inclusion of Entrainment Mixing.

A mechanism was required to warm the bottom waters over the summer months. A clue to the character of this mechanism comes from the observed summer time rise in salinity at 100 m at MCS8. A salinity rise indicates the occurrence of an inflow. At this time of year, the North Channel water is significantly warmer than the Clyde Sea bottom water, since it is well mixed. As discussed in Section 5.3, the observed temperature and salinity at the depth of this observed inflow indicate a very approximate 50 : 50 mix of North Channel and Clyde Sea bottom water. The energy to do this mixing has not originated from the potential energy released when the saline water enters the basin, since the inflow is neutrally buoyant at sill depth. Indeed, a source of mixing energy is required to mix the buoyant inflow downwards. All that is known is that much of this mixing occurred between the sill and the mooring sites, perhaps in the vicinity of the sill. This is outside the domain of the simple box model, which represents a typical point within the basin. In order to incorporate the energy involved in this mixing into the model, a parameterisation representing this mechanism must be introduced.

To this end, a subroutine was added to the model which represents this mixing, and yet makes no assumptions on how it occurred. The energy that mixed the buoyant water down can be estimated from the vertical mass/salinity budget: In the subroutine, a calculation is made of the

density of water which is created when water from the North Channel and the bottom of the Clyde Sea mix in a 50:50 ratio. The level at which this water would be neutrally buoyant was then calculated, and the North Channel inflow was injected into the basin at this depth. During the summer months, this inflow is lighter than the water at the depth of entry, and so mixes upwards. The energy associated with this mixing would be similar to that which must have mixed the observed inflow downwards. Thus, a crude parameterisation for the mixing associated with the entrainment of inflow at times when the inflow is at mid-depths is included in the model. At times when the inflow entered the basin as a bottom current, the mixing energy was estimated from the potential energy released, as in runs A and B.

The results from run C, which incorporates this, 'entrainment mixing' show a significant improvement in the reproduction of the observed deep water properties (Figure 7.4). The results display a continual warming of the bottom waters throughout the summer, yet still retain a deep water stratification similar to that observed. The seasonal minimum in bottom density now occurs near day 340, a week or two later than the observations, the difference possibly resulting from the overestimate of the surface wind mixing, as discussed above. The observed summertime deep water salinity maximum is reproduced well. A salinity inversion at ~100 m is created in the height of summer, similarly to that observed.

Many of the surface salinity features are also well reproduced. Deep mixing occurred following the storm on day 400, as observed, but is too persistent. Following a storm, in the real Clyde, horizontal gradients will relax under estuarine forcing to quickly re-establish stratification, a process not included in the model (Rippeth & Simpson, 1996).

7.4 SUMMARY.

The filling box model of Simpson & Rippeth (1993) has been developed here by the modification of the internal wave mixing mechanism, and the forcing of the inflow to follow the observations. The original version of the model, presented by Rippeth *et al.* (1995), does not reproduce the seasonal variation in salinity, indicating that the physical processes are incompletely represented in the model. In this simulation, the bottom waters in the summer are homogeneous beneath 20 m indicating that too much bottom water mixing was included. The model was then forced with the observed rate of cross-sill exchange, and with the estimate of internal wave mixing made from the new observations. The surface waters became more similar to the observations, with the pycnocline depth increasing to ~ 50 m. However, the bottom waters in the summer remained strongly isolated, as in the original run of Simpson & Rippeth (1993).

A simple parameterisation of the mixing associated with entrainment into inflows at mid-depths was incorporated into the model, which made no assumptions of the character of the mixing mechanism, but was based on the observed properties of the inflow. The result was that for the first time many of the observed features in the deep water were reproduced. However, this new version of the model is no longer independently reproducing the seasonal cycle in the Clyde Sea, as it requires estimates of the observed exchange, and, therefore, it cannot be applied to other periods or fjords. It does however show that the process of entrainment is important at times when the inflow is at mid-depths, and aids the visualisation of this process.

There are two significant features in the observations which are not well reproduced by the model. Firstly, the summer time deep water temperature and salinity are typically 1.0 °C and 0.3 psu lower than those observed, respectively. Secondly, the observed isopycnals are significantly more diffuse than in any of the model runs. These features possibly result from the combination of two simplifications used in the model. Firstly, the surface water outflow is taken entirely from the surface layer, which is the freshest, and in the summer, the warmest, rather than including contributions from other layers down to sill depth, and thus is likely to overestimate the outflux of heat and freshwater. Secondly, other mixing mechanisms may together result in a significant amount of mixing, but are difficult to quantify. These include mixing associated with wind driven motions, flow over complex topography, and shear flows associated with the estuarine circulation.

These results indicate that Hansen-Rattray type exchange applied to the 1-dimensional model, does not account for the observed exchange, such as the increased summer inflow. This will be discussed in later Chapters, following further observational and modelling results.

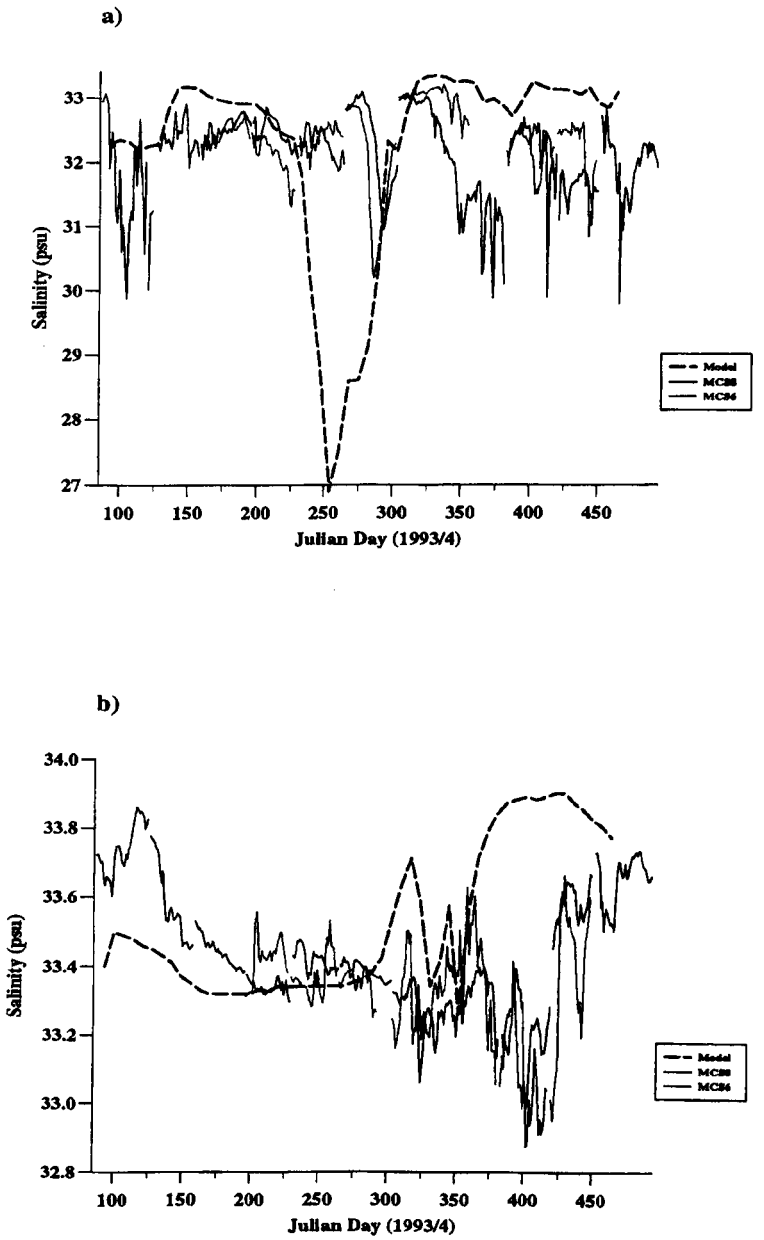

Figure 7.1. Comparison of the hindcast model of Rippeth *et al.* (1995) with the observations at the mooring sites (a) surface salinity (RCMs 60 and 80), and (b) bottom salinity (RCMs 64 and 83).

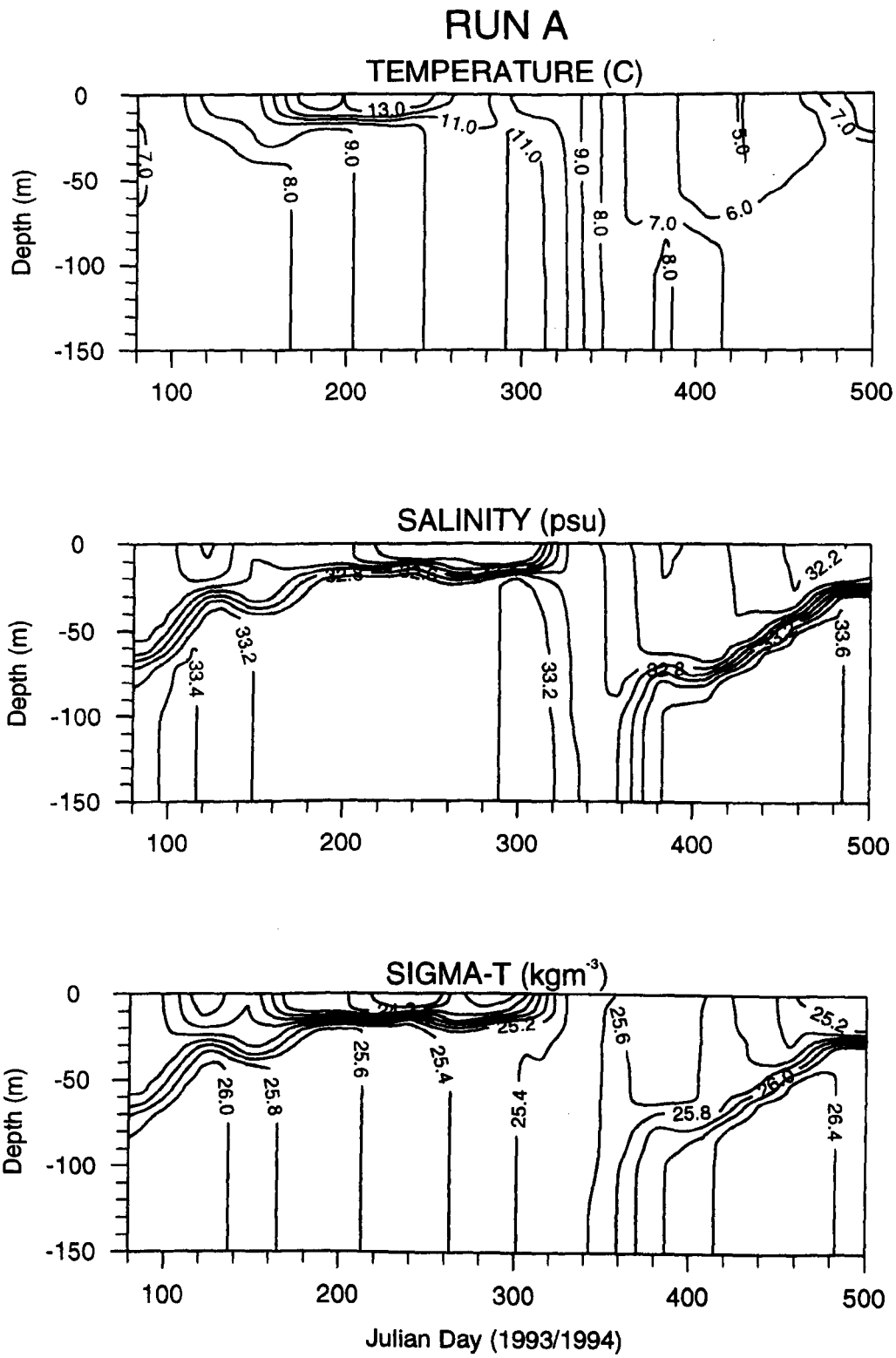

Figure 7.2. RUN A. The original parameterisation. Depth/time plots of temperature, salinity and σ_t.

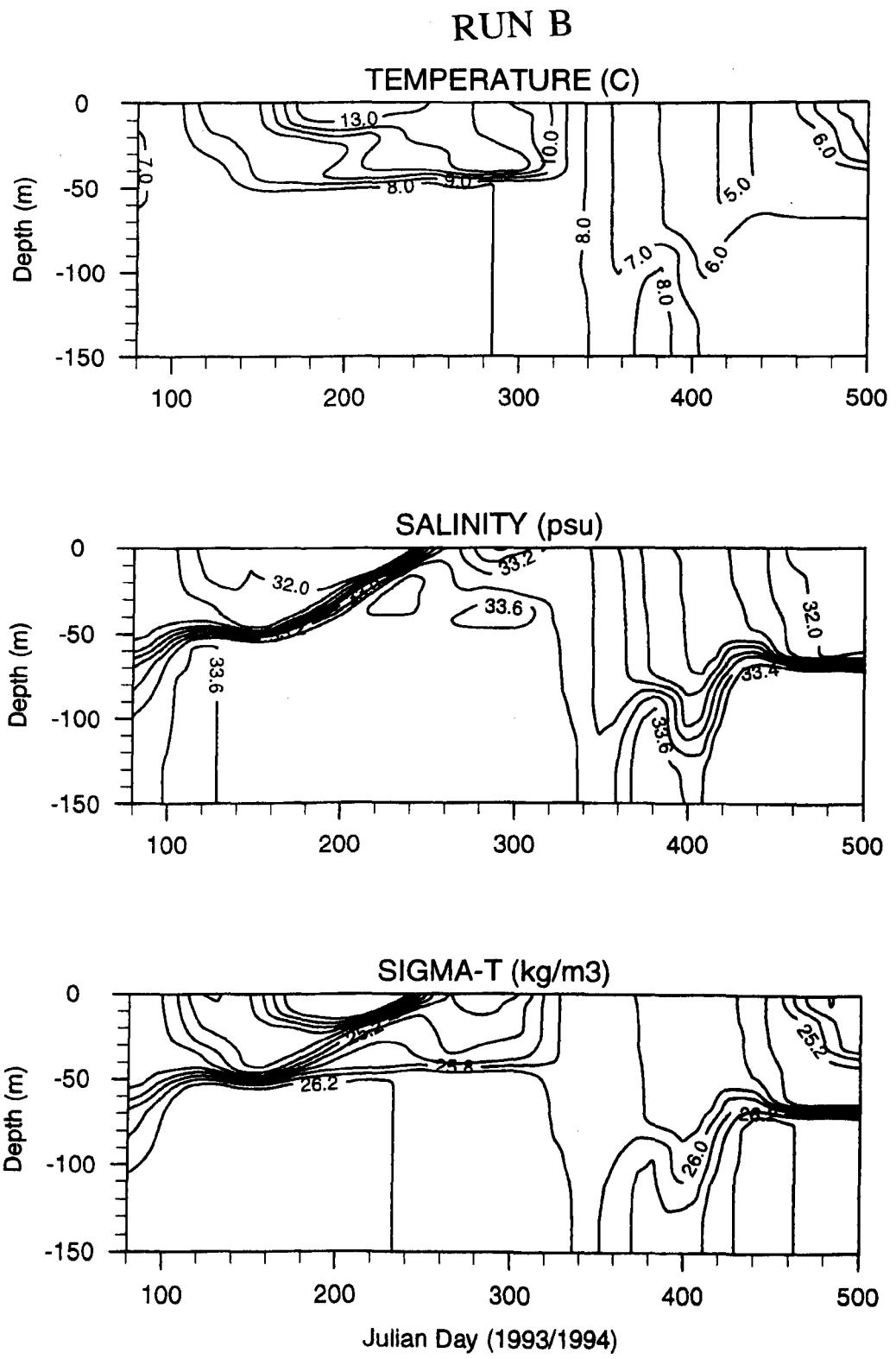

Figure 7.3. RUN B. The best parameterisation from the observations. Depth/time plots of temperature, salinity and σ_t.

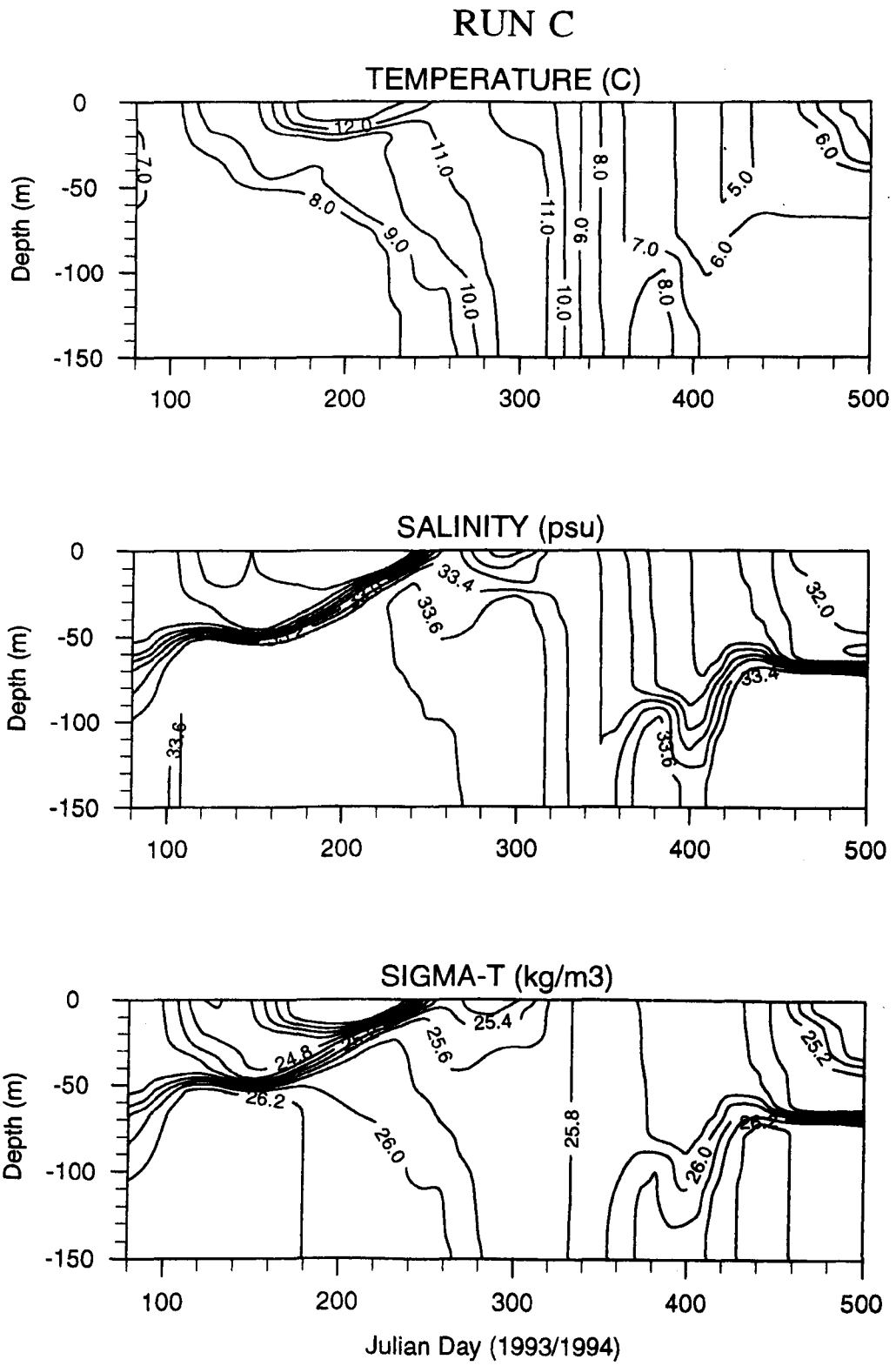

Figure 7.4. RUN C. The inclusion of entrainment mixing. Depth/time plots of temperature, salinity and σ_t.

CHAPTER 8. SILL DYNAMICS; OBSERVATIONS AND INFERENCES.

8.1 INTRODUCTION.

Edwards *et al.* (1986) described a front over the sill which divided the weak estuarine flow in the basin from the tidally well mixed North Channel. They argued that the front was in near geostrophic balance, and so the majority of exchange would occur in the frictional zone near the coasts. The new observations have shown that the exchange rate is variable throughout the year, with maxima in the early spring and the late summer (Section 5.8). If the exchange was solely driven by the density difference between the North Channel and basin bottom waters, it would peak in the winter, when the freshwater inflow is greatest, and be a minimum in the summer. Evidently, there are additional factors which effect the rate of exchange.

To gain further insight into the dynamics of the sill region, new observations were required. The aim was to make observations at times of both high and low cross sill exchange; the seasonal observations described in Chapter 5 indicated that March and September 1995 were such times.

In the following sections, the y-axis and v-component of velocity are defined as positive into the Clyde Sea, and the x-axis and u-component of velocity are positive eastward along the sill.

8.2 EXPERIMENTAL STRATEGY.

On both cruises, observations with shipborne ADCP and CTD were taken on a transect along the sill (stations A-E, Figure 3.1), over a 50 hour spring tide period (18-20/3/1995 and 12-14/9/1995). To calculate the residual water velocity from the ADCP observations, the ship's motion must be subtracted from the observations, which, since it may be ~4 ms^{-1} in comparison to expected water speeds of ~1-10 cms^{-1}, will increase the uncertainty in the data. In order that this be minimised, the ship stopped at each station for a 15 minute period. The enhanced accuracy of this procedure, over the alternative of trailing an undulating CTD along the section, is off-set against the disadvantage of reducing the spatial resolution. Each pass of the transect took ~6 hours, thus achieving a data set of sufficient resolution to remove the semi-diurnal tide. To avoid sample aliassing with the semi-diurnal tide, on occasions it was necessary to stop the ship for an hour at station E.

On the March cruise, in order to investigate the temporal variation of the inflow and possible interaction with the tide, observations were taken alternately at stations D and F, in a similar manner to the transect experiment. These observations continued over 3 tidal cycles between

18:45 21/3/1995 - 08:30 23/3/1995, which was approximately 3 days after the transect experiment.

On the September cruise, a cross-sill section was made to complement the along-sill data by observing the spatial distribution of frontal flows, and investigating possible interactions between the deep water in the Clyde Sea and internal waves at the sill. Over a 24 hour period, 6 passes along a cross-sill transect between CS1 and CS5 (Figure 3.1) were made using the shipborne ADCP and the SEAROVER undulating CTD. On 12/9/1995 two drogues were released in the sill region and tracked during the cruise.

8.3 OBSERVATIONS OF TIDAL OSCILLATIONS.

The ADCP observations at each of the stations along the transect, were fitted, in a least-squares sense, to a semi-diurnal tide of period 12.3 hours (Section 4.3). The amplitude and phase of these observed tides show a high degree of coherence between the March and September cruises (Figures 8.1, 8.2), indicating the success of the experimental procedure. In both cases, the semi-diurnal velocity amplitude increased from ~20 cms^{-1} in the east to ~60 cms^{-1} in the west, with the phase in the west lagging ~60° behind the east. Consequently, tidal stresses will increase by almost an order of magnitude towards the west. The major axis was orientated roughly perpendicular to the sill, with a rotational shift of ~10° anti-clockwise towards the shallow water at both extremes of the section. In comparison, the depth average model of Elliott *et al.* (1992) indicates little amplitude variation across the sill, and a phase change of less than 30° (Figure 2.7).

On both cruises, the residual and the semi-diurnal tide explained 70-80% of the total variance for both cross and along transect flows, with the exception of station E, where only ~50% was explained, indicating that variations on other time scales occur towards the extreme east of the section.

8.4 OBSERVATIONS AT HIGH RATE OF EXCHANGE (MARCH).

During the along-sill transect experiment the wind was very steady and averaged 7 ms^{-1} from 290°, which is roughly parallel to the sill. Later, during the observations at D and F, the wind was steady 9 ms^{-1}, 200°, which is directly into the Clyde Sea. The well mixed waters at CS17 (Figure 3.1), taken as representative of the North Channel, had temperature 7.17 °C and salinity 34.02 psu. The bottom water properties in the Clyde Sea were obtained from CTD profiles taken

at CS7 and CS8, to be temperature 7.1 °C and salinity 33.7 psu.

8.4.1 THE ALONG-SILL TRANSECT.

Any semi-diurnal oscillation was removed from the CTD observations by least-squares analysis, in a similar fashion to the ADCP data. The results revealed that the coolest and least saline water occurred near the surface to the east of the transect (Figure 8.3a-c). The maxima in both salinity and temperature were observed at the bottom in the deepest part of the section, between stations C and D, where the values were close to those observed in the North Channel, thus indicating their origin. The stratification was minimum in the west at <0.2 kgm^{-3}, and increased eastward to a maximum of ~1.2 kgm^{-3} at station D, where there was a strong halocline at 35 m. This may in part be due to the increased tidal amplitude and shallower water to the west. The internal Rossby radius increases from <1 km at A to ~2.1 km at C and D. It is interesting to note that the minimum of depth mean salinity was found in the middle of the transect, at station C, even though saline North Channel water was observed at the bottom here. This indicates that fresh water is not freely moving westward.

Over the period of the survey, the cross-sill residual had a maximum inflow at the bottom in the east of ~10 cms^{-1}, while outflow had a maximum at the surface in the west, also ~10 cms^{-1} (Figure 8.4a). This suggests a simple estuarine circulation modified by the rotation of the Earth. By individually estimating the rates of inflow and outflow across the transect from Figure 8.4a, the rate of cross-sill exchange was estimated to be $4.2 \pm 0.8 \times 10^4 m^3 s^{-1}$. If this rate of exchange were persistent, the entire Clyde Sea would flush in about 30 days.

Along-sill residual currents speeds are generally low (< 8 cms^{-1}) (figure 8.4b). They show an eastward (+ve) residual current east of station B, a direction opposite to that expected from the frontal jet.

8.4.2 THE OBSERVATIONS AT STATIONS D AND F.

The observed temperature and salinity were similar at D and F (Figure 8.5). Surface minima are observed both in salinity and temperature 2 hours after the low tide, presumably at a time when the tide was near its maximum outward excursion. These minima were less saline and cooler than those observed in the transect experiment 3 days earlier, and became progressively fresher and cooler over the observation period.

The semi- and quarter-diurnal tides were removed from the ADCP observations, and the residuals plotted along the vertical mean axis of the semi-diurnal tide (51^0 at D, 42^0 at F; Figure 8.6). Changes in the residuals along the major axis show little temporal correlation, even though they are only 4.1 km apart (Figures 8.6a,c). Periods of enhanced inflow and outflow at D and F neither correlate nor anti-correlate. At F the observed bottom inflows decrease over the observation period from about 8 cms^{-1} to near zero, whilst at D the inflow remains in the range 0-4 cms^{-1}, with no obvious trend. The strong bottom inflow observed on the transect was not observed at either D or F during this experiment.

The residual flows along the minor axis show similar temporal variations at both D and F, indicating that the front moves through both stations at similar times (Figures 8.6b,d).

The mean residual velocity shear along the sill at both F and D is 11 cms^{-1} over 35 m (Figure 8.7). Assuming geostrophy this implies a gradient ~4.0 x 10^{-5} kgm^{-4}. The CTD surveys show that cross-sill gradients are 3-4 x 10^{-5} kgm^{-4}, indicating that the frontal jet is close to geostrophic balance. Residuals along the major axes showed a net inflow of ~2 cms^{-1} at F, and an outflow at D of ~3 cms^{-1} above 35 m.

The percentage of variance explained by the analysis for the cross-sill component of current was 80-85% at both D and F. Similar values were found for the along-sill components below 30 m. Above 30 m, the explained variance dropped to ~50%, indicating that variations occur on other time scales.

8.5 OBSERVATIONS AT LOW RATE OF EXCHANGE (SEPTEMBER).

The North Channel conditions, estimated from a CTD profile at CS17, were temperature 14.53 °C and salinity 34.06 psu. A CTD profile in the interior of the basin at CS7 (Figure 3.1) showed an enhanced salinity at 45 m, the depth of the thermocline, indicating that inflow was restricted to the surface waters (Figure 8.8). During the along-sill transect observations the wind was variable, but averaged 5 ms^{-1} from the south-west. Later, during the cross-sill observations, the wind was from the north and averaged 4 ms^{-1}.

8.5.1 THE ALONG-SILL TRANSECT.

The along-sill transect density profile was similar to that in March in that stratification was minimum west of station B at <0.2 kgm^{-3}, and was maximum over stations C and D, although

the maximum stratification was only ~0.8 kgm^{-3} (Figure 8.9). However the pycnocline was more diffuse and higher in the water column than in March, possibly as a result of the lower wind speeds occurring at this time. The temperature and salinity profiles differed significantly from those observed in March. On either side of station C, the observed salinity below 20 m was ~33.8 psu, which was as high as the maximum bottom salinity observed in March. This is an indicator of the presence of North Channel water, and was probably due to the summer retreat of the front into the basin, following months of low freshwater runoff.

The least saline surface water was observed at the surface at station C (Figure 8.9). A slight salinity inversion also exists at C, with the salinity decreasing below 30 m, while a strong thermal stratification (1 °C in 20 m) stabilised the water column. The bottom water was too cold (12.8 °C) to be of North Channel origin, and can only have originated from the Clyde Sea deep. Its salinity was consistent with being of this origin.

Analysis of the thermal wind shear showed a vertical velocity difference down the water column of ~7 cms^{-1} in the western extreme. The cross-sill ADCP residuals showed a 5 cms^{-1} vertical velocity difference west of station A, resulting in a surface inflow which was in approximate geostrophic balance (Figure 8.10a). In other parts, the cross-sill residuals were weak (<4 cms^{-1}). The Clyde Sea deep water observed near the bottom at station C was apparently outflowing at ~2 cms^{-1}. The rate of cross-sill exchange was estimated from Figure 8.10a, to be $1.2 \pm 0.5 \times 10^4$ m^3s^{-1}. The along-sill residuals were also weak (<4 cms^{-1}) and show divergence between stations C and D (Figure 8.10b).

8.5.2 THE ACROSS-SILL TRANSECT.

The across-sill transect between CS1 and CS5 revealed three distinguishable water masses; (i) fully mixed warm saline North Channel water near CS1, and within the Clyde Sea, (ii) warm brackish surface waters, and (iii) cool deep water of intermediate salinity (Figure 8.11a-c). An increase in the salinity and temperature between 35-50 m in the northern extreme of the section, is indicative of North Channel water. The cool Clyde Sea deep water appeared to have been upwelled onto the sill, which was consistent with the along-sill observations.

Analysis of the thermal wind (Figure 8.11d) shows the frontal jet as a vertical velocity difference of -15 cms^{-1} above the sill. Behind the front, within the Clyde, the thermal wind reversed with a vertical velocity difference of +8 cms^{-1}. Flows on the North Channel side of the frontal region were barotropic. Residual flows from the ADCP observations across the section (Figure 8.11e) showed considerable similarity with the geostrophic picture (Figure 8.11d). The jet was

positioned above the sill, but had a vertical velocity difference a factor of two smaller than the geostrophic estimate. There was a residual reverse flow within the basin, which was also lower than the geostrophic estimate, but extended further northwards to CS5. A barotropic residual was observed at CS1. This flowed parallel to the sill at ~5 cms^{-1}, towards the Rhins of Galloway.

8.5.3 THE DROGUES.

The drogues, set at 23 m, were tracked over much of the September cruise. Drogue 3947, released at 55^0 20.0' N 5^0 12.0' W, ~10 km north of CS3, at 04:55 12/9/1995 followed a south-easterly trajectory for 7 days, when it became grounded near the Ayrshire coast (Figure 8.12a). Drogue 3945, released at CS3 at 05:15 12/9/1995, during a 9 day trajectory, almost completed a full clockwise rotation over the sill region (Figure 8.12b).

8.6 SUMMARY AND DISCUSSION.

Many similarities were observed in the flow structure in March and September 1995, although the rates of exchange were estimated to be very different. In March, a relatively rapid cross-sill exchange was observed (flows ~10 cms^{-1}), which appeared to be essentially estuarine, and influenced by rotation. In contrast, the September cross-sill flows were weak (<4 cms^{-1}) and spatially complex.

From the September observations a conceptual picture of the dynamical structure of the front may be constructed (Figure 8.13). Along the sill the Ekman number decreases from about 0.4 in the west to 0.2 in the east, indicating the increasingly important role of friction in controlling the dynamics towards the west of the sill. The surface flow may be expected to flow out of the basin as it approaches the frictional influence of the coast, with compensating inflow elsewhere, in an estuarine fashion. However, this inflow is partially blocked by the sill, and so much of the surface flow is drawn back into the Clyde basin. Some of this water is then re-circulated, to once again join the frontal jet near the Ayrshire coast, completing a clockwise gyre. Friction induces downwelling in this gyre, which traps buoyant surface water, bringing the density structure closer to a geostrophic balance.

If the estuarine forcing were enhanced due to an increase of freshwater runoff, the frontal gradient would become stronger, with a relative acceleration of the frontal jet. By continuity, the compensating back flow would then be enhanced, and so the gyre would become stronger. The trajectory of drogue 3945 (Figure 8.12b) clearly illustrates this flow structure and its temporal

stability.

The dynamical structure in March was similar to that in September, except that the front and centre of the gyre were located further out to sea, as expected due the relatively large inflow of freshwater into the Clyde during the winter. Additionally, during the March along-sill observations, an enhanced estuarine exchange influenced by rotation was detected. The vertically homogeneous waters to the west outflowed, whilst inflow was concentrated towards the bottom in the east, below the pycnocline. The strong pycnocline, typical of winter months, acted to decouple the bottom inflow from the flows above, so that the observed surface flow structure to the east remained similar to that observed in September.

The rate of exchange inferred from the along-sill observations in March was found to be similar to the peak spring exchange rate deduced from the salinity/mass budgets. However, these rapid exchange flows were not observed 3 days later, at stations D and F, and over the following 3 semi-diurnal tidal cycles, fresh, cool water was observed to gradually accumulate behind the front.

It is suggested that these changes in the exchange rate were the result of changes in the wind direction. During the March along-sill observations, a 7 ms^{-1} wind blew along the sill from the west, whilst 3 days later, a 9 ms^{-1} wind blew directly into the basin. A wind blowing along the sill may tend to drive a surface Ekman flow out of the basin, reinforcing the estuarine flow, whilst a wind blowing into the basin may directly retard the outflow of the surface waters. This phenomena will be discussed in more detail during the modelling study in the next chapter.

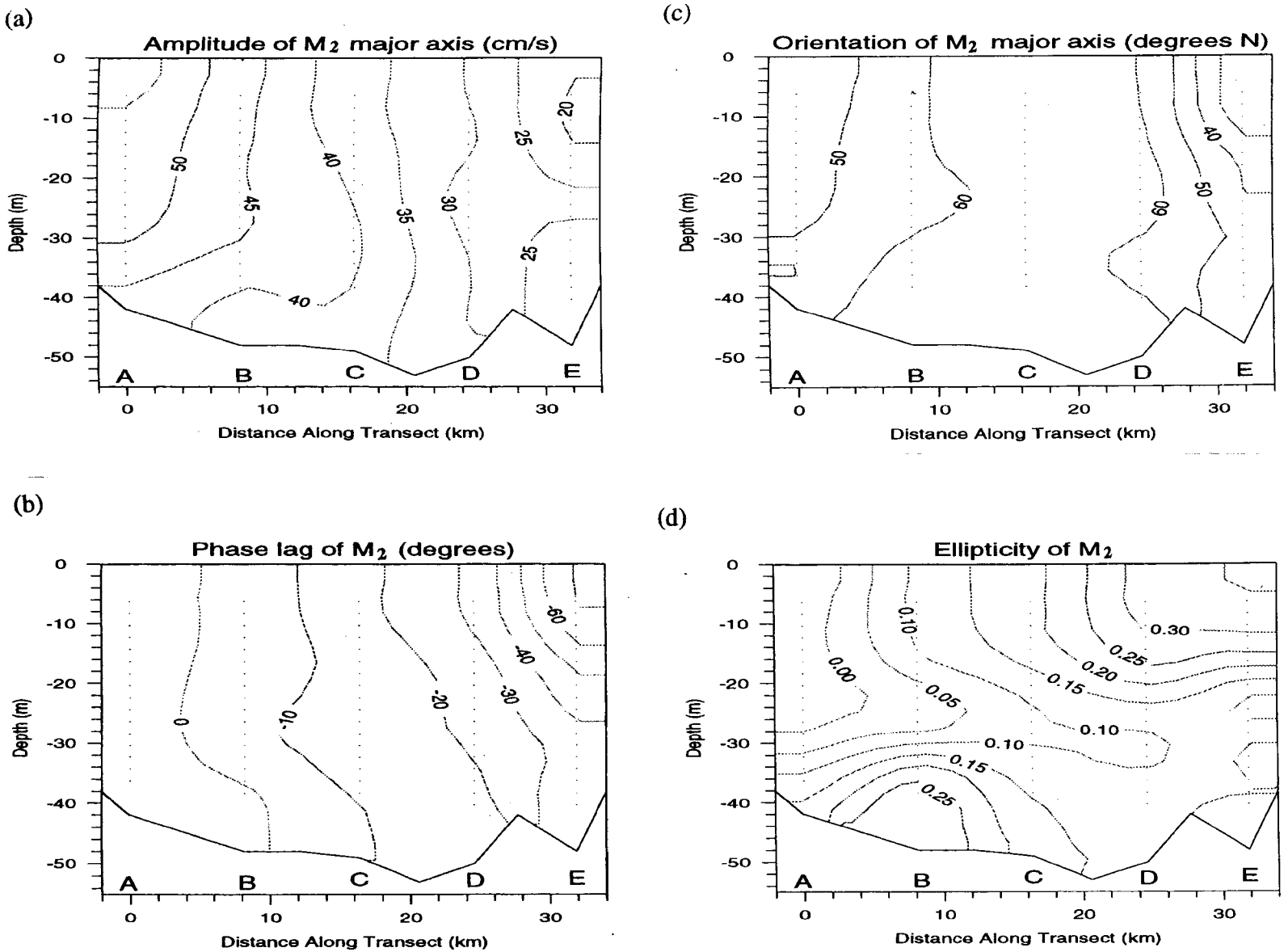

Figure 8.1. Observations of the semi-diurnal tide from the March 1995 transect along the sill. The transect is orientated to face into the Clyde Sea, with positive flows into the basin. (a) Velocity amplitude along the major axis (cms^{-1}); (b) phase; (c) orientation of the major axis (degrees North); and (d) ellipticity.

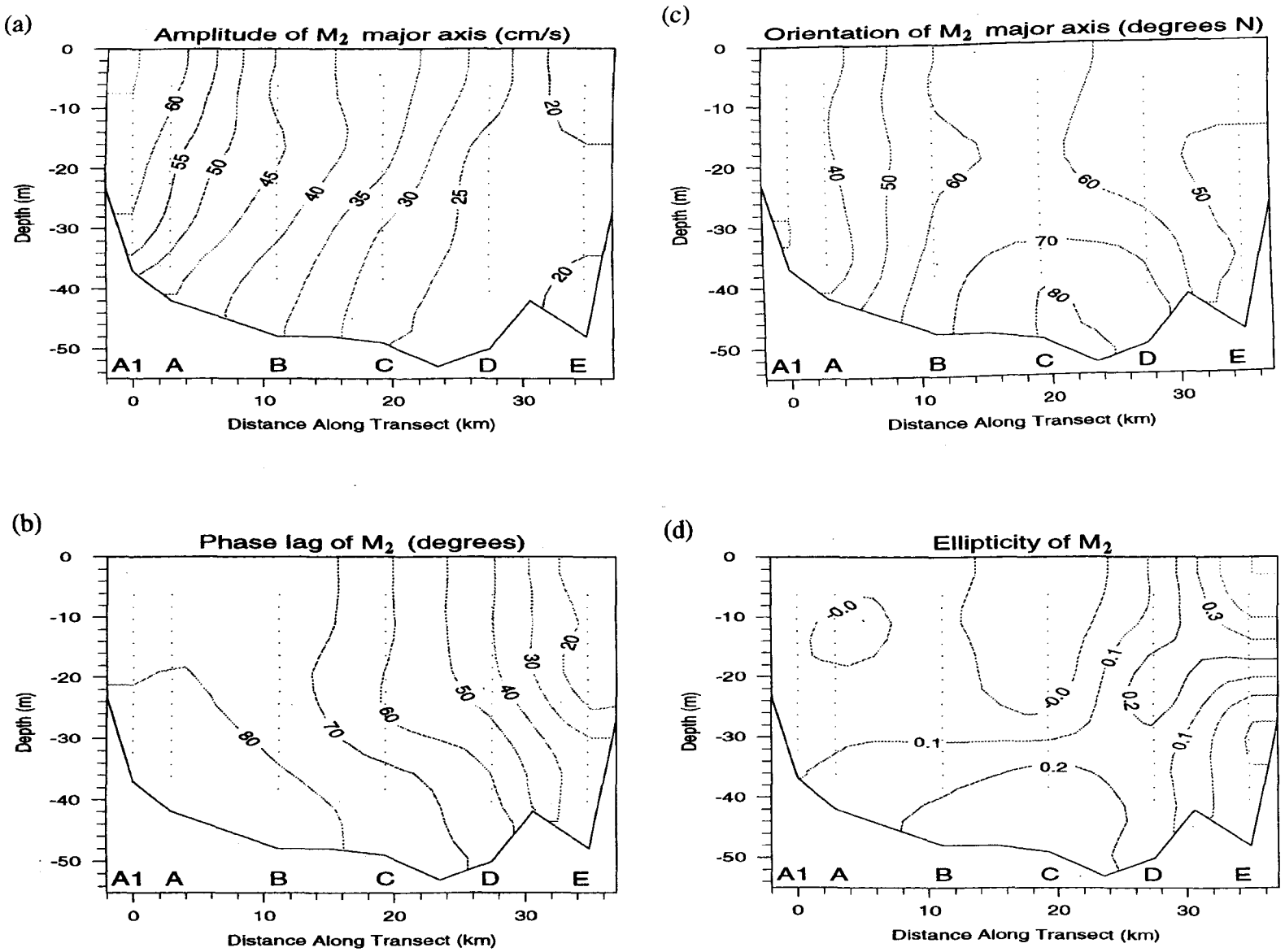

Figure 8.2. Observations of the semi-diurnal tide, from the September 1995 transect along the sill. The transect is orientated to face into the Clyde Sea, with positive flows into the basin. (a) Velocity amplitude along the major axis (cms^{-1}); (b) phase; (c) orientation of the *major axis (degrees North)*; and (d) *ellipticity*.

(a) Temperature (°C)

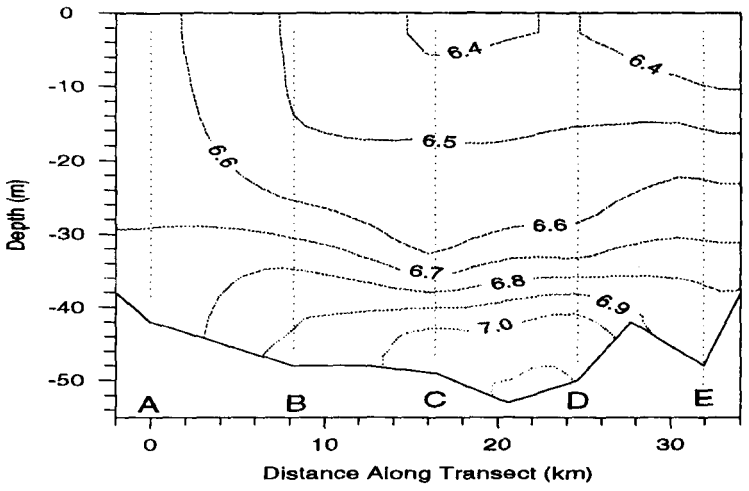

(b) Salinity (psu)

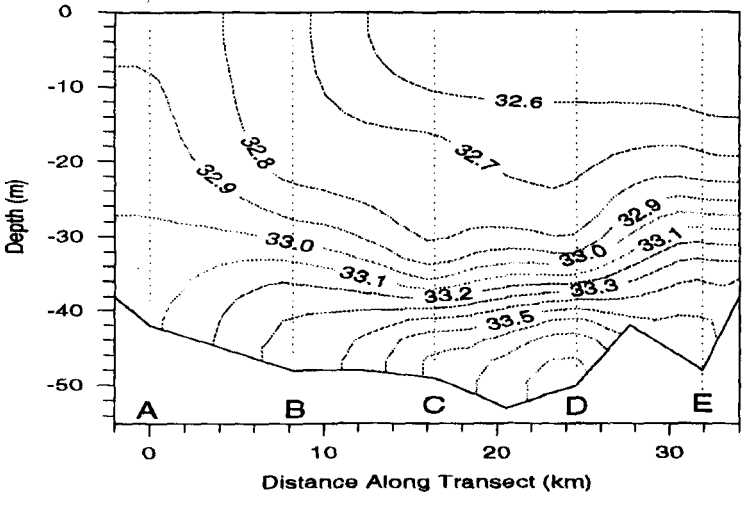

(c) Sigma-t (kgm^{-3})

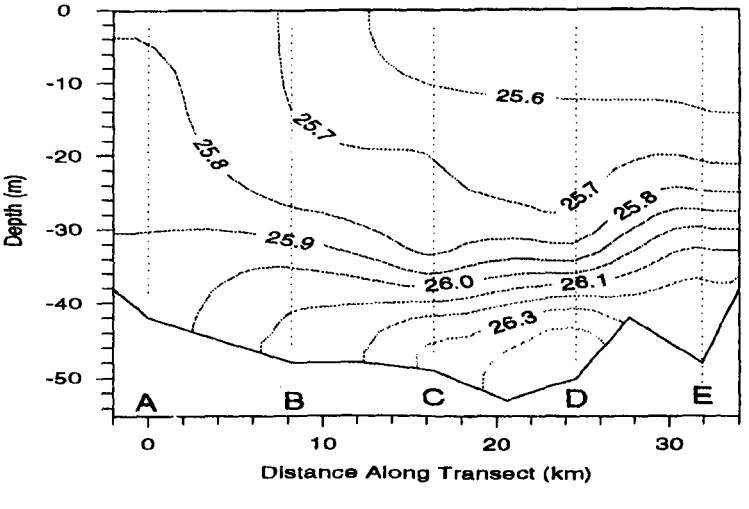

Figure 8.3. Observations from the March 1995 transect along the sill, after removal of semi-diurnal oscillations by tidal analysis. The transect is orientated to face into the Clyde Sea, with positive flows into the basin. (a) Temperature (°C); (b) salinity (psu); and (c) sigma-t (kgm^{-3}).

(a)

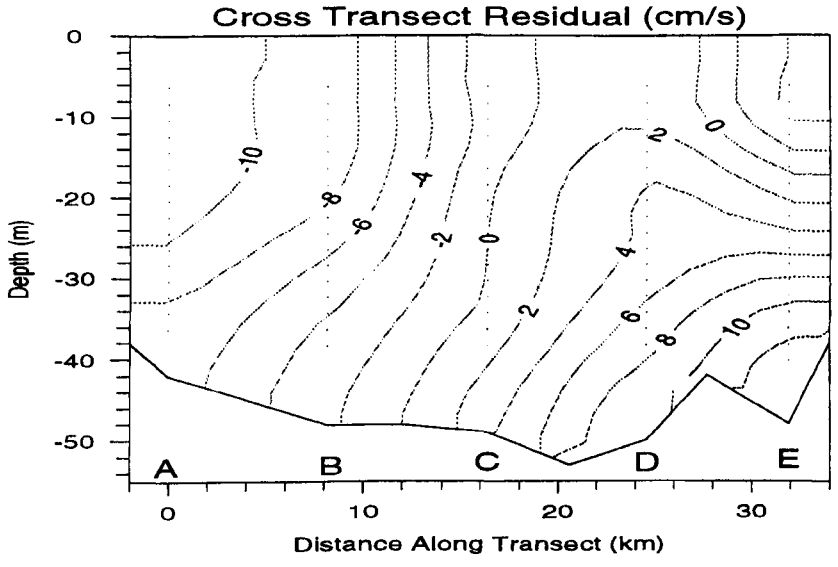

(b)

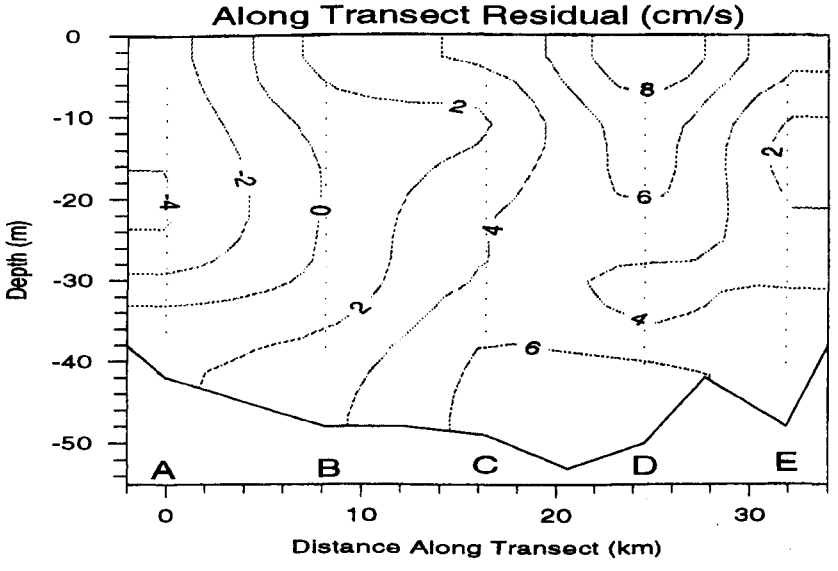

Figure 8.4. Observations of the residual currents, from the March 1995 transect along the sill. The transect is orientated to face into the Clyde Sea, with positive flows into the basin. (a) Cross-transect residual (cms^{-1}); and (b) along transect residual (cms^{-1}).

(a)

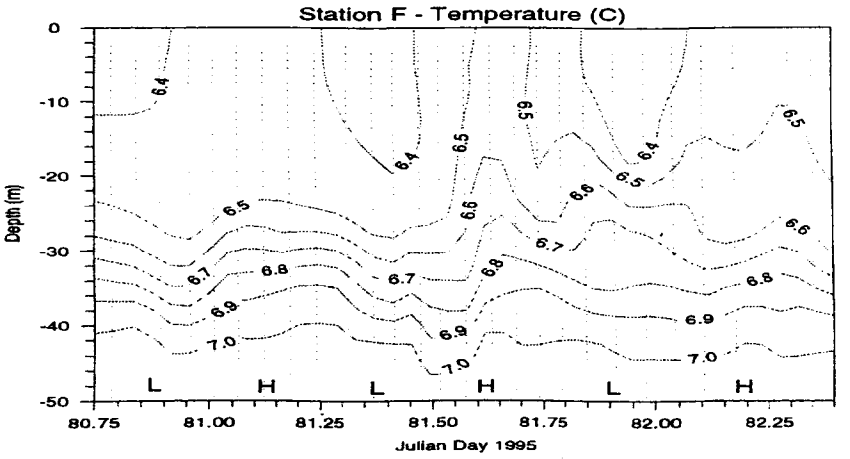

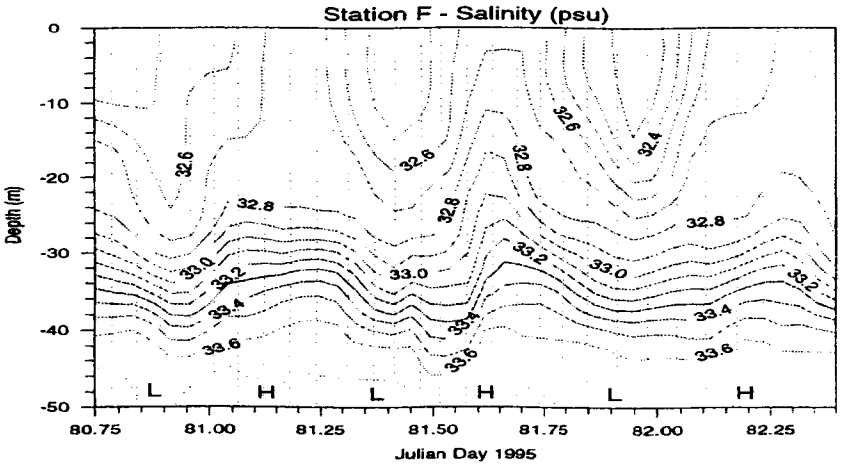

(b)

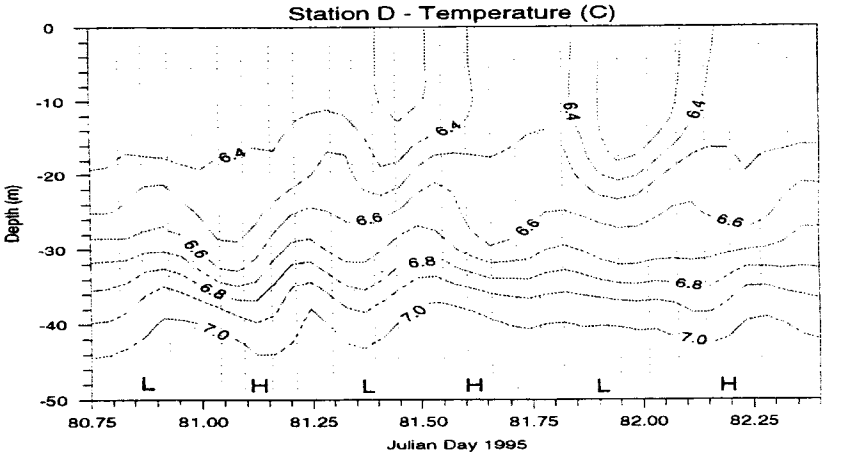

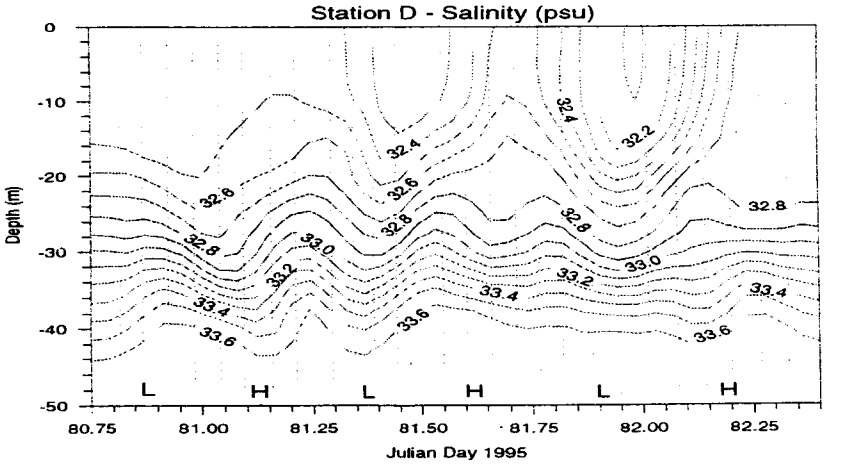

Figure 8.5. Temperature and salinity depth/time plots at (a) station F; (b) station D.

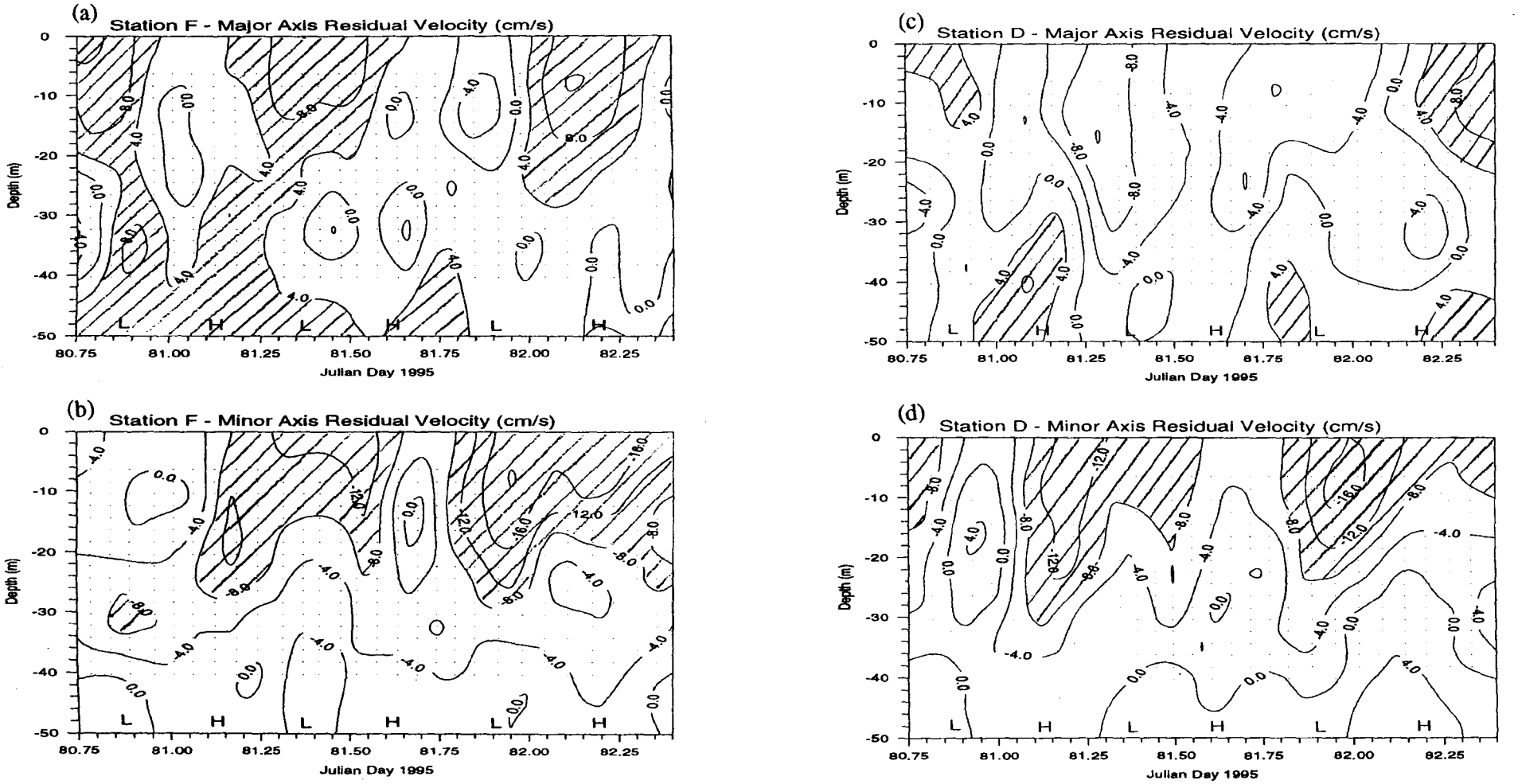

Figure 8.6. Residual velocities after the removal of the semi- and quarter-diurnal tides (cms^{-1}) at station F; (a) along the major axis; (b) along the minor axis, and station D; (c) along the major axis; (d) along the minor axis.

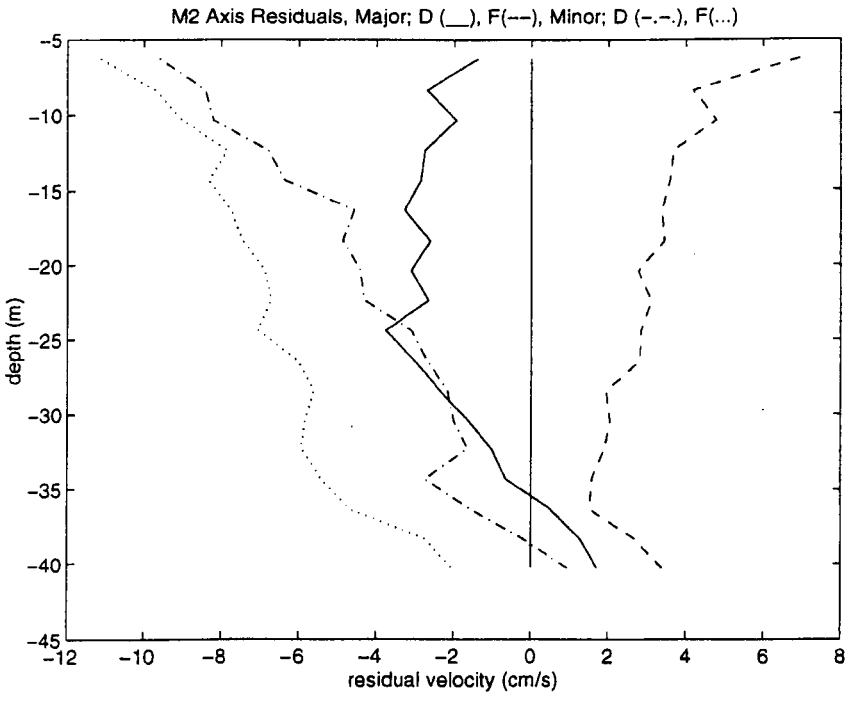

Figure 8.7. Average residual velocity over the 3 tidal cycles at station D; along the major axis, 40° (__); along the minor axis, 220° (-.-.), and at station F; along the major axix, 33° (---); along the minor axis, 210° (....). Positive is defined into the sill and towards the Ayreshire coast.

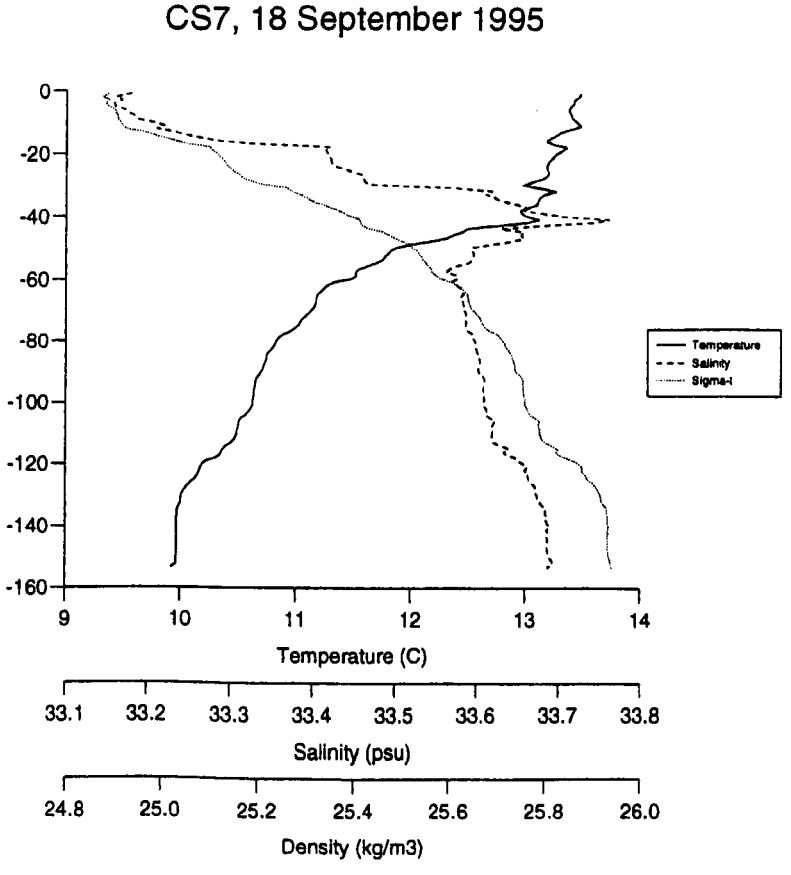

Figure 8.8. CTD profile at CS7 on 18th September 1995. Taken as being representative of conditions within the Clyde Sea basin.

(a) Temperature (°C)

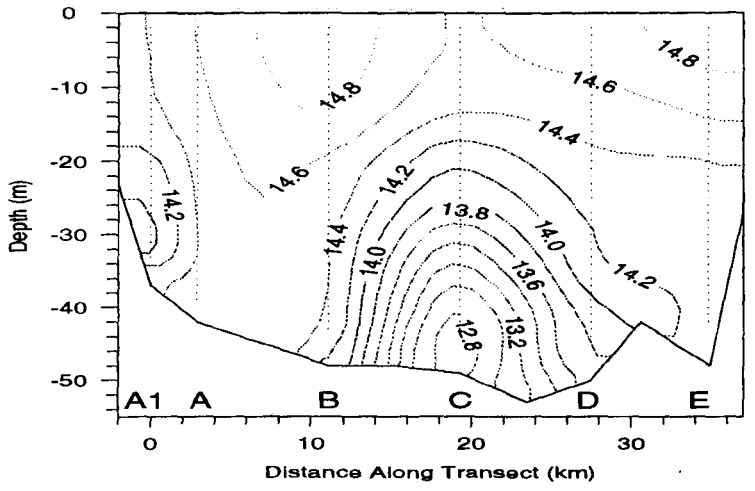

(b) Salinity (psu)

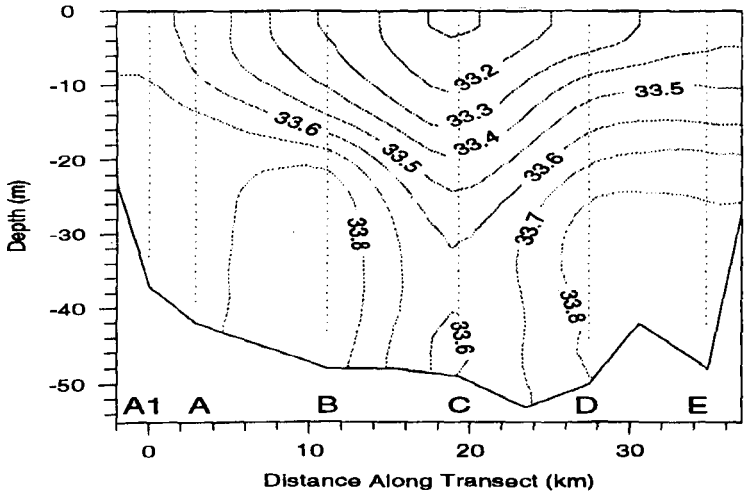

(c) Sigma-t (kgm^{-3})

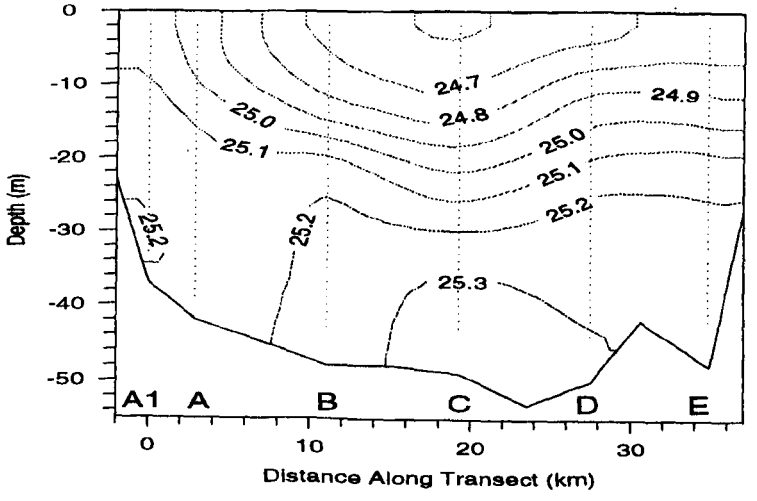

Figure 8.9. Observations from the September 1995 transect along the sill, after removal of semi-diurnal oscillations by tidal analysis. The transect is orientated to face into the Clyde Sea, with positive flows into the basin. (a) Temperature (°C); (b) salinity (psu); and (c) sigma-t (kgm^{-3}).

(a)

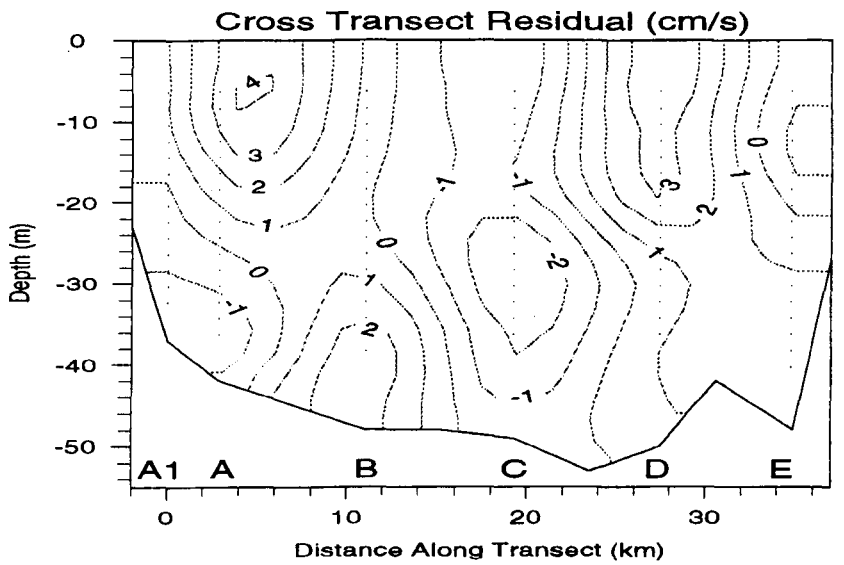

(b)

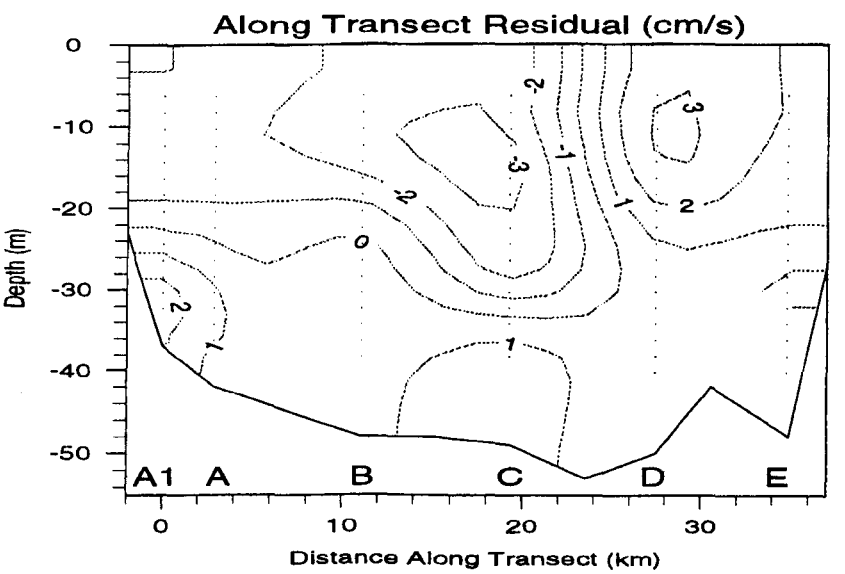

Figure 8.10. Observations of the residual currents, from the September 1995 transect along the sill. The transect is orientated to face into the Clyde Sea, with positive flows into the basin. (a) Cross-transect residual (cms^{-1}); and (b) along transect residual (cms^{-1}).

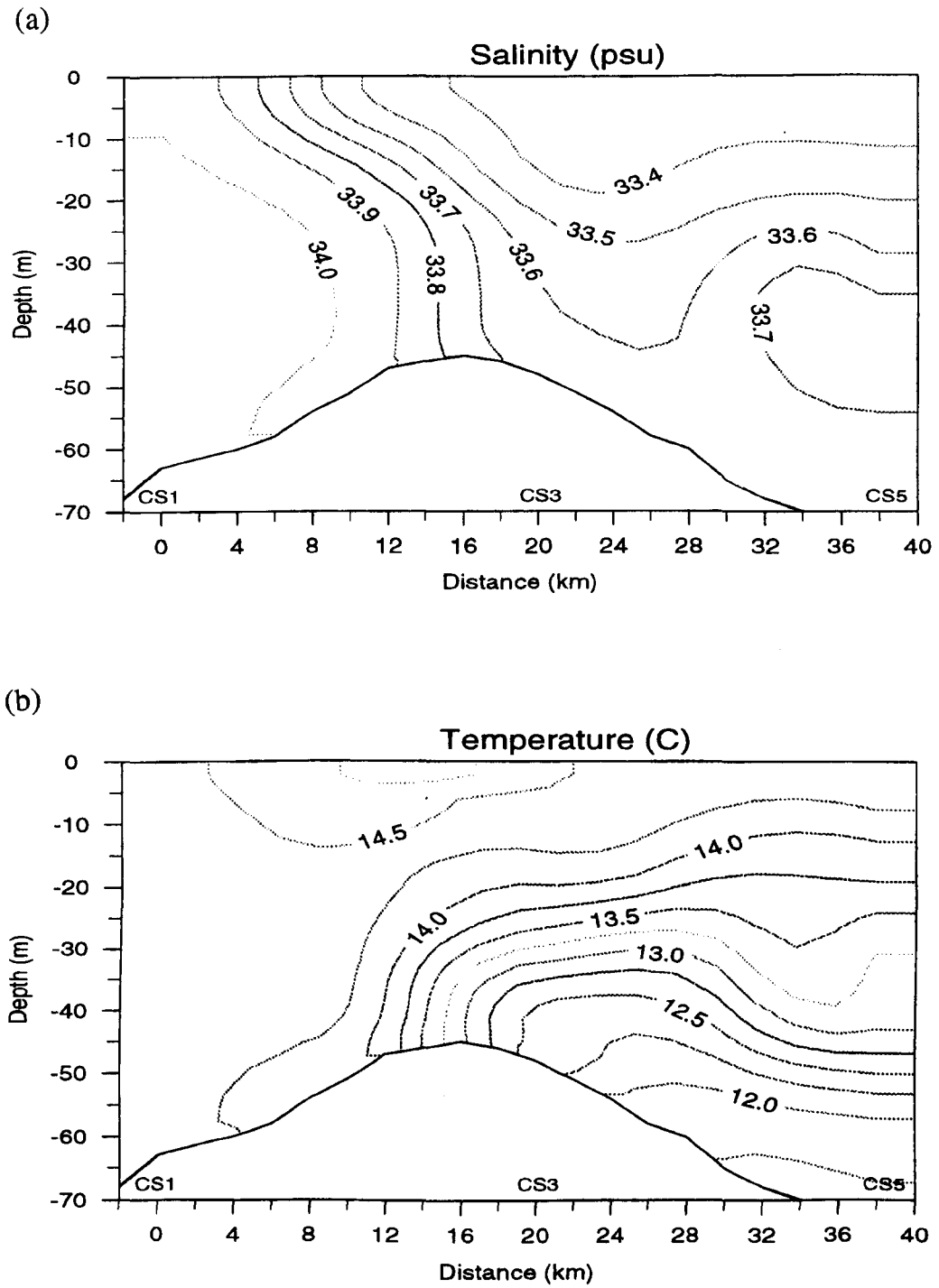

Figure 8.11. Cross-sill transect in September 1995 cruise. The North Channel is on the left and positive flows are into the basin. (a) Non-tidal salinity; (b) non-tidal temperature; (c) non-tidal σ_t; (d) the thermal wind shear, with zero bottom velocity (cms^{-1}); and (e) residual

(c)

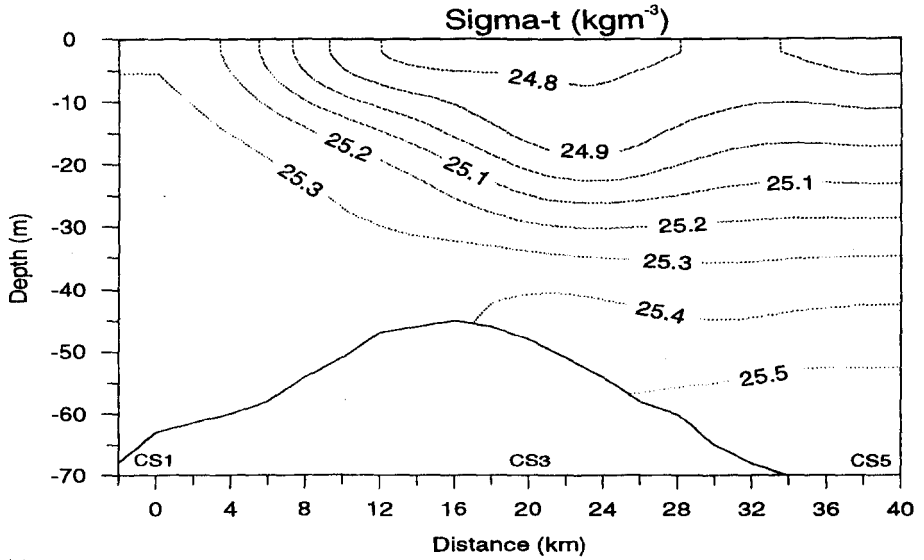

(d)

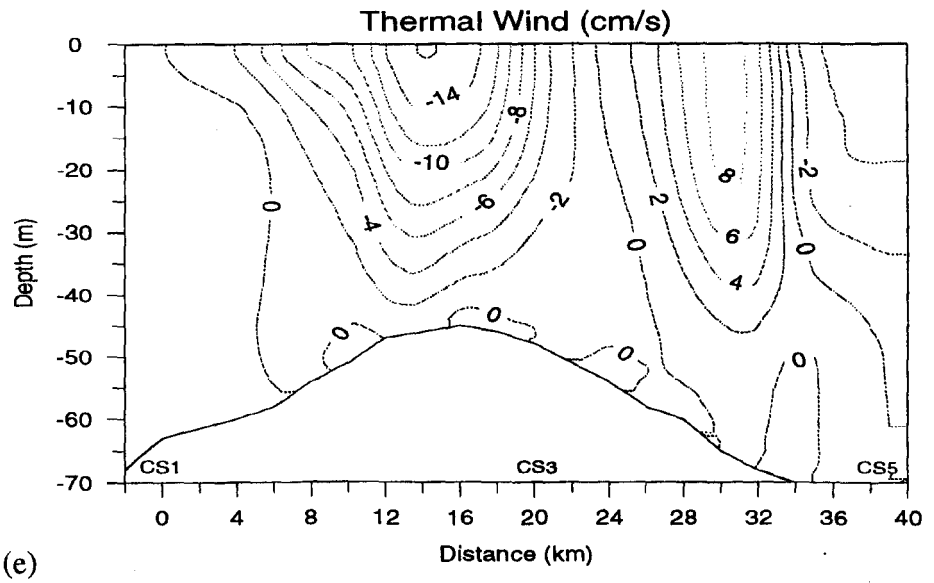

(e)

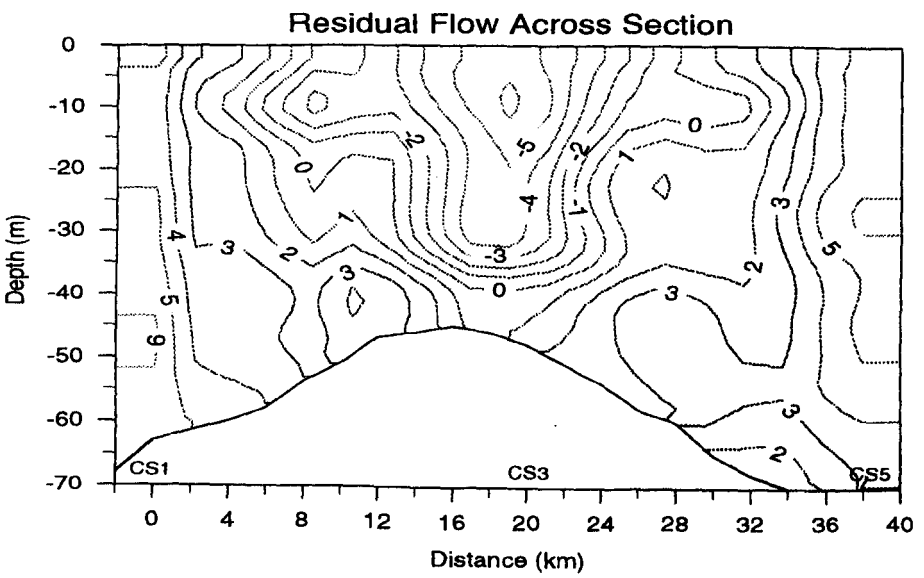

Figure 8.11. Continued.

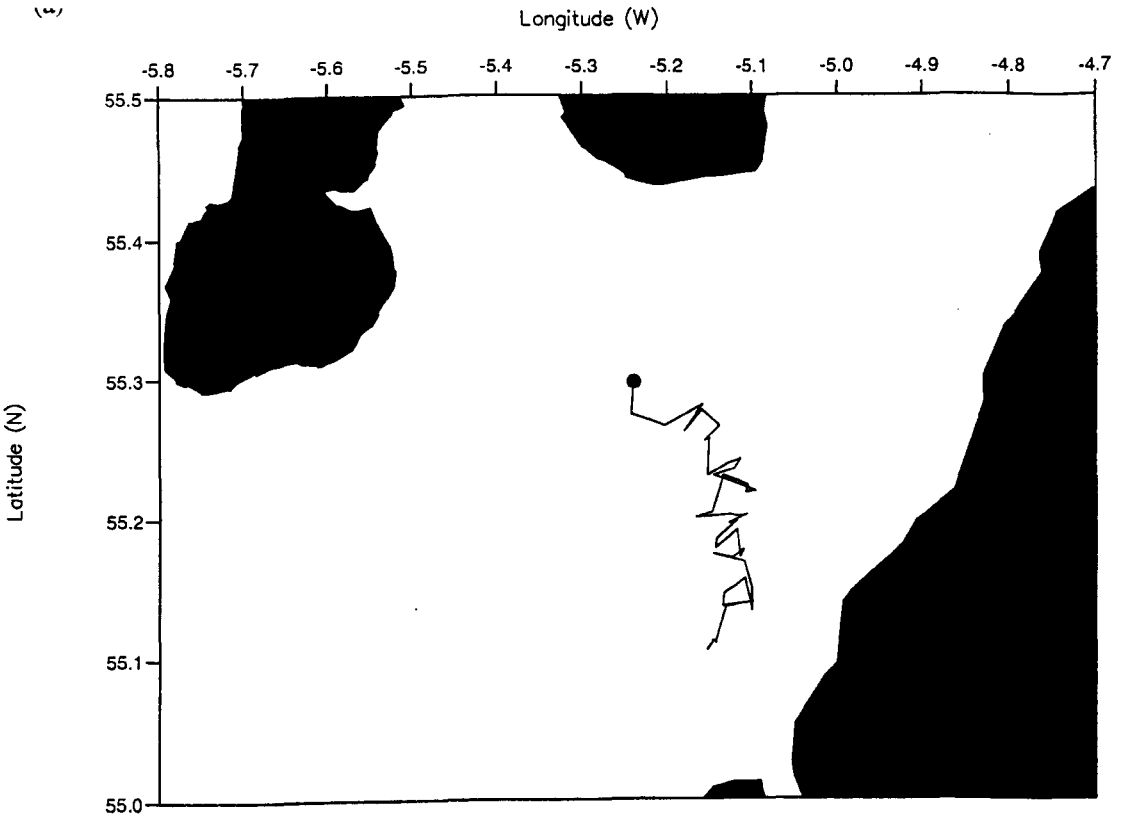

(b)

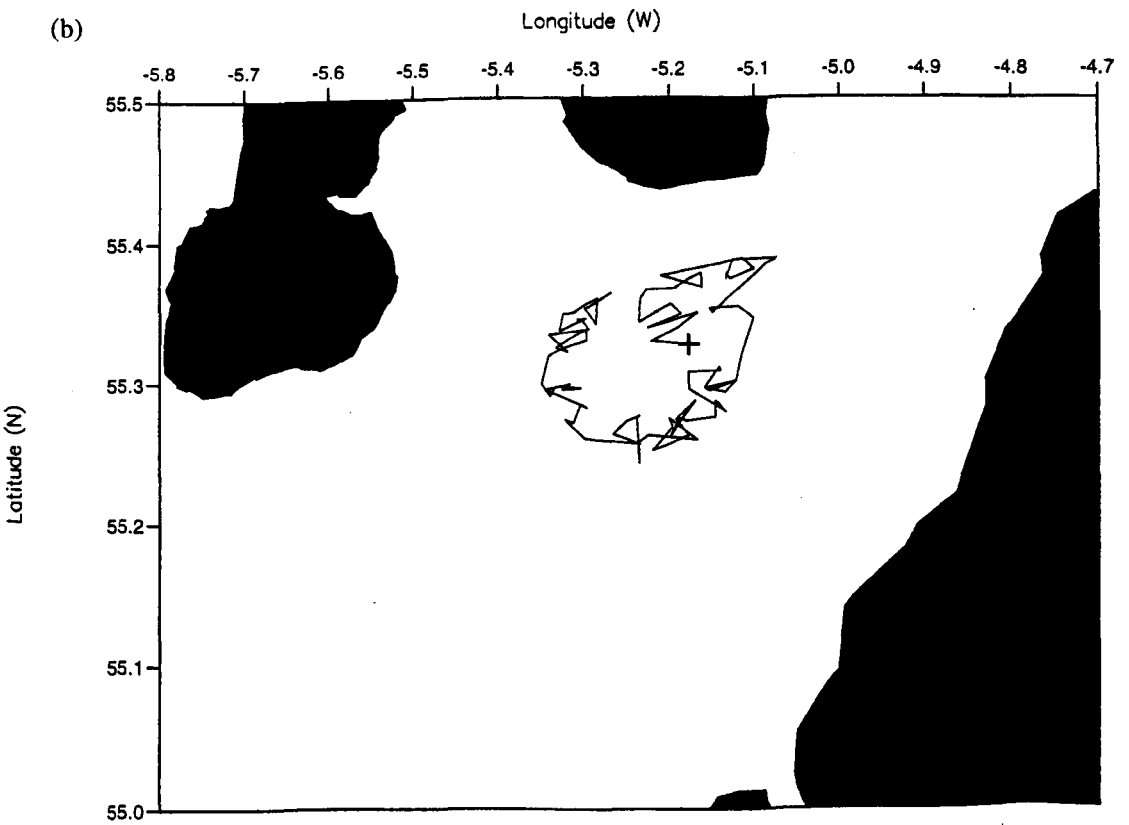

Figure 8.12. Tracks of drogues released on 12/9/1995. (a) Drouge 3945, 9 day trajectory; (b) drogue 3947, 7 day trajectory.

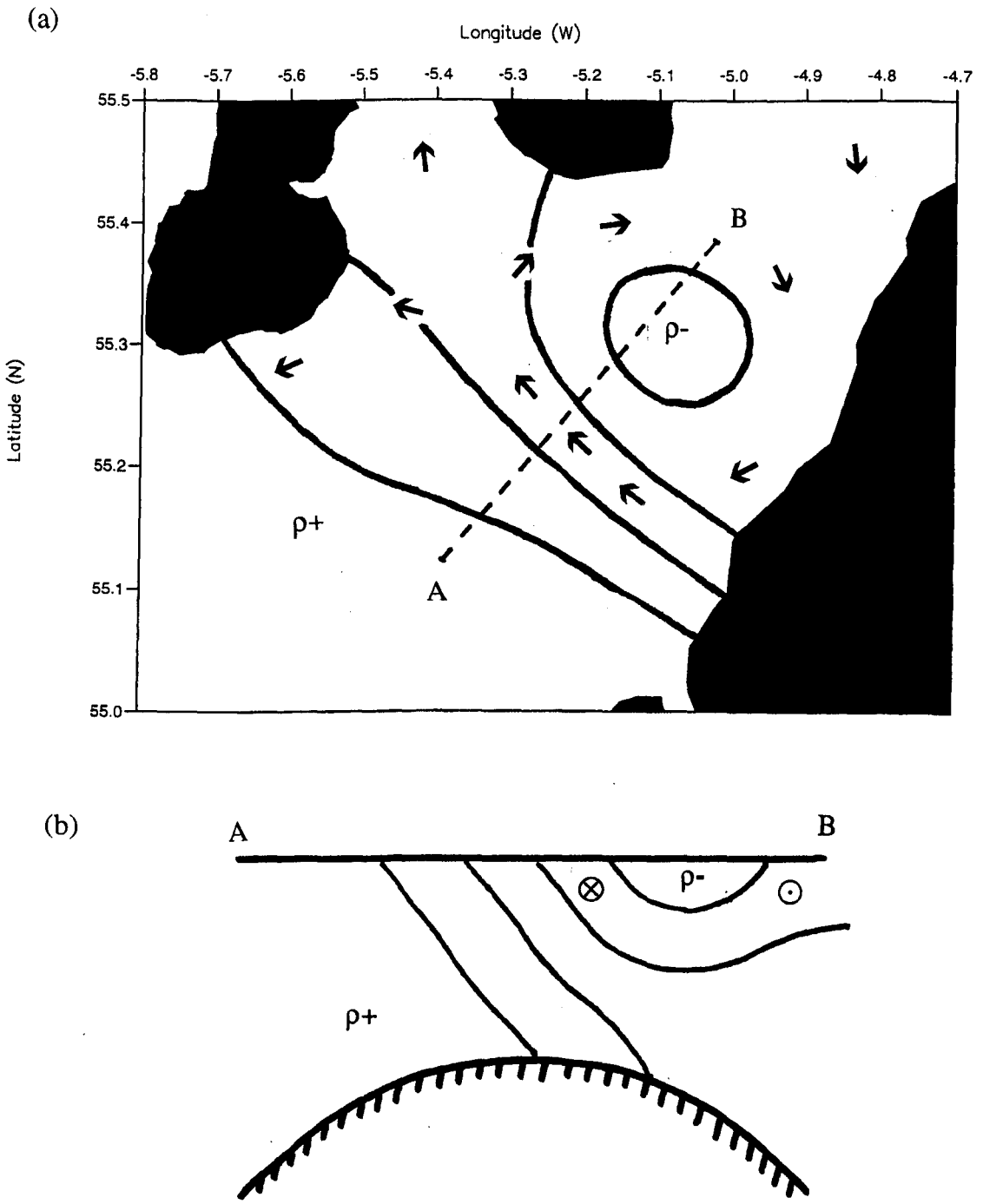

Figure 8.13. Schematic of the flow regime in the sill region, for times of low wind; a) plan view, and b) section AB.

CHAPTER 9. A 3-D MODEL OF THE CLYDE SEA SILL.

9.1 INTRODUCTION.

The inability of the 1-dimensional model (Chapter 7) to reproduce the observed seasonal cycle of cross-sill exchange indicated that factors other than the density differences between the North Channel and the basin bottom water are important in controlling exchange. The observational results presented in Chapters 5 and 8 have been used to identify a number of mechanisms which control the rate of cross-sill exchange, and also their impact upon the circulation in the basin. The dynamics in the sill region has been shown to be complex, being influenced by a combination of density gradients, rotation, topographic, and frictional forces (Section 8.6). The relative importance of each of the proposed mechanisms, and their interaction, is most effectively investigated with the aid of a numerical model. The minimum complexity for such a model would be 3-dimensional with an idealised topography and stratification.

Initially the model should be set up so that it reproduces the main features of the observed flow, as described in previous chapters. It could then be run in an exploratory fashion to investigate the impact of individual mechanisms which control the rate of exchange; (i) the influence upon exchange of the seasonal advance and retreat of the front, as discussed in Section 5.8, and (ii) of wind stress, which was indicated as being significant from the variable rate of exchange observed in March 1995 (Section 8.6). In addition, the influence of both these mechanisms must be considered relative to that of the density difference between the North Channel and the bottom water in the basin. A possible relationship between the observed anti-cyclonic surface circulation about the Isle of Arran observed in Chapter 5, and the dynamics of the frontal region will also be investigated.

9.2 THE MODEL.

The model was developed from the Proctor-James Model in collaboration with Dr. Ian James, at The Proudman Oceanographic Laboratory, Bidston Observatory, Birkenhead, Merseyside, U.K. Much of the work involved in developing the model domain and boundary conditions was done closely with Dr. James, whilst the experimental runs are my own work.

The model uses sigma coordinates and the Piecewise Parabolic Method (PPM) of advection (James, 1996). The advantage of this advection scheme is that it has particularly low numerical diffusion, which is desirable since strong gradients exist over the Great Plateau. This advection scheme is particularly beneficial when sigma coordinates are used, since purely horizontal

motion over a sloping sea bed may introduce strong numerical diffusion in the vertical, resulting in gradients being artificially eroded. For a detailed description of the model and the PPM scheme the reader is referred to James (1996).

Previously, the model has been tested by simulating the tidal advection of an idealised front between stratified and homogeneous fluids over a slope (James, 1996), and it also successfully reproduced the formation of the tidal front, and internal baroclinic features in the southern North Sea (Proctor & James, 1996).

In the model, the Clyde Sea was represented as a rectangle, 40 km wide by 80 km long, with one end open to the shelf sea, and the Isle of Arran a rectangle of land within the basin (Figure 9.1a). The Great Plateau was a simple Gaussian shape (minimum depth 40 m), seated on a linear slope, with the basin being shallower than the North Channel. At the mouth of the Kilbrannan Sound, the addition of a further Gaussian shape formed the Davaar Sill (minimum depth 23 m). The basin was assumed initially to have uniform horizontal stratification, while the North Channel was homogeneous (Figure 9.1b). The model could be run over periods of a few days, when the gradients would come to a quasi-equilibrium, without a significant modification of the initial stratification.

The freshwater runoff was simulated by adding water of 30 psu at a rate of 500 m^3s^{-1} to the head of the gulf. The choice of salinity was not critical since, over timescales of days this inflow will not come into equilibrium with the ambient stratification, but was included since it acted as a tracer of the flow. Radiating boundary conditions were added so that the fresh surface water could flow freely out of the model domain.

Tidal stress, τ, was parameterised by a quadratic drag law which included the tidal velocity amplitude U_t:

$$\tau = k\rho(u + U_t)^2 \qquad (9.1)$$

where u is the non-tidal bottom velocity, k is the bottom drag coefficient, and ρ is the density of water. U_t along the sill crest was estimated from the along-sill observations in Chapter 8, and made inversely proportional to the depth so that tidal mixing became insignificant away from the sill.

The initial stratification in the Clyde Sea was representative of typical conditions in the basin i.e. well mixed from surface to a depth of 25 m, and below 60 m, with the intermediate waters stratified parabolically (Figure 9.1b). The homogeneous North Channel was initially separated

from the Clyde by a vertical front. The model was released from rest and allowed to relax under gravity for a simulated period of 120 hours.

9.3 RESULTS.

A series of eight model runs are presented. The first two are representative of typical conditions occurring in early winter and mid-summer. Runs 3-6 illustrate how exchange responds to changes in cross-front gradient, frontal position and wind direction. The final two runs are control runs in which there is no front. The model runs are presented as surface and section plots of σ_t and velocity. A summary of initial parameters used in the model runs are given in Table 9.1.

RUN	Basin Surface σ_t (kgm^{-3})	Basin Bottom σ_t (kgm^{-3})	North Channel σ_t (kgm^{-3})	Relative Position of Front	Wind Direction
1	25.5	26.2	26.5	forward	-
2	24.5	25.6	25.5	back	-
3	25.5	25.9	26.5	forward	-
4	25.5	26.2	26.5	back	-
5	25.5	25.9	26.5	forward	into basin
6	25.5	25.9	26.5	forward	out of basin
7	25.9	25.9	25.9	-	-
8	25.5	26.2	-	-	-

Table 9.1. *List of model runs, with details of the parameters used.*

9.3.1 EARLY WINTER AND SUMMER CONDITIONS.

Run 1 represents typical early winter stratification, at around day 350, the densest water being found in the North Channel (Figure 9.1a,b). The results show that the surface front has advanced and become more diffuse (Figure 9.2). Dense North Channel water has intruded over the sill and has partially renewed the Clyde bottom water. The velocity section displays a basic estuarine circulation influenced by rotation; the surface waters flow out to the position of the front, whereupon they turn to flow along the sill.

Along section A-B, which is parallel to the sill (Figure 9.1a), inflow is seen to have increased the bottom density, but the effect is constrained to the east coast by rotation (Figure 9.2c). There is no increase in bottom density in the Kilbrannan Sound, indicating that no inflow has taken place over the Davaar Sill.

The frontal jet flows along the region of maximum gradient, and is largely steered out of the Clyde as it approaches the Kintyre coast (Figures 9.2d,e). Some of the jet is redirected into the basin, both in front of the Isle of Arran and at Kintyre coast. This produces a flow reversal and two clockwise (anti-cyclonic) gyres, the largest of which is in the mouth of the Firth of Clyde. A weak anti-cyclonic circulation also fills the entire basin, and forces the outflow of the river, at the centre of the basin head, to the left.

Run 2 represents typical summer conditions, around day 250, and may by compared to the observations from September 1995 (Chapter 8). The initial conditions differ from that in Run 1 in 3 ways; the stratification in the Clyde is stronger, the North Channel has an intermediate density, and initially the front is set 10 km further back towards the head of the gulf (Table 9.1).

Estuarine flow influenced by rotation is again evident, but the inflow does not penetrate to the bottom. The surface conditions (Figure 9.3a,b) are generally similar to those in the winter. The anti-cyclonic circulation which fills the gulf is stronger than in the winter run, and the gyre at the sill appears weaker. This may be due to topographic blocking of the reverse flow in front of the Isle of Arran and is not necessarily a real phenomena due to the use of simplified topography in the model. When the model was run for longer periods, the instability developing in the front became detached and migrated into the Firth.

9.3.2 ENHANCED CROSS-SILL GRADIENTS.

In Run 3 the cross-sill gradients are increased relative to Run 1. This is done by reducing the Clyde Sea bottom water density, thus increasing the density difference between the North Channel water and the bottom water in the basin. The resulting conditions are representative of those in the early spring around day 400, before the onset of the rapid inflows, when the cross-sill density difference is at its seasonal maximum. The results of this run may be compared with the observations made in March 1995.

After 120 hours, the σ_t section X-Y shows that the inflow has penetrated further into the basin, and has a larger volume, than Run 1 (Figure 9.4a). This demonstrates that increasing the cross-frontal density gradient results in an increase in the exchange rate. Section X1-Y1, up the centre

of the Kilbrannan Sound, shows that the front intersects the sill outside the basin, indicating that during this period of high cross-sill gradients, density driven inflow does not occur over the Davaar Sill (Figure 9.4b).

9.3.3 FRONTAL POSITION.

The objective of Run 4 was to test the influence of the position of the front on the rate of cross sill exchange. The initial conditions of Run 4 are again identical to Run 1, except that the front was initially set 10 km back towards the head of the basin. This position of the front is more typical of the summer regime.

The results show significantly more North Channel inflow than in Run 1 (Figure 9.5). This demonstrates that the rate of exchange is enhanced, if the distance the front is located ahead of the sill crest is decreased.

9.3.4 WIND STRESS.

Runs 5 and 6 were used to investigate the effect of stress wind upon the flow. The initial conditions were chosen as those of Run 3 (around day 400), rather than Run 1, to enable comparison of the magnitude of flows induced by the wind stress with those of the maximum observed density gradients. In addition, the results can be directly compared to the observations in March 1995. The amplitude of the wind speed was held constant at 8 ms^{-1}, which was the average speed observed at Machrihanish over the winter.

Run 5 includes the surface stress resulting from an 8 ms^{-1} wind blowing directly into the basin (Figure 9.6a). Estuarine flow is severely impaired in comparison to the no wind scenario of Run 3 (Figure 9.4a), to the extent that little North Channel water entered the basin. In Run 6, an 8 ms^{-1} wind blew directly out of the basin (Figure 9.6b), and considerably more exchange occurred relative to the no wind scenario. The contrast between Runs 5 and 6 demonstrate the governing role that wind direction plays upon the rate of exchange.

The results of other runs, not shown here, indicate that a wind blowing across the sill, from the Kintyre to the Ayrshire coast, also increases the exchange rate. This wind favours upwelling at the mouth of the Clyde, which in turn enhances the estuarine flow. A wind blowing in the opposite direction decreases the rate of exchange. Winds blowing across the mouth of the Clyde appear to have a lower influence upon exchange than winds blowing parallel the basin's axis.

A more quantitative analysis is not possible due to the complex 3-dimensional nature of the flow and the simplified topography used in the model.

9.3.5 CONTROL RUNS.

Runs 7 and 8 are control runs in which there is no front, and are included to investigate the relationship between the front and the anti-cyclonic circulation in the basin. All water in Run 7 was initially homogeneous, while in Run 8 the waters were stratified everywhere with the stratification used in Run 1 (Figures 9.7a,b). The surface velocity fields for both runs show no evidence of anti-cyclonic circulation within the model domain, with the exception of the near surface rotation associated with the inertial outflow from the river. The river outflow at the head of the basin was deflected to the right, as expected in the Northern Hemisphere.

9.4 SUMMARY AND DISCUSSION.

The 3-dimensional model of Proctor & James (1996) has been modified to simulate some of the dynamics of the Clyde Sea. The model has a very much simplified topography, designed to best reproduce the main features in the flow regime over the sill region. After model runs of 120 hours, the frontal gradient was still strong, illustrating the effectiveness of the PPM advection scheme. The model reproduced the essential features of the conceptual picture of the front presented in Section 8.6.

The model allowed the results of other chapters to be synthesised, and supported some of the new interpretations. It has demonstrated that the rate of cross-sill exchange is controlled by three factors:

i) The density difference between the North Channel and the bottom waters in the basin, an increase of which enhances gravitational inflow.

ii) The seasonal advance and retreat of the front. In the summer months, the front is set back, towards the head of the basin, so that the pycnocline is higher in the water column at the sill, allowing the dense North Channel water to flow more freely into the basin.

iii) Wind stress. Winds blowing out of the basin, and from Kintyre towards the Ayrshire coast, enhance exchange, by direct forcing of the surface water, or by inducing upwelling at the mouth of the basin respectively. Winds blowing in the opposite directions inhibited exchange. Winds blowing along the axis of the basin appear to have the greatest impact.

A wind of 8 ms^{-1}, (the average winter wind speed), blowing into the basin reduced exchange to

a small fraction of the no wind rate, under conditions of maximum cross-sill density difference. These are conditions similar to those in March 1995, when the observed exchange was initially rapid whilst a wind blew along the sill from the west, and then decreased as the wind turned to blow into the basin. The modelling results substantiate the suggestion that the changes in exchange rate resulted from changes in the wind direction (Section 8.6). The results indicate that wind stress is the dominant factor influencing exchange, which would explain the episodic nature of the observed bottom salinity in the basin (Section 5.6).

The model also indicated the existence of surface anti-cyclonic circulations, at the mouth and about the Isle of Arran, which were dependent upon the presence of a front over the sill. The anti-cyclonic circulation in the basin was of sufficient magnitude to deflect the outflow from the Clyde river to the left. The strength of this circulation was dependent upon the topography as well as the strength and position of the front, and no simple relationships were evident.

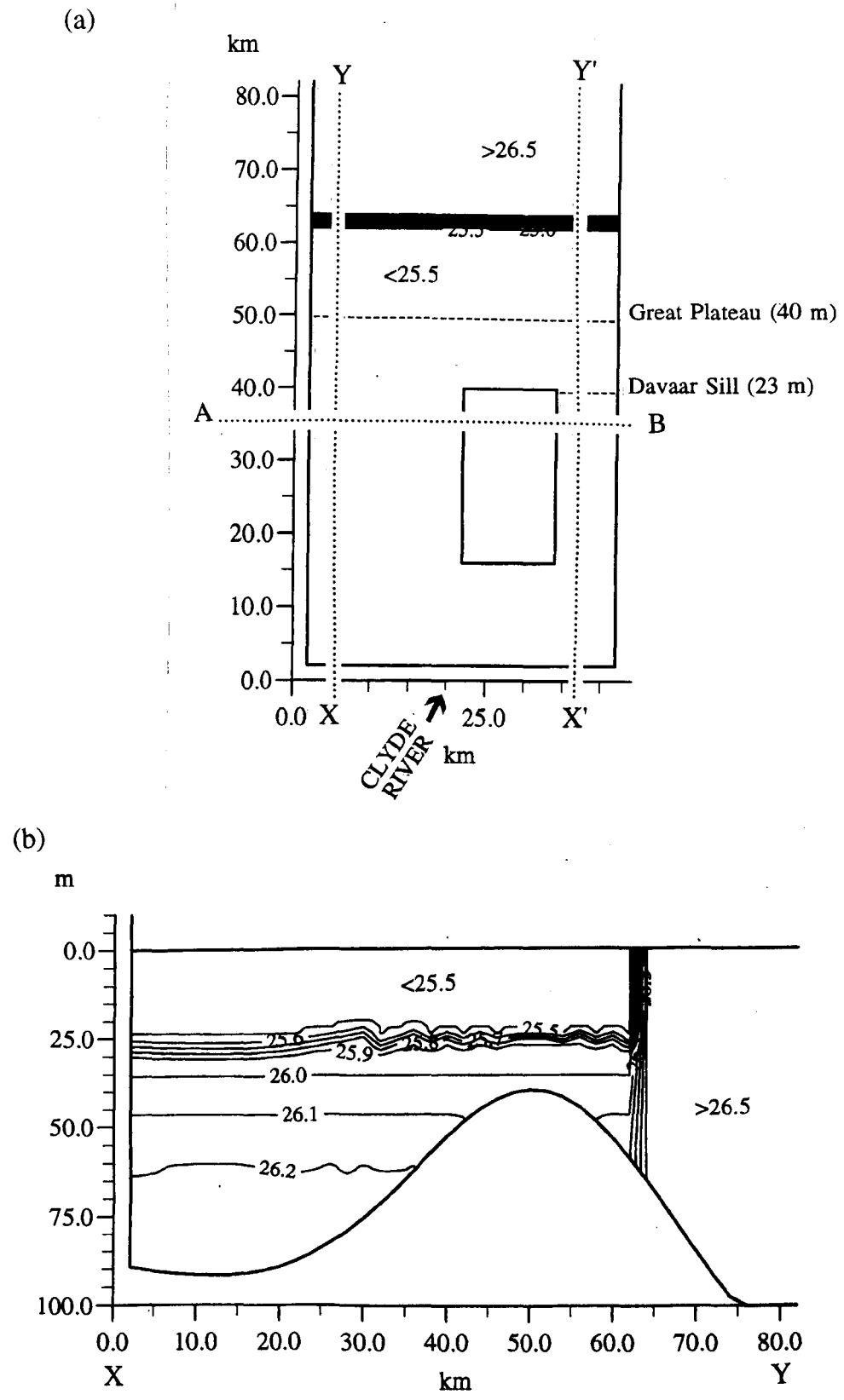

Figure 9.1. Initial conditions for RUN 1; typical winter conditions. (a) Inital surface σ_t, showing the inflow position of the Clyde River, and the peaks of the Gaussians representing the sill, and (b) inital σ_t along section XY. The pertubations in the isopycnals are a result of using sigma co-ordinates.

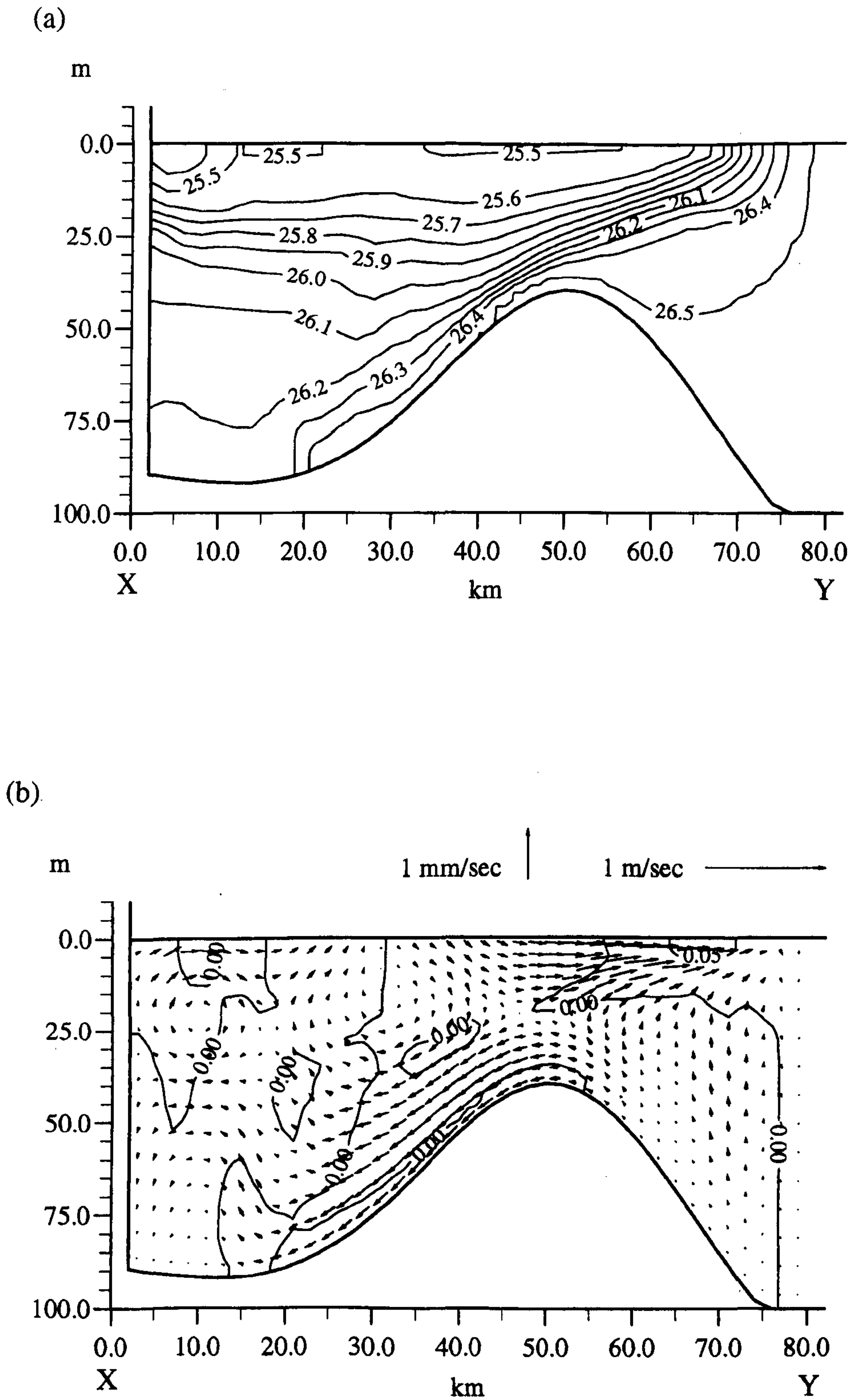

Figure 9.2. RUN 1; typical winter conditions. (a) σ_t along section XY, (b) velocity along section XY (positive is out of the page), (c) σ_t along section AB, (d) surface σ_t, and (e) surface velocity.

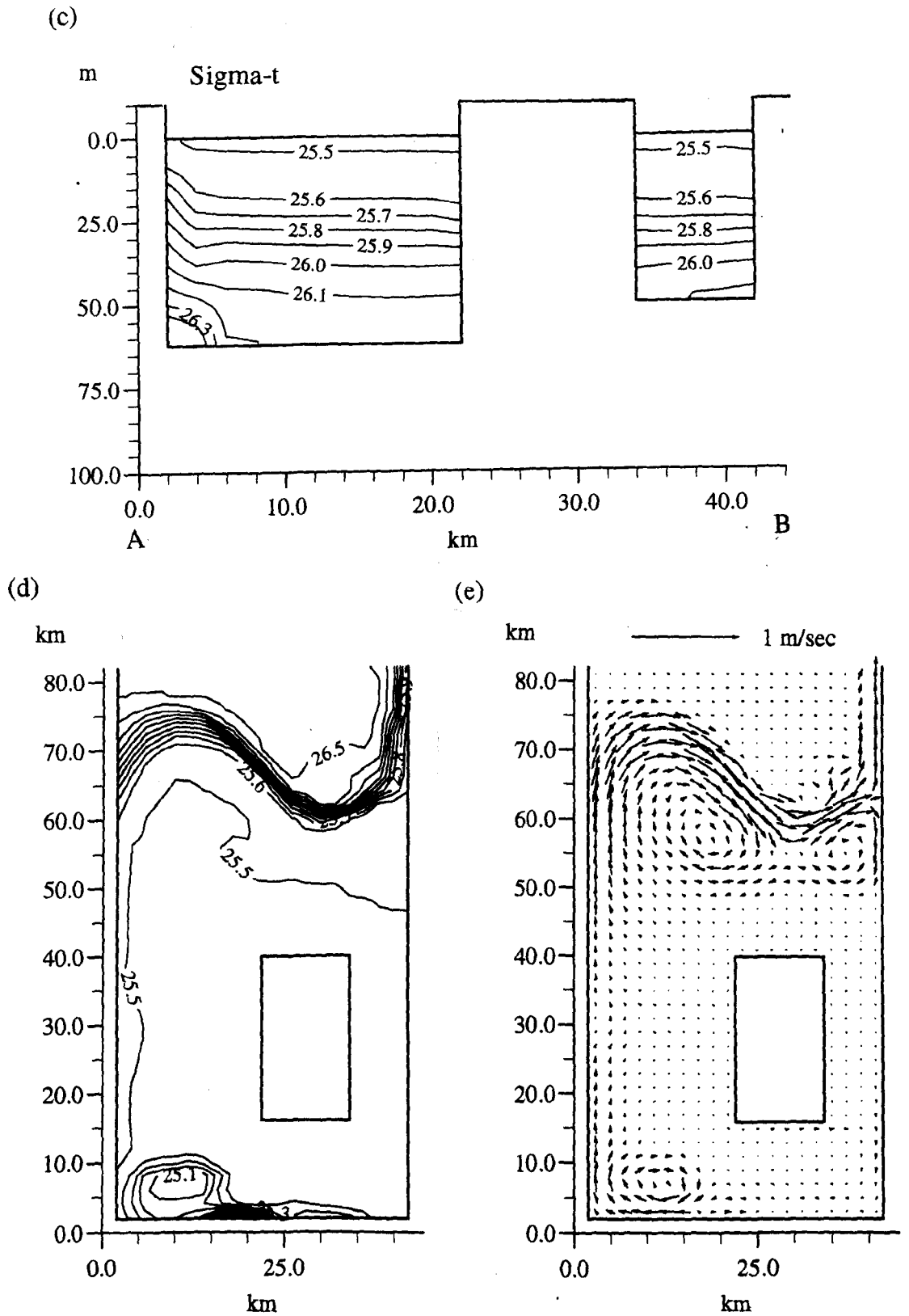

Figure 9.2. Continued.

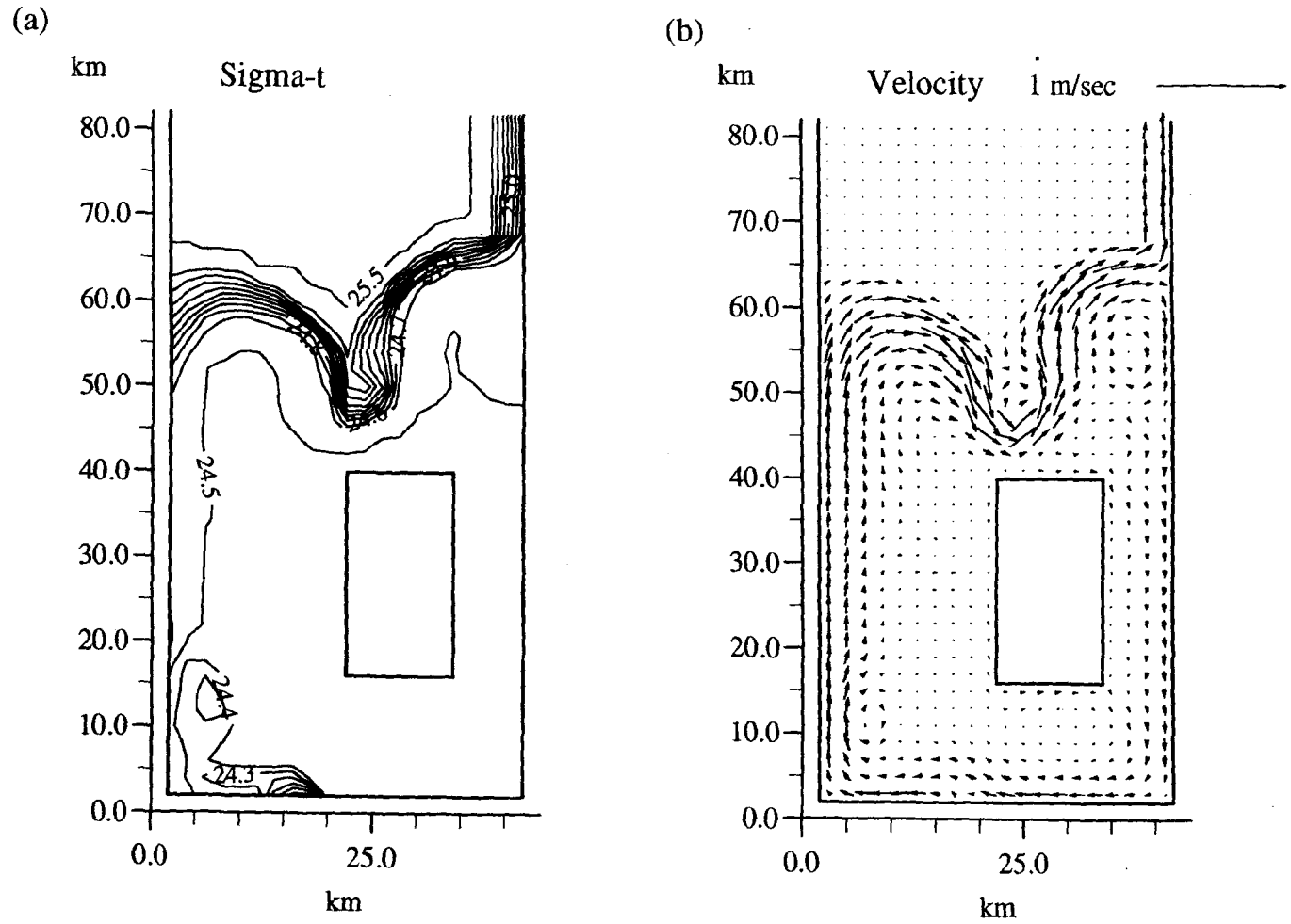

Figure 9.3. RUN 2; typical summer conditions; (a) surface σ_t; (b) surface velocity.

(a)

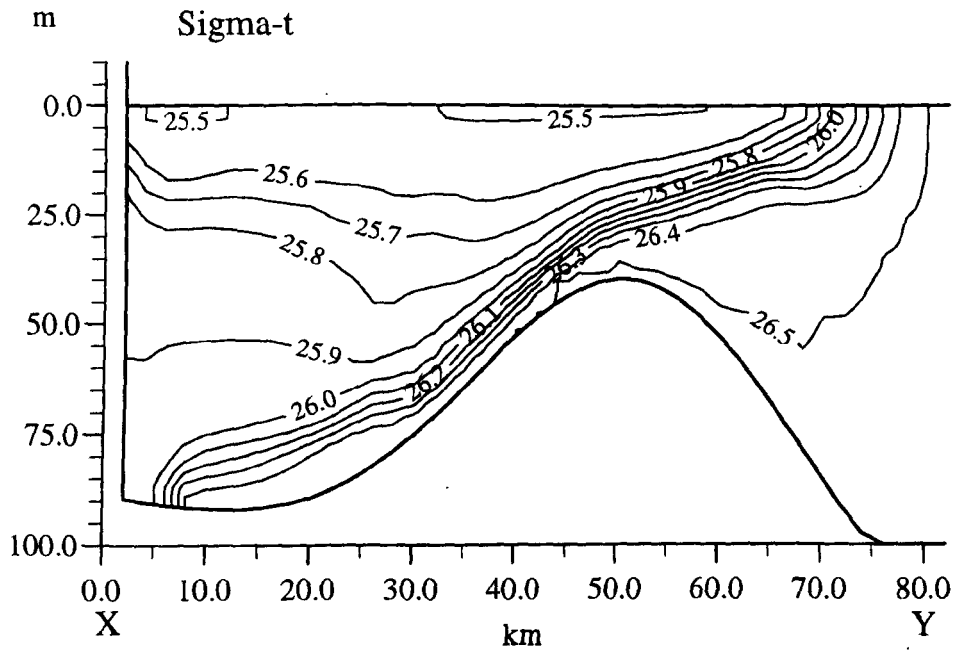

(b)

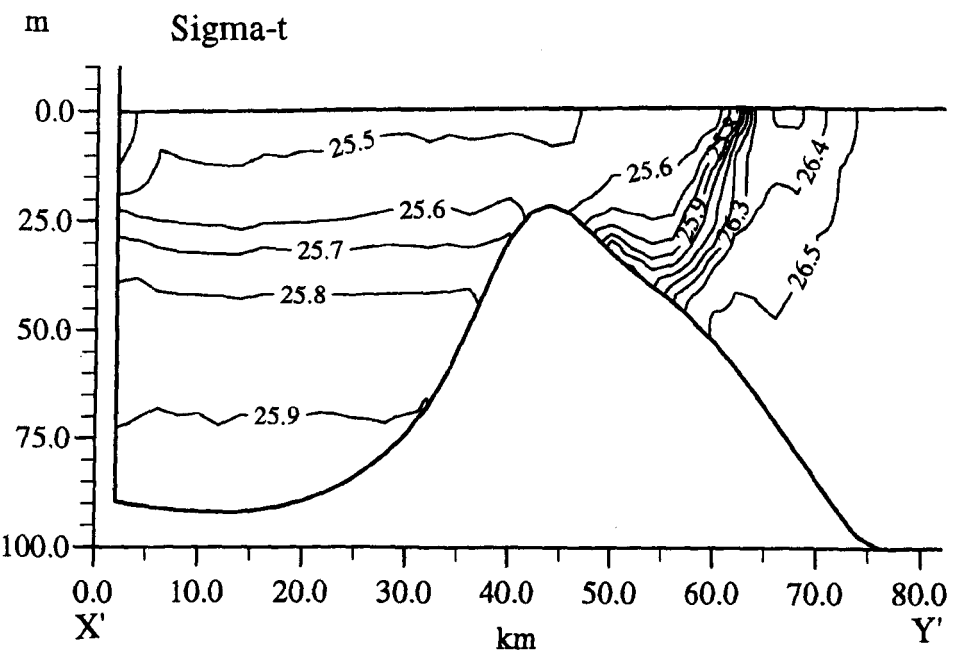

Figure 9.4. RUN 3; increased cross-sill density gradients, typical of early spring conditions; (a) σ_t along section XY; (b) σ_t along section X'Y', in the Kilbrannan Sound.

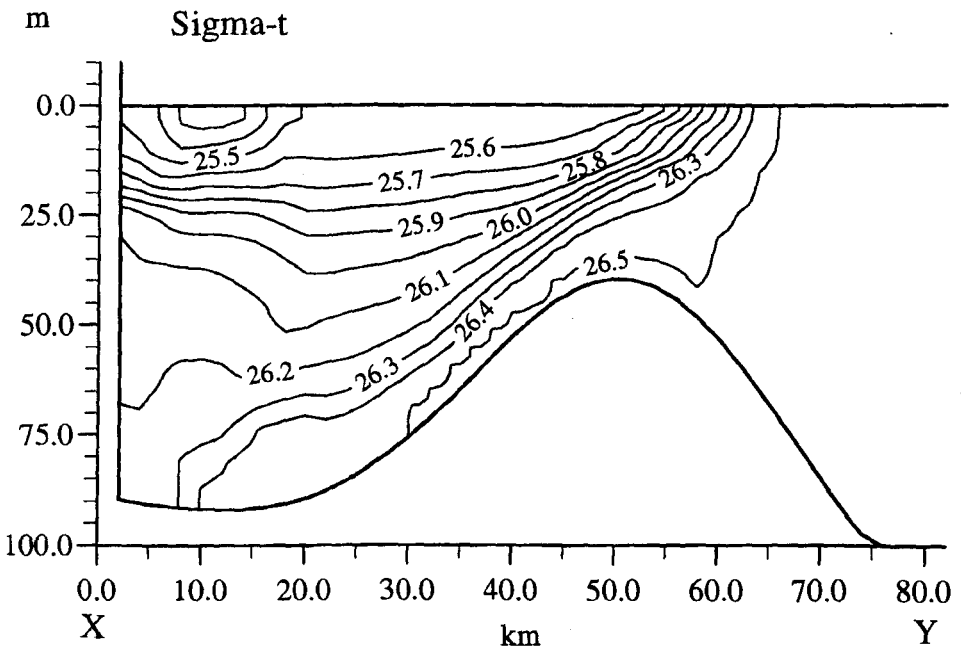

Figure 9.5. RUN 4; σ_t along section XY. As RUN 1, but the front is set back 10 km into the basin.

(a)

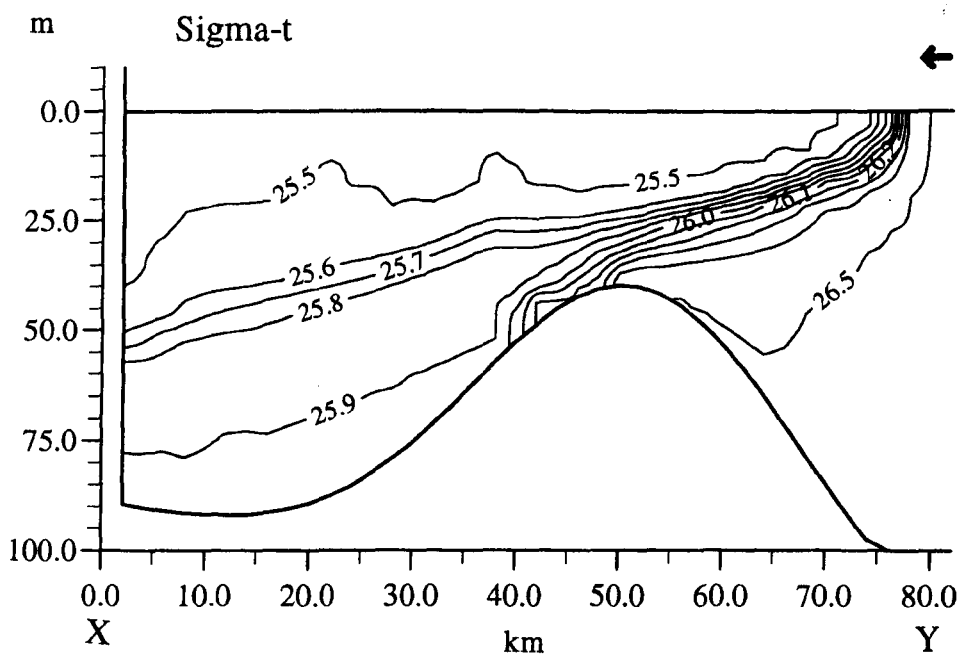

(b)

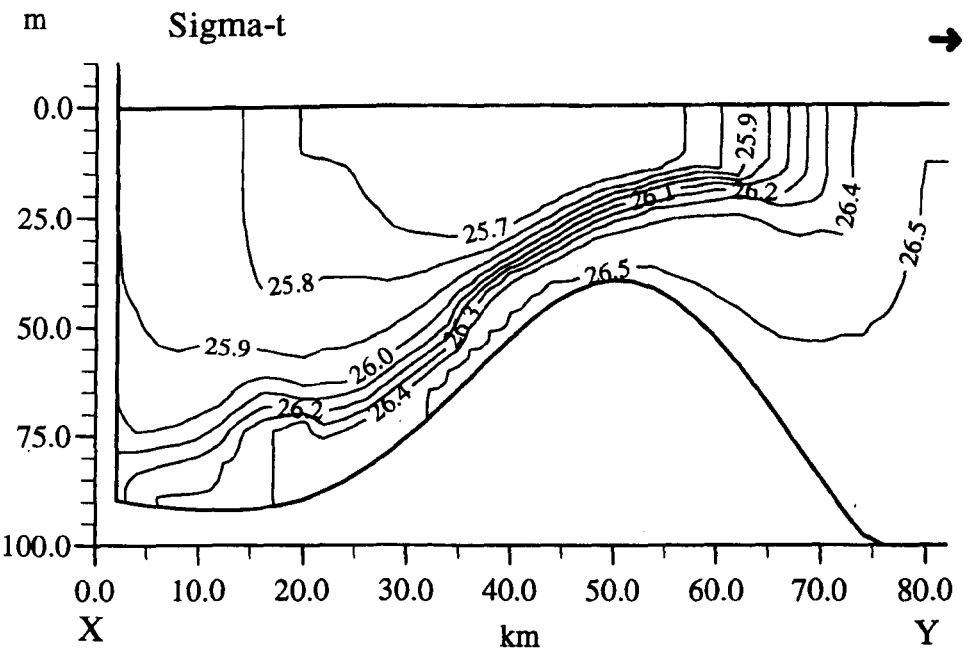

Figure 9.6. The effect of wind stess upon σ_t along section XY. (a) RUN 5, steady 8 ms^{-1} wind blowing into the basin, and (b) RUN 6, steady 8 ms^{-1} wind blowing out of the basin.

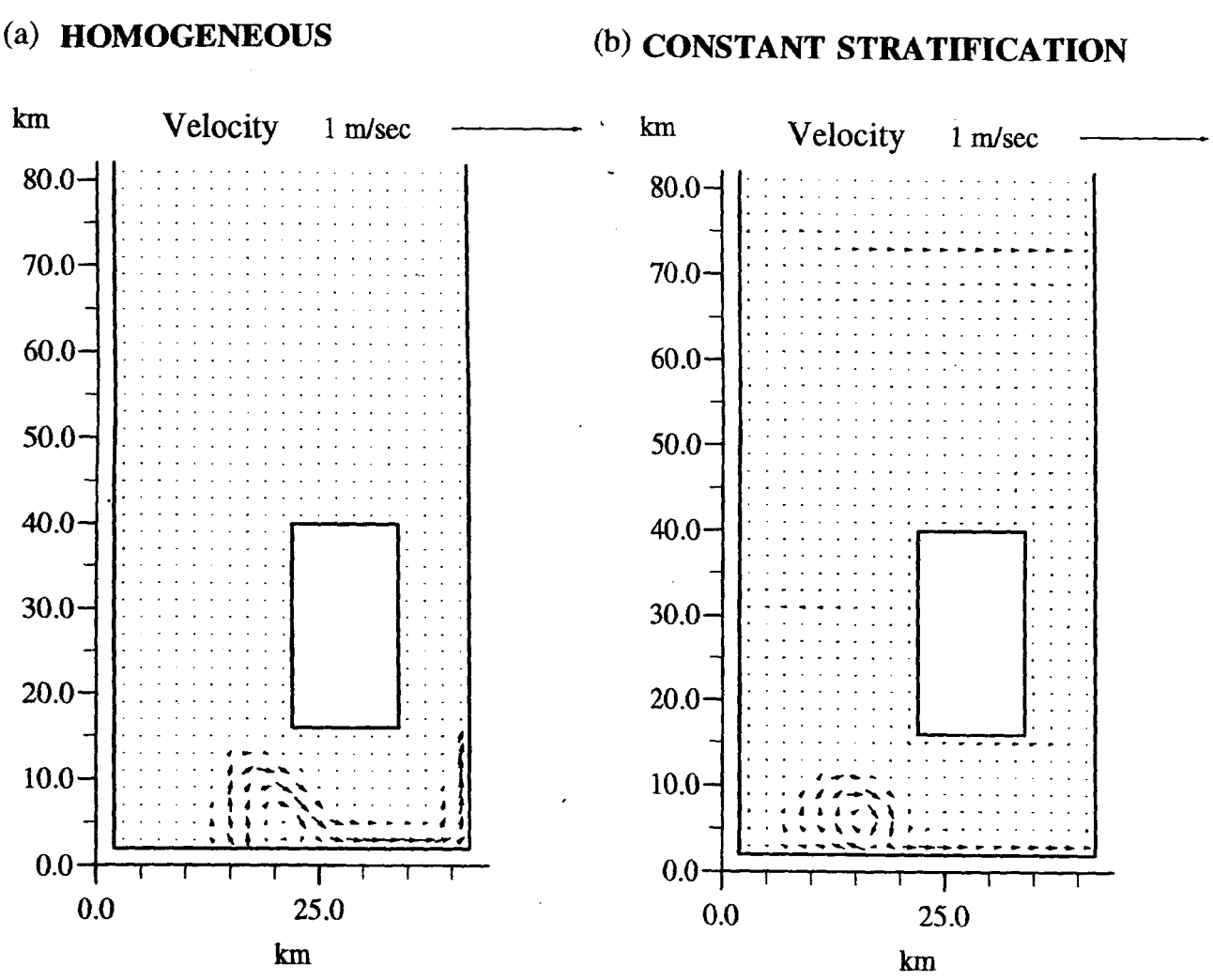

Figure 9.7. Control runs, surface velocity. (a) RUN 7, initial homogeneous conditions, and (b) RUN 8, initial stratified conditions.

CHAPTER 10. SUMMARY AND DISCUSSION.

10.1 INTRODUCTION.

The work presented in this thesis uses an extensive set of new observations, from the Clyde Sea's basin and sill region, together with 1- and 3-dimensional modelling, to improve our understanding of the processes that affect the circulation and mixing, and interaction with the North Channel of the Irish Sea. In this chapter, the principal findings, grouped into five sections, are summarised and discussed, commencing with the new results concerning the seasonal cycle. The next sections concern exchange and mixing processes, with a focus upon new understanding, and a discussion of the observed surface anti-cyclonic circulation. There follows a discussion of the implications of the new work upon the North Channel of the Irish Sea. The thesis concludes with suggestions for future work.

10.2 THE SEASONAL CYCLE IN THE CLYDE SEA.

A continuous set of observations between 27/3/1993 - 11/5/1994 at two locations of the vertical structure of the Clyde Sea over the seasonal cycle has convincingly determined the nature of the seasonal cycle. The stratification has been observed to vary seasonally between being thermally dominated in the summer to entirely haline in the winter (Figure 5.2). The stratification was maximum in the early spring following the build up of surface freshwater over the winter, and an increase in bottom salinity due to deep water renewal. A persistent but weak two layered residual flow has been observed throughout the year (Figure 5.5), with a deep water circulation anti-clockwise about the Isle of Arran, in agreement with previous inferences from observations (Edwards *et al.*, 1986).

Rapid rises of bottom water salinity occurred in three major episodes during the observation period, indicating times during which the effects of inflow were dominant over those of vertical mixing. Two of these episodes, in March 1993 and April 1994, were each sufficient to renew much of the water in the Clyde Sea. Following these two events, for a period of about a month, exchange was reduced to a negligible amount, effectively isolating the Clyde Sea from the shelf sea. The third event was a more persistent inflow in the late summer of 1994, in which North Channel water intruded at mid-depths, leading to a rise in deep water salinity, and a salinity inversion at ~90 m at CS8. The annual mean rate of exchange, based on the salinity and mass budgets was ~1.1 x 10^4 m^3s^{-1}, equivalent to a flushing time of 3.5 months, in satisfactory agreement with estimates based on radiocaesium surveys (Baxter *et al.*, 1979).

The 1-d model of the Clyde Sea (Simpson & Rippeth, 1993) did not reproduce the observed seasonal cycle of salinity (Figures 7.1, 10.1), predicting that the seasonal bottom salinity maximum occurred three months earlier than that observed, at a time at which it was actually at a seasonal minimum. The model was further developed by applying the observational results to estimate the cross-sill exchange and extra mixing of the inflowing water. Although no longer a predictive model, it was now able to reproduce the observations to first order.

10.3 CROSS-SILL EXCHANGE.

The new observations have shown the dynamics of the sill region to be complex. In the late summer and early spring new observations have enabled the mean and tidal flow fields over the sill to be determined, along with their relation to the density structure and topography. Direct measurements of the exchange rate were made. The strong front over the sill lies seaward of a quasi-stationary gyre within the mouth of the Firth, while inflow occurs to the east, beneath this gyre, and outflow to the west.

Density observations show that bottom water renewal is generally energetically possible between day 300 and day 100 the following year (Figure 10.2). However, cross-sill exchange occurs throughout much of the year, at a rate which is governed by three factors, which are discussed below:

10.3.1 The Cross-Sill Density Difference.

The 3-d modelling demonstrated that increasing the density difference between the North Channel and the basin bottom water ($\Delta\rho$) led to an increased inflow rate (Section 9.3.2). However, in winter 1993, when $\Delta\rho$ was at its seasonal maximum, a minimum in the bottom salinity was observed, indicating that mixing effects dominated over those of inflow at that time. Consequently, other factors must influence the rate of exchange.

10.3.2 Wind Forcing.

The episodic nature of fluctuations observed in the bottom salinity in the basin suggest that wind influences exchange. The 3-dimensional modelling study demonstrated that surface wind drag from a wind blowing along the basin axis will significantly reduce or enhance the estuarine flow, depending on whether it is directed into or out of the basin respectively. Winds blowing parallel to the sill also enhance or reduce exchange by inducing up- or downwelling of saline water near the basin mouth, but are not as effective as winds blowing parallel to the basin axis. In March

1995, during a period in which a 7 ms^{-1} wind blew along the sill from the west, the observed exchange rate was ~4 times greater than the average. However, 3 days later, the wind, now averaging 9 ms^{-1}, had turned to blow directly into the basin and the observed exchange was significantly reduced. These observations were made near the time when $\Delta\rho$ was at its seasonal maximum, demonstrating the important role of wind stress upon governing exchange rate.

Mean monthly exchange rate maxima of ~4 x 10^4 m^3s^{-1} occurred in the springs of 1993 and 1994. A positive correlation between strong wind events and bottom salinity increases indicate that much of this exchange may have occurred during a few intense episodes. The clearest example follows day 423, when the daily average wind was 14 ms^{-1} directly out of the Clyde. Between days 424 - 427 RCMs 63 and 64 recorded a salinity rise of 0.8 psu and 0.5 psu respectively, while a 0.2 psu rise was observed between days 420 - 430 at RCMs 83 and 84.

Seasonal bottom salinity maxima were observed in the springtimes of 1985-7 and 1993-4, while bottom salinity minima were observed around February in the years 1985-1988 and 1994, with an isolated low value observed in the spring of 1989 (Figures 10.1, 5.13). The timing of the maxima may result from a combination of the following factors; in the spring (i) the front begins to retreat due to a decline in run-off, (ii) surface waters begin to warm so that the surface temperature inversion is lost, and (iii) the density of the North Channel water is at its seasonal maximum. The last two factors serve to enhance the stratification, aiding the decoupling of the surface gyre from the bottom waters, which may facilitate inflow. Additionally, once a significant volume of inflow has occurred, the pycnocline would be enhanced acting as a positive feedback for exchange.

10.3.3 The Seasonal Migration of the Front.

During the summer of 1993 the inflow rate was estimated to be ~2.3 x 10^4 m^3s^{-1}, significantly above the average. Both $\Delta\rho$ and wind stresses are minimum in the summer, necessitating the existence of another mechanism to induce inflow at this time. This may be associated with the summertime retreat of the front over the sill, typically by 10 km towards the basin head, as the freshwater load diminishes. Saline North Channel water advances closer to the sill crest, where less upwelling is required to induce inflow. 3-dimensional modelling was used to demonstrate that if the front retreats 10 km, then inflow is significantly enhanced. This mechanism is similar, in some respects, to that operating in many Norwegian and New Zealand fjords which renew at times at which dense water is made available at their mouths by upwelling coastal currents (Section 1.4.2).

Indirect evidence of summertime deep water inflow in the Clyde Sea in July 1990 comes from

observed increases in Mn concentration below sill depth (Muller *et al.*, 1996, Muller *pers. com.*). If anoxic conditions exist, Mn oxides will be reduced to the Mn(+II) state, and the element will turn from particulate to water soluble, indicating the sediments as a source for the high levels observed. However, the authors argue that the Mn concentrations in the Firth systematically fall short of those expected. The only available water depleted in Mn was thought to be the North Channel, and thus deep water inflow was inferred.

10.4 MIXING.

The wind was found to be by far the greatest source of mixing energy in the Clyde. Mixing near the sill associated with inflow may also become significant at times of rapid exchange. Some aspects of mixing processes identified by the new work are discussed below.

10.4.1 Internal Tides.

A weak internal tide was observed in the Clyde Sea interior and its contribution to mixing was estimated to be 0.01 mWm^{-2}, two orders of magnitude less than the wind mixing contribution. Hence, the mixing contribution from the internal tide is either negligible, or is concentrated in the vicinity of the sill, south of the moorings.

10.4.2 Low Frequency Internal Oscillations.

A positive correlation was found between the energy of low frequency internal oscillations observed in the basin, and the square of the wind speed, i.e. the surface wind drag (Section 6.4). Although an estimate of the energy contained in these oscillations was made, it was not possible to infer the rate at which they do mixing, although the timing is probably similar to that induced directly through surface stress. Mixing from internal seiching will tend to be concentrated at the pycnocline.

10.4.3 Summer Deep Water Mixing.

In summer 1993, the deep water salinity was enhanced at ~90 m, indicating recent inflow, although the North Channel water was too buoyant to penetrate below sill depth (50 m). To achieve the observed water properties, mixing must have occurred near the sill to mix relatively cold and fresh deep basin water into the inflow. The energy source for mixing may be associated with the kinetic energy of the inflow, or perhaps with internal oscillations. In order to reproduce the deep water properties in the 1-dimensional model, it was necessary to include an estimate of

this mixing, which was determined empirically from the observations.

10.4.4 Winter Deep Water Mixing.

Relatively less stratified areas in the Clyde basin will be more susceptible to deep mixing by the wind. One such area is the Kilbrannan Sound, where buoyant surface water was prevented from entering from the north by the residual anti-cyclonic surface circulation about the Isle of Arran (see Section 10.5). Consequently, the potential energy anomaly, ϕ, observed in the Kilbrannan Sound was typically 60 Jm^{-3} lower than that in the Arran Deep (Figure 5.9d). In both January and February 1994, ϕ was observed in the Kilbrannan Sound to be less than 40 Jm^{-3}. An 8 ms^{-1} wind, persisting for 12 hours, would be sufficient to completely mix this water column. However, the same wind in the relatively stratified Arran Deep would only mix a few tens of metres down (Figure 10.3).

The mixing in the Kilbrannan Sound results in a cooling of the bottom water with only a small reduction in the bottom salinity, and would act in the winter when the wind is strongest. This mixing mechanism was not included in the 1-dimensional model, and may be why the simulated bottom water salinity averaged 0.2 psu greater than that observed in the winter.

It was previously thought that winter inflow acted to cool the Clyde Sea's bottom waters (Edwards *et al.*, 1986, Simpson & Rippeth 1993). However, the bottom salinity in the Arran Deep was lower in December than in October in 1987 (Figure 2.3) and dropped over the winter of 1993/4 (Figures 5.2, 5.13). This indicates that bottom water properties are primarily governed by the effects of mixing, rather than inflow, at these times. In addition, the North Channel water is marginally warmer than the Clyde Sea bottom water during much of this period, due to its greater depth and thus heat capacity (Figure 3.13a), and so cannot be responsible for its cooling.

10.5 ANTI-CYCLONIC CIRCULATION IN THE CLYDE SEA.

If there were no residual surface circulation, freshwater inflow from the Clyde River Estuary would be expected to turn to the right under the influence of the Earth's rotation. The 2-D modelling study of Elliott *et al.* (1992) indicated no barotropic tidal residual about Arran, and no significant residual wind stresses resulting from topographic forcing were apparent in a numerical study of wind in the Clyde Sea region (*pers. comm.* Bethan Jones, UCES). However, residual surface flows observed at MCS8 were persistently southward (Figure 5.5b). Both the new observations and archive data shows, without exception, that the surface waters in the Kilbrannan Sound were more saline than those in the Firth (Figure 10.4). These data indicate

that freshwater from the Clyde River flowed into the Firth and not into the Kilbrannan Sound. A residual surface anti-cyclonic (clockwise) circulation about the Isle of Arran would account for these observations.

Another much smaller scale anti-cyclonic gyre was observed in the mouth of the Clyde Sea (Chapter 8). The observed currents were near geostrophic, and associated with the frontal jet, and a return flow behind the jet, within the basin. In the 3-dimensional modelling study, anti-cyclonic circulation was evident near the mouth of the Firth, and the anti-cyclonic circulation about Arran was sufficiently strong to deflect the outflow from the Clyde River to the left, into the Firth (Figures 9.2,3). When the front was excluded in control model runs, no anti-cyclonic circulation was created, other than that associated with the inertia of the freshwater run-off, and the freshwater was deflected to the right.

Fujiwara (1997) presented an hypothesis which involved the interaction of classical estuarine flow with the effects of rotation (Section 1.6). However, his proposed mechanism will not account for the observed rotation in the Clyde Sea, since it requires the conservation of potential vorticity, which is not satisfied where frictional and baroclinic forces are not negligible. (A mistake in the analysis in which it was assumed that potential vorticity can be linearly added if two water masses mix (Equation 4, second term), led to the incorrect result).

An alternative hypothesis, put forward here, is that the anti-cyclonic circulation in the basin is driven by the currents associated with the density gradient at the mouth.

The along-sill residual flows observed in September 1995 indicate the volume flux of the jet to be ~4 x 10^4 m^3s^{-1}. If this flow turned to the south when it reached the Kintyre coast, the flushing time of the Clyde Sea would be ~4 weeks, and possibly less in the winter, when the cross-sill gradient is higher, significantly shorter than the 3.5 months estimated from the salinity and mass budgets. Therefore much of the water in the frontal jet must be drawn back into the basin. It is this recirculated water that constitutes the anti-cyclonic circulation.

Some fraction of the re-circulated flow is blocked by the Isle of Arran, and redirected up the Kilbrannan Sound, creating a gyre that fills much of the basin. Consequently, the strength of the basin circulation is a complex function of frontal strength, and frontal position relative to the topography, and may thus vary seasonally.

10.6 INTERACTION WITH THE NORTH CHANNEL.

The North Channel is a partially enclosed sea and is consequently itself influenced by any exchange with the Clyde Sea. The peak rate of exchange of ~4 x 10^4 m^3s^{-1} compares with a residual flow of ~6 x 10^4 m^3s^{-1} northwards up the Channel. In the spring of both 1993 and 1994 the North Channel salinity dropped following the periods of high exchange (Figure 5.15), a phenomenon which may have imposed a degree of negative feedback upon the exchange. In 1993, this resulted in a salinity gradient across the channel off Kintyre, which may have enhanced the baroclinic exchange between the North Channel and the Atlantic.

The outflowing jet from the Clyde may modify the circulation of the North Channel. ADCP observations in September 1995 show a south-eastward barotropic residual flow seaward of the front of ~5 cms^{-1} (Figure 8.11e), suggestive of a cyclonic circulation on the seaward side of the front, mirroring the anti-cyclonic circulation in the basin. This flow may explain the persistent eastward advection of drogue 3947 (Figure 8.8b), and may be responsible for the observed patches of low salinity water observed off the Rhins of Galloway in January and August 1985 (Figure 2.2). The influence of this flow upon the North Channel may vary seasonally as the front advances and retreats.

CTD data from the Irish Sea indicate that the salinity observed off Port Erin, Isle of Man (Figure 10.5), is representative of the well mixed region in the north east of the Irish Sea, which is separated seasonally from the North Channel by a thermal front (Hill & Horsbrough *pers. comm.*). Following the autumn breakdown of thermal front, the freshwater held in this region is released into the North Channel and the resultant reduction in density may act to delay the onset of bottom water renewal in the Clyde.

Assuming that, in the winter, water at Port Erin is representative of the source water for the North Channel, there would be a discontinuous increase in salinity of up to 0.5 psu in early 1994 (Figure 10.5). During this period, the northward bottom currents off The Rhins of Galloway were enhanced to about 0.4 ms^{-1}, twice their average (Howarth *et al.*, 1995). These high flows were caused by a storm in February 1994, during which strong winds were directed northwards along the North Channel (Knight, *pers. comm.*). This salinity rise may have enhanced the inflow in the spring of 1994.

10.7 SUGGESTIONS FOR FUTURE WORK.

Future investigation should begin with a study of existing unprocessed data from the sill region, which include surveys over the sill in November 1990 and September 1995. The relationship between exchange and wind may be clarified with continual observations over the sill, although conditions here are not favourable due to frequent bottom water trawling. The question of near sill mixing may be investigated by yo-yoing a CTD at a position near CS4 over a tidal cycle, whilst recording vertically with an ADCP. Sea surface temperature imagery could identify movements of the position of the front, and aid the understanding of how this may influence exchange.

The understanding of the processes in the sill must be improved before the 1-dimensional model may be modified to become a predictive model. This would involve incorporating wind driven exchange, and Hansen-Rattray exchange in a more appropriate manner, perhaps by using the salinity difference over the sill as a boundary condition. Meanwhile, it may be profitable to repeat the nutrient modelling (Jones *et al.*, 1995) with the new version of the model.

Anti-cyclonic circulation in gulfs generally may be investigated with only a slight modification to the 3-dimensional model. The relative importance of the sill topography, frontal strength and position, and the ratio of internal Rossby radius to basin width may be examined. The 3-d Clyde Sea model could be extended to include the North Channel of the Irish Sea, thus investigating the interactions between the two seas, and the significance of flows induce in the Channel, either associated with the front, or the influx of freshwater.

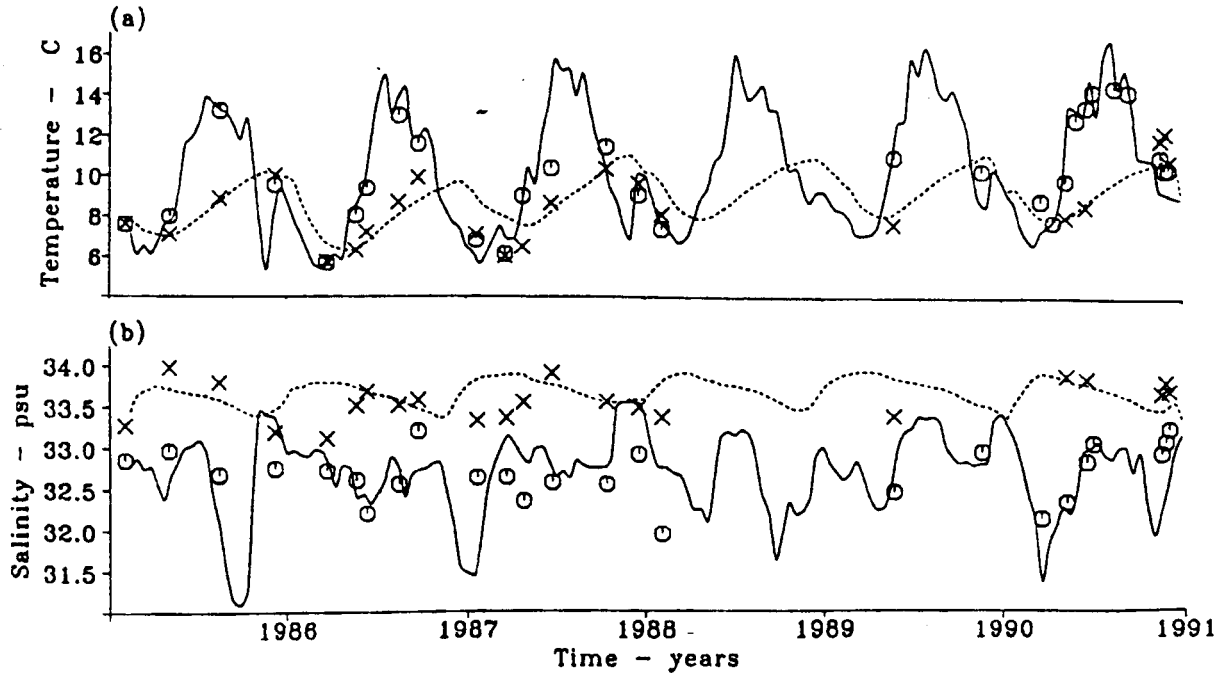

Figure 10.1. Archive temperature and salinity observations in the Firth of Clyde at; (x) surface; (o) 100 m. The continual lines are predections of the original 1-dimensional model; (__) surface; (....) bottom. (Reproduced from Rippeth, 1993).

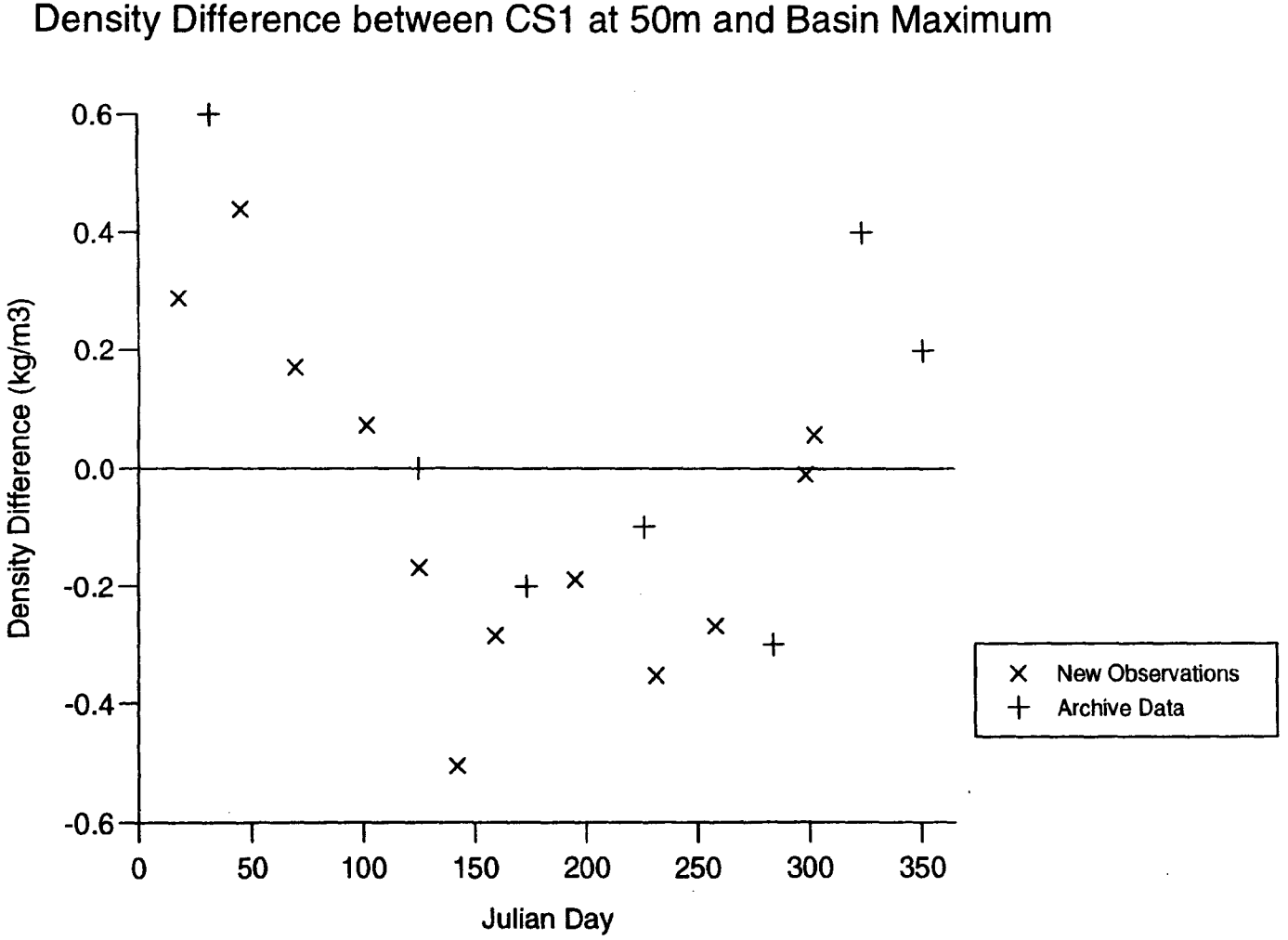

Figure 10.2. Density difference between water outside the sill, at CS1, 50 m, and the maximum observed density in the basin. The difference is positive when the density of water outside the sill is greater than that within, at which time renewal is energetically possible. (Archive data from Edwards *et al.*, 1986; Mitchelson-Jacob *et al.*, 1989; Simpson & Rippeth, 1993).

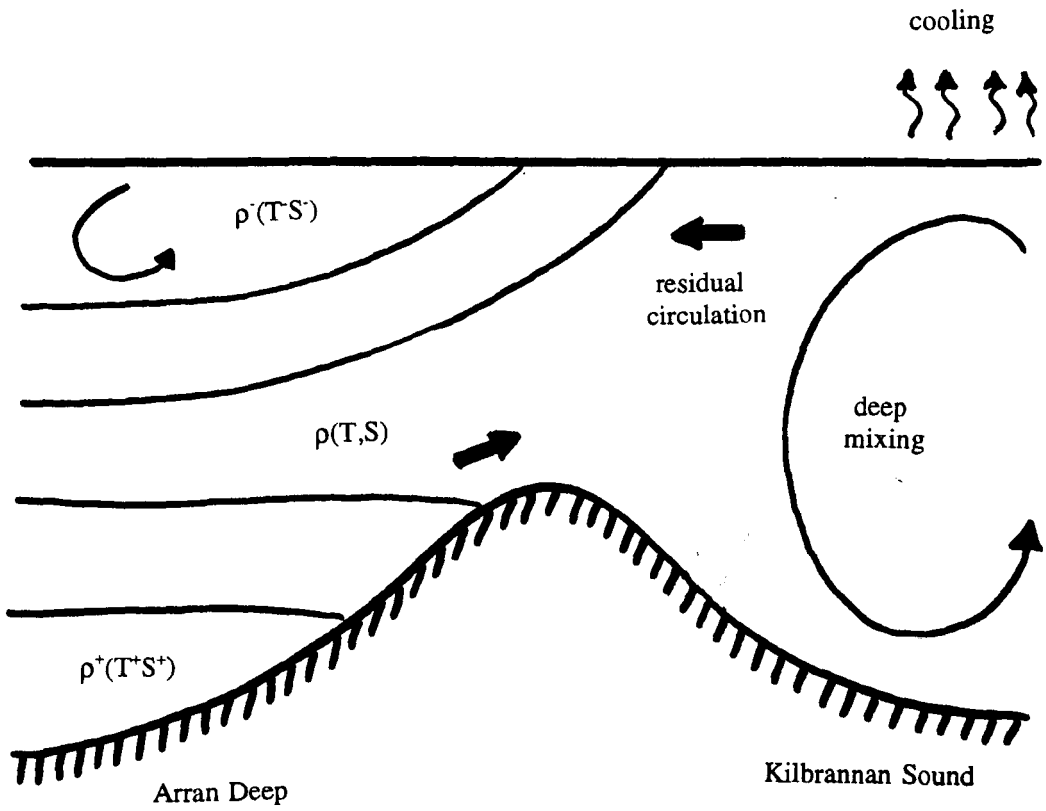

Figure 10.3. Schmatic of density driven flows between the Kilbrannan Sound and the Arran Deep, following a period of moderate wind mixing.

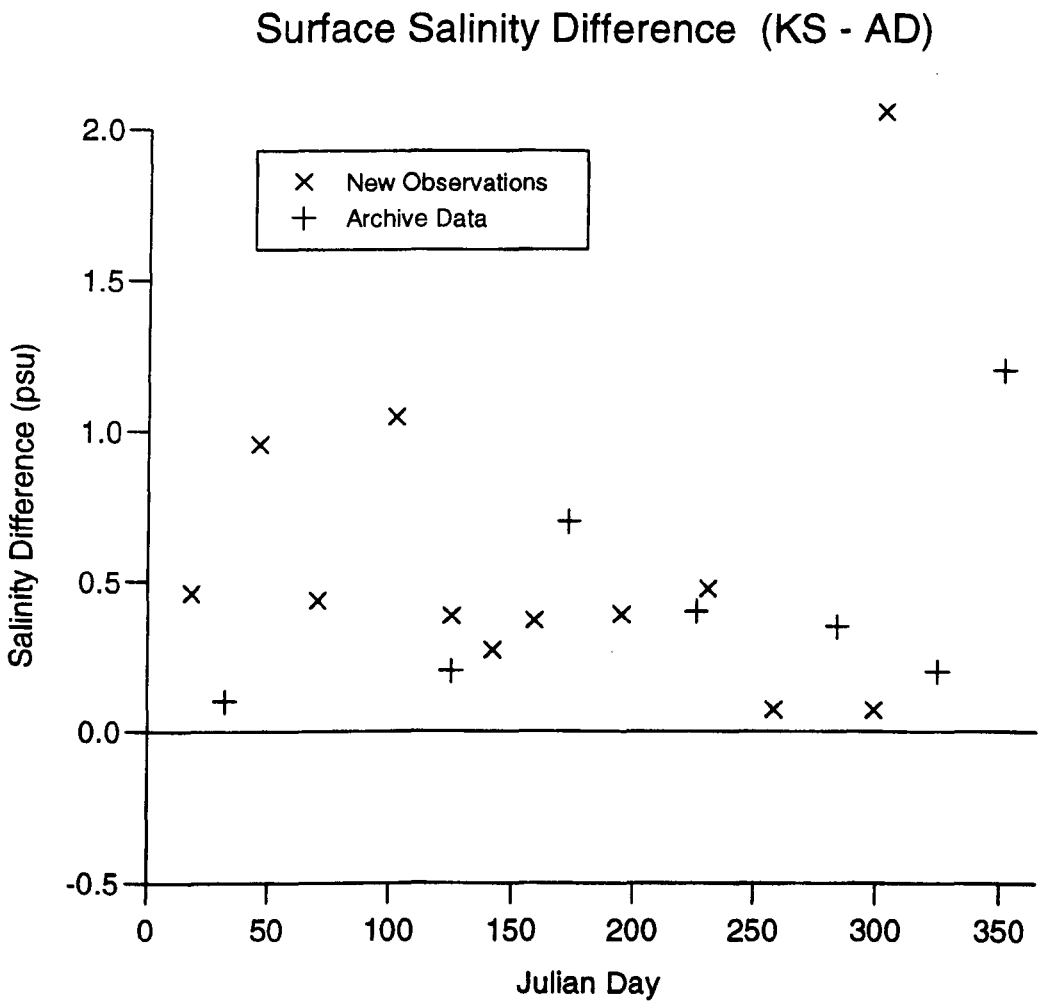

Figure 10.4. Difference in mean surface salinity between the stations in the Arran Deep (CS6, CS7, CS8, CS9) and stations in the Kilbrannan Sound (CS10, CS11, CSE, CS12), from both the new observations and from archive data (Edwards *et al.*, 1986; Mitchelson-Jacob *et al.*, 1989; Simpson & Rippeth, 1993). A positive difference indicates that the Kilbrannan Sound is more saline.

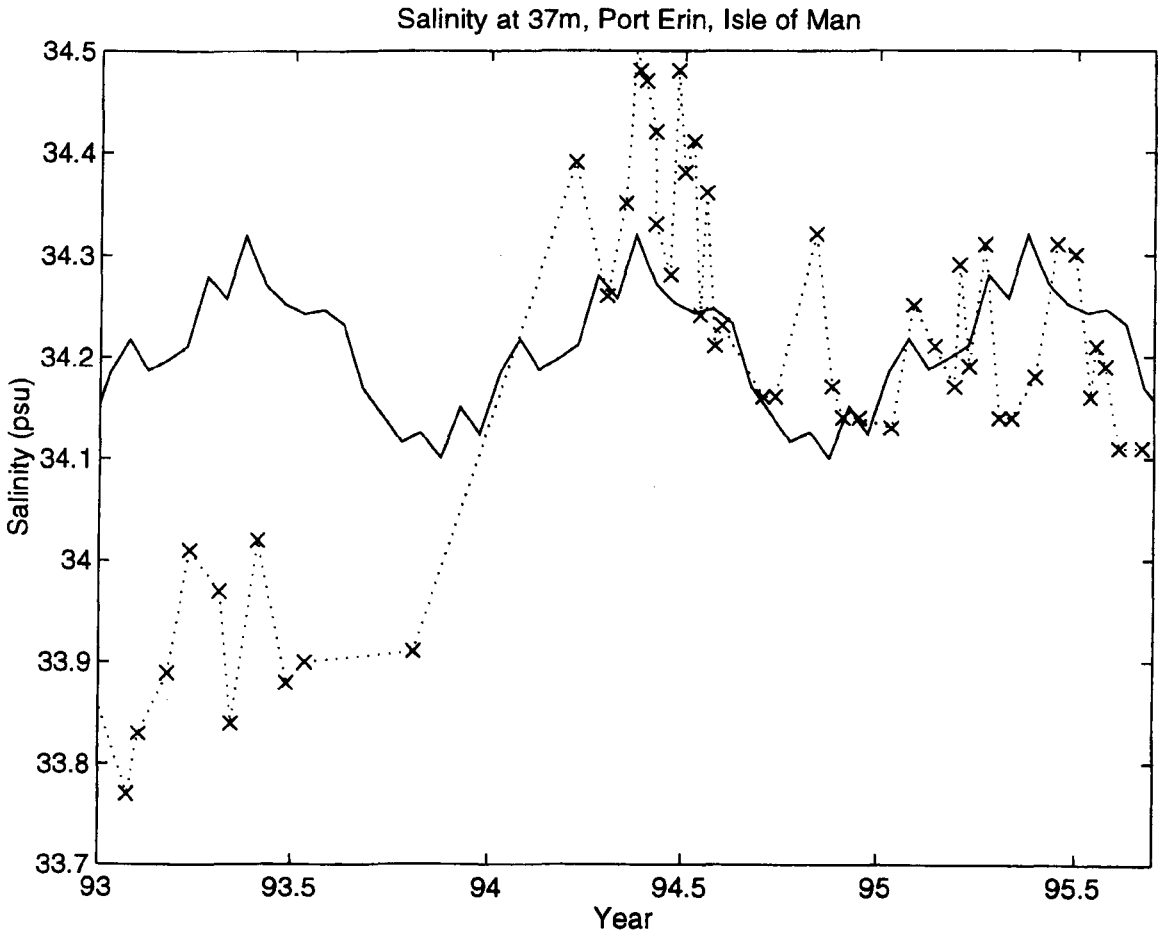

Figure 10.5. Salinity at 37 m, off Port Erin, Isle of Man. (x) observations during the period 1993-5; (__) mean seasonal variation of fortnightly observations taken 1954-1995.

REFERENCES.

Allen, G. 1995. Inflows, mixing and the internal tide of Upper Loch Linnhe. Ph.D. Thesis. U.C.N.W.

Amin, M. 1982. On analysis and prediction of tides on the west coast of Great Britain. *Geophysical Journal of the Royal Astrological Society*, **68**, 57-78.

Asplin, L. 1995. Examination of local circulation in a wide, stratified fjord including exchange of water with the adjacent ocean, due to constant local upfjord wind. In *Ecology of Fjords and Coastal Waters.* Ed. Skjoldal, H.R., Hopkins, C., Erikstad, K.E. & Leinaas, H.P. Elsevier Science B.V. 177-184.

Aure, J. & Stigebrandt, A. 1988. On the influence of topographic factors upon the oxygen consumption rate in sill basins of fjords. *Estuar. Coast. Shelf Sci.* **28**, 59-69.

Bailey, R.S., MacKay, D.W., Morrison, J.A., & Walsh, M. 1986. The biology and management of Herring and other pelagic fish stocks in the Firth of Clyde. *Proceedings of the Royal Society of Edinburgh.* **90B**, 407-422.

Baines, P.G. 1982. On internal tide generation models. *Deep Sea Research,* **29**:307-338.

Barnes, H. & Goodley, E.F.W. 1961. The general hydrography of the Clyde Sea area, Scotland. *Bulletin of Marine Ecology* **5**, 112-150.

Baxter, M.S., McKinley, I.G. MacKenzie, A.B. & Jack, W. 1979. Windscale Radiocaesium in the Clyde Sea area. *Marine Pollution Bulletin* **10**, 116-120.

Borenas, K.M. & Pratt, L.J. 1990. *A Review of Rotating Hydraulics.* L.J. Pratt (ed.), The Physical Oceanography of Sea Straits, 343-371. Kluwer Academic Publishers. Printed in the Netherlands.

Boyd,J.M. 1986. The environment of the Estuary and Firth of Clyde - an introduction. *Proceedings of the Royal Society of Edinburgh,* **90B**, 1-5.

Bretschneider, D.E., Cannon, G.A., Holbrook, J.R. & Pashinski, D.J. 1985. Variability of subtidal current structure in a fjord estuary: Puget Sound, Washington. *J. Geo. Res.* **90**, No. C6, 11949-11958.

Brown, J. & Gmitrowicz, E.M. 1995. Observations of the transverse structure and dynamics of the low frequency flow through the North Channel of the Irish Sea. *Continental Shelf Research* **15**, No. 9, 1133-1156.

Cannon, G.A., Holbrook, J.R., & Pashinski, D.J. 1990. Variations in the onset of bottom-water intrusions over the entrance sill of a fjord. *Estuaries,* **13**, No1, 31-42.

Cowan, E.A. 1992. Meltwater and tidal currents: controls on circulation in a small glacial fjord. *Estuar. Coast. Shelf Sci.* **34**, 381-392.

Craig, R.E. 1959. Hydrography of Scotish coastal waters. *Marine Research* **2.**

Craig, P.D. 1987. Solutions for internal tide generation over coastal topography. *Journal of*

Marine Research, **45**, 83-105.

Cushman-Roisin, B. & Svendsen, H. 1983. Internal gravity waves in sill fjords: vertical modes, ray theory and comparison with observations. In: *Coastal Oceanography,* H.G. Gade, A. Edwards & H. Svendon, eds., Plenum Press, New York. 373-396.

Cushman-Roisin, B. & Svendsen, H. 1994. Upwelling in broad fjords. *Continental Shelf Research,* **14**, No. 15, 1701-1721.

Curran, J.C. 1981. A finite element model of population in the Clyde estuary: formulation, validation and utilisation. *Applied Mathematical Modelling* **5**, 137-142.

Daziel, S.B. 1990. *Rotating two-layer sill flows.* L.J. Pratt (ed.), The Physical Oceanography of Sea Straits, 343-371. Kluwer Academic Publishers. Printed in the Netherlands.

de Young, B. & Pond, S. 1987. The internal tide and resonance in Indian Arm, British Columbia. *J. Geo. Res.* **92**, No. C5, 5191-5207.

de Young, B. & Pond, S. 1988. The deep water exchange cycle in Indian Arm, British Columbia. *Estuar. Coast. Shelf Sci.* **26**, 285-308.

Dooley, H.D. 1979. Factors influencing water movements in the Firth of Clyde. *Estuarine, Coastal and shelf Science* **9**, 631-641.

Drinkwater, K.F. & Osborn, T.R. 1975. The role of tidal mixing in Rupert and Holberg Inlets, Vancouver Island. *Limnol. Oceanogr.* **20**(4), 518-529

Dyer, K.R. 1977. *Estuaries: a physical introduction.* John Wiley & Sons, London, p45.

Edwards, A., Baxter, M.S., Ellet, D.J., Martin, J.H.A., Meldrum, D.T. & Griffiths, C.R. 1986. Clyde Sea Hydrography. *Proceedings of the Royal Society of Edinburgh,* **90B,** 67-83.

Edwards, A.D.J. & Edelsten, M.A. 1977. Deep water renewal of Loch Etive: a three basin Scottish fjord. *Estuar. Coast. Mar. Sci.* **5**, 575-595.

Edwards, A.D.J., Edelsten, M.A., Saunders, S.O. & Stanley. 1980. Renewal and Entrainment in Loch Eil; a periodically ventillated Scottish fjord. In: *Fjord Oceanography.* H.J.Freeland, D.M.Farmer & C.D.Levings, eds. Plenum Press, London, 523-530.

Ellet, D.J. & Edwards, A. 1983. Oceanography and inshore hydrography of the Inner Hebredes. *Proceedings of the Royal Society of Edinburgh,* **83B,** 143-160.

Elliot, A.J., Gillibrand, P.A. & Turrell, W.R. 1990. Tidal mixing near the sill of a Scotish sea loch. In Coastal and Estuarine Studies: Dynamics and exchanges in esruaries and the coastal zone. Ed Prandle, D. American Geophysical Union, Washington DC.

Elliott, A.J., Perry, O.B. 1992. Tidal currents in the Clyde Approaches. *The Hydrographic Journal, 64, 11-15.*

Elliott, A.J., Perry, O.B. & Li, Z. 1991. A modelling study of the Clyde Approaches. *Report for Hydraulics Research Ltd,* Wallingford, Oxon.

Farmer, D.M. & Smith, J.D. 1980. Generation of lee waves over the sill in Knight Inlet. In: *Fjord oceanography,* H.J. Freeland, D.M. Farmer & C.D. Levings, eds., Plenum Press, New York. 259-269.

Farmer, D.M. & Freeland, H.J. 1982. The physical oceanography of fjords. *Prog. Oceanog.* ***12****, 147-220.*

Fujiwara T., Sandford L.P., Nakatsuji K. & Sugiyama Y. 1997. Anti-cyclonic Circulation Driven by the Estuarine Circulation in a Gulf Type ROFI. *Journal of Marine Systems*, **12**, 83-99.

Gade, H.G. & Edwards, A. 1980. Deep water renewal in fjords. In: *Fjord oceanography,* H.J. Freeland, D.M. Farmer & C.D. Levings, eds., Plenum Press, New York. 453-490.

Geyer, W.R. & Cannon, G.A. 1982. Sill processes related to deep water renewal in a fjord. *Journal of Geophysical Research,* **87**, No. C10, 7985-7996.

Gill, A.E. 1977. The hydraulics of rotating-channel flow. *Journal of Fluid Mechanics*, **80**, 641-671.

Gill, A.E. 1982. *Atmosphere-Ocean Dynamics*. Academic Press.

Gillibrand, P.A., Turrell, W.R., Elliot A.J. 1995. Deep water renewal in the upper basin of Loch Sunart, a Scottish Fjord. *Journal of Physical Oceanography*, **25**, 1488-1503.

Gillibrand, P.A., Turrell, W.R., Moore, D.C. & Adams, R.D. 1996. Bottom water stagnation and oxygen depletion in a Scottish Sea Loch. *Estuarine, Coastal and shelf Science,* **43**, 217-235.

Hansen, D.V. & Rattray, Jr. 1966. New dimensions in estuary classification. *Limnolgy and Oceanography,* **11**, 319-326.

Harker, G. 1994. ADCP study of the North Channel. M.Sc. Thesis, UNCW.

Hislop, J.R.G. 1986. The demersal fisheries in the Clyde Sea area. *Proceedings of the Royal Society of Edinburgh.* **90B**, 423-438.

Howarth, M.J., Harrison, A.J., Knight, P.J. & Player, R.J.J. 1995. Measurement of net flow through a channel. *Pub. 12 of the LOIS Community Research Program*, NERC.

Hughes, B.A. 1978. The effect fo internal waves on surface wind waves. 2. Theoretical analysis. *J. of Geo. Res.* **83**, 455-465.

Ivey, G.N. & Nokes, R.I. 1989. Vertical mixing due to the breaking of critical internal waes on sloping boundaries. *Journal of Fluid Mechanics*, **204**, 479-500.

James, I.D. In Press. Advection schemes for shelf sea models. *Journal of Marine Systems*, **254**.

Jardin, W.G. 1986. The geological and geomorphical setting of the Estuary and Firth of Clyde. *Proceedings of the Royal Sociey of Edinburgh* **90B,** 25-42.

Jeffries, D.F., Steele, A.K. & Preseton, A. 1982. A further study on the distribution of ^{137}Cs in the British Coastal waters - 1. Irish Sea. *Deep Sea Research*, **29**, 713-738.

Jones, K.J., Ayres, P., Bullock, A.M., Roberts, R.J. & Tett, P. 1982. A red tide of gyrodinium Aureolum in Sea Lochs of the Firth of Clyde and associated mortality of pond-reared salmon. *Journal of the Marine Biological Association, U.K.*, **63**, 771-782.

Jones, K.J., Grantham, B., Ezzi, I., Rippeth, T.P. & Simpson, J.H. 1995. Physical controls on phytoplankton and nutrient cycles in the Clyde Sea, a fjordic system on the west coast of Scotland. In *Ecology of Fjords and Coastal Waters.* Ed. Skjoldal, H.R., Hopkins, C., Erikstad, K.E. & Leinaas, H.P. Elsevier Science B.V. 93-104.

Kay, S.M. 1988. Modern Spectral Estimation - Theory & Application. Prentice Hall, Englewood Cliffs, New Jersey 07632.

Keeley, J.R. 1984. Observations of an internal resonance in a fjord. *J. Mar. Res.* **42**, 873-891.

Lavin-Peregrina, M.F. 1984. The seasonal cycle and variability of stratification in the western Irish Sea. Ph.D. Thesis, UCNW, 154pp.

Le Blond, P.A. & Mysak, L.A. 1978. *Waves in the Ocean.* Elsevier, New York.

Lynn, P.A. & Fuerst, W. 1990. *Digital Signal Processing with Computer Applications.* John Wiley & Sons Ltd.

Mackay, D.W. & Halcrow, W. 1976. The distribution of nutrients in relation to water movements in the Firth of Clyde. In *Freshwater on the Sea,* eds. skreslet, S., Leinebo. r, Mathews, J.B.L. & Sakshayg.E. pp109-118. Oslo: Association of Noregian Oceanographers.

Marsden, R.F. & Greenwood, K.C. 1994. Internal tide observed by an Acoustic Doppler Current Profiler. *Journal of Physical Oceanography*, **24**, 1097-1109.

Mason, J. & Fraser, D.I. 1986. Shellfish fisheries in the Clyde Sea area. *Proceedings of the Royal Society of Edinburgh.* **90B**, 493-450.

McKinley, I.G., Baxter, M.S. & Jack, W. 1980. A simple model of radiocaesium transport from Windscale to the Clyde Sea. *Estuarine, Coastal and Shelf Science,* **13**, 59-67.

Mill, H.R. 1892. The Clyde Sea area. *Transactions of the Royal Society of Edinburgh,* **36**, 641-729.

Mitchelson, E.G., Hill, A.E. & Simpson, J.H. 1989. A report on CTD data collected west of Scotland during the winter of 1987-1988 as part of the Scottish Coastal current and Autumnal circulation experiment (ACE) programmes, UCNW Internal Report.

Münchow, A. & Garvine, R.W. 1993. Dynamical properties of a buoyancy-driven coastal current. *Journal of Geophysical Research*, **98**, No. C11, pp 20,063-20,077.

Ozretich, J.R. 1975. Mechanisms for deep water renewal in Lake Nitinate, a permanently anoxic fjord. *Estuaries, Coastal and Marine Science*, **3**, 189-200.

Pedersen, F.B. 1980. A monograph on turbulent entrainment and friction in two-layer stratified flow. Tech. Univ. of Denmark, Inst. of hydrodynamics and hydraulic eng. Series paper No. 25.

Perkin, R.G. & Lewis, E.L. 1978. Mixing in an arctic fjord. *Journal of Physical Oceanography*

8, 837-880

Poodle, T. 1986. Freshwater inflows to the Firth of Clyde. *Proceedings of the Royal Sociey of Edinburgh,* **90B,** 55-66.

Phillips, O.M. 1977. *The Dynamics of the Upper Ocean.* 2st ed. Cambridge University Press, London. 199-255.

Pollard, R.T., Rhines, P.B. & Thompson, R.O.R.Y. 1973. The deepening of the wind-mixed layer. *Fluid Dyn.* **4**, 381-404.

Prandle, D. 1984. A modelling study of the mixing of ^{137}Cs in the seas of the European continental shelf. *Philosophical Transactions of the Royal Society of London*, **A310**, 407-436.

Pratt, L.J. & Lundberg, P.A. 1991. Hydraulics of rotating strait and sill flow. *Annual Revew of Fluid Mechanics*, **23**, 81-106.

Proctor, R. & James, I.D. 1996. A Fine-Resolution 3D Model of the Southern North Sea. Journal of Marine Systems, **257**, IN PRESS

Pugh, D.T. 1987. Tides, surges and mean sea-level. N.E.R.C., John Wiley & sons, Swindon, U.K.

Research Developemetn Instruments. 1989. *'ADCP Princlples of operation: a Practical Primer.'* 9855 Businesspark Av., San Diego, Californai, U.S.A.

Rippeth T.P. 1993. The control of stratification in a fjordic system (the Clyde Sea). Ph.D. thesis. U.N.C.W.

Rippeth, T.P., Midgley, R.P., & Simpson, J.H. 1995. The seasonal cycle of stratification in a Scottish fjord. In *Ecology of Fjords and Coastal Waters.* Ed. Skjoldal, H.R., Hopkins, C., Erikstad, K.E. & Leinaas, H.P. Elsevier Science B.V. 85-92.

Rippeth, T.P. & Simpson, J.H. 1995. The frequency and duration of episodes of complete vertical mixing in the Clyde Sea. *Continental Shelf Research,* **16,** No. 7, 933-947.

Rodhe, J. 1995. The Baltic and the North Sea - a process-orientated review of the physical oceanography. Department of Oceanography, Göteborg, Sweeden.

Seibert, G.H., Trites, R.W. & Reid, S.J. 1979. Deepwaterexchange processes in the Saguenay Fjord. *J. Fish. Res. Bb. Canada.* **36**, 42-53.

Simpson, J.H. 1981. The shelf-sea fronts - Implications of their existence and behaviour. *Philosophical Transactions of the Royal Society of London Series A - Mathematical and Physical Sciences.* Vol 302, No. 1472, 531-542.

Simpson, J.H. & Bowers, D.G. 1981. Models of stratification and frontal movement in shelf seas. *Deep Sea Research*, **28**, 727-738.

Simpson, J.H. & Bowers, D.G. 1984. The role of tidal stirring in controlling the seasonal heat cycle in shelf seas. *Annales Geophysicae*, **2(4)**, 411-416.

Simpson, J.H. & Hunter, J.R. 1974. Fronts in the Irish Sea. *Nature, london* ***250****, 404-406.*

Simpson, J.H. & Rippeth, T.P. 1993. The Clyde Sea: a model of the seasonal cycle of stratification and mixing. *Estuarine, Coastal and Shelf Science,* **37**, 129-144.

Simpson, J.H. In Press. Physical Processes in the ROFI regime. *Journal of Marine Systems.*

Sherwin, T.J. 1988. Analysis of an internal tide observed on the Malin Shelf, North of Ireland. *Journal of Physical Oceanography,* **18**, No. 7.

Skreslet, S. & Loeng, H. 1977. Deep water renewal and associated processes in skjomen, a fjord in north Norway. *Estuarine and Coastal Marine Science,* **5**, 383-398.

Smith, K. 1986. The climate of the Estuary and the Firth of Clyde. *Proceedings of the Royal Society of Edinburgh* **90B**, 43-54

Stacy, M.W. & Zedel, L.J. 1986. The time-dependent hydraulic flow and dissipation over the sill of Observatory Inlet. *Journal of Physical Oceanography* **16**, 1062-1076.

Stacy, M.W. 1984. The interaction of tides with the sill of a tidally energetic inlet. *Journal of Physical Oceanography* **14**, 1106-1117.

Stanton, B.R. 1986. Winter oceanographic conditions in some New Zealand fjords. *New Zealand Journal of Marine and Freshwater Research,* **20**, 299-314.

Stigebrandt, A. 1976. Vertical diffusion driven by internal waves in a sill fjord. *Journal of Physical Oceanography,* **6**, 484-495.

Stigebrandt, A. 1977. On the effect of barotropoic current fluctuations on the two-layer transport capacity of a constriction. *Journal of Physical Oceanography* **7**, 118-122.

Stigebrandt, A. 1979. Observational evidence for vertical diffusion driven by internal wavesof tidal origin in the Oslofjord. *Journal of Physical Oceanography* **9**, 435-441.

Stigebrandt, A. 1980. Some aspects of tidal interactions with fjord constrictions. *Journal of Physical Oceanography* **11**, 151-166.

Stigebrandt, A. 1981. A mechanism governing the estuarine circulation in deep strongly stratified fjords. *Estuarine Coastal and Shelf Sea Science* **13**, 197-211.

Stigebrandt, A. 1990. On the response of the horizontal mean vertical density distribution in a fjord to low freqency density fluctuations in the coastal water. *Tellus* **42A**, 605-614.

Stigebrandt, A. & Aure, J. 1989. Vertical mixing in basin waters of fjords. *Journal of Physical Oceanography,* **19**, 917-926.

Svendsen, H. 1995. Physical oceanography of coupled fjord-coast systems in northern norway with special focus on frontal dynamics and tides. In *Ecology of Fjords and Coastal Waters.* Ed. Skjoldal, H.R., Hopkins, C., Erikstad, K.E. & Leinaas, H.P. Elsevier Science B.V. 149-164.

Tett, P.R., Gowen, B., & Jones, K. 1986. The phytoplancton ecology of the Firth of Clyde sea-lochs Striven and Fyne. *Proceedings of the Royal Society of Edinburgh.* **90B**, 223-238.

Tivy, J. 1986. The geography of the Estuary and Firth of Clyde. *Proceedings of the Royal Society of Edinburgh.* **90B**, 7-23.

Townson, J.M. & Collar H.F. 1986. Water movement and the simulation of storm surges in the Firth of Clyde. *Proceedings of the Royal Society of Edinburgh* **90B**, 85-96.

Turner, J.S. 1973. Boundary effects in fluids. Cambridge University Press. pp367

Turner, J.S. 1981. Small scale-mixing processes. In: *Evolution of physical oceanography.* B. Warrren & C. Wunsch, eds., The MIT Press. 236-262.

Valle-Levinson, A., O'Donnel, J. 1994. Tidal Interaction with buoyancy-driven flow in a coastal plain estuary. Seventh Bienial International Conference on the Physics of Estuaries and Coastal Seas, Woods Hole, MA.

Valle-Levinson, A., Wilson, R.E. 1994. Effects of sill bathymetry, oscillating barotropic forcing and vertical mixing on estuary/ocean exchange. *Journal of Geophysical Research*, **99**, No. C3, 5149-5196.

Whitehead, J.A., Leetmaa, A., Knox. R.A. 1974. Rotating Hydraulics of strait and sill flows. *Geophysical Fluid Dynamics*, **6**, 101-125.

Webb, A.J. & Pond, S. 1986. A modal decomposition of the internal tide in a deep, strongly stratified inlet: Knight Inlet, British Columbia. *Journal of Geophysical research*, **91**, No. C8, 9721-9738.

Wong, Kuo-Chuin 1994. On the nature of transverse variability in a coastal plain estuary. *Journal of Geophysical research*, **99**, No. C7, 14,209-14,222.

Appendix 1: CTD station positions

Station	Latitude (North)	Longitude (West)	Approx. water depth (m)
NC1	55°02.0'	05°35.0'	120
NC2	55°00.6'	05°40.6'	140
NC3	54°58.3'	05°46.8'	100
NC4	54°56.2'	05°51.0'	50
PD5	54°38.3'	05°28.9'	30
PD4	54°41.9'	05°23.7'	110
PD3	54°44.0'	05°18.6'	130
PD2	54°46.9'	05°14.0'	150
PD1	54°49.5'	05°08.8'	40
MK1	55°13.9'	05°40.3'	90
MK2	55°15.4'	05°48.1'	130
MK4	55°13.0'	05°55.0'	140
MK5	55°10.4'	05°58.0'	120
PE1	55 17.1'	05 04.5'	50
PE2	55°10.5'	05°05.9'	40
PE3	55°06.3'	05°11.4'	50
PE4	55°00.7'	05°21.1'	140
GP1	55°09.2'	05°36.3'	100
GP4	55°21.1'	05°17.2'	40
GP5	55°23.3'	05°14.5'	50
AD5	55°23.8'	04°51.7'	60
AD4	55°25.3'	04°57.0'	60
AD3	55°31.2'	04°47.0'	60
AD2	55°31.2'	04°53.1'	70
AD1	55°39.7'	04°56.5'	65
LF5	55°58.1'	05°22.6'	150
LF4	55°55.6'	05°23.1'	140
LF3	55°53.4'	05°23.0'	160
LF2	55°50.6'	05°19.8'	150
LF1	55°49.1'	05°16.2'	150
CE4	55°56.3'	04°53.8'	50

CE3	55°52.0'	04°56.6'	30
CE2	55°46.7'	04°58.8'	70
CE1	55°43.7'	04°58.9'	110
CS1	55°09.5'	05°22.3'	70
CS2	55°13.9'	05°15.0'	45
CS3	55°18.0'	05°11.3'	40
CS4	55°21.8'	05°04.7'	50
CS5	55°26.7'	05°01.3'	110
CS6	55°32.2'	05°59.0'	100
CS7	55°38.4'	05°01.8'	170
CS8	55°41.9'	05°08.9'	160
CS9	55°46.1'	05°15.5'	120
CS10	55°42.6'	04°20.1'	110
CS11	55°40.3'	05°25.4'	160
CSE	55°35.4'	05°25.4'	110
CS12	55°30.1'	05°26.5'	80
CS13	55°26.0'	05°28.9'	30
CS14	55°22.5'	05°18.8'	40
CS15	55°17.0'	05°27.7'	40
CS16	55°14.7'	05°33.3'	70
CS17	55.05.3'	05.30.1'	120

CTD stations visited March 1995: CS1, CS2, CS4, CS5, CS6, CS7, CS8, CS9, CS10, CS11, CSE, CS12,CS13, CS14, CS15, CS16, CS17, PE4, MK1, A, B, C, D, E, F.
CTD stations visited September 1995: CS17, CS1, CS2, CS3, CS5, CS7, A1, A, B, C, D, E.E2-E8 in the Irish Sea.

CTD STATION	LATITUDE North	LONGITUDE West
A	55.35	5.45
B	55.33	5.33
C	55.30	5.20
D	55.28	5.08
E	55.25	4.96
F	55.29	5.13
A1	55.24	5.48

CTD stations new to this work, and not given in Rippeth et al., 1995b.

APPENDIX 2.

Profiles anti-clockwise about Arran of selected CTD observations.

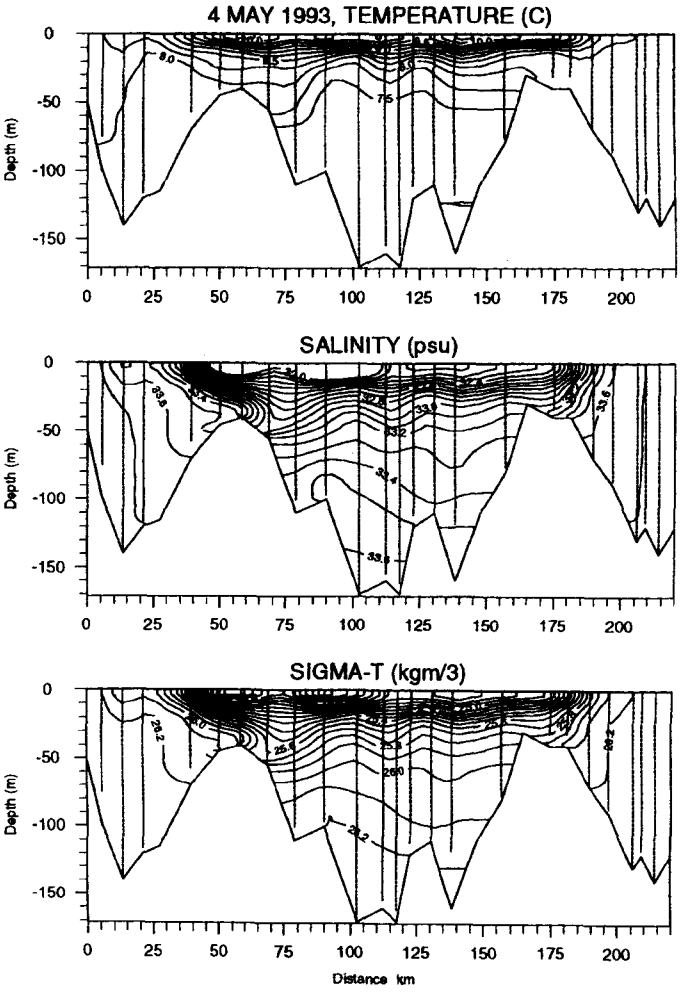

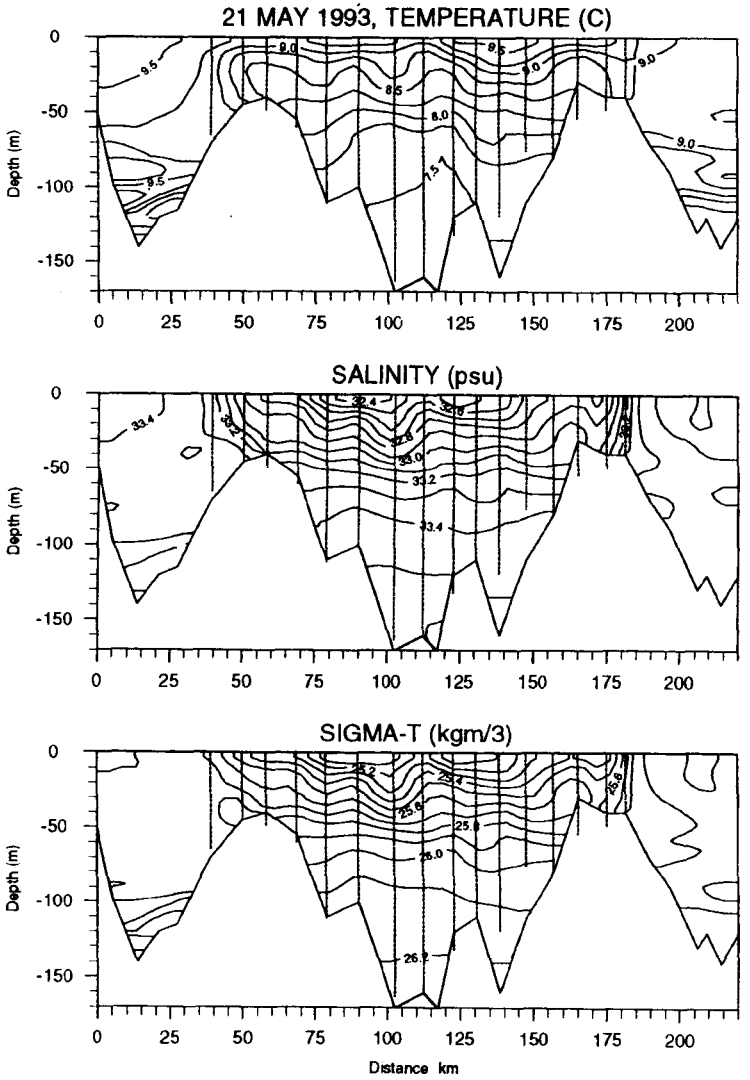
21 MAY 1993, TEMPERATURE (C)
SALINITY (psu)
SIGMA-T (kgm/3)
Depth (m)
0
-50
-100
-150
0 25 50 75 100 125 150 175 200
Distance km

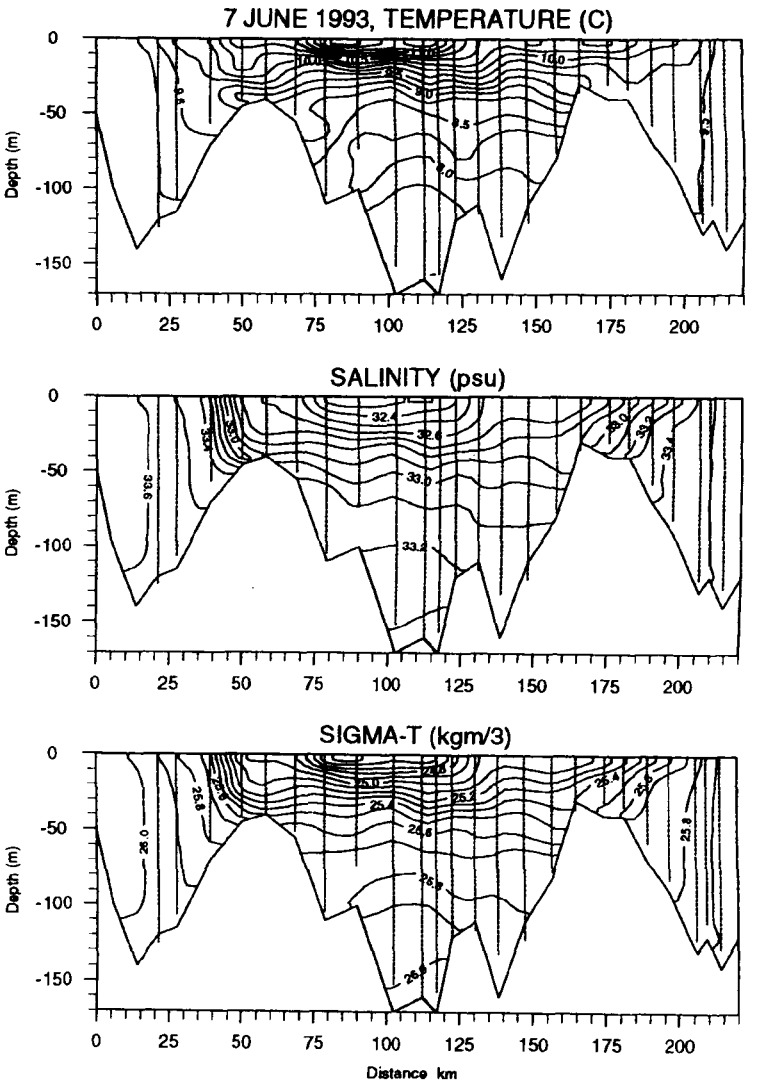
7 JUNE 1993, TEMPERATURE (C)
SALINITY (psu)
SIGMA-T (kgm/3)
Depth (m)
0
-50
-100
-150
0 25 50 75 100 125 150 175 200
Distance km

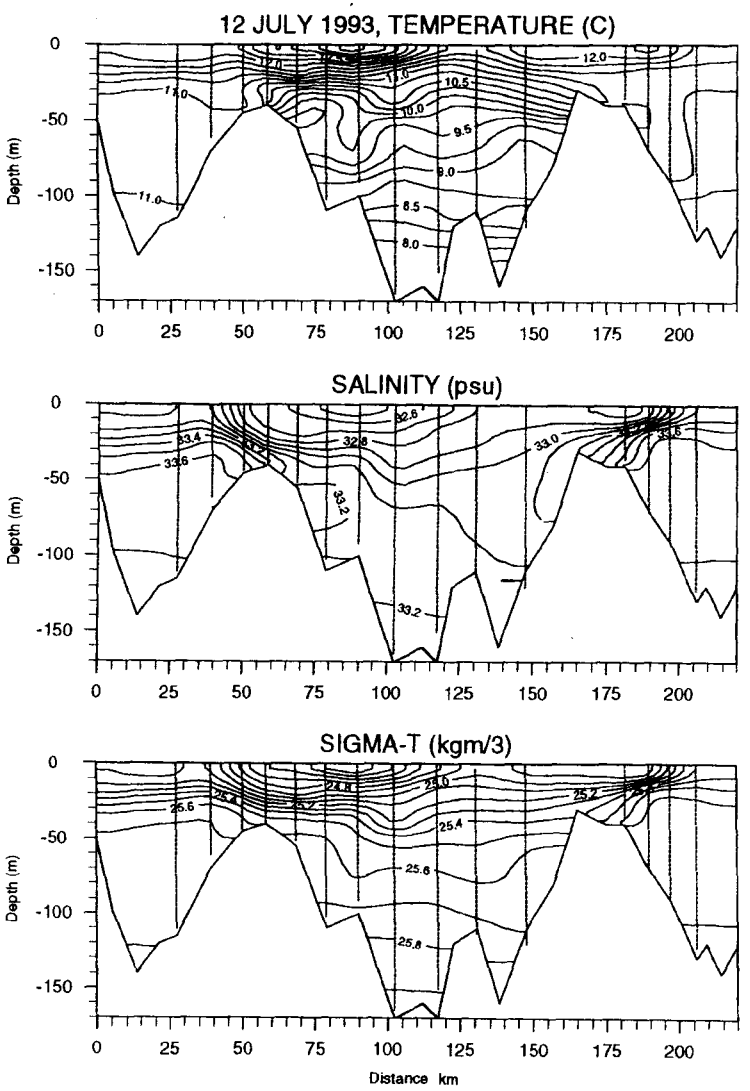
12 JULY 1993, TEMPERATURE (C)
SALINITY (psu)
SIGMA-T (kgm/3)
Depth (m)
Distance km

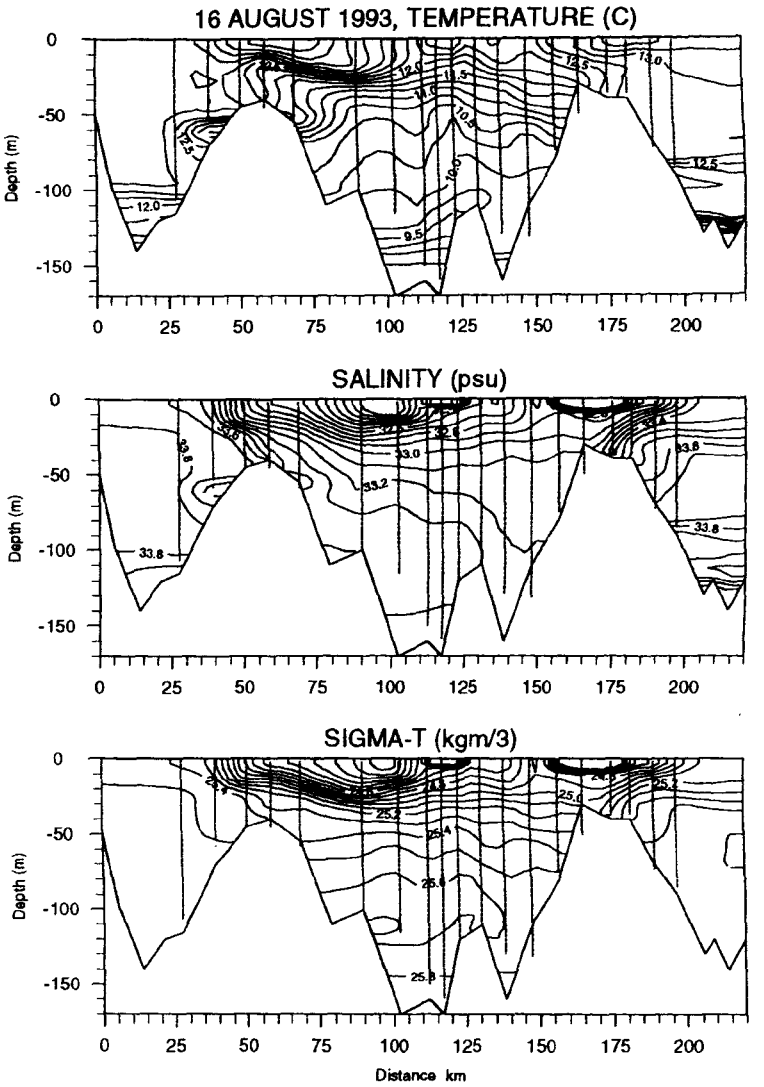
16 AUGUST 1993, TEMPERATURE (C)
SALINITY (psu)
SIGMA-T (kgm/3)
Depth (m)
Distance km

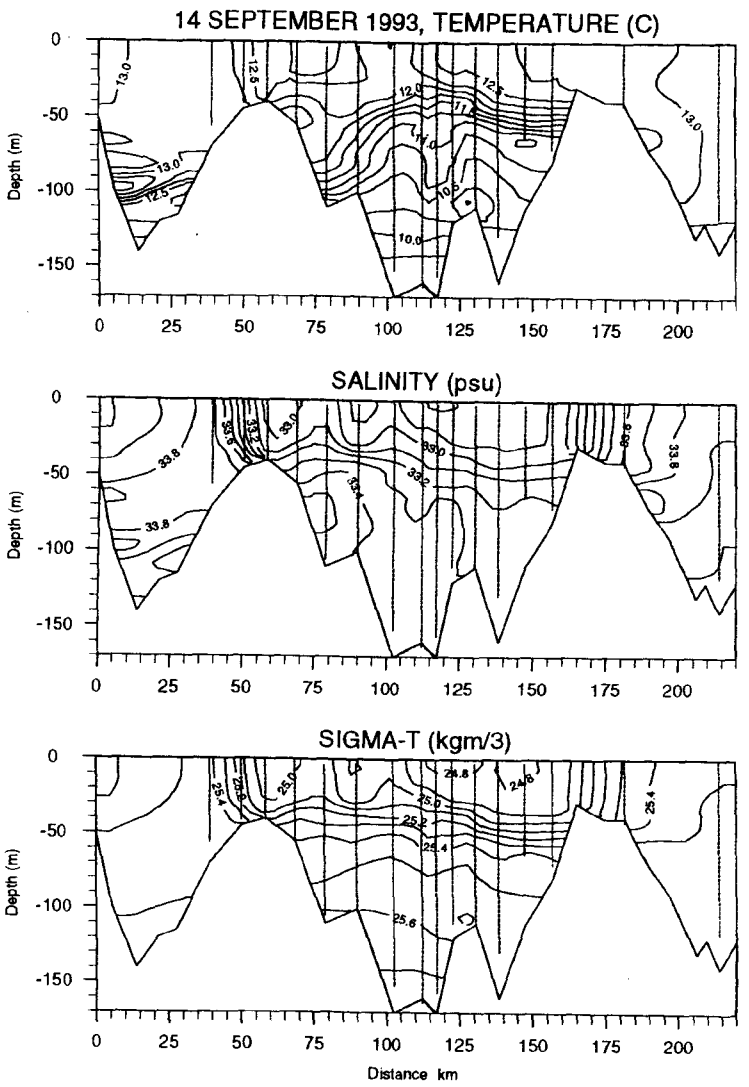
14 SEPTEMBER 1993, TEMPERATURE (C)
SALINITY (psu)
SIGMA-T (kgm/3)
Depth (m)
Distance km

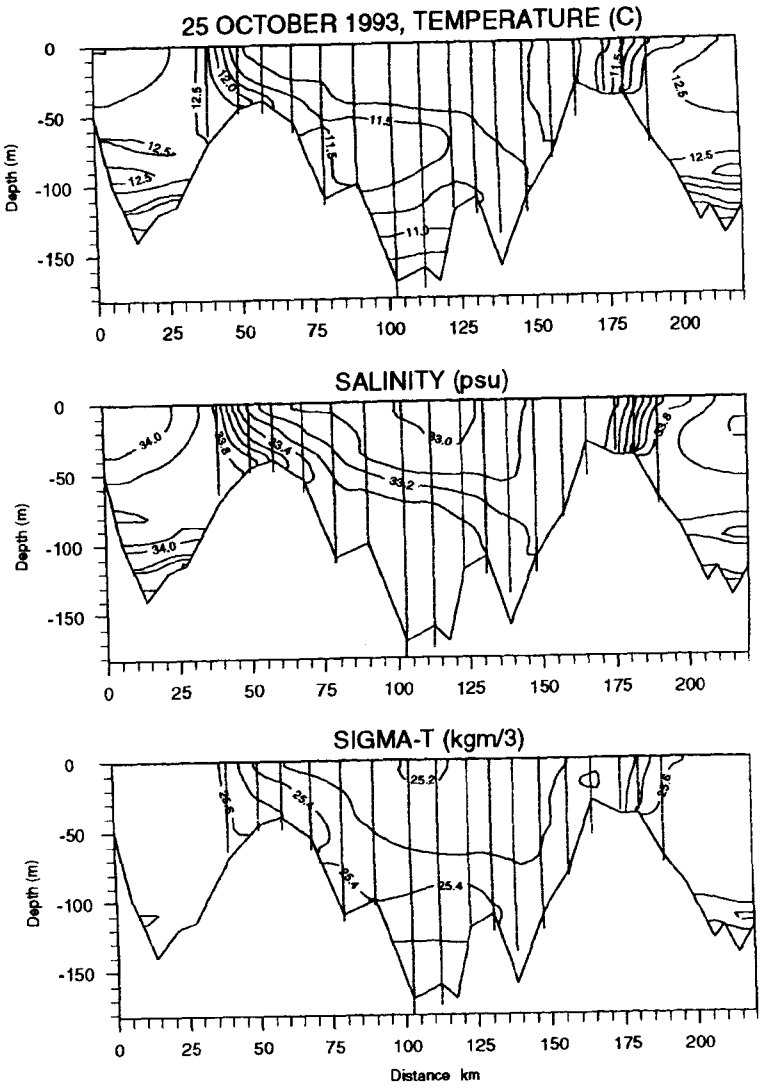
25 OCTOBER 1993, TEMPERATURE (C)
SALINITY (psu)
SIGMA-T (kgm/3)
Depth (m)
Distance km

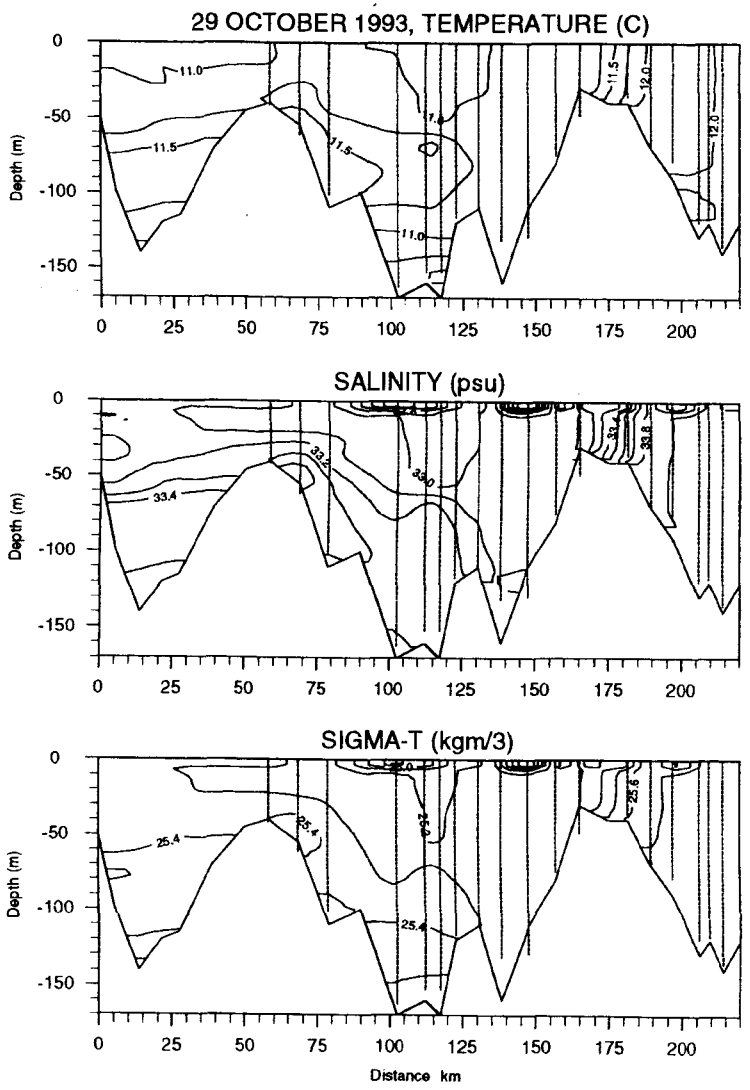
29 OCTOBER 1993, TEMPERATURE (C)
SALINITY (psu)
SIGMA-T (kgm/3)
Depth (m)
0
-50
-100
-150
0 25 50 75 100 125 150 175 200
Distance km

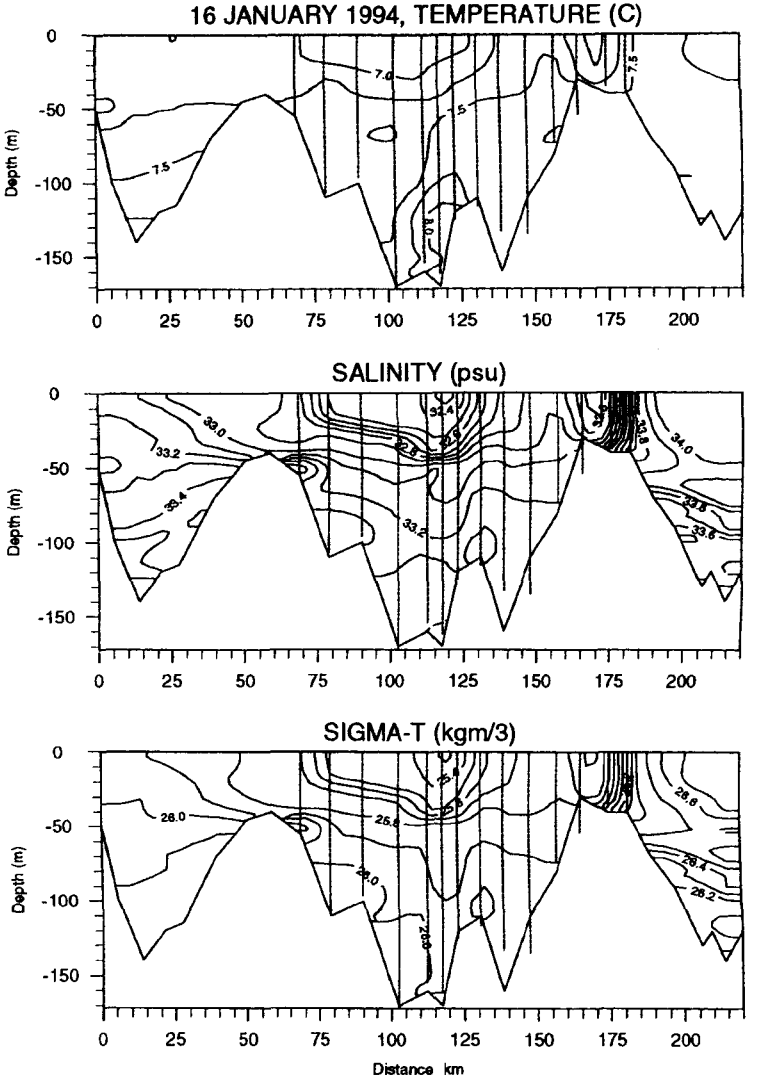
16 JANUARY 1994, TEMPERATURE (C)
SALINITY (psu)
SIGMA-T (kgm/3)
Depth (m)
0
-50
-100
-150
0 25 50 75 100 125 150 175 200
Distance km

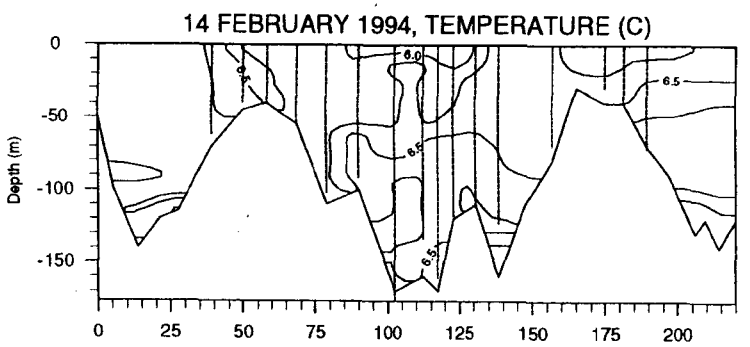
14 FEBRUARY 1994, TEMPERATURE (C)
Depth (m)
0
-50
-100
-150
0
25
50
75
100
125
150
175
200
6.0
6.5

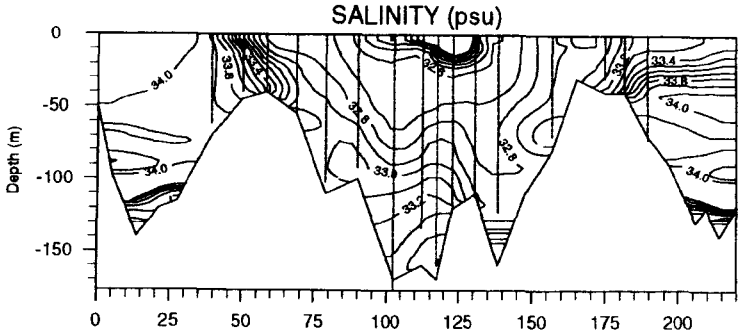
SALINITY (psu)
Depth (m)
0
-50
-100
-150
0
25
50
75
100
125
150
175
200
34.0
33.8
33.4
32.8

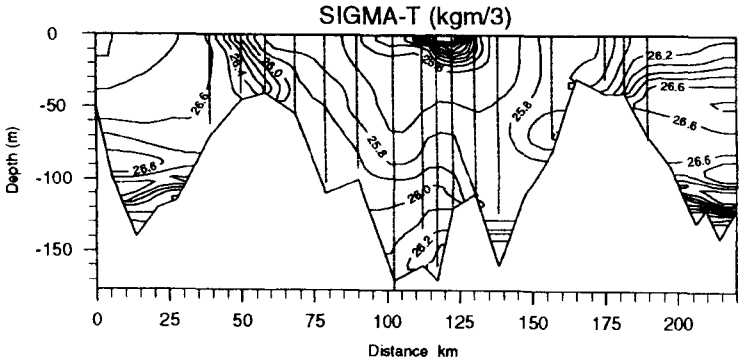
SIGMA-T (kgm/3)
Depth (m)
0
-50
-100
-150
0
25
50
75
100
125
150
175
200
Distance km
26.2
26.6
26.8
25.8
26.0

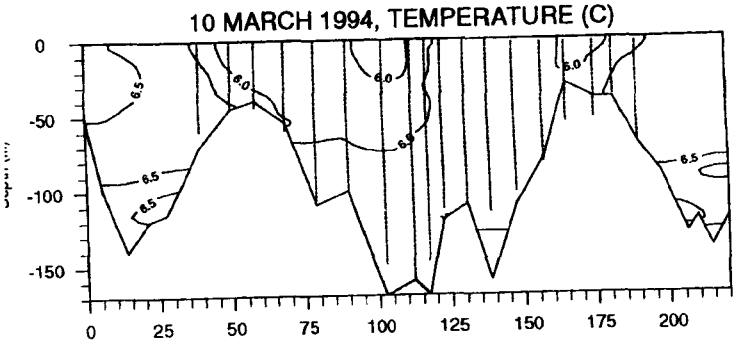
10 MARCH 1994, TEMPERATURE (C)
0
-50
-100
-150
0
25
50
75
100
125
150
175
200
6.0
6.5

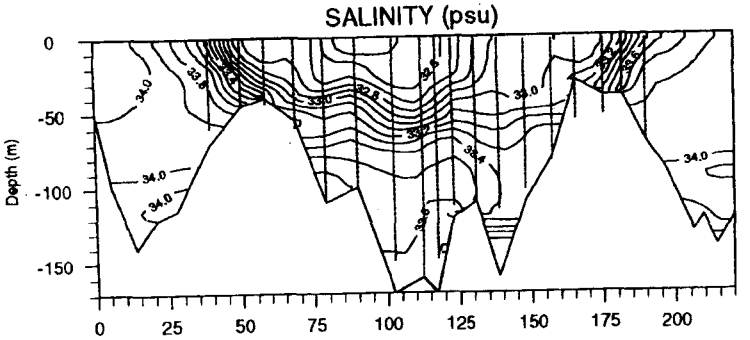
SALINITY (psu)
Depth (m)
0
-50
-100
-150
0
25
50
75
100
125
150
175
200
34.0
33.8
33.4
32.8

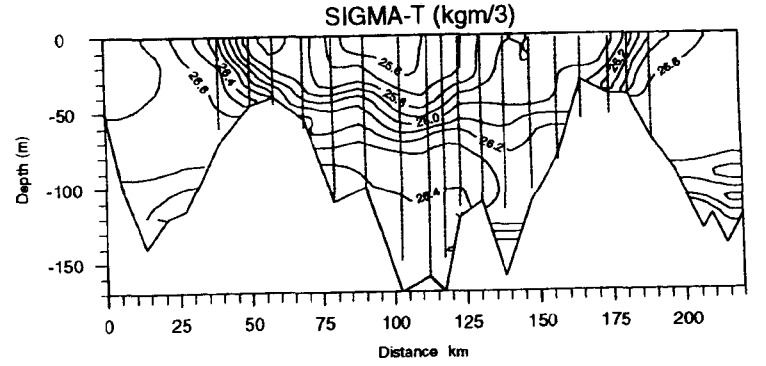
SIGMA-T (kgm/3)
Depth (m)
0
-50
-100
-150
0
25
50
75
100
125
150
175
200
Distance km
26.0
26.2
26.4
26.8

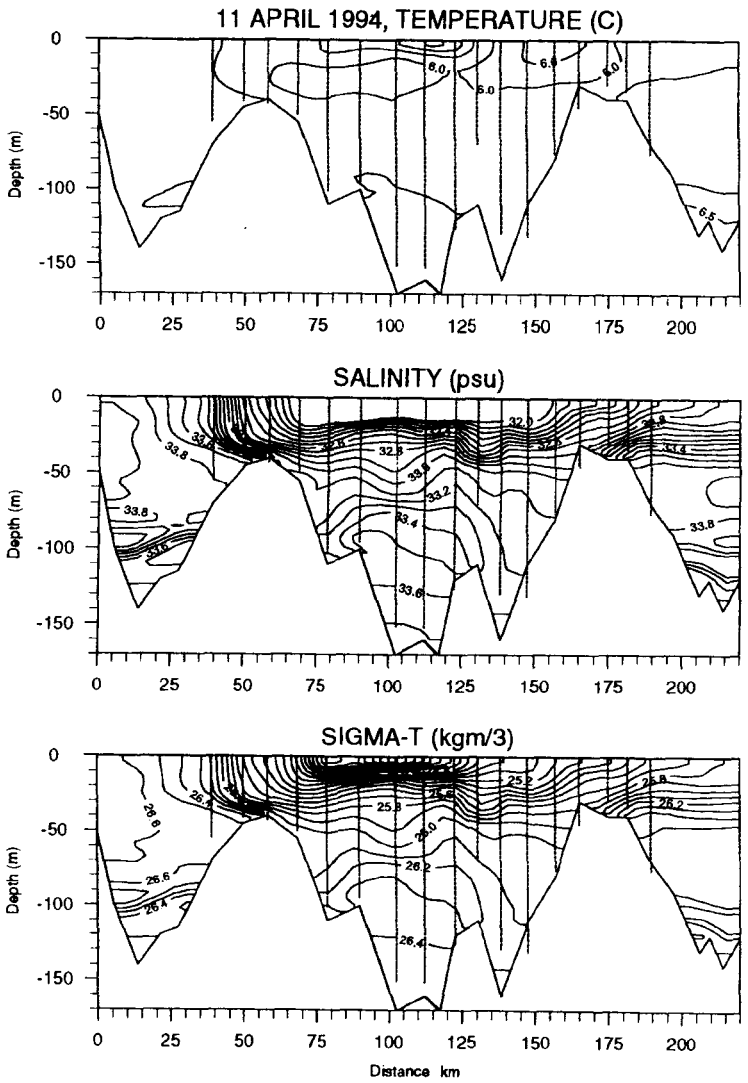
11 APRIL 1994, TEMPERATURE (C)
SALINITY (psu)
SIGMA-T (kgm/3)
Depth (m)
Distance km

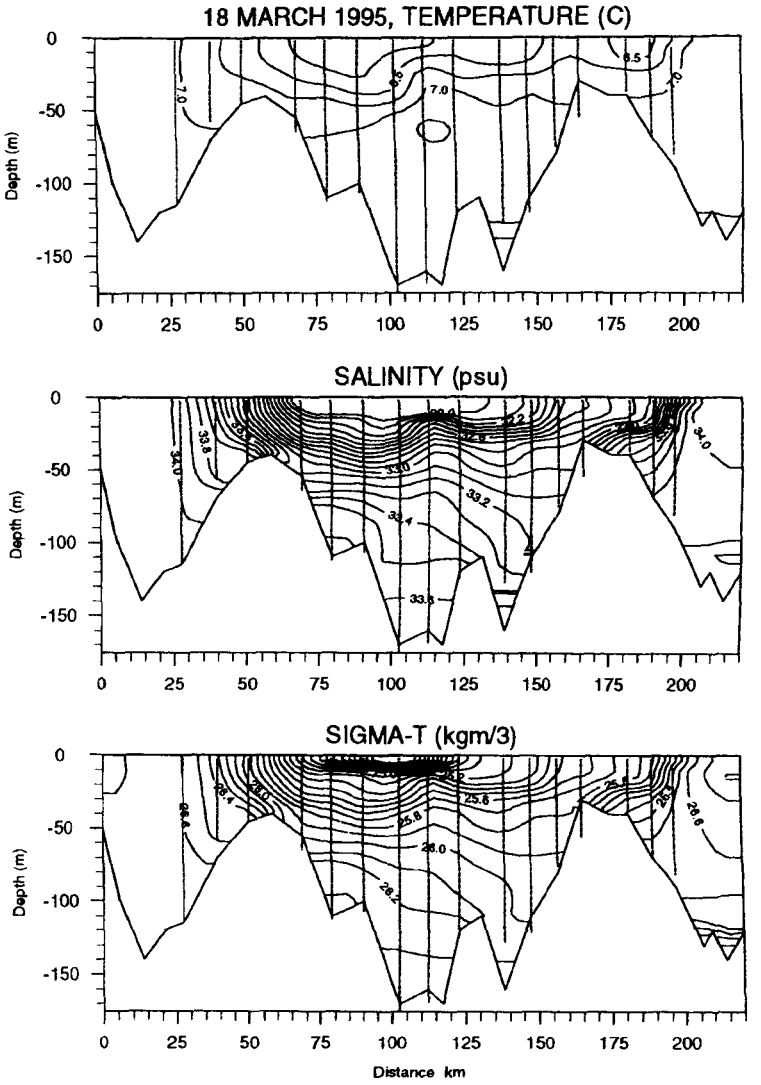
18 MARCH 1995, TEMPERATURE (C)
SALINITY (psu)
SIGMA-T (kgm/3)
Depth (m)
Distance km